

Reservoir characterisation and facies classification of the detrital deposits adjacent to a travertine system in Denizli, Turkey

Michaël VERBIEST

Promotor: Prof. Dr. Rudy Swennen
KU Leuven

Begeleider: Dr. Jeroen Soete
KU Leuven

Proefschrift ingediend tot het
behalen van de graad van
Master of Science in de geologie

Academiejaar 2015-2016

© Copyright by KU Leuven

Without written permission of the promoters and the authors it is forbidden to reproduce or adapt in any form or by any means any part of this publication. Requests for obtaining the right to reproduce or utilize parts of this publication should be addressed to KU Leuven, Faculteit Wetenschappen, Geel Huis, Kasteelpark Arenberg 11 bus 2100, 3001 Leuven (Heverlee), Telephone +32 16 32 14 01.

A written permission of the promotor is also required to use the methods, products, schematics and programs described in this work for industrial or commercial use, and for submitting this publication in scientific contests.

Preface

The discovery of the Lula (also known as Tupi) oil field sparked the interest in continental carbonates. These hydrocarbon reservoirs are located deep offshore near the coast of Brazil and are commonly referred to as the Pre-Salt plays. Continental carbonates are considered to be a possible analogue for a part of these oil reservoirs and has thus been studied at the KU Leuven by several master and PhD students. The studied analogue in the Ballık area is encased by detrital deposits (ranging from conglomerates to laminated marls). It is likely that comparable detrital deposits are also present in the Pre-Salt deposits, making them part of the system targeted for oil exploration. In order to increase the understanding of the sedimentological and volumetric characteristics, field analogues near the city of Denizli (Turkey) were studied.

Four main objectives were defined for this research:

- The first objective was to describe the detrital deposits that are encasing the so-called Ballık “travertine dome”. This description mainly took place in the field itself and aimed to increase the understanding of the lateral and vertical continuity of these deposits.
- The second objective was to classify the detrital deposits in different sedimentary facies. This was achieved by integrating data acquired from numerous techniques, as for example petrography, medical CT, SEM, Furthermore, the depositional setting of each facies was discussed and if possible visualised with a proposed conceptual model. The aim of these models is to unravel the depositional mechanisms of the sedimentary facies, with a quick and visual overview.
- The third objective was to evaluate whether the lacustrine sediments can be used to characterise each detrital sequence (either by a unique clay mineralogy or geochemistry) in order to correlate a sequence throughout different quarries rather easily and with great certainty.
- The fourth objective was to characterise these detrital deposits by their petrophysical properties. This data was used in order to differentiate porous from non-porous lithologies, in order to place them within the framework of the reservoir analogue.

During this research several people helped me out with specific problems.

At first I would like to start with thanking my promoter, prof. dr. Rudy Swennen, who gave me the opportunity to go in the field and look to these detrital deposits myself. I am also grateful for his quick and efficient meetings and for the time he spend in reviewing my thesis.

I would also like to thank the people who guided me in the field itself. Dr. Jeroen Soete, thank you for guiding me around in *your* quarries! I really appreciate the time you took in discussing our field observations in the field itself. Of course, I cannot forget to mention Drs. Cihan Aratman, who not only helped me out with several problems, but also volunteered as a jukebox while driving to the quarries. Furthermore, I would like to thank Prof. Dr. Mehmet Özkul for his interesting comments in the field itself.

However, once I returned from the field, I had to count on the expertise of several people. I would like to thank Herman Nijs for the time he spend in preparing my thin sections (which was not always a straightforward and easy task at all). Furthermore, I would also like to thank Ria Brepoels and Dr. Nancy Weyns, who both helped me out tremendously with XRD-measurements and several other procedures. I really enjoyed working with both of you. During the interpretation of the XRD measurements I could count on the experience of Dr. Rieko Adriaens and Drs. Sofie Hollanders, for which I'm grateful. Furthermore, I would also like to thank Dr. Elvira Vassilieva, who guided me with the geochemical analyses. I would also like thank Drs. Ophélie Fay-Gomord, for helping me to get started with the SEM. Lastly, I would like to thank Drs. Marcelle Marques Erthal for giving me a crash course in bio-mineralisation.

Of course I would like to thank my parents, who allowed me to study this incredibly interesting branch of science. Furthermore, I cannot forget to thank my friends from my hometown, who have always been supportive throughout the years. I know I have missed our last barbeque meetings, but we will soon make up for this! Nevertheless, in the past five years I also enjoyed the vibrant atmosphere within our group. Nevertheless, I would like to thank Nathan, Glenn and Pieter more specifically. Thanks for all the adventures we had the past five years you guys!

Abstract

In 2006, the Lula (also known as Tupi) hydrocarbon reservoir was discovered in the deep offshore of the Brazilian coast. This reservoir consists of a mixture of lacustrine carbonates, continental carbonates and detrital deposits, which are commonly described as Pre-Salt deposits. The discovery of this *new* reservoir type, lead to the creation of the Joint Industrial Project focusing on the sedimentology of several continental carbonate analogues.

The area, which was studied during this research, is known as the Ballık area and is located near the city of Denizli (Turkey). The continental carbonates in this area have been studied for numerous years and are considered to be one of the best reservoir-scaled analogues worldwide. However, the analogues are also characterised by the presence of detrital deposits, encasing the carbonate sediments. This thesis aims to increase the understanding of the processes that lead to these non-travertine lithologies and to evaluate their petrophysical properties.

In order to achieve these goals, numerous methods have been used. Classic field observations (acquiring lithologs and describing large scale sedimentary features) and petrographical analyses (conventional, fluorescence and cathodoluminescence microscopy) lead to initial observations, which were used in the facies classification. Additionally, Medical Computed Tomography (CT) was used to visualize the internal structure of certain hand samples. In total seven different lithologies could be differentiated (massive marls, laminated marls, polygenetic conglomerates, tabular sandstones, monogenetic breccias, gastropod-rich carbonates and coquina beds). Each of these lithologies are classified in five different sedimentary facies, being the lacustrine, the fluvial, the debris-flow, the gastropod and the coquina facies. The petrophysical properties of these facies were evaluated and the results were combined with the other methods, in order to come up with a proposed depositional setting. Since this thesis still focuses on the sedimentological characteristics of an analogue, it was also important to keep in mind that the diagenetic processes differ from the ones of the true reservoir. The possible behaviour of these deposits during diagenesis was briefly addressed as well.

X-Ray Diffraction (XRD) was used in order to evaluate whether it is possible to characterise the lacustrine sediments by a unique (clay) mineralogy. Additionally, SEM was used in order to differentiate authigenic from allogenic clay minerals. Furthermore, the geochemical composition of these sediments was assessed trough Inductively Coupled

Plasma Optical Emission Spectroscopy (ICP-OES). Additionally, the total amount of organic carbon (TOC) was evaluated by Elemental Analysis – Isotope Ratio Mass Spectrometry (EA-IRMS). All these observations lead to a proposed depositional model of the lacustrine facies, which is characterised by indicators of an arid and evaporitic depositional environment (with palygorskite, authigenic dolomite, fluctuating carbonate content, ...). The fluvial facies consists of three different lithologies (massive marls, tabular sandstones and polygenetic conglomerates) and tend to develop horizontally and vertically interconnected reservoir bodies. These reservoirs are characterised by porosity values ranging between 5.6 and 14.9 % and permeability values ranging between 0.04 and 142 mD. Furthermore, a grain size analysis has been performed on the unconsolidated conglomerates in order to get an idea about the clast sizes. The debris-flow facies consists of the monogenetic breccia lithotype and is characterised by a different depositional setting as the fluvial facies. In comparison to the fluvial facies, the volume of this facies is rather limited and the deposition was dominated by gravity-driven processes. The fourth facies consists of the gastropod facies, which is characterized by isolated moldic porosity. This facies was observed in great proximity of the travertine dome and the lacustrine facies, since they are deposited in a sub-horizontal environment. Lastly the coquina facies is described, however, only a limited petrographical study was done within this thesis.

It can thus be concluded that in great proximity of the travertine dome, five different sedimentary facies are present. Each of these facies are characterised by an unique depositional setting and controlling parameters. These detrital deposits will further increase the understanding of the depositional setting of the travertine analogue in the Ballık area.

Samenvatting

Voor de kust van Brazilië werd in 2006 een olie- en gasreservoir van wereldklasse ontdekt. Dit reservoir staat momenteel bekend als het Lula veld en was vroeger ook wel gekend als het Tupi veld. Het reservoir bestaat uit lacustriene carbonate, continentale carbonaten en detritische afzettingen, die ook wel gekend zijn als de Pre-Salt afzettingen. Het type reservoir gesteente die deel uitmaken van het Lula veld zijn eerder uniek en werden tot voor de ontdekking van dit olie- en gasveld zelden bestudeerd.

In het kader van dit onderzoek werd een reservoir analoog voor continentale carbonaten, gekend als de Ballik travertijnen gelegen nabij Denizli (Turkije), bestudeerd. Dit analoog werd hiervoor al voor verscheidene jaren bestudeerd door verschillende onderzoekers aan de KU Leuven en wordt beschouwd als een goed analoog voor de continentale carbonaten van het Lula veld. Het voorafgaande onderzoek heeft zich tot nu toe voornamelijk gefocust op de carbonaten zelf, zonder al te veel aandacht te besteden aan de detritische afzettingen die nabij de continentale carbonaten worden waargenomen. Het zijn net deze detritische afzettingen die centraal staan in dit onderzoek, met als doel om deze afzettingen te classificeren in verschillende sedimentaire facies. Verder worden ook de mogelijke processen, die tot deze afzettingen geleid hebben en hun bijhorende petrofysische eigenschappen geëvalueerd.

Tijdens dit onderzoek werden verschillende methodes gebruikt. De initiële terreinobservaties (lithologs en grootschalige sedimentaire structuren) en de petrografie (conventionele, fluorescentie en cathodoluminescentie microscopie) werden verwerkt in een facies classificatie. Hiernaast werd 'Medical Computed Tomography' (Medische CT) gebruikt om de interne structuren van deze sedimenten te visualiseren. In totaal werden er zeven verschillende lithologiën beschreven (massieve mergels, gelamineerde mergels, polygenetische conglomeraten, tabulaire zandstenen, monogenetische breccias, carbonaatgesteente rijk in gastropodes en coquina banken). Deze lithologiën werden onderverdeeld in vijf verschillende facies: de lacustriene, de fluviatiele, de debris-flow, de gastropode en coquina facies. Elke facies werd gekenmerkt door specifieke petrofysische eigenschappen, waarop de lacustriene facies een uitzondering vormt. Dit onderzoek focust ook op de sedimentaire eigenschappen van een analoog, waardoor het belangrijk is om de mogelijke diagenetische processen in rekening te brengen. Bijgevolg werd de diagenetische invloed op de reservoir karakteristieken van elke facies kort besproken.

Om na te gaan of het mogelijk is om de verschillende lacustriene afzettingen van elkaar te onderscheiden, werd er gebruik gemaakt van X-Ray Diffractie (XRD). Het doel hiervan was om na te gaan of de lacustriene sedimenten gekenmerkt worden door een unieke (klei) mineralogie. Hiernaast werd er ook gebruik gemaakt van 'Scanning Electron Microscope' (SEM) om de authigene van de allogene klei mineralen te onderscheiden. Aanvullend werd de geochemische samenstelling van deze sedimenten ook geëvalueerd aan de hand van 'Inductively Coupled Plasma Optical Emission Spectroscopy' (ICP-OES). Verder werd ook de totale hoeveelheid organisch koolstof gemeten aan de hand van 'Elemental Analysis – Isotope Ratio Mass Spectrometry' (EA-IRMS). Deze observaties (authigene palygorskiet en dolomiet) worden samengebracht in een deponitioneel model voor de lacustriene facies, dat gekenmerkt wordt door een evaporitische en ariede omgeving. De fluviatiele facies bestaat uit drie verschillende lithologiën (massieve mergels, tabulaire zandstenen en polygenetische conglomeraten) en leidt vaak tot horizontale en verticale reservoir-eenheden die met elkaar verbonden zijn. Deze reservoir-eenheden worden gekenmerkt door een porositeit tussen 5.6 en 14.9 % en een permeabiliteit van 0.04 tot 142 mD. Om meer informatie te vergaren over de grootte van de verschillende keien, werd een korrelgrootte analyse uitgevoerd. De debris-flow facies bestaat uit monogenetische breccias en wordt gekenmerkt door een verschillend afzettingsmilieu van de fluviatiele facies. In vergelijking met de fluviatiele facies, werden deze sedimenten gedurende de depositie gedomineerd door zwaartekracht gerelateerde processen. Het vierde sedimentaire facies, geclassificeerd als het gastropode-rijke carbonaat facies, wordt gekenmerkt door geïsoleerde poriën en kan geobserveerd worden in de nabijheid van de verschillende travertijn lichamen en de lacustriene facies. De coquina facies werd voornamelijk beschreven op het terrein. Slechts een beperkte petrografische studie kon uitgevoerd worden, gezien staalname ten gevolge van de geringe lithificatiegraad van dit sediment bijna onmogelijk was.

Uit deze studie kan worden besloten dat in de nabijheid van de travertijn koepel, in de Ballik regio, vijf verschillende sedimentaire facies aanwezig zijn. Elke van deze facies wordt gekenmerkt door een uniek afzettingsmilieu met specifieke afzettingscondities. De vergaarde kennis, over deze detritische afzettingen, zal er toe leiden dat het grootschalige afzettingsmilieu van de continentale carbonaat analogen beter wordt begrepen.

Glossary

cf.: *Confer (compare).*

CL: *Cathodoluminescence.*

Coquina: *Sedimentary rock dominantly made of transported or mechanically-sorted shell fragments.*

CP: *Crossed polars.*

Detrital particles: *particles that consist of lithic fragments (particles of recognisable rock) or of monomineralic fragments (mineral grains). The latter are transported through sedimentary processes.*

e.g.: *Example gratia (for example).*

Effective porosity: *All open pores, through which a medium can flow. The total porosity minus the closed porosity (e.g. isolated pores in the gastropod facies).*

Extracellular Polymeric Substances

(EPS): *Molecular compounds secreted by microorganisms into their environment.*

Facies association: *Group of sedimentary facies that are characteristic for a general depositional environment (e.g. all facies occurring in the distal part of an alluvial fan).*

Facies: *Distinctive rock (e.g. grain size, fossil content ...) unit forming within a specific depositional environment.*

Geobody: *Volumetric unit made of sedimentary deposits.*

Lamination: *Alternation of fine layers, characterised by, for example, a different colour, grain size ... (e.g. laminated marl lithotype).*

Lithotype: *A sedimentary deposit, described by its characteristics in the field (e.g. laminated marls).*

Marl: *Calcium carbonate rich mudstone, containing variable amounts of clays and silt.*

Monogenetic: *Having only one specific origin (e.g. monogenetic conglomerates composed solely of travertine clasts).*

Polygenetic: *Having more than one origin (e.g. polygenetic conglomerates composed of different clast types).*

PP: *Parallel polars.*

Sequence: *Sequence of rocks arranged in chronological order (during this research a sequence refers to a relative continuous deposit of detrital sediments).*

Table of contents

| | |
|--|------------|
| Preface | I |
| Abstract | III |
| Samenvatting | V |
| Glossary | VII |
| Table of contents | IX |
| Chapter 1 Introduction | 1 |
| Chapter 2 Setting of the Ballık travertines | 3 |
| 2.1 Geographical setting | 3 |
| 2.2 Geological evolution of the region | 4 |
| 2.3 Geological structure of the region..... | 5 |
| 2.4 Formations of the Ballık area..... | 8 |
| 2.4.1 Menderes Massif..... | 8 |
| 2.4.2 Lycian nappes: Lycian mélange and the Lycian metaclastics and metacarbonates – Early Eocene | 9 |
| 2.4.3 Denizli molasses – Oligocene to Miocene | 9 |
| 2.4.4 Denizli/Belevi group – Neogene | 10 |
| 2.4.5 Depositional evolution during the Neogene | 13 |
| 2.4.6 Quaternary evolution..... | 13 |
| Chapter 3 Methodology | 15 |
| 3.1 Field work | 15 |
| 3.2 Petrography | 15 |
| 3.2.1 Thin section scans | 15 |
| 3.2.2 Optical microscopy..... | 16 |
| 3.2.3 Fluorescence microscopy..... | 16 |
| 3.2.4 Cold Cathodoluminescence (CL)..... | 16 |
| 3.2.5 Scanning Electron Microscopy (SEM) | 16 |
| 3.3 Computed Tomography (CT) | 17 |
| 3.4 Bulk X-Ray Powder Diffraction (XRD) | 17 |
| 3.4.1 Sample preparation..... | 17 |
| 3.4.2 XRD measurement..... | 18 |
| 3.4.3 XRD analysis with Quanta..... | 18 |
| 3.5 X-Ray Diffraction on oriented clay slides (XRD) | 19 |
| 3.5.1 Sample selection..... | 19 |
| 3.5.2 Jackson treatment..... | 19 |

| | | |
|--------------------------------|--|-----------|
| 3.5.3 | XRD measurement | 19 |
| 3.5.4 | XRD analysis | 20 |
| 3.6 | Elemental Analysis – Isotope Ratio Mass Spectrometry (EA - IRMS) | 20 |
| 3.6.1 | Sample selection | 20 |
| 3.6.2 | Sample preparation..... | 21 |
| 3.6.3 | Sample measurement..... | 21 |
| 3.7 | Carbonate content | 21 |
| 3.8 | Grain size analysis..... | 22 |
| 3.9 | Inductively Coupled Plasma Optical Emission Spectrometry (ICP-OES)..... | 22 |
| 3.9.1 | Four acid digestion method..... | 23 |
| 3.9.2 | Reference samples | 23 |
| 3.9.3 | Detection limit | 24 |
| 3.10 | SketchUp Pro..... | 24 |
| 3.11 | Petrophysical characterisation | 25 |
| 3.11.1 | Specific gas permeability | 25 |
| 3.11.2 | Helium porosimetry | 26 |
| 3.11.3 | Porosity estimations through image analysis | 26 |
| Chapter 4 Results | | 27 |
| 4.1 | Lithology description | 27 |
| 4.1.1 | Sedimentary architecture | 27 |
| 4.1.2 | Marls..... | 28 |
| 4.1.3 | Polygenetic conglomerates & tabular sandstones..... | 30 |
| 4.1.4 | Monogenetic breccias | 33 |
| 4.1.5 | Gastropod-rich carbonate | 34 |
| 4.1.6 | Coquina | 36 |
| 4.2 | Petrography | 37 |
| 4.2.1 | Laminated marls | 37 |
| 4.2.2 | Polygenetic conglomerates | 42 |
| 4.2.3 | Monogenetic breccias | 45 |
| 4.2.4 | Gastropod-rich carbonate | 46 |
| 4.2.5 | Coquina | 47 |
| 4.2.6 | Computed Tomography (CT) | 48 |
| 4.3 | X-Ray Diffraction (XRD)..... | 52 |
| 4.3.1 | Bulk XRD: Overall mineralogical composition. | 52 |
| 4.3.2 | Bulk XRD: Specific mineralogical composition of individual laminae within the laminated marls..... | 53 |
| 4.3.3 | Clay-specific XRD: Laminated marls..... | 54 |
| 4.3.4 | Clay-specific XRD: Argillaceous travertine (Bouman, 2016)..... | 55 |

| | | |
|--|--|------------|
| 4.4 | Total Organic Carbon (TOC) | 55 |
| 4.5 | Carbonate content..... | 56 |
| 4.6 | Grain size analysis | 57 |
| 4.7 | Geochemical trace and major element analysis | 58 |
| 4.7.1 | Detection limit | 58 |
| 4.7.2 | Results..... | 58 |
| 4.8 | SketchUp Pro..... | 60 |
| 4.9 | Reservoir characteristics | 61 |
| 4.9.1 | Specific gas permeability and helium porosimetry | 61 |
| 4.9.2 | Image analysis | 62 |
| Chapter 5 Discussion | | 65 |
| 5.1 | Facies classification | 65 |
| 5.1.1 | Lacustrine facies | 65 |
| 5.1.2 | Fluvial facies | 74 |
| 5.1.3 | Debris-flow facies..... | 76 |
| 5.1.4 | Gastropod facies..... | 78 |
| 5.1.5 | Coquina facies | 78 |
| 5.2 | Reservoir characteristics | 79 |
| 5.2.1 | Lacustrine facies | 79 |
| 5.2.2 | Fluvial facies | 80 |
| 5.2.3 | Debris-flow facies..... | 81 |
| 5.2.4 | Gastropod facies..... | 81 |
| 5.2.5 | Coquina facies | 81 |
| 5.2.6 | Summary | 81 |
| Chapter 6 Conclusion..... | | 83 |
| Chapter 7 Future research | | 85 |
| 7.1 | Petrophysical assessment..... | 85 |
| 7.2 | Mapping of the broader region | 85 |
| 7.3 | Lacustrine facies | 85 |
| 7.4 | Provenance analysis | 86 |
| 7.5 | Sequence stratigraphy | 86 |
| 7.6 | Clay-analysis..... | 86 |
| Bibliography | | 87 |
| Appendices | | 93 |
| Appendix A – Field report..... | | 95 |
| Appendix B – ID-charts for detrital facies in the Ballık area | | 117 |
| Appendix C – Jackson treatment..... | | 123 |

| | |
|--|------------|
| Appendix D – EA-IRMS procedure..... | 129 |
| Appendix E – Sample list | 135 |
| Appendix F – Bulk XRD diffraction patterns | 139 |
| Appendix G – Bulk XRD diffraction patterns: Laminae | 143 |
| Appendix H – XRD diffraction patterns oriented clay slides..... | 147 |
| Appendix I – ICP-OES results | 151 |
| Appendix J – Porosity and permeability measurements..... | 155 |

Chapter 1

Introduction

In 2006 a new oil-play was discovered in the deep-offshore of the Brazilian coast, leading to the discovery of the largest hydrocarbon field of the last 40 years (Galpenergia, 2015). This reservoir might contain 8 – 12 billion barrels of recoverable oil, with a possible peak production reaching 2.1 – 3.5 million barrels per day (The Economist, 2011). The explorative well indicated that the reservoir is made of continental carbonates, lacustrine carbonates and detrital deposits. Prior to this discovery there was nearly no interest in this type of carbonates, however, after 2006 this changed drastically.



Figure 1.1: Location of the Lula oil field in the Pre-Salt area (after The Economist, 2011).

This discovery led to the formation of a research team at KU Leuven, which was dedicated to studying the properties of continental carbonate analogues. Until now, this team focused mainly on the carbonate lithologies in, for example, the Denizli Basin in Turkey (Soete, 2011 & Claes, 2011), in Rapolano Terme & Trivoli in Italy (Honlet, 2013 & Janssens, 2015) or in Sütto in Hungary (Claes & Török, 2016). Since it is unlikely that the true reservoir consists purely of continental carbonates, it is also important to take into account the non-carbonate lithologies that are closely associated with these travertine deposits. The characteristics of the latter were assessed in this study as well as their petrophysical properties.

The presented study took place in the Ballık area, which is well-known for its world-class travertine deposits. The area is located near the city of Denizli, in Turkey. All detrital deposits that were encasing the travertine dome and that were spread over an area of 5 km by 1 km, were studied in this research. This study thus presents additional information towards the existing analogue model of the continental carbonates in the Ballık area, which is important in order to assess the complexity and the variability of the detrital deposits, encasing a travertine deposit.

Chapter 1 - Introduction

This study thus aimed to characterise all the detrital facies, encasing the continental carbonate deposits, associated with their petrophysical properties. In the end, for each of these facies a depositional model was proposed, in order to clarify the processes that lead to the deposition of these sediments. Furthermore, the geochemical and mineralogical composition of these detrital deposits were evaluated, in order to verify whether they could be used to identify specific detrital sequences. To achieve these goals, a multidisciplinary approach was used. This integrated the field observations, petrography (conventional microscopy and SEM), petrophysics, geochemistry, XRD-analyses & grain size analysis in order to deal with the four objectives defined in this research.

Chapter 2

Setting of the Ballık travertines

This chapter contains a brief overview of the geographical and geological setting of the studied analogue.

2.1 Geographical setting

The area, studied in the framework of this thesis, is located just east of Denizli. This city is the capital of the Denizli province, located within the Aegean region in the south-west of Turkey. Denizli is located 175 kilometre in the north-west of Antalya, 180 kilometre in the east of Izmir and 400 kilometre in the south-west of Ankara. The approximate location of the Denizli municipality can be seen in Figure 2.1.



Figure 2.1: Geographical location of the Denizli municipality.

Since the emphasis of this thesis lied in understanding the interaction between the travertine-dome and detrital interlayers, several quarries were studied. These quarries are known as Alimoglu-Tasarim, Basaranlar, Cakmak, Cinkaya, Ece, Faber, Faber-West, Metamar (abandoned) and Siray. All of these quarries are located in the lower domal area, as described by Soete (2011). The approximate location of all quarries can be seen in Figure 2.2. These quarries are located about 25 kilometres in the east of Denizli, just north of the city of Honaz.

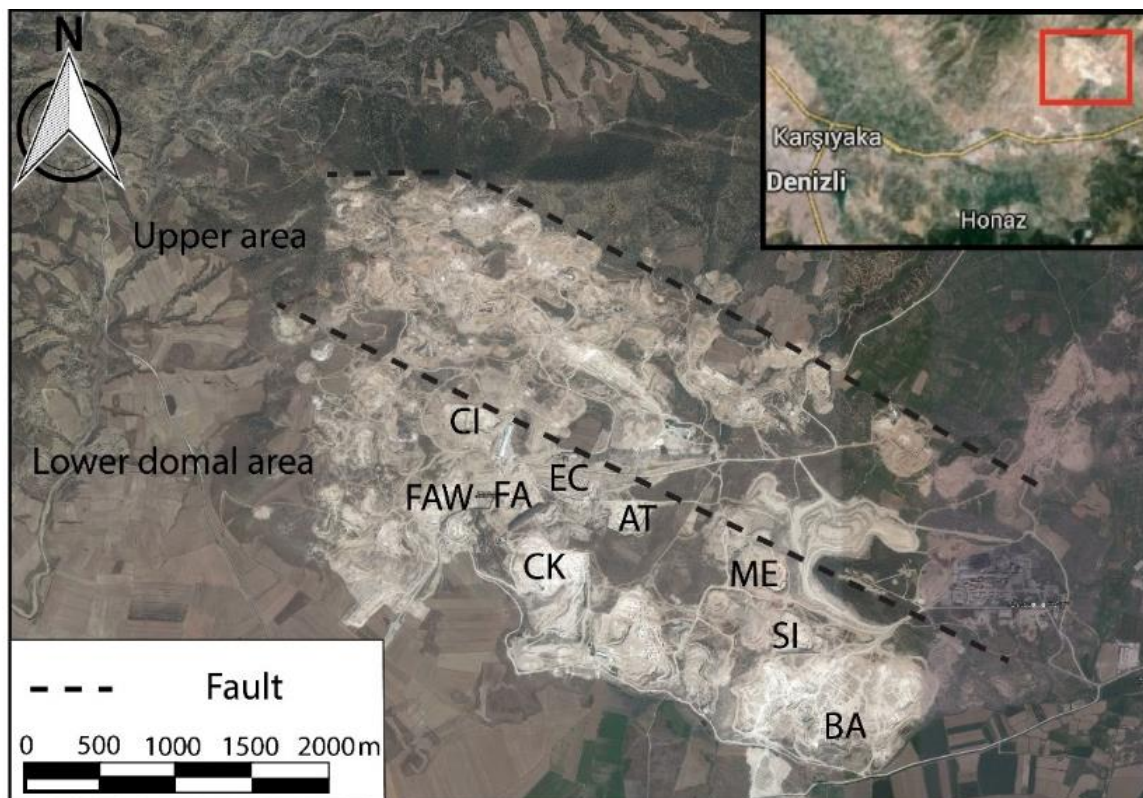


Figure 2.2: Location of the studied quarries in the lower domal area (Basaranlar, BA; Cakmak, CK; Cinkaye, CI; ECE, EC; Faber, FA; Faber West, FAW; Metamar, ME and Siray, SI).

2.2 Geological evolution of the region

The region of Western Turkey is located in the Alpine-Himalayan orogenic belt, at the collisional boundary between Gondwana and Laurasia. The paleogeological setting of this region is thus characterised by the closure of several Mesozoic-Cenozoic Neo-Tethyan oceanic basins, followed by continental collision and post-orogenic processes (Dilek & Pavlides, 2006; Taymaz et al., 2007).

During the Triassic, these oceanic branches of the Neo-Thethys started to open, while as they closed during the Late Cretaceous to Eocene. This closure lead to the development of several suture zones (e.g. Vardar, Bitlis-Zagros ...) and ophiolites/mélanges in the Jurassic-Cretaceous period (Erdogan & Güngör, 2002; Taymaz et al., 2007). This evolution can be seen in the cross-sections in Figure 2.3, where the formation of oceanic branches is visualised. This formation is followed by an obduction in the Late Cretaceous leading to the metamorphic transformation of the Menderes massif (Erdogan & Güngör, 2002).

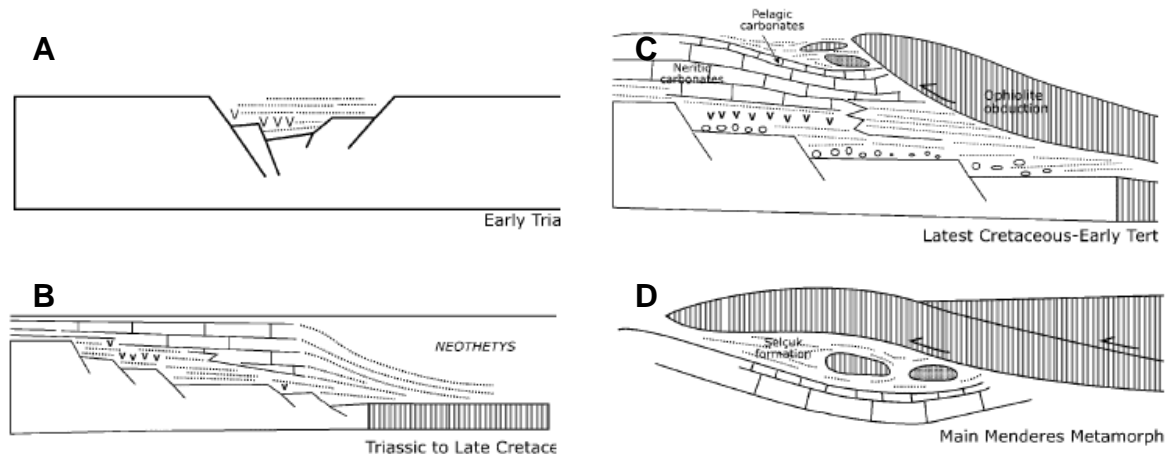


Figure 2.3: Conceptual cross-sections of the evolution of the study area during the Early Triassic to the Early Tertiary. A & B – Visualisation of the opening of the oceanic branches. C & D – Obduction taking place during the Late Cretaceous, followed by the formation of the Menderes Massif (after Erdoğan & Güngör, 2002).

The closure of these oceanic basins also resulted in crustal thickening, followed by a phase of post-orogenic extension in the Aegean extensional province. This region is characterised by a NNE-SSW oriented extension since the latest Oligocene to Early Miocene (Dilek & Pavlides, 2006; Taymaz et al., 2007). This continental extension resulted in two different structural styles, of which the first one reflects the rapid exhumation of deep-burial metamorphic rocks (1). These rocks are exposed in the footwall of the low-angle normal faults and express a shift in deformation style from ductile to brittle (due to mylonites which are overprinted by breccias). The second structural style is associated with the formation of grabens (2) along high-angle normal faults of Pliocene-Quaternary age (which is the latest and most recent phase of extension). This extensional phase leads to the exposure of several core-complexes (as for example the Menderes Massif) and the east-west trending grabens (Taymaz et al., 2007).

2.3 Geological structure of the region

The study area is located in the Denizli Basin, which currently is an asymmetric WNW-ESE graben with a length of about 50 km and a width of 20 km. The basin itself is bounded by major escarpments, which are interpreted to correspond to footwalls of a succession of normal faults. These faults formed in order to accommodate the N-S extensional forces (Westaway et al., 2012). In Figure 2.4 a general geological map of Western Turkey can be seen, on which it is clear that the broader region of south-western Turkey is characterised by the presence of several fault-systems and ophiolite-complexes. A more detailed map can be seen in Figure 2.5.

Chapter 2 – Setting of the Ballık travertines

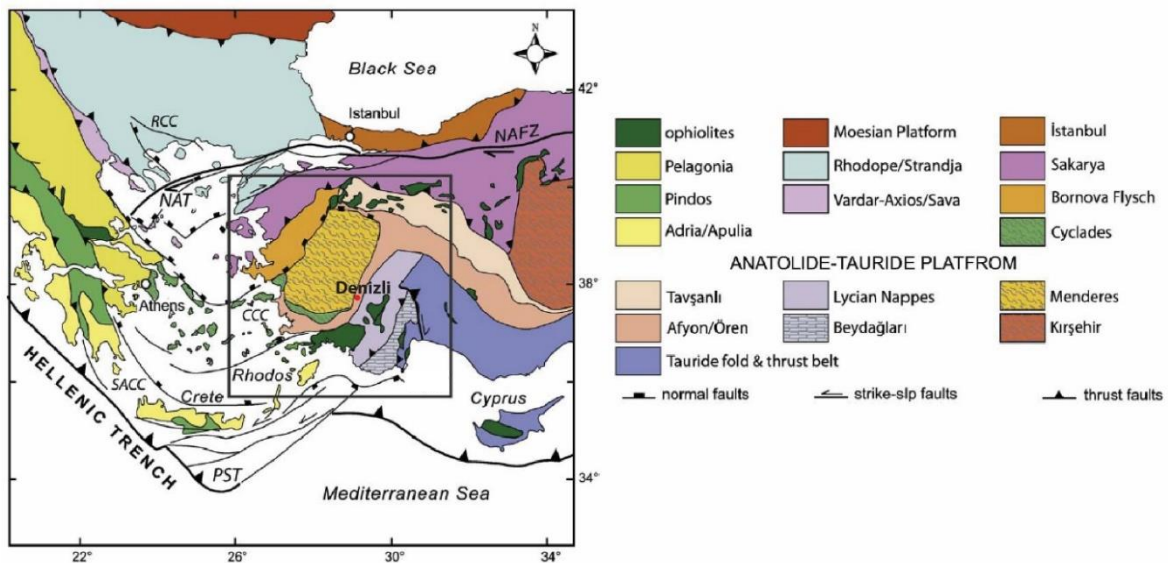


Figure 2.4: Geological map of western Turkey with all the major terranes. NAFZ = North Anatolian Fault Zone; NAT = North Anatolian Trough; PST = Pliny & Strabo Trenches; CCC = Cycladic core-complex; RCC = Rhodope core-complex (modified after Hinsbergen et al. 2010).

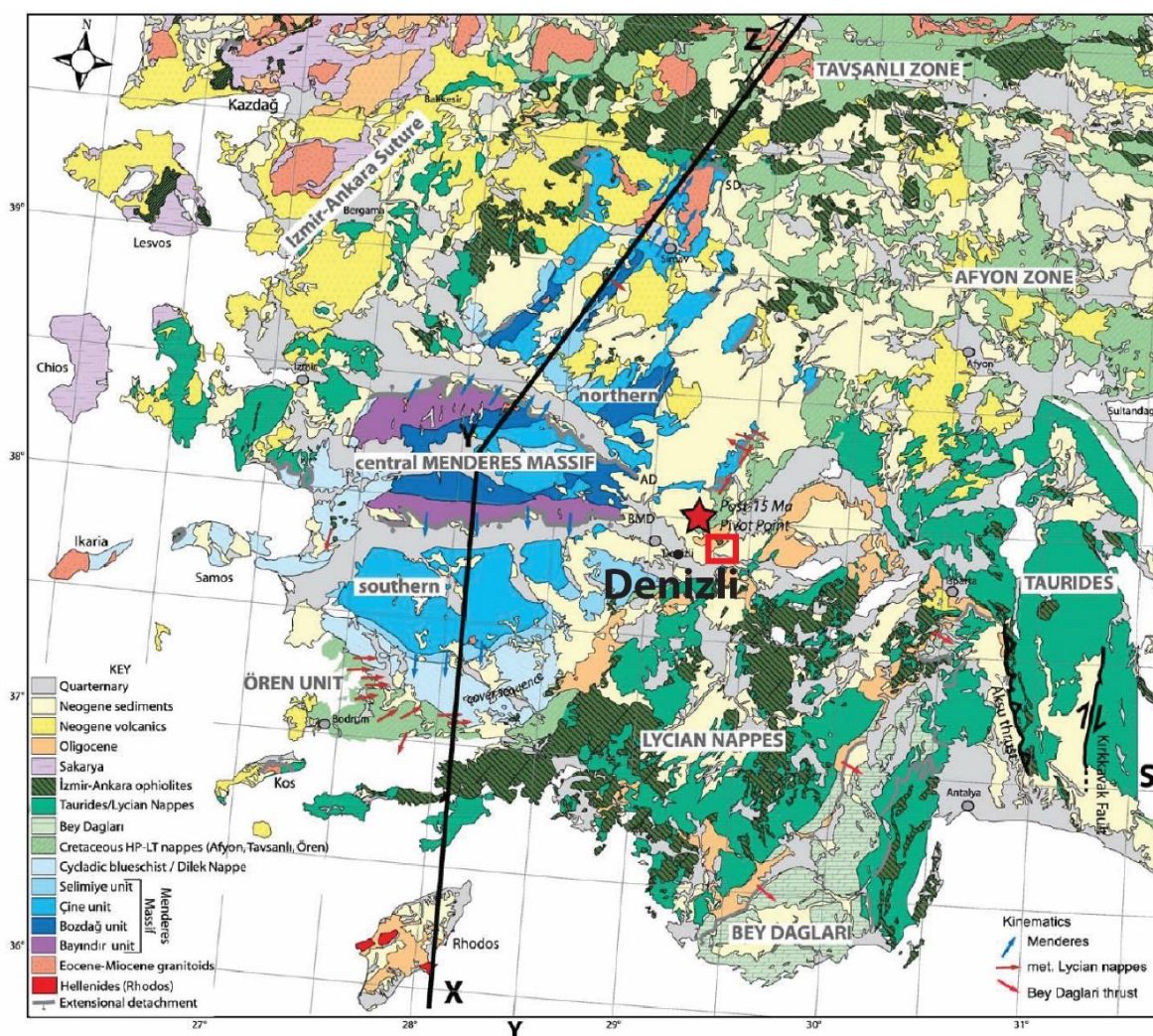


Figure 2.5: Detailed geological map with the major geological features near the city of Denizli and the study-area (red square, modified after Hinsbergen et al. 2010).

Chapter 2 – Setting of the Ballık travertines

As can be seen in Figure 2.5, the region of Denizli is made of 4 major geological units. The oldest one is the Menderes Massif (1), which can be found mainly in the north and east of the study area (Hinsbergen et al., 2010). The Lycian nappes can be divided in two sub-units, the first one being the Lycian mélangé (2) and the second one the metaclastic and metacarbonate rocks (3). These three units are covered by more recent deposits (4), which will be addressed in more detail in the upcoming section. A simplified geological map near the study area can be seen in Figure 2.6.

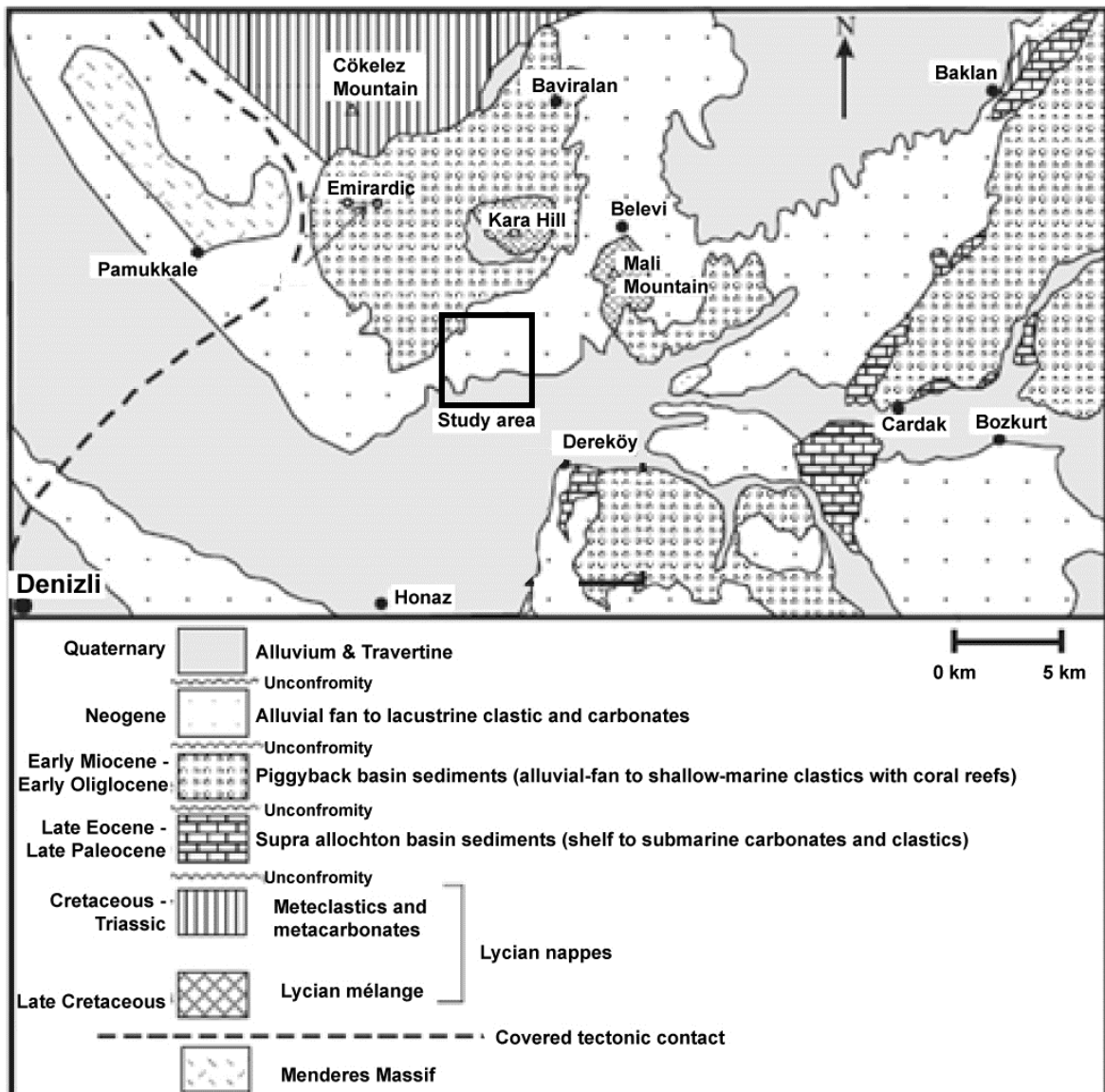


Figure 2.6: Simplified geological map of the study area (black square, modified after Sözbilir, 2002).

2.4 Formations of the Ballık area

The different formations that are present within the study area are visualized in Figure 2.7. The latter, and the facies association in which they are divided, are described based upon literature in this section.

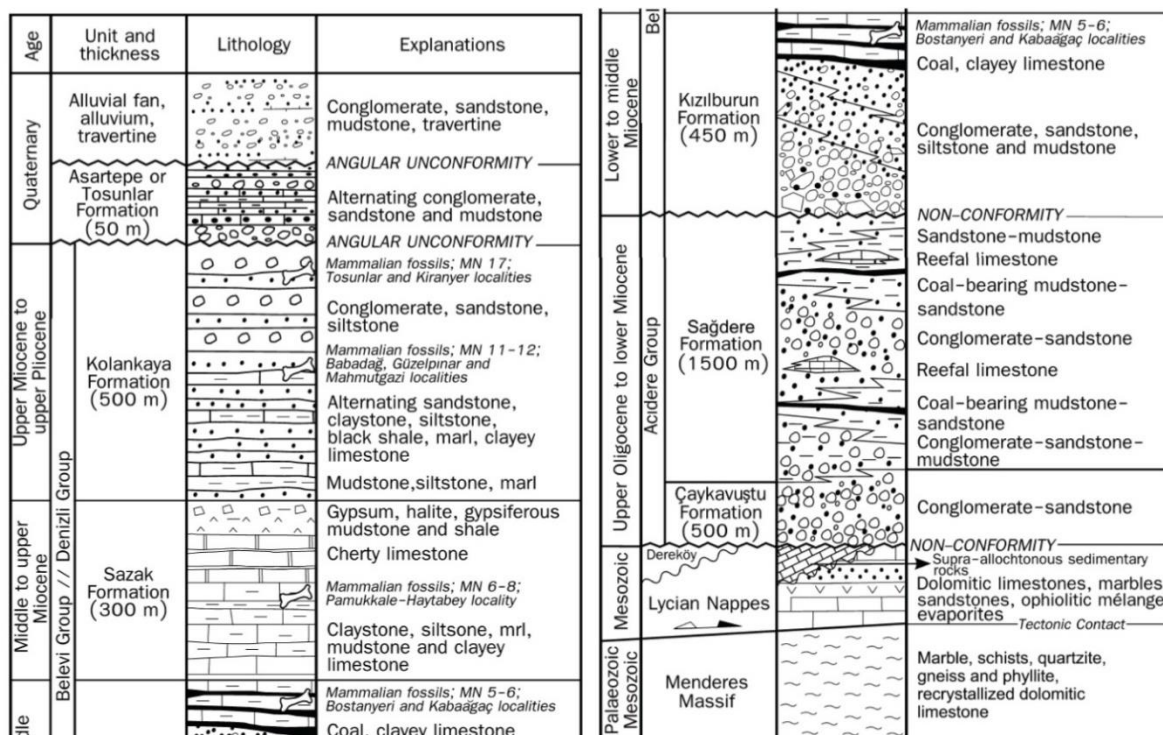


Figure 2.7: Unscaled lithostratigraphic section of the Denizli basin (after Alçiçek et al., 2007).

2.4.1 Menderes Massif

Sozbilir (2002) described the outcrops of the Menderes Massif just north of Pamukkale as an alternation of metaquartzite, mica schists and kyanite-chloritoïd schists. In the broader region the Menderes Massif has undergone a Barrovian-type of metamorphism. The three uppermost formations of the Menderes Massif in this region correspond to the Pinarlar Formation, the Yılanlı Formation and the Zeybekölen Formation (Okay, 1989).

2.4.1.1 Pinarlar Formation – Permian to Carboniferous

This formation dominantly consists of slightly metamorphosed quartzites. The colours of these quartzites are ranging from pink to bluish-grey. Next to these quartzites fine to medium red sandstone occurs, together with red to greenish shales and yellowish-white dolomite. Within this formation the presence of foraminifera of the fusulinada family is also a remarkable characteristic (Okay, 1989).

Chapter 2 – Setting of the Ballık travertines

2.4.1.2 *Yılanlı Formation - Mesozoic*

The Yılanlı Formation consists of light grey carbonate rocks, enriched in gastropods. A typical feature of these neritic carbonate rocks at the edge of the Mendere Massif (near Denizli) are the bauxite horizons within the carbonates (Okay, 1989).

2.4.1.3 *Zeybekölen Tepe Formation*

This formation consists of slightly metamorphosed light grey to red limestones with chert nodules. The latter can have a thickness of up to 2-3 cm (Okay, 1989).

2.4.2 Lycian nappes: Lycian *mélange* and the Lycian metaclastics and metacarbonates – Early Eocene

The timing of the emplacement of the Lycian nappes is considered to be Early Eocene and they can be divided in two sub-units (Okay, 1989). The Lycian *mélange* is a heterogeneous sequence of blocks of all sizes, which are embedded in a sheared matrix of turbiditic and serpentinitized materials. This formation contains blocks of recrystallized limestones, bauxite-bearing limestones, dolomitic limestones, gabbros and submarine volcanic rocks. This unit is also referred to as the ophiolitic *mélange* (Muechez et al., 2008). In the area of Sagalassos, located 60 km towards the east of the study area, this ophiolitic *mélange* is subdivided in 3 different subunits by Muechez et al. (2008). The first subunit consists of serpentinite rocks (i) and is dominantly made of serpentine and chlorite. The second subunit is a tectonic *mélange* (ii), occurring below the serpentinite unit, which is characterised by blocks (both sedimentary and intrusive) embedded in a green-greyish matrix of extrusive rocks, serpentine and deep-sea sediments. The last subunit consists of volcanic and sedimentary rocks (iii), being limestone, radiolarite, sandstone, serpentinite, gabbroid rocks and volcanics (Muechez et al., 2008).

The second subunit, the Lycian meta-clastics and meta-carbonates (2), is exposed well north of the study-area (west of the Cökölez mountain, Figure 2.6). At the base of the sequence red meta-conglomerates (with (sub-)rounded clasts of quartz, quartzite and carbonates) can be observed. Towards the top, the thickness of these meta-conglomerates decreases and they alternate with metasandstones. The upper part of this sequence consists out of meta-carbonates with thin to medium bedded limestones (Sözbilir, 2002).

2.4.3 Denizli molasses – Oligocene to Miocene

According to Akgün & Sözbilir (2001) the Denizli basin is characterised by a transgressive sequence, which is unconformably overlying the pre-Oligocene basement rocks. The

landward margins of this molasse sequence is fault-controlled. The sequence starts with alluvial fan deposits but transforms into fan delta to shallow marine deposits on top. This sequence is known as the Acidere group and can be subdivided in several formations.

2.4.3.1 *Caykavustu Formation – Chatian*

The basal part of the Acidere group, which consists of reddish-brown conglomerates intercalated with lithic sandstones, is the Caykavustu Formation (Akgün & Sözbilir, 2001).

2.4.3.2 *Sagdere Formation – Chattian to Aquitanian*

The Sagdere Formation is characterised by a deltaic-marine sequence, in which reef carbonates and coal lenses can be observed. Additionally, this formation consists of massive to planar cross-bedded and wave-rippled sandstones, bioturbated and fossiliferous mudstones and alterations of sand- and mudstone. These coal lenses formed on the delta plain (terrestrial part of the fan-delta), while the patch reefs can be observed as individual lenses on the delta-front slope (Akgün & Sözbilir, 2001).

2.4.4 Denizli/Belevi group – Neogene

The deposits of the Denizli group are resting unconformably on the older deposits from the Sagdere Formation.

2.4.4.1 *Kizilburun Formation – FA1 proximal to medial alluvial fan deposits*

The lower part of the Kizilburun Formation (*FA1*) consists of proximal to medial alluvial fan deposits. The thickness of this part increases towards the fault at the margin of the basin and has a limited basinwards extension, indicating the close association with the proximity of the margin-fault. This association is characterised by tabular-bedded, amalgamated conglomerates. These deposits are interpreted to be deposited in a braided river system, in which the gravel-rich deposits are associated with flash floods in ephemeral streams (Alçiçek et al., 2007).

2.4.4.2 *Kizilburun Formation – FA2 distal alluvial-fan deposits*

The more distal equivalent of the Kizilburun Formation is made of reddish to yellowish, planar cross-stratified sandstones, ripple cross-laminated sandstones, parallel-laminated sandstones and horizontally stratified sandstones. Additionally, finer sediments can be observed as laminated to massive mudstones together with ostracod- and gastropod-bearing limestones and coal beds. These deposits are interpreted to be distal fan and fluvial sandflat deposits, in which the sandstone beds represent channel belts and crevasses splays. The mudstone, coal beds and clayey-limestone are interpreted to be floodplain deposits or infill in an oxbow lake. The deposition of these deposits is

associated with an increased inundation of the floodplain (e.g. due to a rising lake or ground water level). The surfaces underlying these coal-lenses are also interpreted to be maximum flooding surfaces (Alçiçek et al., 2007).

2.4.4.3 Sazak Formation – FA3 marginal lake deposits

At the lower part of the Sazak Formation this facies association occurs as horizontally stratified sandstones, laminated marls, organic-rich mudstones bioclastic and clay-rich limestones. This association is laterally continuous over several hundreds of m and lies directly on the distal alluvial-fan deposits of FA2. These deposits are characteristic for carbonate lakes and are associated with water-level fluctuations. The clayey limestones and laminated marls would in that case be deposited during episodes of a high Ca^{2+} -supply from the source area and a significant influx of fresh water in the lake area. The organic-rich mudstones indicate that these lakes underwent a (temperature) stratification at a local scale, leading to dys- or anoxic conditions (Alçiçek et al., 2007).

2.4.4.4 Sazak Formation – FA4 shallow lacustrine deposits

This facies association consists of cherty limestone and is well developed near the southern and northern margin of the basin. The precipitation of these limestones could be triggered by an abrupt lowering of alkalinity (e.g. due to inflow of groundwater with a low pH) (Alçiçek et al., 2007).

2.4.4.5 Sazak Formation – FA5 saline lake deposits

The last facies association of the Sazak Formation consists of saline lake centre and margin/mudflat deposits. The sediments, which were deposited in the centre of the lake, consists of an alteration of gypsarenite, selenite, diatomite-bearing gypsiferous halite and organic-rich mudstones. The sediments, which were deposited near the margin of the lake, consists of gypsiferous mudstones and white shales. The selenite gypsum is interpreted to reflect deposition at the sediment-brine interface in shallow waters. These conditions could be reached in restricted environments as for example marginal ponds. Several mechanisms are proposed for the formation of the gypsarenites. The first one would be reworking of selenite gypsum due to waves and the second one would be that gypsum grains form at the water surface which settle afterwards (Alçiçek et al., 2007).

2.4.4.6 Kolankaya Formation – FA6 shallow lake deposits

This association occurs at the margins of the basin and has a lateral continuity of several hundreds of m. The lithology mainly consists of laminated mudstones with an intercalation of thinly laminated marl facies. The laminated aspect of these deposits is an indicator for

a rather calm depositional environment, dominated by suspension fallout, characteristic for lake-sedimentation (Alçıçek et al., 2007).

2.4.4.7 Kolankaya Formation – FA7 deep lake deposits

This facies association consists of diatomite-bearing laminated marls, laminated claystones, black shales, clayey limestones and massive sandstones. This association contains fossils of brackish water molluscs and ostracods. The clayey limestones are interpreted to be deposited during a fast lake-level rise (limiting the deposition of clastic sediments to the margins of the lake). The laminated marls represent a low-energy environment, with clay suspension fallout (deep lake deposits), while as the massive sandstones are interpreted to be sheet floods (margin deposits) (Alçıçek et al., 2007).

2.4.4.8 Kolankaya Formation – FA8 lake shoreface deposits

The lake shoreface deposits consist of planar cross-stratified pebbly sandstones, horizontally stratified sandstones and ripple cross-laminated sandstones. All of these lithologies are also characterised by fresh water molluscs and ostracods and commonly coarsen upwards. The depositional environment is placed near the lake-shoreface (which extends mainly above the fair-weather wave base). The coarsening upwards trend is associated with shoreline progradation (Alçıçek et al., 2007).

2.4.4.9 Kolankaya Formation – FA9 lake foreshore deposits

This facies association is made of well-sorted, planar cross-stratified conglomerates intercalated with planar cross-stratified pebbly sandstones and ripple cross-laminated sandstones. These conglomeratic beds represent a lake shoreline, while as the pebbly sandstones are associated with a low-energy beach (shoreface) setting. Just as FA8 this association is also characterised by fresh water molluscs and ostracods (Alçıçek et al., 2007).

2.4.4.10 Kolankaya Formation – FA10 alluvial-fan facies

The last facies association, that is part of the Kolankaya Formation, consists of matrix- and clast-supported conglomerates, planar cross-stratified conglomerates inter-bedded with planar cross-stratified and horizontally stratified sandstones. The strata are interpreted as braided-stream channels in the medial part of the alluvial fans. The matrix-supported conglomerates, however, are interpreted as cohesive debris-flows. The thickness of these deposits increases towards the margin-faults, due to proximity towards the apex of the alluvial fans (Alçıçek et al., 2007).

2.4.5 Depositional evolution during the Neogene

In the early Miocene, the Denizli basin subsided with the depocenter located in the southern margin. This led to the formation of alluvial fans, making up the Kizilburun formation. The proximal facies (*FA1*) gradually evolves into the more distal facies (*FA2*). Based on isotopic data it can be deduced that precipitation was abundant, leading to the development of dense forests with an anastomosed fluvial system and rather small lakes. Within these lakes, located in paleolows, algal controlled carbonate production was possible.

During the initial phase of the Middle Miocene, the lake level continued to rise, leading to a broader deposition of lake carbonates. Rhythmic alterations between organic-rich mudstones, marls and clayey limestones, suggest that during the deposition of organic-rich intervals the lake was relatively deep. This led to the stratification of the lake system, creating dys- or anoxic conditions in the bottom part of the lake.

The lake gradually became more alkaline, leading to the deposition of sulphur-bearing cherty limestones (*FA4*). According to Alçiçek et al (2007) this alkaline-enrichment was closely associated with the influx of calcium from the drainage basin.

At the end of the middle Miocene to the beginning of the late Miocene, the alkaline lake gradually became enriched in sulphates. Associated with a decreasing lake level was the deposition of sulphate bearing sediments. The main controlling conditions leading to these evaporitic conditions were climatic and tectonic in origin. Climatologically a transition from a semi-arid to an arid climate occurs, this led to the formation of an evaporitic trap in combination with several faults.

During the late Miocene this saline lake, became gradually more brackish in composition, most likely due to a shift from an arid to a humid climate. During the Pliocene the lake became gradually a fresh water lake. During this period the lake margins became an area of shifting alluvial fans, beach and shore face settings (Alçiçek et al., 2007).

2.4.6 Quaternary evolution

The subsidence of the Denizli basin decreased significantly after the late Pliocene, leading to the current-day fluvial dominated basin. During the Quaternary the Tosunlar Formation was deposited, which is covered by the most recent siliciclastic and travertine deposits (Alçiçek et al., 2007). The massive travertine deposition was dated to have a minimum age of 1.1 Ma and a maximum age of 1.78 Ma (Claes et al., 2015).

Chapter 3

Methodology

In this chapter the aim of each method is presented, together with a brief description of the method itself.

3.1 Field work

In the framework of this thesis a field trip was organized which took place from the August 25th till September 7th 2015 . On the consolidated lithologies, sampling was performed by drilling horizontally oriented plugs. The unconsolidated lithologies were sampled either as blocks, which could be studied as thin sections after impregnation, or as loose clasts in the case of the conglomerates. A detailed description of these field observations can be found in Appendix A – Field Report.

3.2 Petrography

Since the emphasis of this thesis also lied in describing each sequence with their specific lithological characteristics, a petrographical study of the samples was necessary. With the use of petrography the knowledge of the different cement-, pore- and fabric types could be deduced. This could then be combined with the petrophysical data, in order to verify whether a relationship exists between the petrophysical data and the petrographical observations. In total 34 thin sections were made from samples taken at different locations, of which the exact location can be found in Appendix E – Sample list. All thin sections have been impregnated by a fluorescent resin, partly due to the rather unconsolidated state of several samples, but also to facilitate the study of porosity distribution.

3.2.1 Thin section scans

In order to have a broader view of the sedimentological structures, that could be observed within each thin section, the latter were scanned in advance. These scans were completed with an EPSON transmitting light scanner at a resolution of 1200 dpi. From each thin section a parallel polars (PP) and crossed polars (XP) scan was taken with the use of polarizing papers.

3.2.2 Optical microscopy

The goal of this approach was to acquire a detailed insight in the characteristics of laminations in the laminated marls and the distribution of porosity within each facies. Additionally, the cement types and the angularity of the grains were also accessed through petrographical analyses.

During the petrographical study a microscope of the type Olympus BX41 was used, with a magnification ranging from 50 – 100 – 200 – 500 times. A computer, connected to a camera that was mounted on a Leica DM LP microscope, was used in combination with the Deltapix software in order to capture striking sedimentological features. Afterwards a scale was added to these pictures by the computer program of AxioVision.

3.2.3 Fluorescence microscopy (FL)

For the fluorescent light microscopy a microscope of the type Olympus BX41 was used, with a magnification ranging from 50 to 500. In order to achieve fluorescent light a source of the brand Leica (of the 12V/100W-type) was connected to the microscope. In combination with this light source a BP450-490/LP515 filter was used.

This technique can be a useful tool to observe microporosity within the matrix of the rock samples, highlighting poorly-cemented zones. Additionally, this technique also allowed the observation of intercrystalline porosity, which can often be observed within the fractures that were present throughout the samples.

3.2.4 Cold Cathodoluminescence (CL)

Cathodoluminescence is a widely applied technique in the study of carbonate rocks and their diagenetic history. It can be used to highlight certain features (due to a changing chemical composition), which are invisible by conventional microscopy. In the framework of this thesis, cathodoluminescence was used in order to obtain more information on certain cement phases (visible in pores and fractures) and to differentiate dolomite clasts from clasts made of calcite. The device that has been used is a modified Techosyn Model 8200 Mark II.

3.2.5 Scanning Electron Microscopy (SEM)

Scanning Electron Microscopy, also known as SEM, is a widely used tool in the petrographical study of geological samples. It was opted to use SEM pictures in the framework of this thesis, in order to (semi-)quantify the presence and abundance of authigenic and detrital chlorites. Furthermore, it would also allow to study the distribution of specific clay-minerals.

The basic concept behind this technique is the collision of a highly-accelerated electron beam with the atoms of the studied sample, taking place under high vacuum conditions. Due to this interaction, several electronic signals are generated (ranging from secondary electrons to backscattered electrons and to characteristic XRD). It are these signals that are used by the SEM in order to create an image of the studied sample (García-Veigas et al., 2012). In total 6 different rock samples of the lacustrine facies were selected and prepared for SEM study. The samples were coated three times (120 seconds, 90 seconds and 60 seconds), in order to achieve a good gold-coating of the sample.

3.3 Computed Tomography (CT)

X-ray computed tomography has proven to be a very powerful tool to characterise different rock properties, as for example porosity, density, depositional patterns, etc. (Jacobs & Cnudde, 2009). Since it was rather difficult to sample large cores, often due to the unconsolidated nature of the samples, CT-scans were acquired from hand samples. The main goal was to increase the knowledge of the internal stacking pattern in several conglomerates. The medical computed tomography was performed at the University Hospital of Gasthuisberg in Leuven (Belgium). The device that was used is a Siemens Sensation 64, with a resolution of 230 μm for one slice (X and Y directions) and a spacing of 500 μm between successive slices (Z direction).

3.4 Bulk X-Ray Powder Diffraction (XRD)

Due to the polygenetic composition of the conglomeratic units, they could not be used to differentiate each sequence from one another (based upon their mineralogical composition). That is why the XRD-analysis focused on the laminated marls, in order to verify whether the clay mineralogy differs between the different sequences (Appendix A – Field report). This would make it possible to characterise the different sequences based upon their mineralogical composition.

3.4.1 Sample preparation

At least 20 grams of each sample was taken, in order to end up with an representative sample. This material was pulverized in a porcelain mortar, with the shock-impact technique in order to keep the clay minerals intact. Afterwards, this sample was passed through a 500 μm sieve. Of this sieved fraction 2.7 grams was weighed and 0.3 grams of the internal standard ZnO was added. As a grinding agent 5 mL of ethanol was used and the resulting mass was then micronized for 5 minutes with the use of the McCrone Micronizing Mill, filled with corundum rollers. This in order to obtain a very fine particle size

(<20 μm), leading to an increased accuracy of the measurement. The resulting paste was transferred in a porcelain cup which was covered with plastic foil, in order to enhance recovery after the paste was completely dry.

Once the paste was dry, the powder was transferred to an agate mortar, after which it was passed through a 250 μm sieve. This step is crucial to ensure a homogenous distribution of the internal standard throughout the powder. This powder was then transferred to a sample holder with the use of the side-loading technique, in order to end up with a randomly orientated sample, reducing any preferred orientation.

3.4.2 XRD measurement

The measurements were performed with a PW1050/37 goniometer, that was connected with a PW1830 generator and equipped with a Cu-K α -radiation. The detector was proportional to the detector type PW3011/00 and the diffractometer has a Bragg-Brentano $\theta / 2\theta$ setup (respectively for the source and detector). The EDWIN-2 settings were used (measurement duration: 1h40, step size: 0.02° 2 θ , counting time per step: 2 seconds and range: 5 – 65 °2 θ) in order to measure the bulk-clay compositions of each sample.

3.4.3 XRD analysis with Quanta

The analysis of a XRD pattern is a fast and often applied technique in order to determine the mineralogical composition of sediments. The classical Rietveld-refinement technique is not suitable for the analysis of these samples, due to the abundance of clay minerals (Moore & Reynolds, 1997).

The analytical analysis of clay minerals is complicated due to their chemical and structural properties. Examples of these properties are the varying chemical composition (due to substitution) and the abundance of crystal-lattice defects. All of these aspects give rise to a broad range in intensity for XRD-reflections, making it rather hard to model each of these reflections theoretically (e.g. the Rietveld method) (Srodon et al., 2001 & Dirix, 2010).

Quanta is a program, allowing the quantification of XRD-patterns through a different approach. In contrast with the Rietveld method, this software uses experimentally measured patterns in order to determine which minerals are present within the sediments. This software represents the quantitative data as specific groups (Kaolinite, 2:1 Fe-rich clay minerals, 2:1 Al-rich clay minerals, chlorite & muscovite). This in order to take into account the mixed-layer type of clay minerals (Srodon et al., 2001).

3.5 X-Ray Diffraction on oriented clay slides (XRD)

The middle-, upper- and cover siliciclastic sequence all contain clay-bearing laminated marls (Appendix A – Field Work). Based upon the initial bulk measurements, it was decided to analyse the clay minerals in specific. The general idea was to investigate whether the different sequences possess an unique clay-assemblage, which would allow them to be identified based upon their mineralogical composition.

3.5.1 Sample selection

In order to extract these clays - *and get rid of the non-clay matrix* - the Jackson treatment was applied to six samples. In total four of these samples were selected from the laminated marls lithotype. Two additional samples were selected from the Basaranlar quarry. These samples represent two of the most clay-enriched lithologies, corresponding to a marly travertine and a paleosol (Bouman, 2016).

The samples of Basaranlar were analysed during this research, in order to verify whether the clay content in these lithologies would match with the clay content in one of the lacustrine facies. Both of these samples were characterised by a very low clay content.

3.5.2 Jackson treatment

The general steps, applied during the Jackson treatment (used to remove carbonate cements, organic matter and Fe-(hydro)oxides) can be found within Appendix C – Jackson treatment. However, since two of the analysed samples consisted nearly purely of carbonates, some additional comments are given. This would actually have been one of the first times (at the KU Leuven) that this treatment was used to extract clays from carbonates. Due to this carbonate matrix, the standard procedure was slightly adapted and the samples were treated six times (instead of only three) with an acid buffer. From the resulting clay fraction ($< 2\mu\text{m}$) glass plates were prepared by using the sedimentation technique. In optimal conditions at least 140 mg of material should be used to form these glass plates.

3.5.3 XRD measurement

The measurements were performed with a PW1050/37 goniometer, that was connected with a PW1830 generator and equipped with a Cu-K α -radiation. The detector is proportional to the detector type PW3011/00 and the diffractometer has a Bragg-Brentano $\theta / 2\theta$ setup (respectively for the source and detector). The following settings were used: 0h38 (measurement duration), $0.02^\circ 2\theta$ (step size), 1 seconds (counting time per step) and $2 - 47^\circ 2\theta$ (range).

3.5.4 XRD analysis

Due to the presence of multiple different clay minerals, it is rather difficult to truly model the quantitative composition of the resulting clay fraction (Adriaens, pers. communication). The flow chart, published by the USGS in 2001, was used in order to identify the different clay minerals, based upon the distinctive peaks in air-dried and glycol-saturated conditions.

3.6 Elemental Analysis – Isotope Ratio Mass Spectrometry (EA - IRMS)

The visual presence of alternating laminae within the laminated marl lithotype lead to questions regarding the involved sedimentary processes. The latter are commonly characterised by a difference in organic, chemical and/or mineralogical compositions (Zolitschka et al., 2015). In order to verify whether these alternating laminae possess variable amounts of organic matter, the total amount of organic carbon (TOC) of eleven samples was analysed

3.6.1 Sample selection

In total three different deposits were selected of which at least two successive laminae were analysed. By analysing the successive laminae it was possible to verify whether the TOC-content acts as a controlling parameter within these marls. An example of two successive laminae from the Cakmak quarry can be seen in Figure 3.1. Additionally, three measurements of horizons, that were visually behaving as a marker horizon, were included as well.

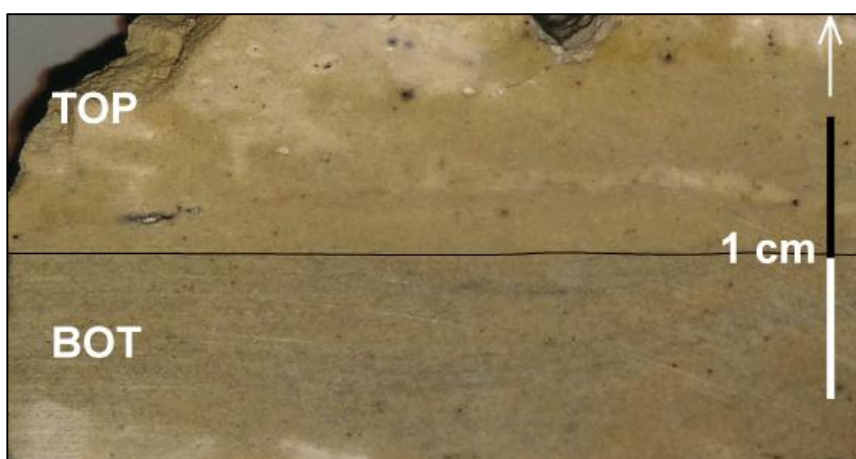


Figure 3.1: Two alternating laminations of the laminated marl lithotype, as could be observed in the quarry of Cakmak. Visually the top layer has a lighter colour as the layer at the bottom (wetted sample in order to increase colour contrast).

3.6.2 Sample preparation

In general, the EA-IRMS method is applied to soil samples, which in general do not contain a lot of carbonates. Since our samples consisted at least for 40% of carbonates (both calcite and dolomite) a slightly different approach was used as the one being described in Appendix D – EA-IRMS procedure.

It is essential for this method that all carbonates are removed before measurements can be carried out, since this method measures the total C-content of each sample. Initially 10 mg of each sample was selected, of which the carbonates were removed by the addition of HCl (1.5 N). This causes an initial reaction at room temperature and the volume of HCl should be large enough to make sure that there was still reactive acid left within each container after all calcite was gone. After 12 hours, these containers were brought to a temperature above 60 °C, in order to remove trace amounts of dolomite.

Afterwards the remaining product was cleansed two times with demineralized water and the remaining liquid was removed after being centrifuged for 5 minutes. The remaining product was then placed in a bowl with a plastic foil (in order to easily extract the dried product) and placed in an oven for 12 hours at 60°C. It is this dried product, free of any carbonates, that was used in order to measure the total carbon content.

3.6.3 Sample measurement

At last about 20 mg of each processed sample was weighed and sealed within small Ag-cups. These cups were then measured within a Carlo Erba elemental analyser. In here the sealed cups were burned by a pulse of pure (99.99%) oxygen. The resulting gasses were then carried away by the non-reactive helium carrier gas. Next to N₂, nitrogen may also be present as NO_x, and thus it was necessary to convert these NO_x-gasses to N₂ with the use of a copper catalyst. In a next step the carbon was converted to CO₂ and water vapour was removed from the gas mixture. The resulting cleaned gasses were then passed through a gas chromatograph, which measured the gas-content based upon its thermal conductivity. The detailed procedure of the EA-IRMS analyses, can be found in Appendix D – EA-IRMS procedure.

3.7 Carbonate content

The carbonate content of the laminated marls could already be deduced from the bulk XRD-measurements. Nevertheless, the method that was applied to deduce the mineralogical content is based on Quanta and may not always result in reliable

estimations. As discussed in 3.6, all carbonates had to be removed from the samples prior to measuring the total carbon content.

This procedure thus allowed an accurate estimation of the non-carbonate phase within each sample, due to the fact that the plastic foil leads to a recovery rate of almost 100%. Based upon the dried sample weight and the weight of the dried resulting product, it was possible to calculate the amount of dissolved carbonates.

3.8 Grain size analysis

Since grain sizes of deposited materials are related to the proximity of their source, a grain size analysis of the described conglomerates (Appendix A – Field report) might lead to usefull information (McLaren & Bowles, 1985).

The observed conglomerates tend to form small aggregates, due to the precipitation of a carbonate mud. Because of this dry sieving will not lead to correct results. That is why the technique of wet sieving was used, separating the fractions of 1 cm, 2 mm, 250 µm and 62 µm. After each fraction was separated from one another, the fractions were placed in an oven at 60°C for 24 hours.

Each of these fractions were weighed and finally consist of individual grains. In order to increase the amount of grain classes, the resulting grains were dry sieved additionally at 4 cm, 1 mm, 500 µm and 125 µm .

3.9 Inductively Coupled Plasma Optical Emission Spectrometry (ICP-OES)

Since the geochemical composition of the laminated marls (Appendix B – Field report) might lead to some insights into its sedimentary depositional system, ICP-OES analyses were also performed in the framework of this research. Similar data were already acquired by Soete (2011) and Swennen et al. (2013) and a geochemical comparison between both datasets would thus be possible. The device that was used for measurements during this research is a Varian of the type 720-ES.

Of all studied lithotypes, the laminated marls were the most homogenous one. This in comparison with, for example, the conglomerates that contained *exotic* pebbles. A geochemical analysis of these conglomerates would thus depend upon the types of clasts that were analysed, which were heterogeneously distributed. The laminated marl lithotype, however, was characterised by the absence of coarse grained material and consists dominantly out of clays and carbonates. It was possible that this depositional system received water (and thus weathered products) from both the travertine system and a

specific provenance region, what might be confirmed based on the geochemical composition.

3.9.1 Four acid digestion method

The four acid digestion method is a commonly used method for *near total* elemental analysis of carbonates. This method uses four different acids (HNO_3 , HClO_4 , HF and HCl) all breaking down specific mineral groups. Initially each sample was mortared and sieved at $250\ \mu\text{m}$, after which 100 mg of it was weighed in a Teflon container. The first acid, HNO_3 , was used for the primary decomposition of the sample and after 3 mL has been added the Teflon containers were placed on a hotplate.

The second acid, HClO_4 , was used as a strong oxidizing and dehydrating agent. This acid is characterised by a high boiling point and replaces all other acids in their salts. Two mL of this acid was added to the samples and afterwards the mixture was put on the hotplate and brought to boil. As a next step 3 mL HF was added to the containers, which is known to react with silicates, leading to a Si-free solution. After this final step the container was placed on a hot plate and the solution was digested until the residue was nearly dry. After this step the residue was dissolved in 7 mL HCl (2.5 N) and the resulting solution was diluted with MQ-water to a total volume of 25 mL. Fifteen mL of this diluted solution was then transferred to an ICP-OES measuring tube, after which the solutions were ready for analysis.

A possible disadvantage of this digestion method is the inability to break down chromite and zircon (Totland et al., 1992). This thus means that some caution should be used when interpreting results of Ti, Zr, Cr and W. Additionally, it is not possible to measure the Si-content of a sample, since this has been removed by HF. On the other hand, this method will not lead to a volatile phase of other elements, while as LiBO_2 -fusion may lead to a loss of Pb, Sb, Cu, Sn and Zn (Totland et al., 1992 & Wang et al., 2004).

3.9.2 Reference samples

In order to calibrate the ICP-OES and take into account matrix effects, four different reference samples were analysed as well. The first two being CCH-1 (crinoidal limestone) and GFS-401 (limestone) (Flanagan, 1986; Roelandts & Duchesne, 1988). Additionally, BCR-1 (basalt) was used as well, which is characterised by an elevated Ni, Ti, Cu and Mn content (Pecora, 1968). The last reference that was used is GBW-7114, which is a dolomite (Bartha & Bertalan, 1997). Additionally 5 custom made references were used as well, spanning a whole range of concentrations.

Next to these references, two blanks were included as well, in order to take into account any possible contamination and matrix effects that are introduced during the digestion procedure.

3.9.3 Detection limit

When dealing with geochemical information, it is important to be aware of the significance of the measured concentrations themselves. The detection limit is defined by McNaught & Wilkinson (1997) as the sum of the mean concentration – *of a certain element* – in a blank with 3 times the standard deviation of the same element (measured in the same solution). Additionally the Limit of Blank (LoB), was calculated as well. In this research the LoB is equal to the highest value of analyte concentration that could be measured in the blanks (Vassilieva, pers. communication). In the specific case that the LoB would surpass the LoD, valid for Ca during these analyses, the Practical Quantification Limit (PQL) is equal to the LoB (Figure 3.2). In any other cases, the PQL is equal to the LoB.

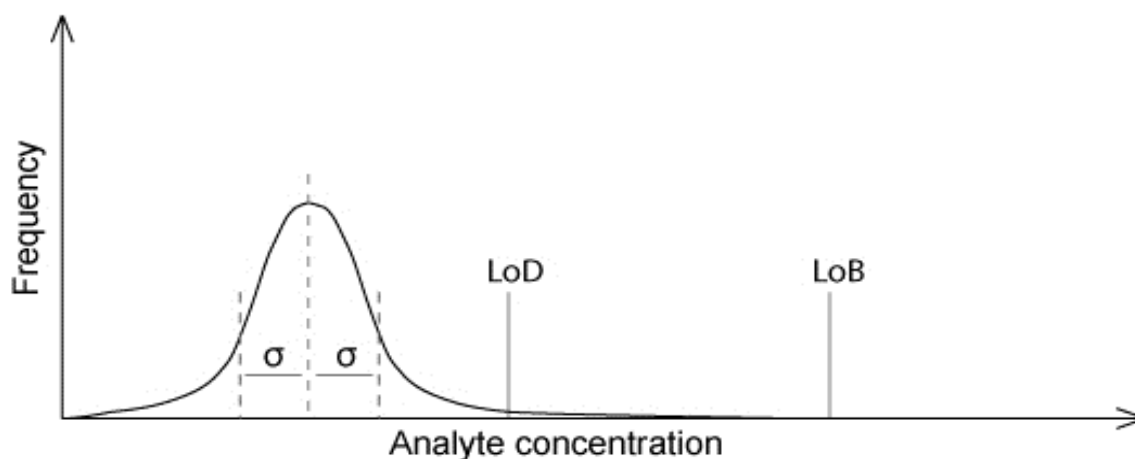


Figure 3.2: Visual representation of the Limit of Detection (LoD) and Limit of Blank (LoB). In this specific case the Practical Quantification Limit (PQL) is equal to the Limit of Blank (LoB).

3.10 SketchUp Pro

Due to the large scale of the studied area, a summarizing model is of major importance in order to visualise the observations. A general model of the overall Ballik area was made in SketchUp Pro. The advantage of this program is that it allows the construction of a geometric model, which respects the metric properties of the quarries and sequences.

The blue print of this model was based on satellite images. This allows the model to be constructed at a correct scale and with a correct distance in between each quarry. The detailed structure of each quarry, however, was based upon photogrammetry of the specific quarry itself. The major advantage of such a three-dimensional model is that it gives a clear overview of the relation between each sedimentary sequence.

3.11 Petrophysical characterisation

Since this thesis is part of the Joint Industrial Project on travertines, it was also important to characterise the studied deposits with regard to porosity and permeability. This would allow to integrate the petrophysical characteristic of the clastic deposits with the neighbouring travertine system.

In total 21 plugs were used for the conventional porosity and permeability analysis. Due to the fact that these samples are taken from outcrops, these are all orientated in a horizontal direction and will thus represent the horizontal permeability. These samples were send to the geo-consultancy company of PanTerra. In order to prepare these plugs they were cut off at the end, leading to a clean and horizontal surface. After this preparational step, the samples were dried in an oven of 60 °.

3.11.1 Specific gas permeability

The gas permeability of the samples was determined with a nitrogen permeameter. The advantage of this device is that it can be used with a core holder, allowing the measurements to be executed at a pressure of 400 psig (simulating reservoir conditions). During the measurements a steady-state gas flow was established and the flow rate, pressure differential, gas temperature and ambient pressure were recorded. These parameters, combined with the length and the diameter of the plug, were then used to compute the permeability from Darcy's equation (Formula 3.1).

$$K_g = \frac{M \times Q_b \times P_b \times L}{A \times D_p \times P_m}$$

Formula 3.1: Darcy's Law for gases. K_g = gas permeability (Darcy), M = Gas viscosity (centiPoise), Q_b = gas flow rate (mL/sec), $P_m = (P_1 + P_2)/2$, P_1 & P_2 = up- and downstream pressure in core sample in absolute units (atmosphere), mean pore pressure (atmosphere), P_B = atmospheric pressure in units (atmosphere), D_P = differential pressure in absolute units (atmosphere), L = plug length (cm), A = plug cross-sectional area (cm²).

In order to take into account the gas-slippage, the gas permeability was corrected with the empirical correlation, leading to the Klinkenberg permeability (Formula 3.2).

$$K_l(< 400 \text{ mD}) = 0.68 \times P_g^{1.06}$$

$$K_l(> 400 \text{ mD}) = K_g \left(\left[\frac{K_g}{1000} \times 0.005 \right] + 0.95 \right)$$

Formula 3.2: The empirical correlations for the Klinkenberg permeability, for permeability values below and above 400 mD. K_l = Klinkenberg gas-slippage corrected gas permeability (Darcy).

3.11.2 Helium porosimetry

The helium porosity was determined by a helium expansion porosimeter and allows the determination of the effective porosity of each plug. This data can be used in order to verify into what extent 2D porosity estimations through image analysis yields trustworthy results and may be of interest in the interpretation of the Ballik travertine system as a reservoir analogue.

3.11.3 Porosity estimations through image analysis

In comparison to helium porosimetry, image analysis is a cost-efficient way to deduce porosity from a 2D section. Additionally, this technique also visualizes the porosity distribution, which increases the understanding of the porosity results. The disadvantage, however, is that it is not possible to take into account the three-dimensional distribution and the final estimation is limited by the resolution of microscopic observations. Since 21 samples were characterised by helium porosimetry, it was possible to estimate the possible error associated with porosity estimations through image analysis. This evaluation is important in order to interpret the final results of the image analysis correctly.

Image analysis took place on several scales (cf. upscaling), based on a scanned thin section and microphotographs. The microphotographs could be scaled due to the presence of the scale bar, however, for the scanned thin sections this scale bar was absent. Since all thin sections were scanned at a resolution of 1200 dots per inch, the pixel size can be calculated. Each scan contains 427.44 dots per cm, what lead to a pixel size of 0.021 mm. In order to end up with 2D-porosity estimations, J-MicroVision was used. This software has two different approaches to calculate the two dimensional porosity, both with their own (dis)advantages.

In order to estimate the 2D-porosity in the conglomeratic beds, which are specifically enriched in quartz, point-counting was used. With this approach it is the user who determines whether something will be classified as a pore or not, allowing him to differentiate pores from quartz grains. This was important to differentiate quartz from pores in the polygenetic conglomerates, since they both were characterised by a black colour in crossed polars. For all other lithologies, object extraction was used. The advantage of this approach is that it will truly evaluate the whole photograph, in contrast with point counting. The only requirement is that pores can visually be differentiated from the matrix (e.g. moldic gastropod pore from calcite matrix).

Chapter 4

Results

Results of previously described methods are discussed in detail in the upcoming chapter.

4.1 Lithology description

The classification of the observed lithologies and the interpretation of their paleo-environmental setting are crucial parts of an analogue study. In total 6 different lithologies were differentiated in the detrital deposits, encasing the travertine dome. These lithologies were classified as marls, polygenetic conglomerates, sandstones, monogenetic breccias, gastropod-rich carbonate and coquina beds. Detailed field-observations can be found in Appendix A – Field report.

4.1.1 Sedimentary architecture

The travertine dome in the Ballık area was encased by four separated sedimentary sequences. An overview with three of these sequences can be found in Figure 4.1, next to a schematic model with the relative timing of these sequences. The oldest sequence (lower conglomerates) consisted of polygenetic conglomerates and monogenetic breccias and was observed in the quarry of Faber and Ece. A thick detrital unit, referred to as the middle siliciclastic sequence, was present in between the subhorizontal travertine

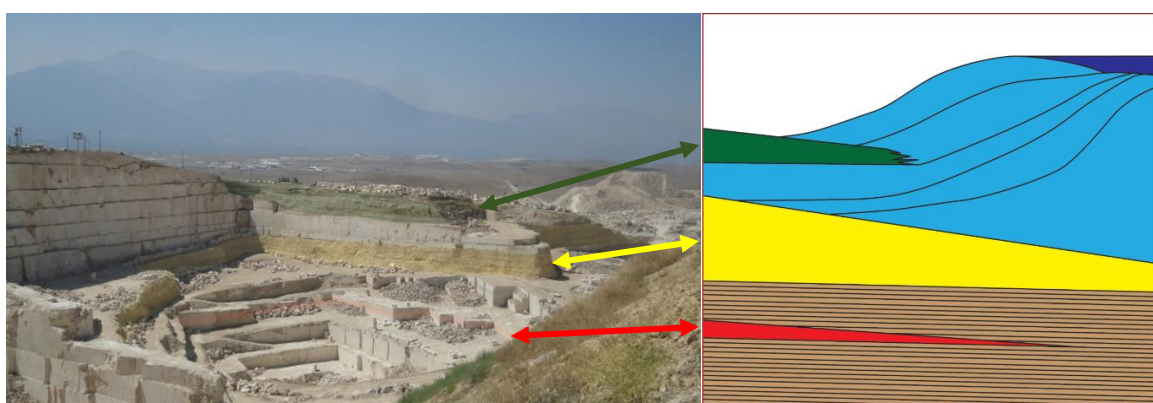


Figure 4.1: *Right* - Overview of the quarry of Faber, where three sequences can be observed. *Left* – Simplified overview of all four detrital sequences (Lower conglomerates = red, Middle siliciclastic sequence = yellow, Upper siliciclastic sequence = green, Cover siliciclastic sequence = dark blue, Subhorizontal travertine = brown and domal travertine = blue).

lithologies and the domal travertine lithologies. This facies consisted of several lithologies ranging from laminated marls to polygenetic conglomerates.

The third sequence, known as the upper siliciclastic sequence, developed contemporaneous with the domal travertine lithologies. Both massive and laminated marls were abundantly present, next to polygenetic conglomerates, monogenetic breccias, gastropod-rich carbonates and coquina beds. The youngest sequence, referred to as the cover sequence, covered the domal travertine lithologies and consisted of laminated marls, polygenetic conglomerates, tabular sandstones and coquina beds.

4.1.2 Marls

In the Ballık area, thick and laterally extensive marls could be recognised. These marls were characterised by fine grained particles and could be observed in the field as two different lithotypes. With exception of the lower conglomerates (described in the quarries of Ece and Faber) the marls were observed in all sequences present within the area.

The first lithotype consisted of a brownish and rather massive marl, which does not show a clear internal architecture. This type of marls was often observed in close relationship with the polygenetic conglomerates and had a rather limited thickness of up to 1 m (Figure 4.2 A). In close proximity to polygenetic conglomerates, reed-like structures developed within these marls, leading to locally well-cemented horizons. In the field, the top of these massive marls were often characterised by an erosive surface. Furthermore, they also contained iron- and manganese oxidized root-traces. In general, this lithotype is poorly-cemented and thus rather difficult to sample.

The second lithotype had several different characteristics in comparison to the massive marls. These marls, however, expressed a clear horizontal lamination (with thicknesses of each laminae ranging from 0.5 – 4 cm), could be up to 12 m in thickness and contained root traces (Figure 4.2 C). In certain cases, secondary laminations within these primary laminae were observed as well. Furthermore, they contained several correlative horizons that could be traced for up to 300 m. The alternation, which was a unique aspect of this lithotype, could partly be observed due to the different colours of the successive layers (being brown-green or white, Figure 4. B & C). Additionally, a different degree of cementation highlighted the alternating nature of this lithotype. The latter seems to be controlled by the proximity towards the travertine dome (as was observed in the quarry of Cakmak). Near the travertine system itself, these laminated marls were almost completely cemented, while they became less-cemented with increasing distance towards the travertines. Furthermore, the thickness of these laminations was not constant and varied

between 0.5 cm to 4 cm (Figure 4.2 B). Additionally, these marls were often affected by tectonic influences. This expressed itself in the formation of water-escape and ball-and-pillow structures.

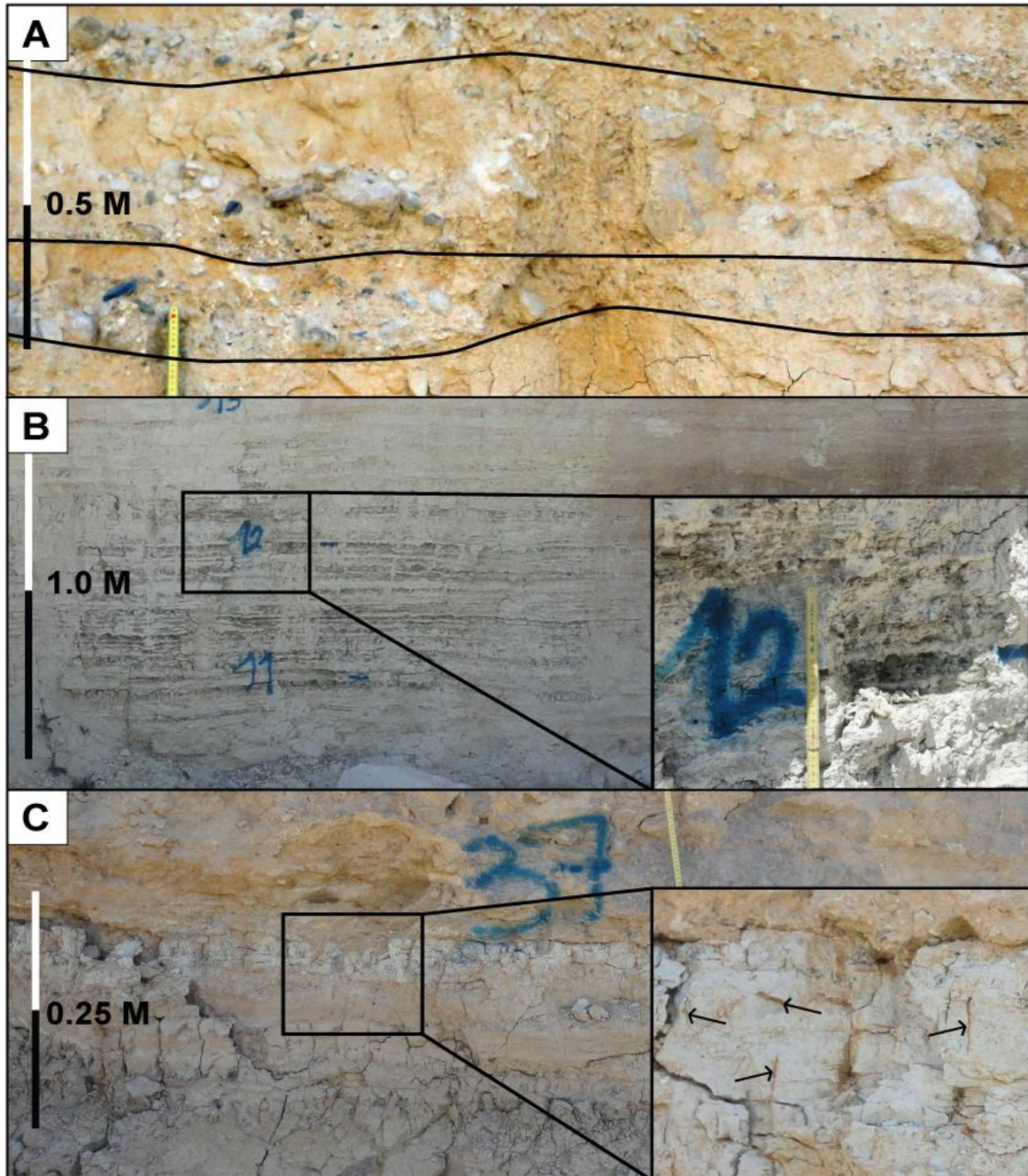


Figure 4.2: Illustration of both marl lithotypes. *A* - Rather massive marl deposits, with erosive contacts of polygenetic conglomerates highlighted by black lines (lower siliciclastic sequence in Faber). *B* - Laminated marl deposits with layers of varying thickness, strongly affected by cementation (Cakmak). *C* - Horizontally laminated deposits with root traces (black arrows, Faber).

4.1.3 Polygenetic conglomerates & tabular sandstones

The polygenetic conglomerates were characterised by their erosive nature. This lithology consisted of (sub-) rounded clasts, with a varying composition and colour (limestone, marble, dolomite, travertine, quartzite, periodite ...). The size of these clasts could vary significantly, ranging from 0.5 cm (microconglomerates) to 30 cm (often sub-angular travertine boulders of the sub-horizontal facies). The finer fragments were often well-rounded in nature and travertine fragments seemed to be absent within the fine fraction. All of the polygenetic conglomerates were characterised by a fining upwards trend and tended to form amalgamated structures of several channels on top of one another (Figure 4.3 C). This lithology was characterised by an important variability in cementation, since some of these polygenetic conglomerates were welded together by travertine or cemented by transparent calcite. Next to these cemented conglomerates, there were also other conglomerates embedded within a poorly-cemented muddy matrix. In general, the degree of cementation varied within a short distance and seemed to be associated with the proximity to the travertine system (as for example in the quarry of Faber).

These lithologies could often be observed within channel-like structures with a varying dimension. Their width ranged from 1 to 15 m and their thickness could vary from 0.2 to up to 6 m (for amalgamated conglomerates). Furthermore, these conglomerates often displayed imbricated structures (Figure 4.3 C). Throughout the whole sequence, the abundance of these conglomerates varied in space, leading to certain sections where nearly no conglomerates could be observed at all. Furthermore, certain polygenetic conglomerates were deposited contemporaneous, but within a distance of up to 100 m in between two channels. The space in between these channels was filled up by the massive marl lithotype, as was discussed in 4.1.2 Marls.

Tabular sandstones were closely associated with these polygenetic conglomerates. These sandstones consisted of coarse to medium sized grains with a brownish colour. Crossed lamination was observed within these sandstones, often in a preferential direction indicating a flow direction towards the south (Figure 4.3 B). The thickness of the latter was rather limited (up to 20 cm), while they were lateral continuous for up to 500 m. In general, these sandstones were poorly cemented and disintegrated rather easy, making it difficult to sample this lithology.

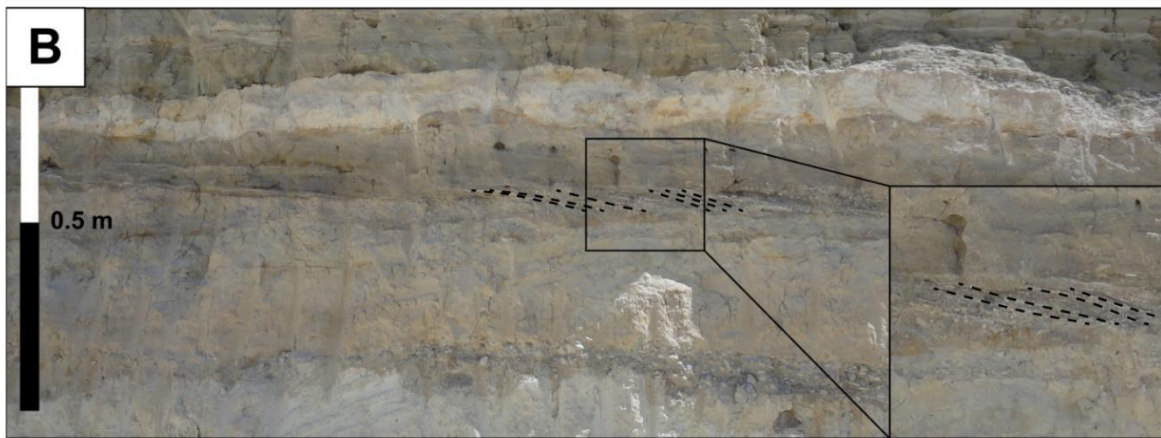
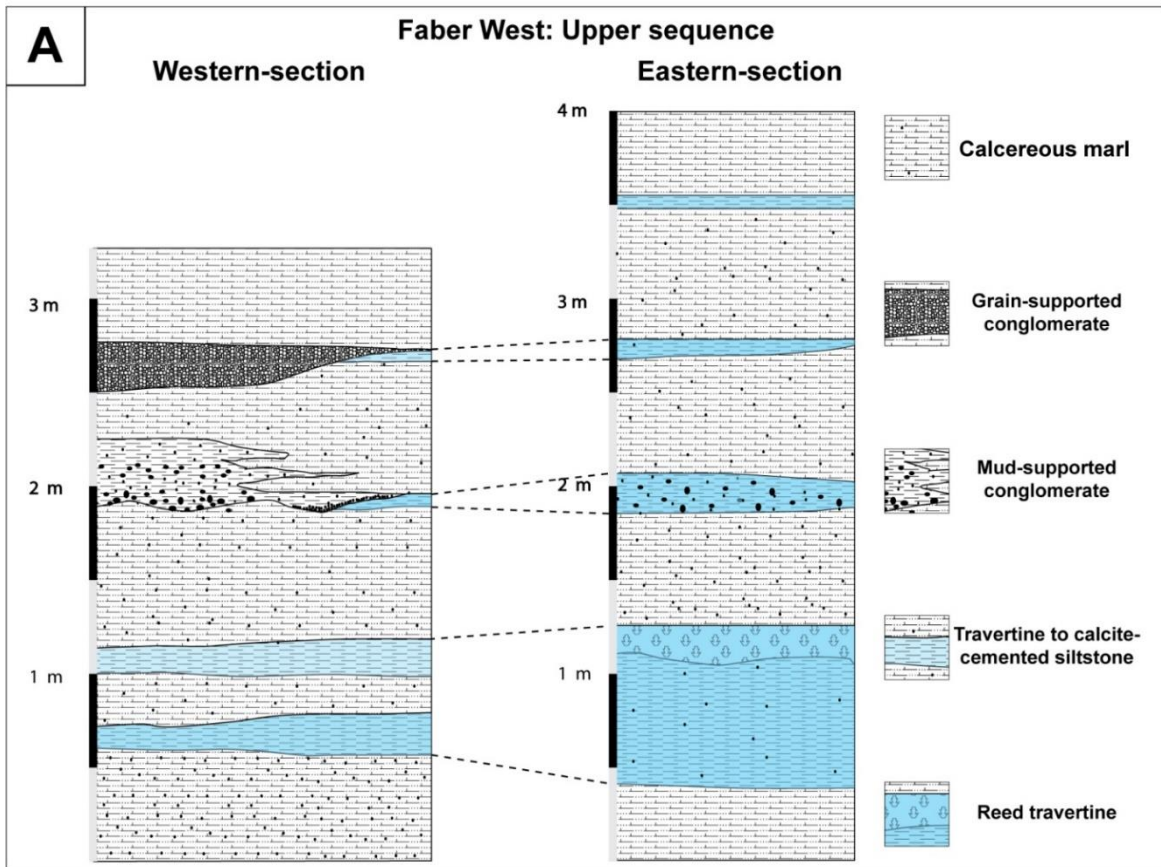
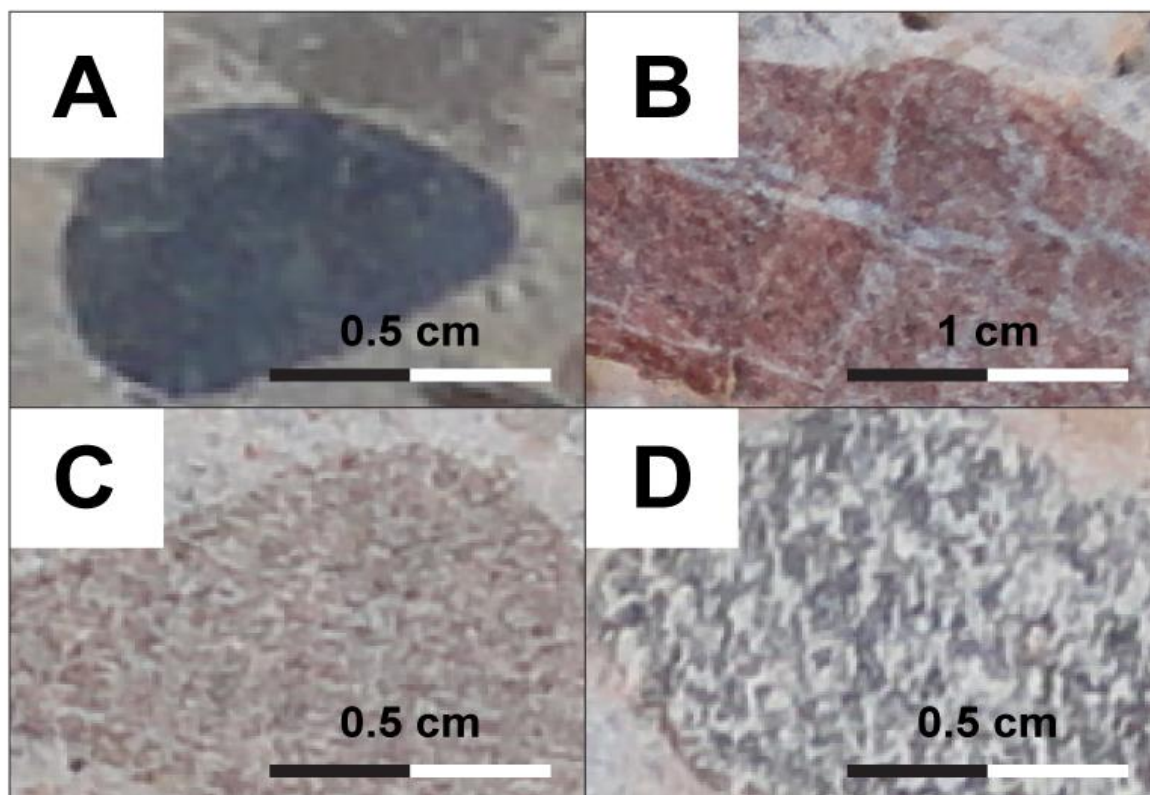


Figure 4.3: Representative outcrops for the polygenetic conglomerates and tabular sandstones in the Ballık area. *A* - Simplified litholog, highlighting the spatial relation between the polygenetic conglomerates, the massive marls and reed-travertine (Faber West). *B* - Tabular sandstone with cross-lamination highlighted by dashed black lines (Alimoglu Tasarim). *C* - Amalgamation of erosive river channels, of which the contacts are highlighted in black, filled with polymict conglomerates giving rise to imbrication structures (thick black lines, Faber).

4.1.3.1 *Clast composition*

The polygenetic conglomerates consisted of clasts with a varying composition. The larger clasts (up to 30 cm) were often made of the subhorizontal travertine facies and were sub-angular in shape. The other clast types had a (sub-)rounded shape and generally had a diameter below 10 cm. These clasts could be divided in four different groups, being carbonate rocks, siliciclastic rocks, metamorphic rocks & metamorphic ultramafic rocks. The carbonate rocks were either made of a light grey limestone or a dark (sulfur smelling) dolomite (Figure 4.4, A). The siliciclastic clasts were dominantly made of either dark red to brown sandstones and brownish siltstones and were abundantly present within the conglomeratic beds (Figure 4.4, B & C). The third type consisted of several different rock types. Clasts of white marbles were regularly present within the conglomeratic beds, next to clasts with a gneiss texture (Figure 4.4, D). The last clast type was only present as rather small clasts (diameter below 0.5 cm) and was characterized by a mustard green colour. This clast type could be classified as serpentinite (Figure 4.4, E & F).



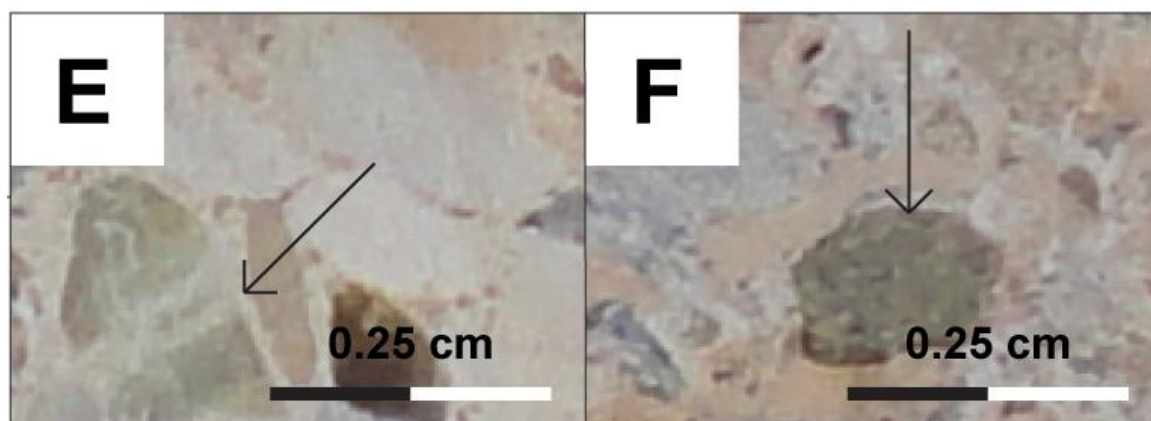


Figure 4.4: Different clast types in the polygenetic conglomerates. *A* – Dark blue (sulfur rich) dolomite. *B* & *C* – Red and brown sandstones. *D* – Clast with a gneiss texture. *E* & *F* – Small clasts with a mustard green colour, possibly serpentinite.

4.1.4 Monogenetic breccias

The monogenetic breccias consisted almost purely of fine angular travertine clasts, with a size ranging from 0.5 to 20 cm. Furthermore, these breccias were often mud-supported, leading to clasts that float within a matrix of calcareous mud (Figure 4.5 A). In some cases, poorly-developed imbrication structures were observed. However, they tended to be less consistent in comparison to the polygenetic conglomerates.

In the study area, this lithology only represented a rather limited volume with respect to the other detrital deposits. The maximal thickness of this lithotype was about 1 m and it had a rather limited length of 10 – 20 m. Furthermore, this lithology was closely associated with the presence of paleoslopes (Figure 4.5 B). Internally, a coarsening upwards trend could often be observed in these deposits. A last characteristic of this lithology is the absence of erosive power with respect to the underlying sediments. This caused the underlying deposits to be draped by these monogenetic breccias.

It was thus clear that the monogenetic breccias were characterised by different features when compared with the polygenetic conglomerates. In contrast to the polygenetic conglomerate lithologies, the clasts of these breccias were angular and dominantly made of travertine. Furthermore, these lithologies were not observed in channel-like structures, but upon often steep paleoslopes. A typical example of this lithotype could be observed in the Cakmak quarry, where the cascade facies acted a paleoslope. This paleoslope was covered by a monogenetic breccia with a thickness of about one metre and an abundance of angular travertine clasts (Figure 4.5 B). In the close-up shot in figure 4.5B, what was described as the *frozen* structure of these clasts, can be seen. This frozen structure was characterised by angular clasts, oriented in all possible directions, in between contacts were rather rare, since the interparticle space was filled up by a calcareous mud.

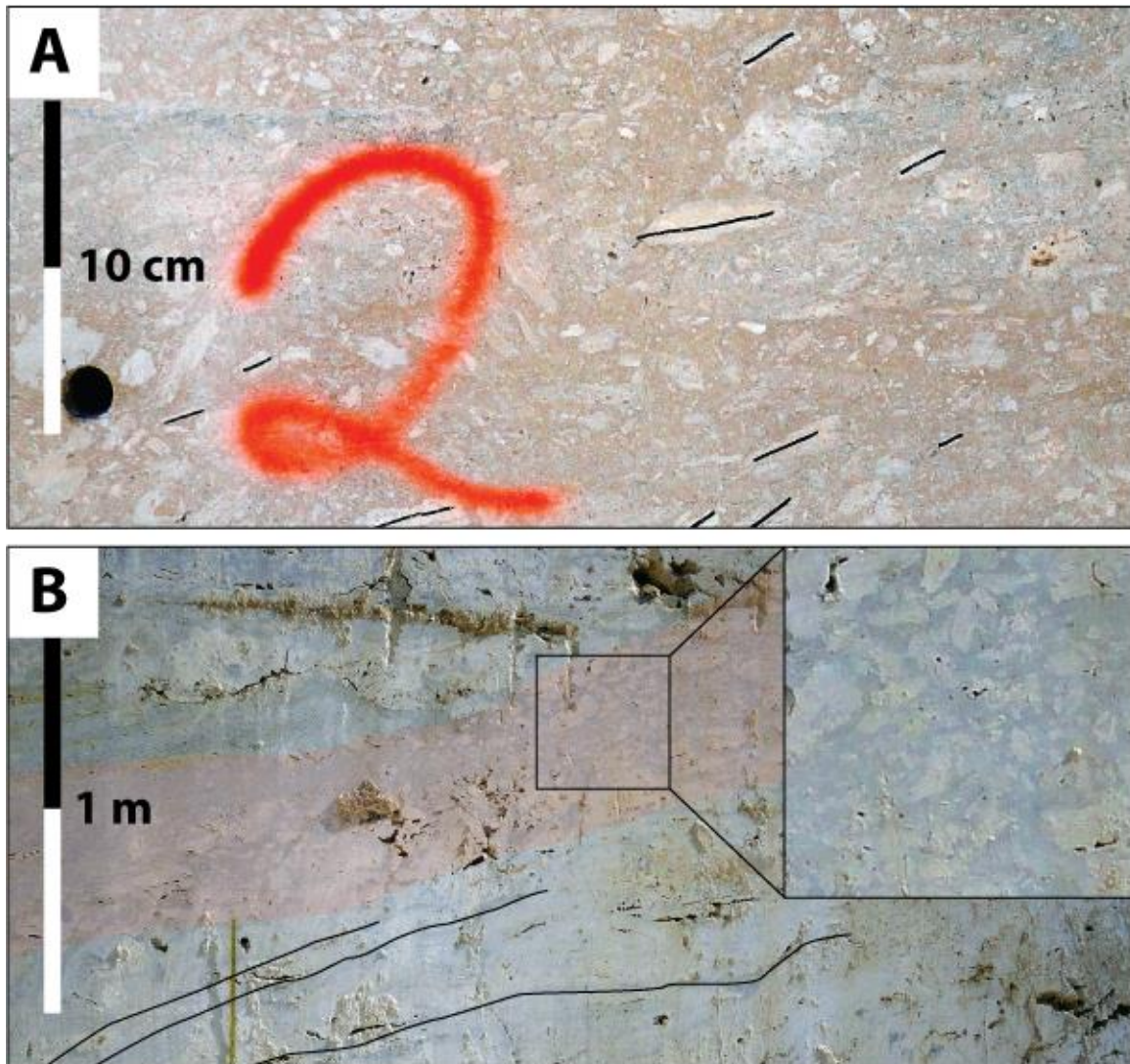


Figure 4.5: *A* - Close-up of the monogenetic breccia lithology, made of angular travertine clasts within a matrix of calcareous mud. Within this picture, poorly developed imbrication structures are highlighted in black (Ece). Monogenetic breccia (red) on top of an inclined (paleo-) surface (highlighted in black), which is interpreted as the cascade facies. *B* - The clasts of this breccia tend to develop a coarsening upwards succession and are floating in the matrix (Cakmak). The colours of both pictures are visually enhanced, in order to highlight the presence of the angular clasts.

4.1.5 Gastropod-rich carbonate

This lithology consisted dominantly of either dissolved or intact gastropod shells, that were embedded in a travertine matrix. The latter was often observed in proximity of both the travertine system and the laminated marls (Figure 4.6 B). In general, this lithology did not contain a lot of detrital fragments, however, some coarse to very coarse sand grains could be observed (Figure 4.6 A, red box). This lithology did not make out a significant part of the total volume of the studied system. Overall, the thickness of this lithology reached at most 50 cm, while its horizontal extend was limited to about 20 m.

Most of the gastropod shells tended to be intact and they were distributed homogeneously throughout the travertine matrix (Figure 4.6 A). However, it could sometimes be observed that the gastropods tended to align in horizontal layers (Figure 4.6 B, black line). In most cases, the gastropods themselves were dissolved, leaving behind a moldic porosity (Figure 4.6 A & B).

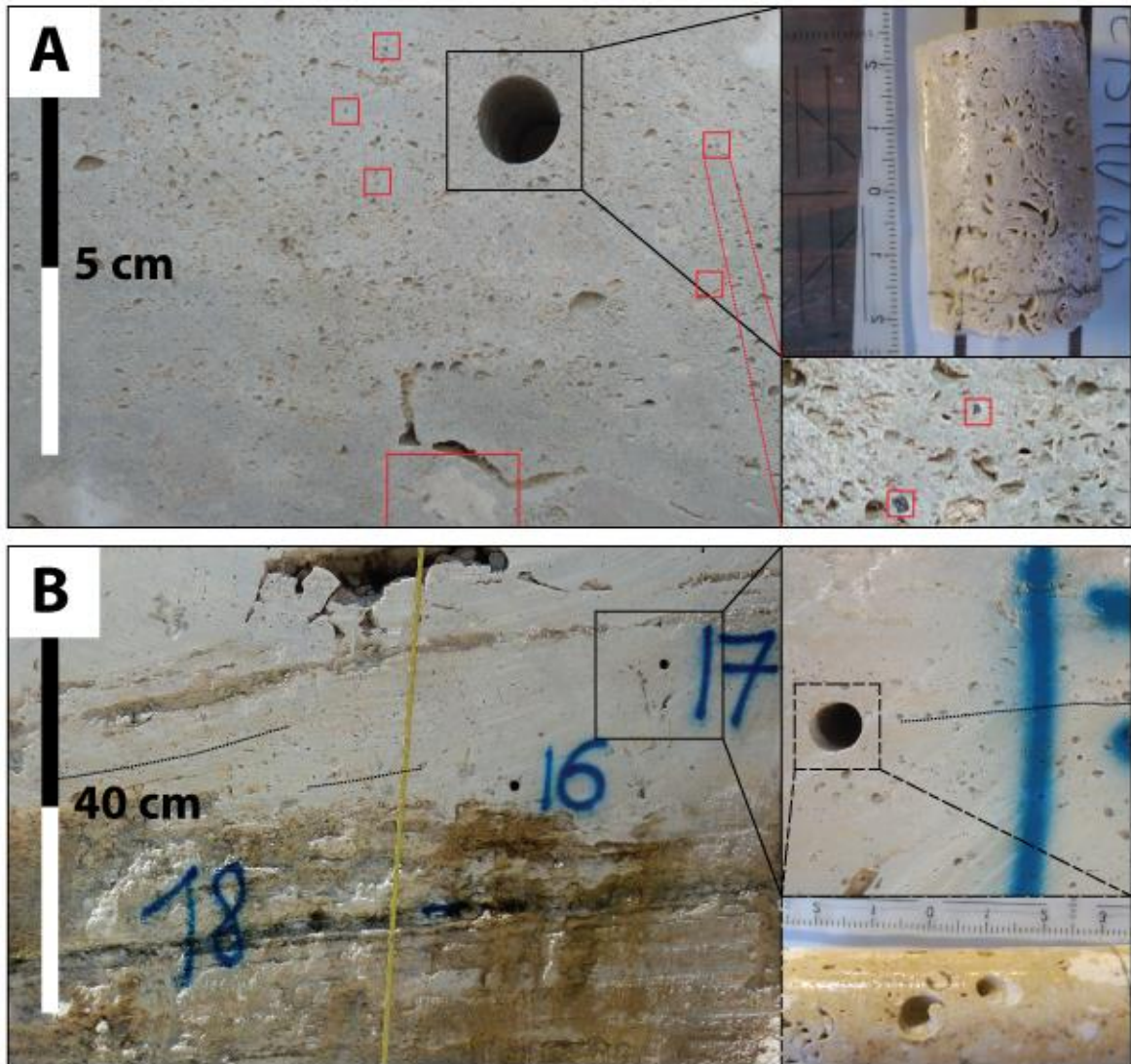


Figure 4.6: Outcrop and zoomed-in sections, representative for gastropod-rich carbonate. *A* - Homogenously distributed gastropods, within a travertine matrix with some detrital fragments that are highlighted by the red box (Cinkaya). *B* - The gastropod-rich lithology was closely associated with the laminated marl lithology and the travertine system. Moldic pores were the most dominant macroscopic pore-type of this lithology, which sometimes tended to align horizontally (black line, Cakmak).

4.1.6 Coquina

This lithology was almost purely made of gastropod shells, both intact and fragmental, classifying these deposits as a coquina bed (Figure 4.7 A). In certain cases, this lithology also tended to develop beds of gastropods embedded within a sandy matrix (Figure 4.7 B). This lithology was found throughout most quarries and tended to be closely associated with the tabular sandstones. In general, the latter was dominated by poorly-cemented beds, which often possessed a certain form of crossed-bedding (Figure 4.7 A). The thickness of this lithology was rather limited, ranging from several cm to 50 cm. However, the thicker beds in specific tended to be lateral continuous for up to 200 m.

This lithology differed from the gastropod-rich carbonate deposits, due to the different matrix and the undissolved nature of the gastropod shells. Furthermore, this lithotype was closely associated with the tabular sandstones, while this was not the case for the gastropod-rich carbonate. Furthermore, the crossed-lamination was also a characteristic that was not observed in the gastropod-rich carbonate lithotype.

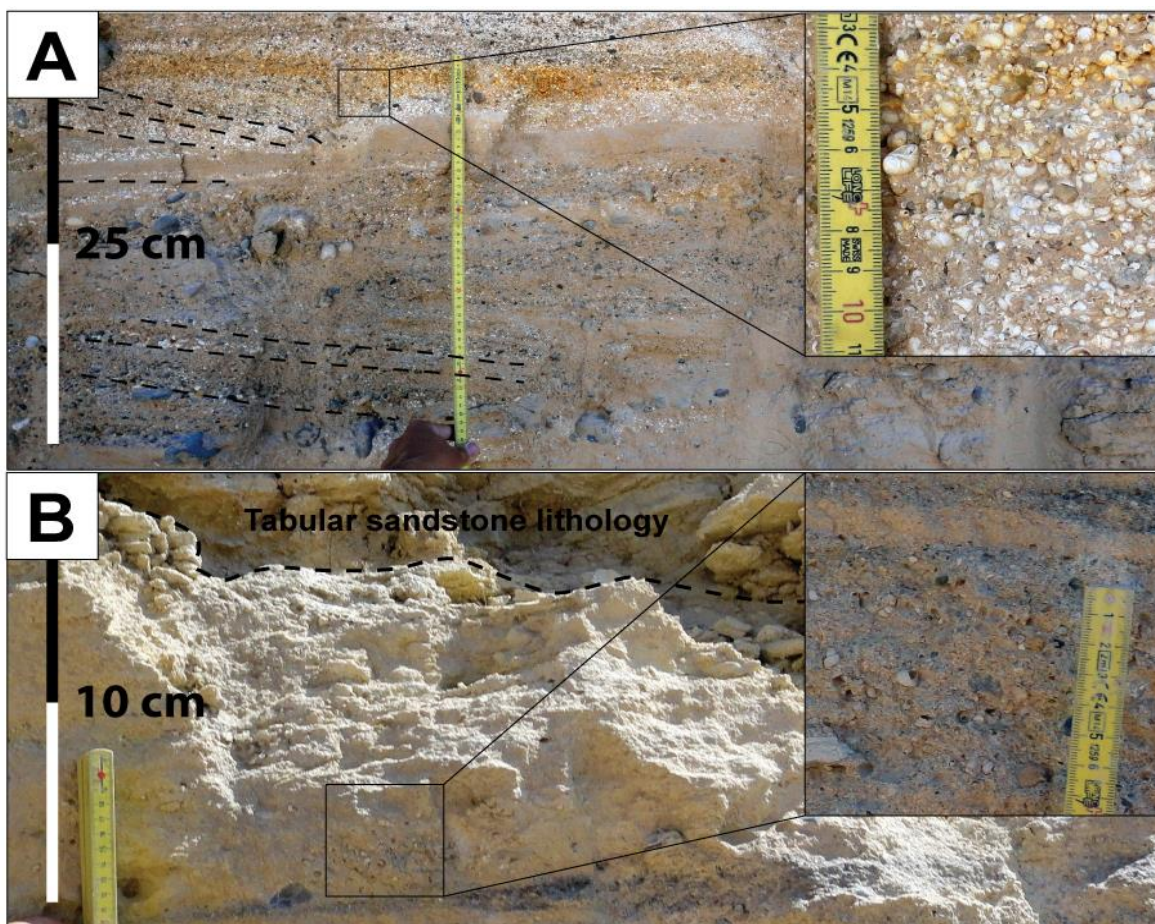


Figure 4.7: Figures illustrating the coquina lithotype, as observed in the field. *A* - Thick gastropod-supported grainstones, with the development of crossed-bedding (dashed lines, Alimoglu Tasarim). *B* - Coquina bed with a sandy matrix. Closely associated with these coquina beds were the tabular sandstones (dashed lines, Faber).

4.2 Petrography

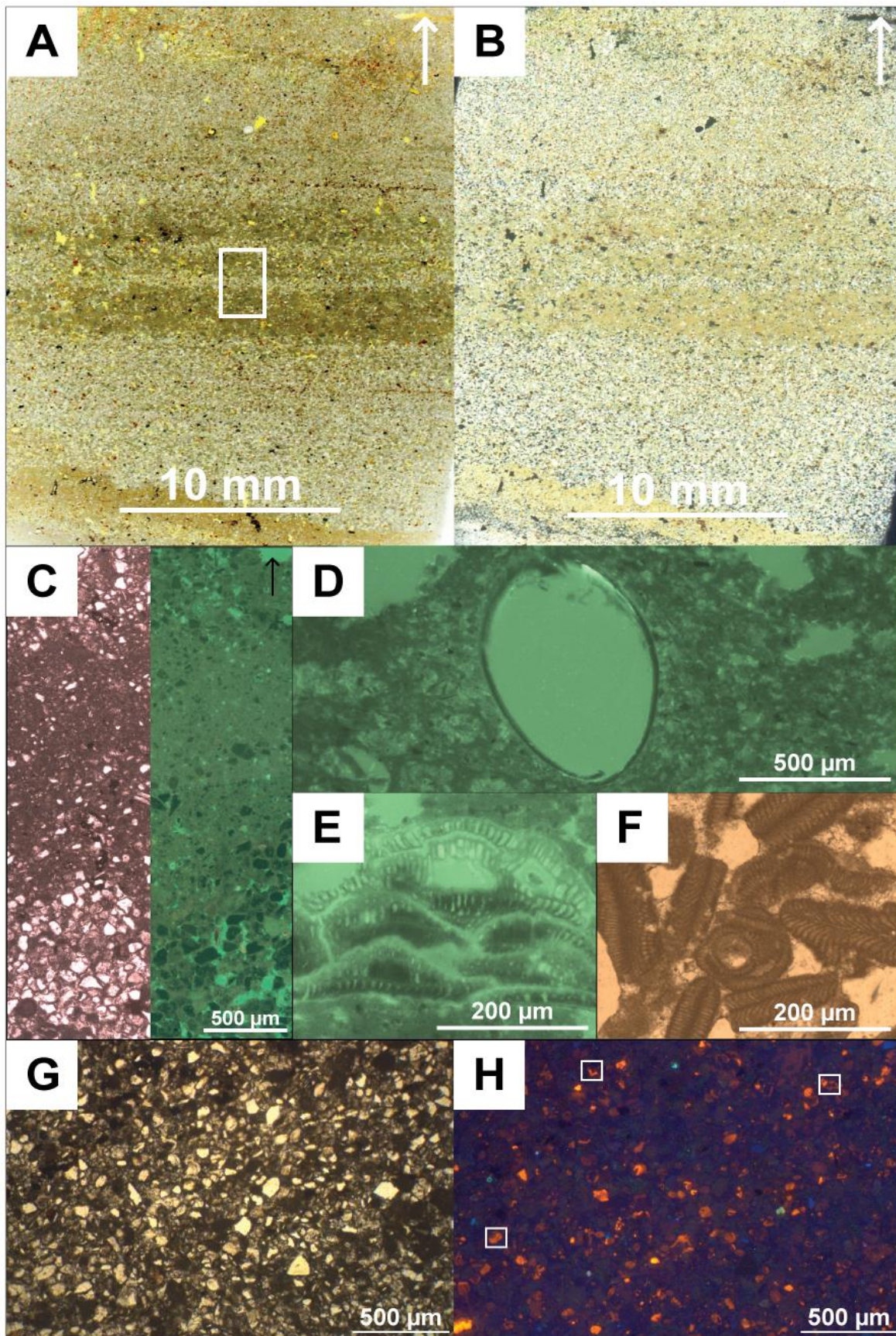
The results of the cathodoluminescence, fluorescence and conventional microscopy are discussed within this section. These results were linked to the recognised lithotypes, in order to compare macroscopic with microscopic observations. In the upcoming section a facies classification will be made, integrating these observations.

4.2.1 Laminated marls

On a macroscopic scale the laminated marl lithotype was characterised by a alternation of laminations. These laminations tended to be rather thick, making it difficult to study a full assemblage by microscopy. It has to be mentioned that the textural variability of this lithotype was rather high (degree of cementation, mineral content, porosity ...). In general, this lithology translated into thin laminae, which were either made of calcite and quartz grains or of a muddy material (Figure 4.8 A & B). The porosity was mainly concentrated within the bright layers, which dominantly consisted of calcite grains (Figure 4.8 A & B, thin sections).

On a microscopic scale it was observed that these alternating laminae were made of two different fabrics. The first fabric could be observed within the bright laminae, which had a packstone texture and were dominantly made of angular calcite grains (Figure 4.8 C). Furthermore, these calcite grains often developed a zonation of bright and non-luminescent calcite rims (Figure 4.8 E, white box). Next to these calcite grains, some quartz grains and peloids could be observed as well. With regard to the pore-network, these grainstones tended to develop intergranular pores and thus seemed to contain the largest volumetric share of porosity of the laminated marl lithotype. However, the muddy matrix also contained a significant amount of microporosity as deduced from fluorescence microscopy (see Figure 4.8 C). The second fabric could especially be observed within the darkish laminae. In contrast to the bright ones, these laminae were almost entirely made of mud without any grains present (Figure 4.8 C). The latter developed a mud- to wackestone texture, in which peloids could be observed as well. Overall, macroscopic pores were rather rare, due the absence of a grain-supported fabric. Nevertheless, these laminae were still quite porous, due to the presence of microporosity within the mud itself (based on fluorescence microscopy, Figure 4.8 C). Furthermore, algal structures and intact ostracods were present as well (Figure 4.8 D). These algal structures could be observed either as horizontally laminated or as branched-like structures (Figure 4.8 E & F). The horizontally laminated structures were observed within small build-up geometries (Figure

4.8 E). Other minerals that could be observed throughout the matrix were feldspars, expressing a bright blue or bright green luminescence (Figure 4.8 H).



Chapter 4 – Results

Figure 4.8: Representative pictures of a thin section of the laminated marl facies, visualised at different levels of detail. *A & B* - Thin sections highlighting the laminated nature of the marls (PP & CP). *C* - Assembly of two pictures, focusing on three successive laminae, visualising the alternation of grainstone texture and mud- to wackstone laminae (FL & PP). *D, E & F* - Intact ostracods and algal structures, which were often observed within these marls (FL & PP). *G & H* - Bright calcite grains, often with internally zoned CL-fabric (white boxes, PP & CL).

With regard to the zoned calcite crystals, striking observations were made in the laminated marl facies of the Cakmak quarry. These marls were characterised by an increased degree of cementation, in which a poorly-visible horizontal lamination could be observed (Figure 4.10 A & B). On a microscopic scale these marls were not characterised by the presence of laminae and they tended to develop a honeycomb texture (Figure 4.10 C & D). Furthermore, these cemented marls were entirely made of closely-packed calcite grains, with all porosity located in between the grains themselves. Next to calcite, dolomite and feldspars could also be observed in these thin sections (Figure 4.10 D, white box).

The calcite grains, within these well-cemented marls, were characterised by a zoned fabric (Figure 4.10 E & F). The core of these grains was made of non-luminescent (or weakly luminescent) calcite and was sub-rounded in nature (Figure 4.9, NL – C). This nuclei was coated by a bright calcite cement, which seemed to coat a preferential part of the grain, exhibiting an equant crystal habitus (Figure 4.9, BL – R1). On the other side of the crystal this bright calcite coating was almost absent. Furthermore, a rim of non-luminescent (NL – R1) and bright calcite cement (BL – R2) was encasing the previous generation of bright cements, in a similar manner as was described before (Figure 4.9, NL – R1 & BL – R2). Finally, these zoned calcite crystals were embedded within a non-luminescent calcite matrix. The zonations were associated by a certain preferential growth direction, of which the orientation was not consistent for the whole thin section. However, the largest crystals tended to be oriented within the same growth direction.

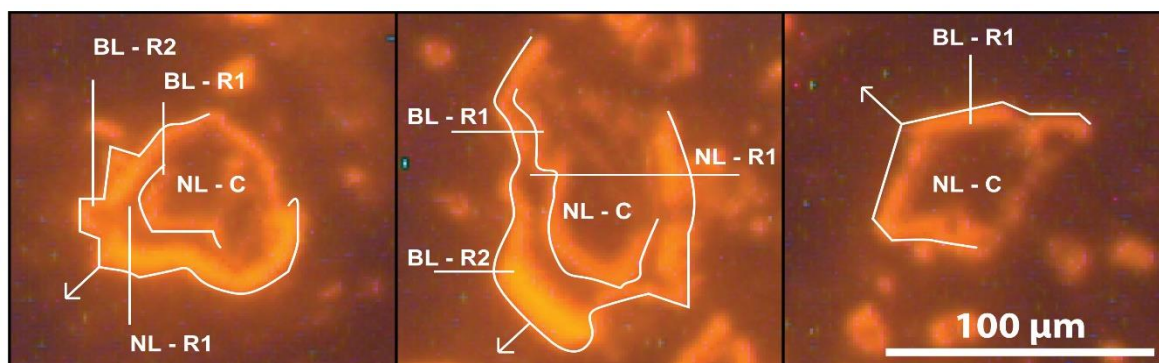


Figure 4.9: Detailed images of several zoned crystals, highlighting their zoned nature. The subrounded core was made of non-luminescent calcite (Non-luminescent core, NL – C), surrounded by bright (Bright-luminescent rim, BL – R1 & BL – R2) and non-luminescent (Non-luminescent rim, NL – R1) equant cements. The preferential growth direction of these cements is indicated by a white arrow.

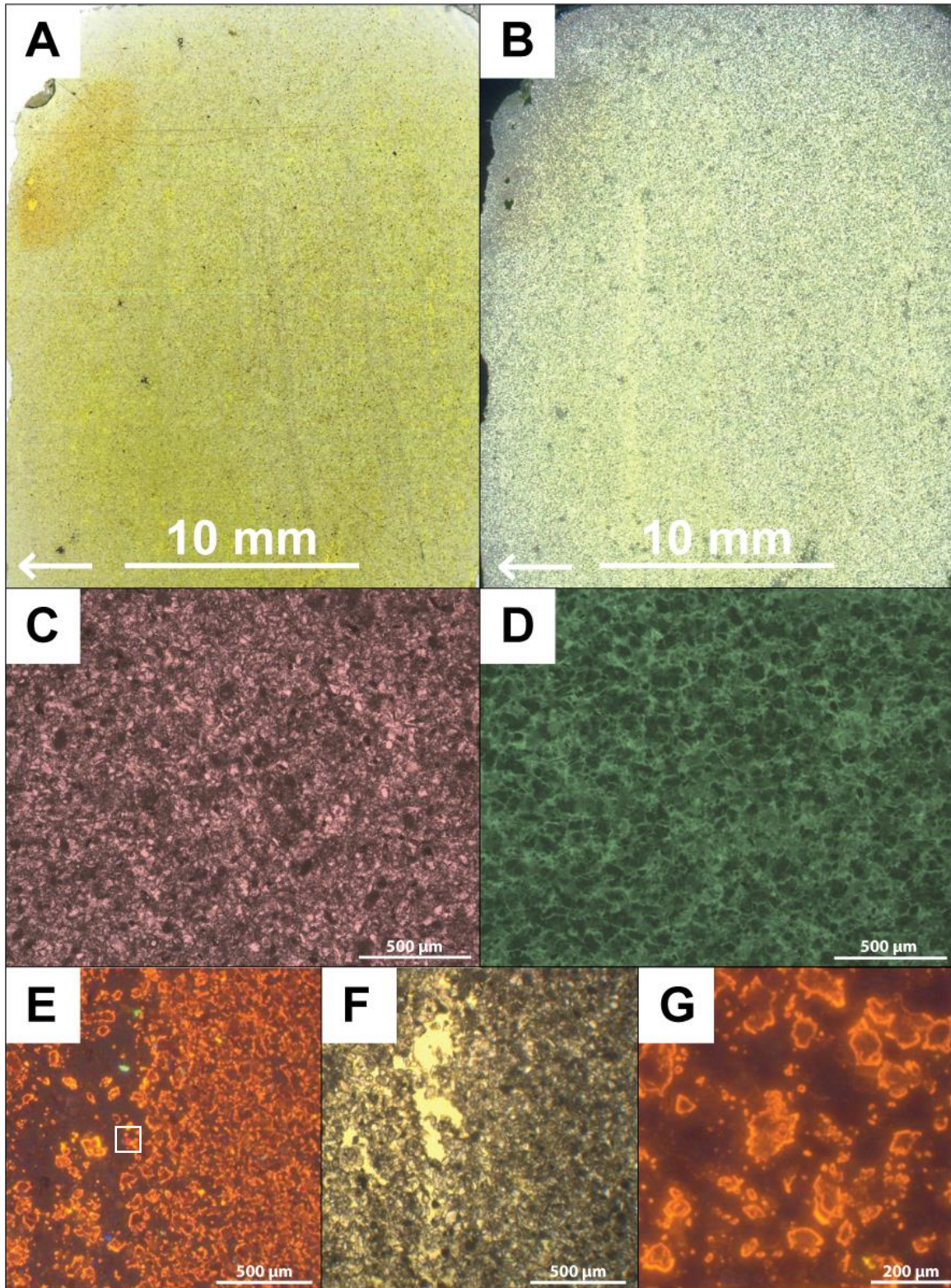


Figure 4.10: *A & B* - Well-cemented horizontally laminated marls, as they could be observed in a thin section (PP & CP). *C & D* - The internal structure of these well-cemented marls, dominated by a densely packed framework of calcite crystals (PP & FL). *E & F* - Internally zoned calcite crystals, with the presence of feldspars and dolomite phases (white box, CL & PP). *G* - Close-up of the previous picture, where the CL-zonations of the calcite phases are highlighted (CL).

In general, the laminated marl samples, that were observed under SEM, were characterised by a framework of grains. In between these grains, a rather significant amount of (micro-)porosity could be observed. Regarding the clay-content of this lithology, certain particles were completely coated by authigenic illite (Figure 4.11 A). Additionally, the clay mineral corrensite was present and formed rather small patches with a honeycomb texture (Figure 4.11 B). On the surface of certain grains, small (1 μm) and needle-like clay minerals were present. These clays were rather straight, which was the major difference when compared to the fibrous and curly illite clays. These needles could be classified as palygorskite, however, the resolution was not sufficiently high enough to really confirm this observation.

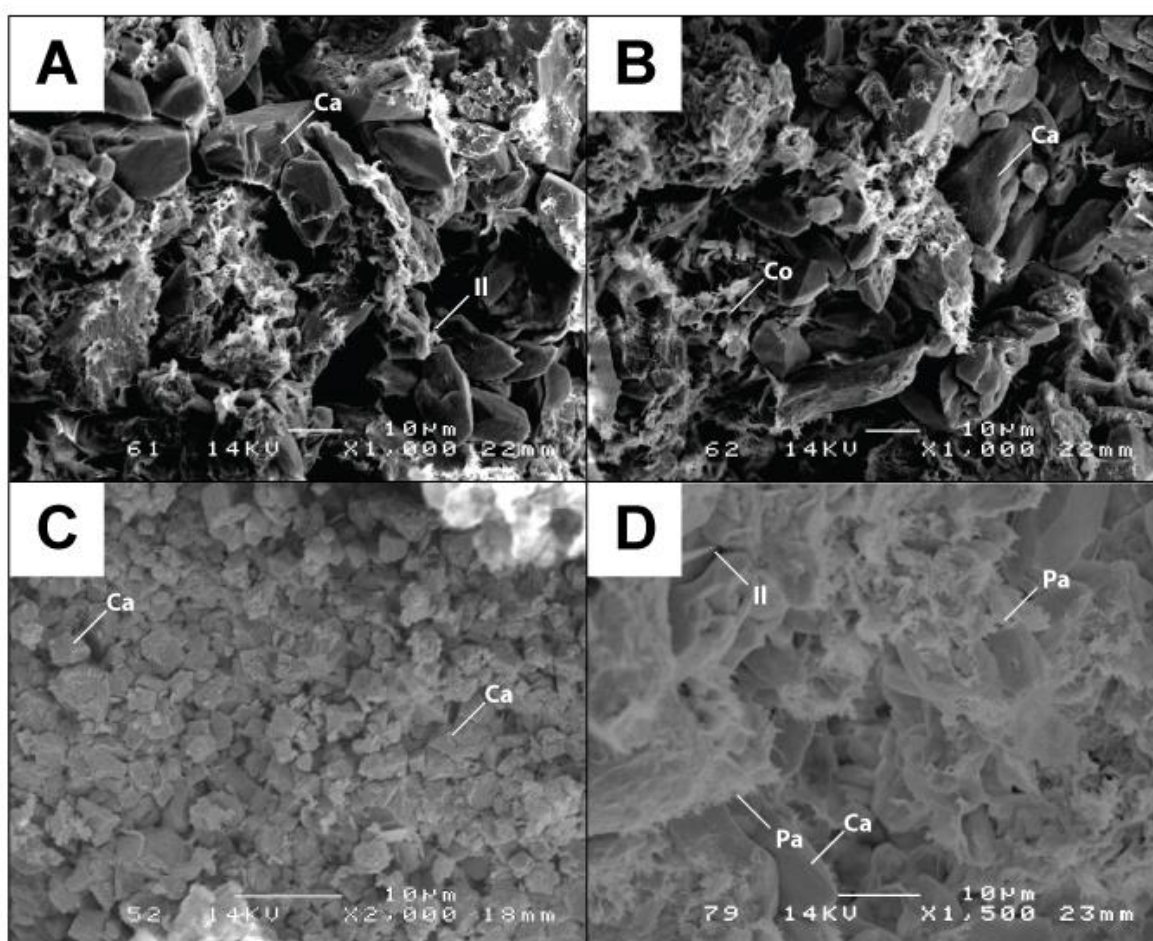


Figure 4.11: Snapshots of the laminated marl lithotype, as observed through SEM. Calcite grains coated by illite (A). Similar framework of calcite grains, but with the possible presence of corrensite clays (B). Clean section, consisting almost purely out of calcite grains, without a major presence of clays (C). Heavily coated calcite grains, both with illite and what could correspond to be palygorskite (D).

4.2.2 Polygenetic conglomerates

In section 4.1.3, both polygenetic conglomerates and tabular sandstones were discussed. However, no thin sections were available from these sandstones, due to their unconsolidated nature. This section will thus only deal with the petrographical description of the polygenetic conglomerates. An initial observation was that these conglomerates can be classified into three different groups, based on their petrographical characteristics, namely:

- The first group, being the poorly-cemented conglomerates, was supported by a carbonate mud (Figure 4.12 A). In general, these conglomerates were rather poorly sorted and characterised by a wide range of clast-sizes. These clasts had a rounded shape and their matrix was characterised by the absence of crystalline calcite cements. The muddy matrix, however, did contain a significant amount of microporosity, as could be observed through fluorescence microscopy (Figure 4.12 E). It were also these micropores that dominate the pore-network of this type of conglomerate, since intergranular pores were nearly absent. Furthermore, in this type of conglomerates veins were rarely observed.
- The second group of conglomerates were classified as the mud-supported conglomerates. In general, these conglomerates were rather similar to the previously described group, however, the matrix of these conglomerates was very fine grained and more cemented in comparison to the poorly-cemented conglomerates. This makes the matrix of this type of conglomerates rather cemented, leading to a lower amount of microporosity. Additionally, these conglomerates were often cross-cutted by several calcite veins (Figure 4.12 B).
- The third group consisted of well-cemented grain-supported conglomerates, with clasts ranging from rounded to sub-angular (Figure 4.12 C & D). It has to be mentioned that larger clasts were often more rounded, in comparison to the smaller ones. Furthermore, these conglomerates were rather well-sorted, leading to a very narrow clast size distribution. The matrix of these conglomerates was made of a crystalline calcite cement, welding all individual grains together (Figure 4.12 C). The dominant type of porosity was intergranular and seemed to be isolated in 2D, due to the presence of the calcite cements. Additionally, secondary porosity was created by the (partial) dissolution of certain grains and shell-fragments. Similar to the mud-supported conglomerates, several veins could be observed within these lithologies (Figure 4.12 C). In general, the calcite within these veins was dull-luminescent, with an exception of a rather thin rim of slightly brighter calcite.

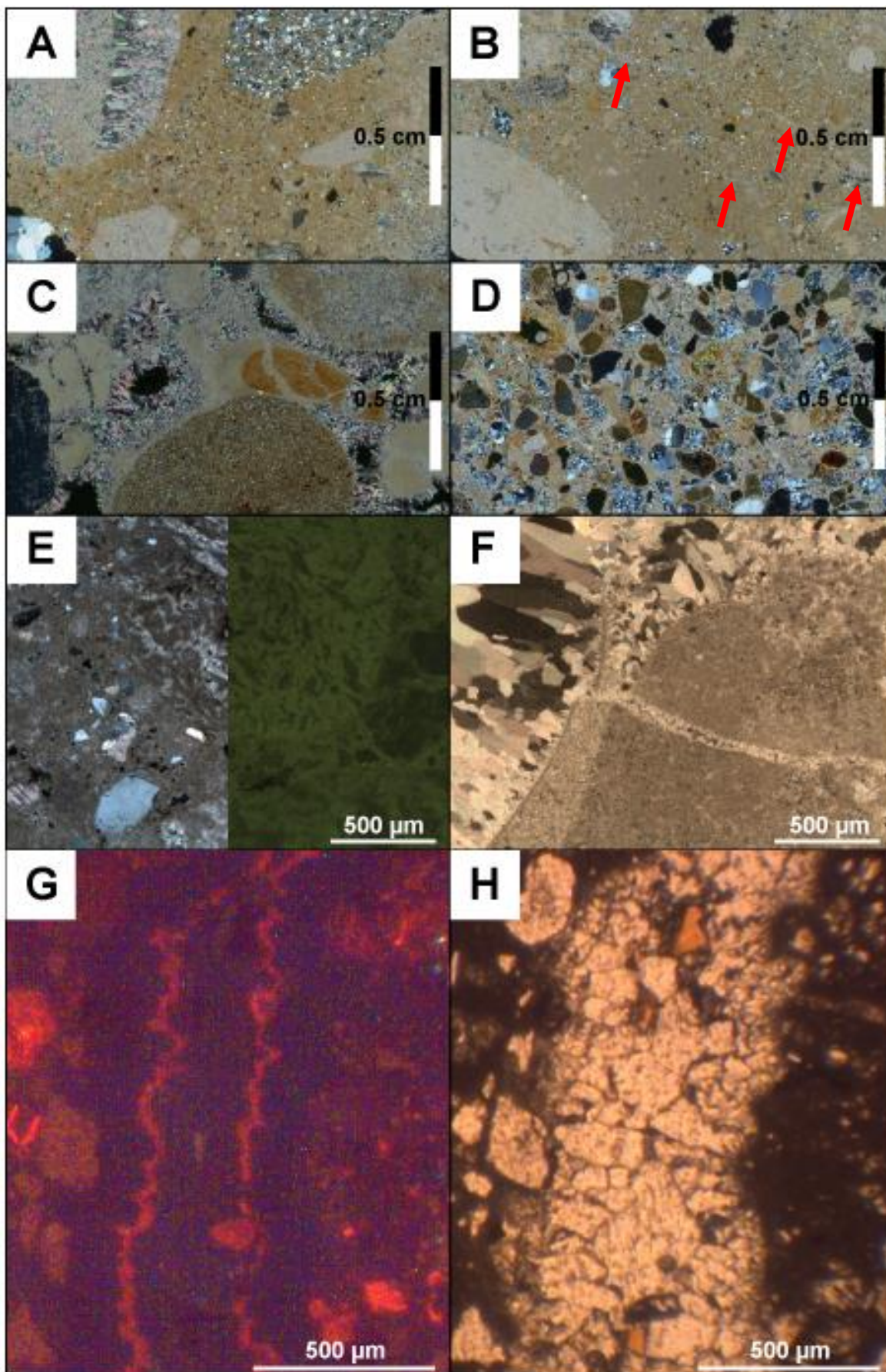
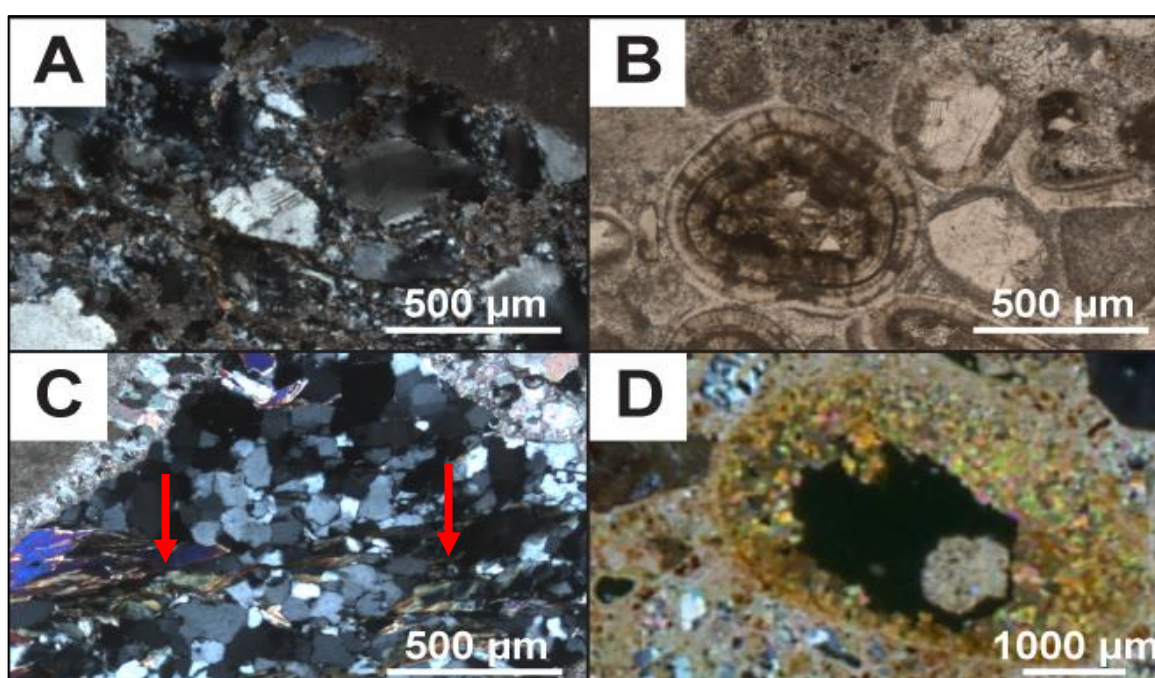


Figure 4.12: Representative pictures of the polygenetic conglomerates, summarizing the characteristics of the three different types. *A* - Poorly-cemented conglomerates with rounded clasts of a varying size (CP). *B* - Mud-supported conglomerates of which the matrix was more cemented and tended to contain veins (red arrows, CP). *C* & *D* - Well-cemented conglomerates, both grain-supported in nature, with a narrow grain size distribution (CP). *E* - Microporosity within the poorly-cemented conglomerates, leading to a continuous network of microscopic pores (CP & FL). *F* - Abundance of crystalline calcite cement, filling up the intergranular pore space within the well-cemented conglomerates (CP). *G* & *H* – Example of a calcite vein, that can be observed in both the mud-supported and well-cemented conglomerates, with a rather thin rim of slightly brighter cement in the otherwise dull cements (CL & PP).

4.2.2.1 *Clast composition*

Due to the heterogeneous nature of the polygenetic conglomerates not all clasts types, that were observed in the field, could be identified in the thin sections. The identified clasts were only briefly discussed, since this study did not specifically focus on the clast types itself. Nevertheless, fragments of both coarse sandstones and greywacke lithologies were observed abundantly. These greywackes were characterised by angular quartz, embedded in a matrix of fine quartz grains, feldspar and micas (Figure 4.13 A). Furthermore, several carbonate lithologies, ranging from travertine to oolitic limestone, were present as well (Figure 4.13 B). Metamorphic lithologies occurred rarely in the thin sections, however, several fragments with a gneiss texture could be identified. These fragments were made of quartz with interlobate grain boundaries, in between which (aligned) micas were present (Figure 4.13 C). Lastly, partly weathered rock fragments, composed of grains with high birefringence colours were observed in certain thin sections. These grains were identified as olivine and possibly orthopyroxene. These small fragments could possibly be identified as periodite (Figure 4.13 D).



Chapter 4 – Results

Figure 4.13: *A* – Greywacke clast, composed of coarse and fine quartz grains, feldspars and micas (XP). *B* – Oolitic carbonate (PP). *C* – Clast with a gneiss texture, composed of quartz with interlobate grain boundaries and aligned micas (red arrow, XP). *D* – Partly weathered clasts, composed of individual grains with high birefringence colours (XP).

4.2.3 Monogenetic breccias

In a thin section, this lithology was characterised by a dominance of intergranular pores in between rather angular clasts. These clasts were dominantly made of travertine and were (sub-)angular in nature (Figure 4.14 *A* & *B*). The clast composition was one of the major differences with respect to the polygenetic conglomerates, since it strongly affected the porosity distribution within this lithology. These travertine clasts were characterised by a significant amount of microporosity, while as this was not the case for most of the clasts of the polygenetic conglomerates (Figure 4.14 *C* & *E*).

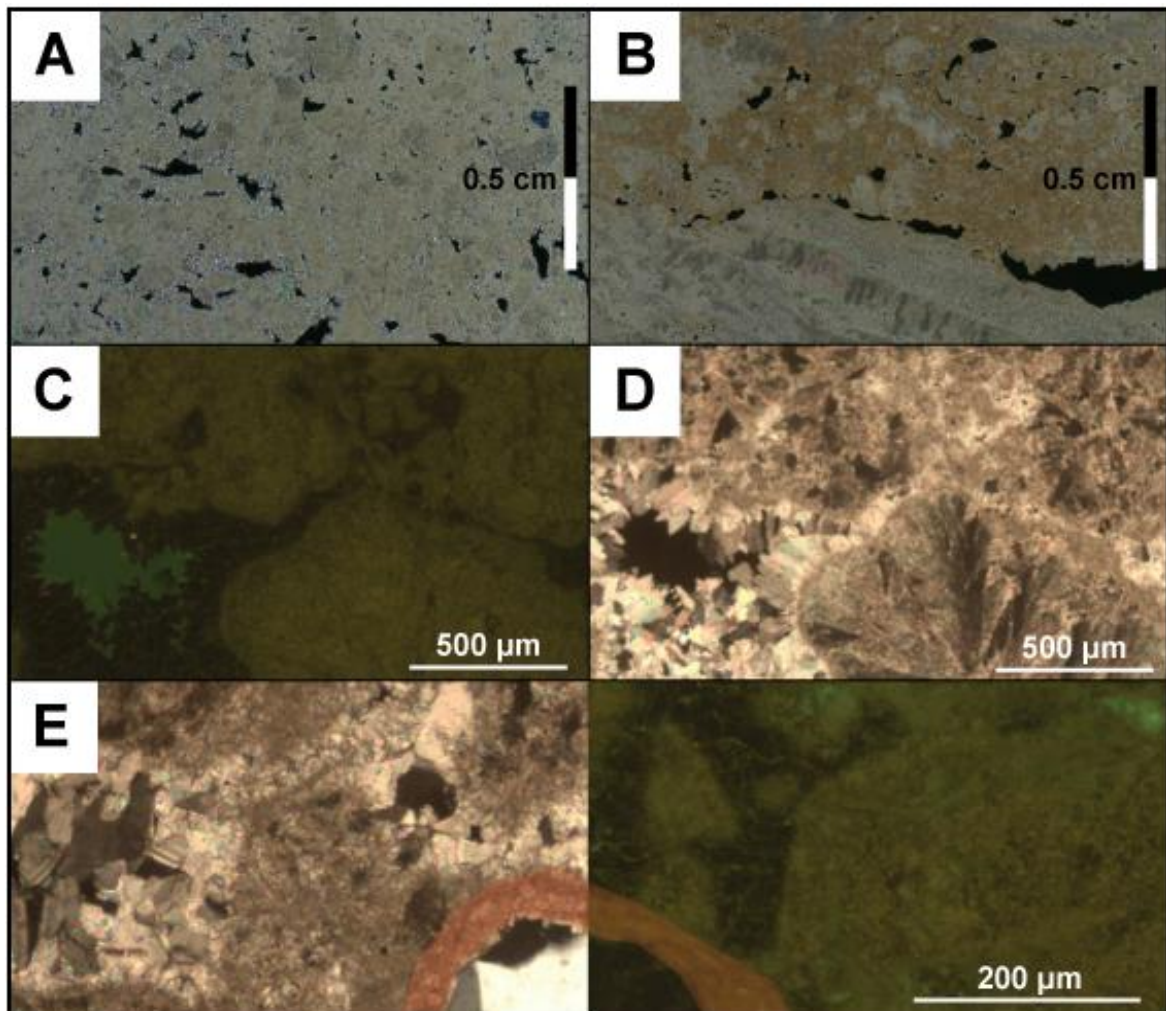


Figure 4.14: *A* & *B* – Two thin sections of the monogenetic breccia facies, highlighting the abundance of angular clast fragments. *C* & *D* – Two detailed picture of this facies, highlighting the abundance of microporosity within the matrix and the clasts and the presence of dogtooth calcite (FL & CP). *E* – A compiled picture (left XP, right FL) of the same part of a thin section, highlighting the presence of a micritic rim (red) around a quartz grain.

The presence of this microporosity, both within the clasts themselves as well as within the matrix, possibly created a well-connected network. Furthermore, some intergranular pores could be observed in between these travertine clasts (Figure 4.14 C, D & F).

In certain cases, the presence of clearly developed equant cements could be observed (Figure 4.14 D). The latter could affect the connection between the matrix and the microporous clasts, leading to a poorly connected pore-network. Additionally, prior to these crystalline calcite cements a micritic phase could be observed, encasing most of these clasts (Figure 4.14 E, red surface).

4.2.4 Gastropod-rich carbonate

In general, this lithology consisted of a crystalline to locally micritic matrix, which was rather impermeable. The porosity was distributed rather heterogeneously on the scale of a thin section, however, most of these pores were isolated in a 2D-planar view (Figure 4.15 A & B). The dominant pore type within this facies was moldic gastropod porosity, with nearly no matrix porosity at all (Figure 4.16 A & B). In general, detritals were rather rare within this lithology and are dominantly belonging to the sand fraction. Furthermore, a remnant part of a gastropod shell was still present in certain thin sections, while commonly the largest part was dissolved (Figure 4.16 A). In certain cases the gastropod shells themselves tended to be micritized (Figure 4.16 C & D). Additionally, a micritic infill could often be observed within these gastropods (Figure 4.16 B). In general, the micrite was restricted to the surface of these gastropod shells, with as exception areas with a dense accumulation of gastropods. Here the matrix was locally made of micrite. Overall, these micritized patches were still embedded in a crystalline and equant calcite matrix. Furthermore, in certain cases, shrub-like morphologies could be observed in the matrix (Figure 4.16 E & F)

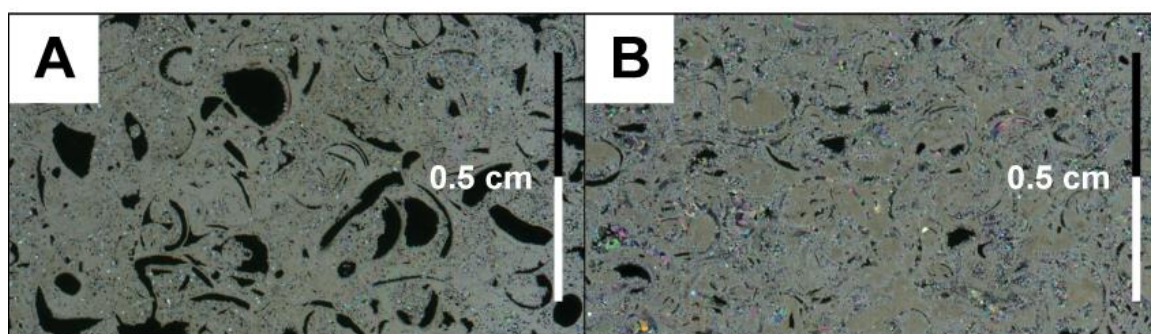


Figure 4.15: A & B - Illustration of the gastropod-rich carbonate lithology. Fabric of this lithology on the scale of a thin section, highlighting the dominance of (isolated) moldic porosity (CP).

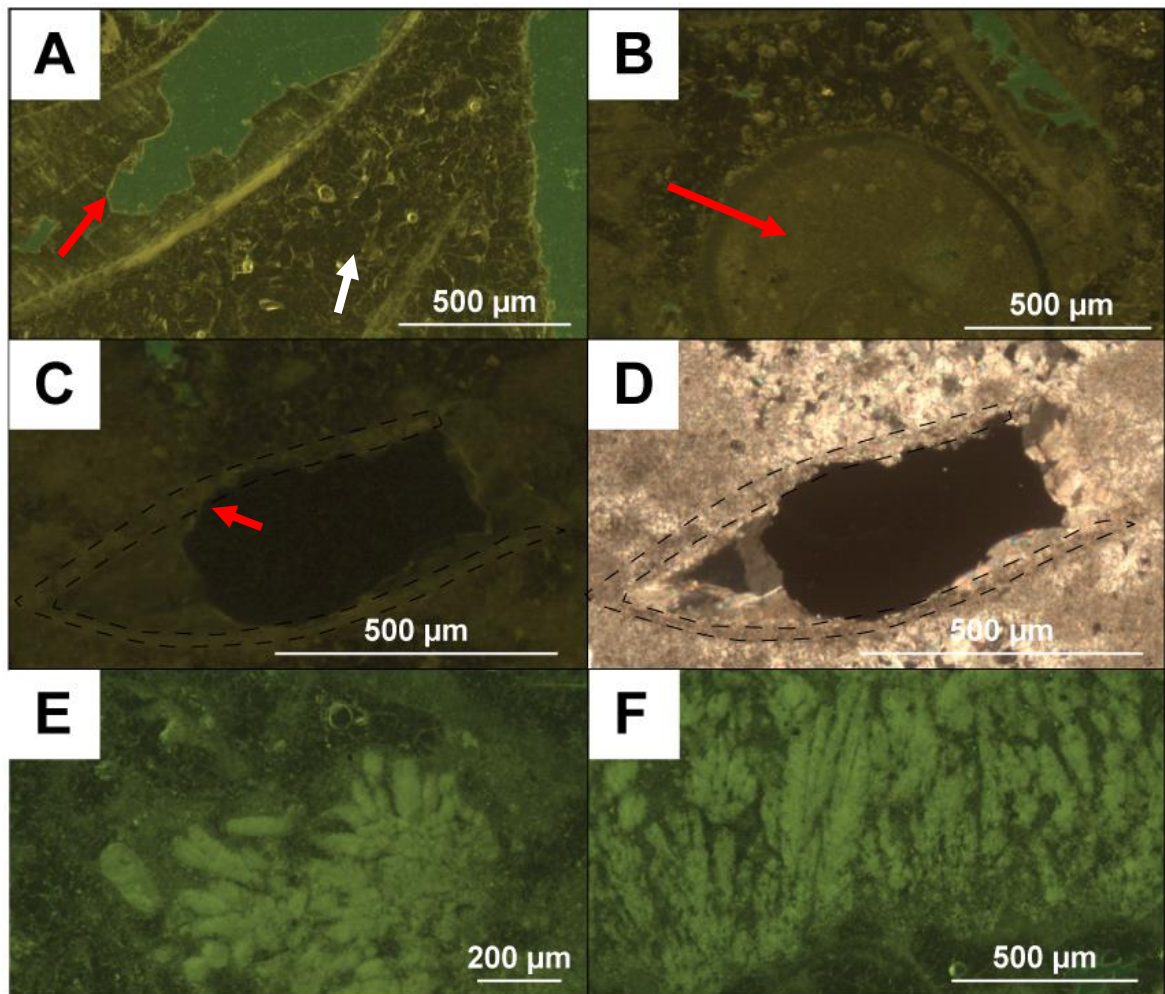


Figure 4.16: *A* - Detailed image of a partly dissolved gastropod shell (red arrow), embedded within a crystalline matrix (white arrow, FL). *B* - Intact gastropod shell with a micritic infill (red arrow, FL). *C* & *D* - Micritized gastropod shell of which the outlines were highlighted by a dashed line (FL & CP). *E* & *F* - Shrub-like structures that are present throughout the gastropod-rich carbonate (FL).

4.2.5 Coquina

The petrographical study of the coquina facies was limited to only one thin section. This lithology was characterised by high porosities (Figure 4.17). The dominant type of porosity was moldic, either due to the dissolution of broken shell fragments, coated grains or quartz grains. The matrix consisted of remnant isopachous cements (blue arrow, Figure 4.17 D). Furthermore, peloids were present as well and were often (partially) dissolved.

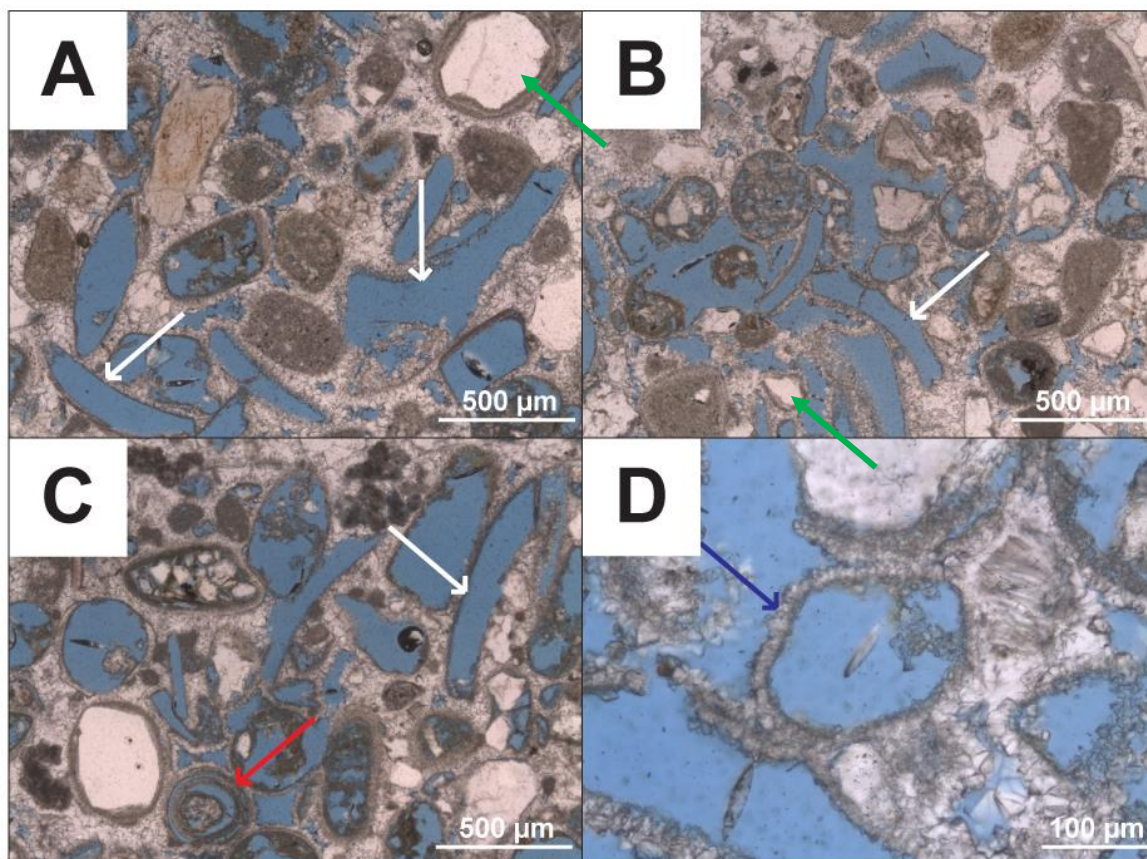


Figure 4.17: A, B & C – Overall fabric of the coquina lithologies, dominated by moldic porosity, originating from the dissolution of broken shell fragments (white arrows), coated grains (red arrow) or quartz grains (green arrows). D – The matrix of this lithology consisted of remnant isopachous cements.

4.2.6 Computed Tomography (CT)

Results of the CT-scans were discussed briefly, with an emphasis on the internal structure of the studied samples. Since all samples were composed of clasts with a varying composition (travertine, quartz, marble, dolomite, ...) it was currently still impossible to clearly model the pores and different clast types.

4.2.6.1 Massive marls

In section 4.1.2 the massive marls, that occurred adjacent to channels filled with polygenetic conglomerates, were described. Within these marls, the presence of reed-like structures could be observed, closely related to the proximity of these channels. Internally these marls were cross-cutted by several of these reed-stems, which occurred in different orientations. The outer part of these reed stems was well-cemented and thus less-porous, however, within these structures elongated voids could be observed (Figure 4.18, black arrows). The matrix contained a significant amount of microporosity and was

characterised by the presence of several open and discontinuous fractures (Figure 4.18, white arrows).

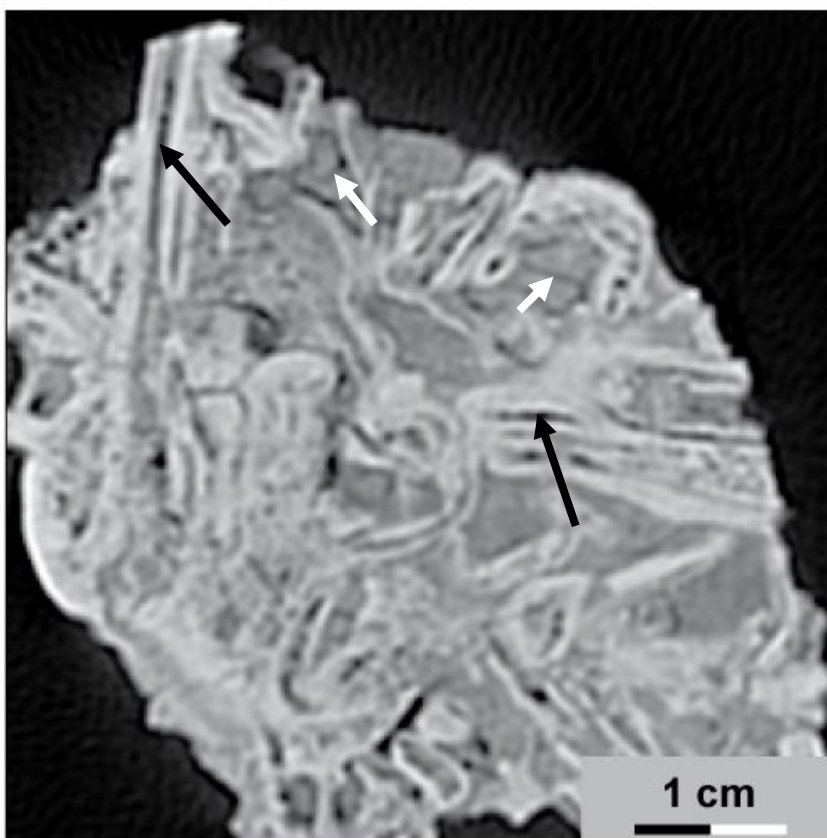


Figure 4.18: Massive marl with presence of reed-like structures. The center of these structures tended to contain elongated voids (black arrows) and open cracks could be observed within the matrix (white arrows).

4.2.6.2 Polygenetic conglomerates

On the CT-scans of these conglomerates, some macroscopic pores could be observed, of which most were located between particles (Figure 4.19 A, black arrows). Furthermore, some voids with similar dimensions and angularities as the neighbouring clasts could be observed as well, classifying them as solution enhanced porosity (Figure 4.19 B, black boxes). The matrix tended to be slightly more porous, especially in comparison to the clasts. This indicated that the matrix might be microporous, as was inferred from microscopy.

The clasts did not seem to be porous at all, meaning that the majority of the pore network was located in between them, either as intergranular or microscopic porosity (Figure 4.19 A & B). Furthermore, these clasts were stacked rather densely, partly due to their (sub-)rounded geometry.

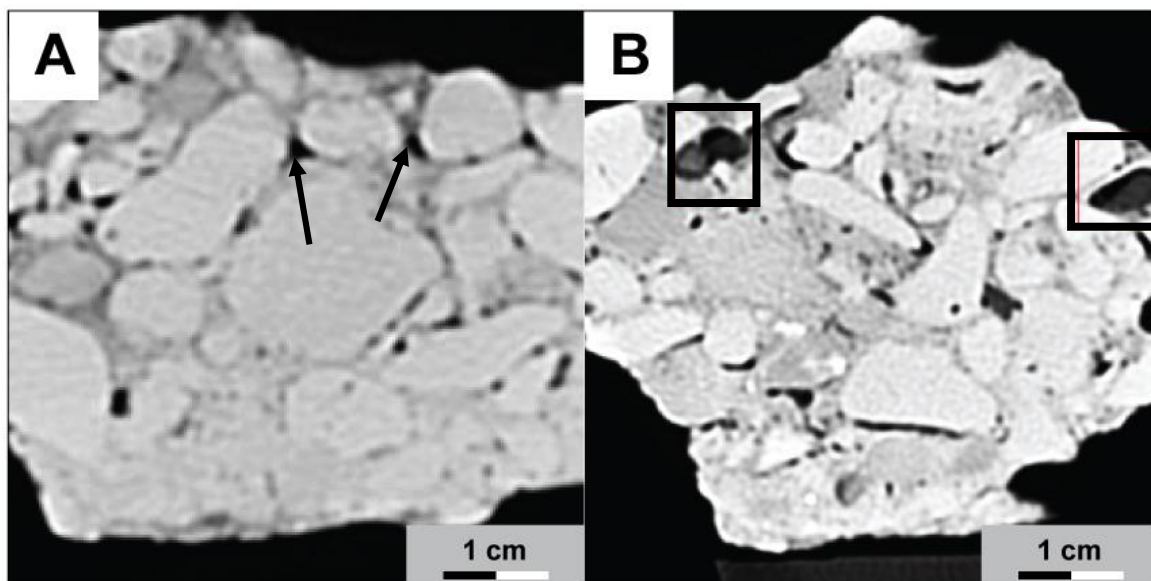


Figure 4.19: *A* – Medical CT images of polygenetic conglomerate. Mud-supported conglomerate with sub-rounded clasts. The macroscopic pores of this sample were restricted to the intergranular pore space (black arrows). *B* – Well-cemented conglomerate, made of elongated and sub-rounded clasts. Both interparticle pores and solution enhanced (black box) pores could be observed.

4.2.6.3 *Tabular sandstones*

The tabular sandstones were characterised by cross-lamination, present throughout the whole sample (Figure 4.20). These laminae were erosive with respect to one another, leading to erosive contacts between different laminae. The lamination translated itself to an alternating porosity distribution, however, the resolution of the resulting scans was not sufficiently high enough to truly confirm this.

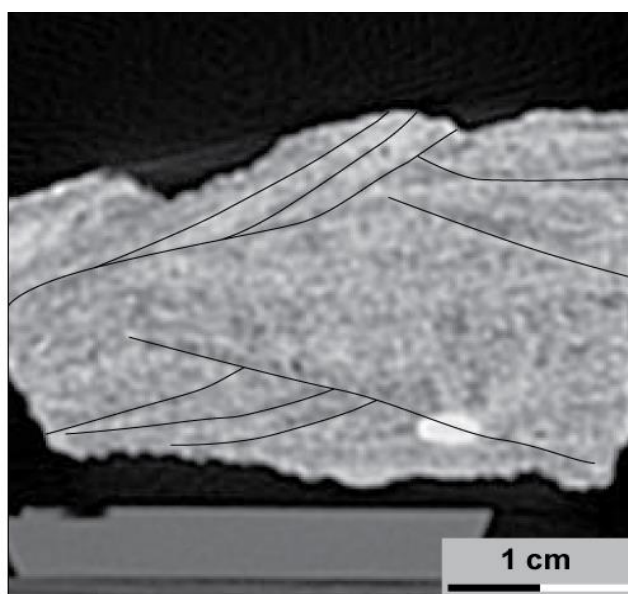


Figure 4.20: Section through tabular sandstone perpendicular to the cross-bedded lamination. Several different laminae were visualized in black, highlighting their erosive nature.

4.2.6.4 *Monogenetic breccia*

The monogenetic breccias did not exhibit a clear internal stacking, as was already observed in the field. On the contrary, the angular clasts were floating within the matrix, often without any clear internal ordering (Figure 4.21 A & B). Furthermore, several open cracks could be noticed in the CT-scans (Figure 4.21 B, black arrow). In general, macroscopic pores were absent, but the matrix itself was rather porous.

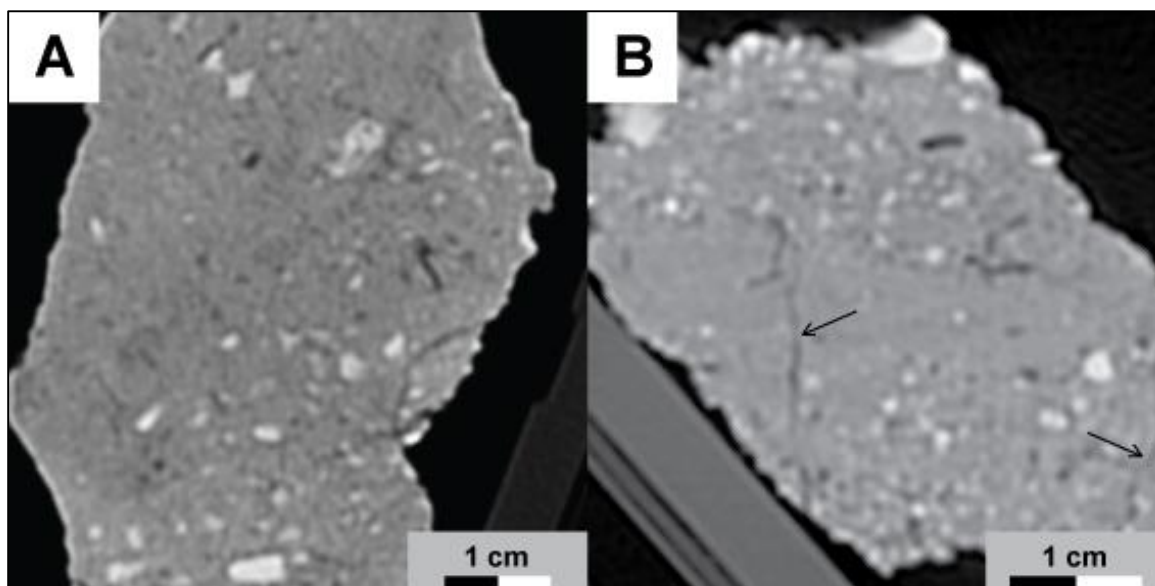


Figure 4.21: Two CT-slices of the monogenetic breccia, which have been visually enhanced in order to increase contrast between clasts and matrix. In certain samples, open cracks could be observed (highlighted by a black arrow, B).

4.2.6.5 *Gastropod-rich carbonate*

The gastropod-rich carbonate was characterised by the presence of moldic porosity. Through CT it was confirmed that most of these pores tended to be isolated and will thus not develop a connected pore-network, at least not at the resolution of the medical CT (Figure 4.22). Furthermore, the distribution of these moldic pores was concentrated within horizontal layers. The matrix of this rock did not seem to contain any other macroscopic porosity and was, in general, rather dense. This confirmed the petrographical observations, which already concluded that the matrix itself was rather non-porous.

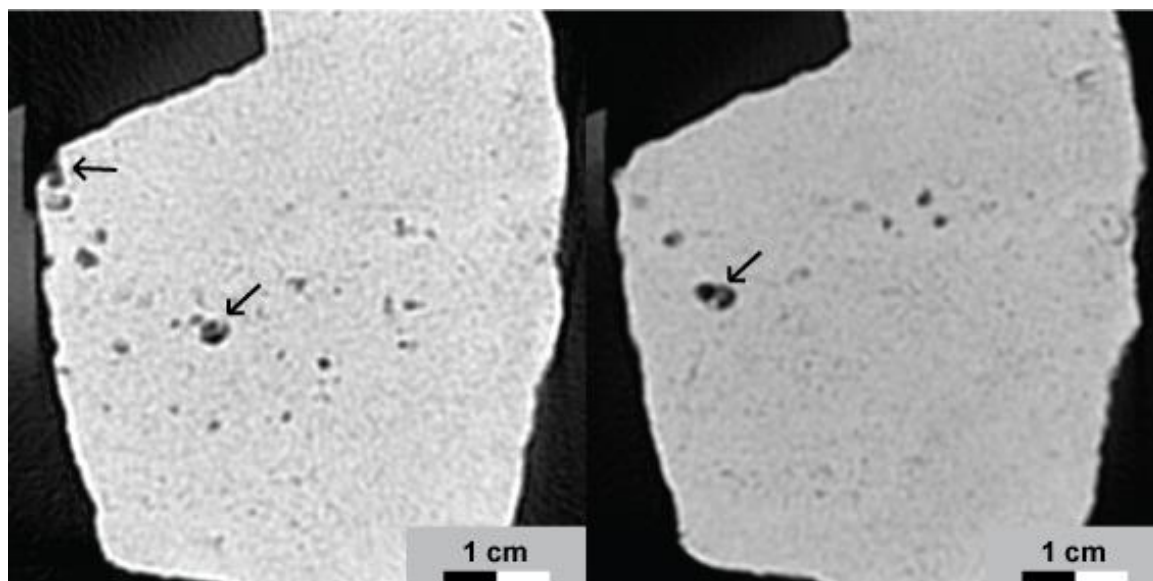


Figure 4.22: Visually enhanced slice of the gastropod facies, where isolated moldic pores (highlighted by a black arrow) are the dominant macroscopic pore-type.

4.3 X-Ray Diffraction (XRD)

This section addresses the results of both the bulk-XRD measurements and the clay-XRD measurements. The diffraction patterns themselves can be found in Appendix F – Bulk XRD diffraction patterns and Appendix G – Bulk XRD diffraction patterns: Laminae.

4.3.1 Bulk XRD: Overall mineralogical composition.

The bulk XRD measurements were used in order to assess the broad (clay) mineralogical composition of the laminated marls. It could be observed that the latter contained higher amounts of calcite (23 - 75%) and possessed a rather elevated amount of quartz as well (with as an exception DE15MV112). Next to calcite and quartz, traces of K-feldspar, plagioclase and dolomite could be detected. The type of clay minerals did not vary significantly in between each of the four sedimentary sequences, as described in 4.1.1

| Sample | Non-carbonates | | | Carbonates | | | Clays |
|-----------|----------------|---------------|---------------|--------------|--------------|---------------------|---------------|
| | Quartz (wt. %) | Kspar (wt. %) | Plag. (wt. %) | Cal. (wt. %) | Dol. (wt. %) | Total carb. (wt. %) | Kaol. (wt. %) |
| DE15MV011 | 43 | 2 | 7 | 22 | 1 | 23 | 3 |
| DE15MV022 | 11 | 3 | 2 | 31 | 8 | 39 | 2 |
| DE15MV067 | 16 | 2 | 4 | 32 | 2 | 34 | 1 |
| DE15MV071 | 18 | 1 | 5 | 43 | 3 | 47 | 1 |
| DE15MV112 | 3 | 0 | 0 | 76 | 3 | 79 | 0 |

| Sample | Clays | | | | | | |
|-----------|--------------------|--------------------|-----------------|---------------------|---------------|---------------------|-----------------|
| | 2:1 Al cl. (wt. %) | 2:1 Fe cl. (wt. %) | Mg-chl. (wt. %) | Tri 2:1 cl. (wt. %) | Musc. (wt. %) | Sum 2:1 cl. (wt. %) | Sum cl. (wt. %) |
| DE15MV011 | 3 | 9 | 4 | 1 | 5 | 12 | 25 |
| DE15MV022 | 0 | 28 | 3 | 3 | 9 | 28 | 44 |
| DE15MV067 | 3 | 24 | 6 | 0.8 | 9 | 27 | 44 |
| DE15MV071 | 0 | 14 | 3 | 0.6 | 10 | 14 | 28 |
| DE15MV112 | 2 | 14 | 1 | 0 | 0 | 17 | 18 |

Table 4-1: Quantitative results of the analysis of the XRD-patterns for all 6 bulk samples (in this table clay is abbreviated as cl., chlorite as chl., muscovite as musc., dolomite as dol., calcite as cal., K-feldspar as Kspar and plagioclase as plag.).

Sedimentary architecture. In this table DE15MV011 and DE15MV022 represented the middle siliciclastic sequence, DE15MV067 and DE15MV071 the upper siliciclastic sequence and DE15MV112 represented the cover siliciclastic sequence. In general, all samples were characterised by the presence of Mg-chlorites, which made up a weight fraction between 1 and 6 wt. %. Additionally muscovite (0 – 10 wt. %), kaolinite (0 – 3 wt. %) and several other clay groups were identified. The detailed mineralogical composition of each sample could be found in Table 4-1.

The lateral variability of the mineralogical composition could be assessed through the comparison of samples DE15MV067 and DE15MV071, which were both taken in the same horizon located in the Cakmak quarry. The XRD analysis indicated that the compositional variability within one layer was rather high. The calcite content ranged from 31 to 40 % and might be due to a different distance with respect to the travertine system, translating in a different degree of cementation. However, the clay-content of this horizon fluctuated as well, where both the chlorite content (0 – 16 wt. %) and muscovite content (13 – 21 wt. %) were displaying significant variations.

4.3.2 Bulk XRD: Specific mineralogical composition of individual laminae within the laminated marls

The specific clay content of several successive laminae in the laminated marl lithotype was assessed, in order to evaluate whether the latter displays systematic mineralogical trends. It has to be mentioned that sometimes within these layers, secondary internal laminations could be observed (as for example in Figure 4.23 C). However, during sample preparation these laminae were homogenized as a whole.

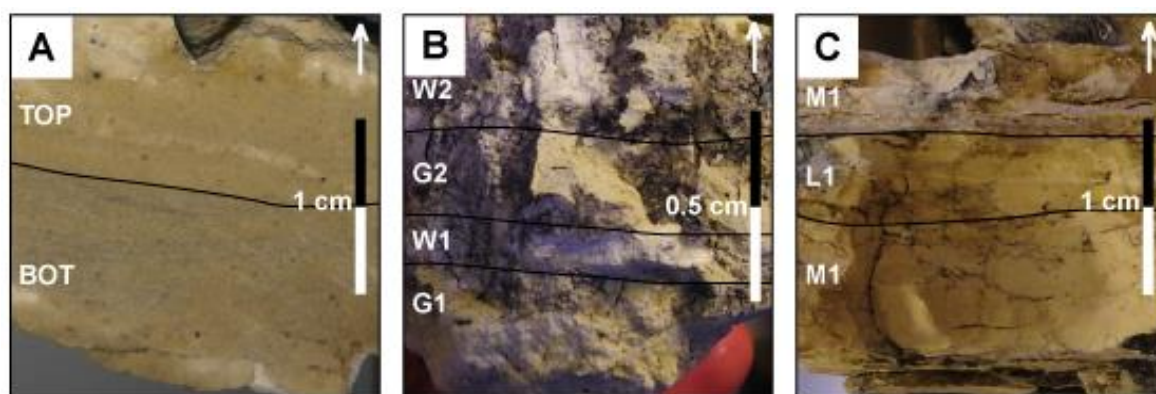


Figure 4.23: Hand samples of DE15MV071 (A), DE15MV068 (B) and DE15MV102 (C). (W = white, G = green, M = massive, L = laminated)

The analysis of the XRD-pattern indicated that there did not seem to be a rhythmic variation with respect to the laminae themselves. An exception was the carbonate-content of these laminae, as could be observed in the mineralogical composition of the laminated

Chapter 4 – Results

marls of Cakmak (Figure 4.23 A). In this sample, the colours of the successive layers were correlated with the clay- and carbonate content, being respectively 22 wt. % and 63 wt. % for the dark bottom layer and 10 wt.% and 68 wt. % for the whiter upper layer. A similar pattern could be observed for DE15MV102 (Table 4-2).

| Sample | Non-carbonates | | | Carbonates | | | Clays |
|--------------|----------------|---------------|---------------|--------------|--------------|---------------------|---------------|
| | Quartz (wt. %) | Kspar (wt. %) | Plag. (wt. %) | Cal. (wt. %) | Dol. (wt. %) | Total carb. (wt. %) | Kaol. (wt. %) |
| DE15MV068G1 | 19 | 0.9 | 11 | 33 | 0 | 33 | 2 |
| DE15MV068G2 | 23 | 1 | 4 | 45 | 0 | 45 | 0.9 |
| DE15MV068C2 | 15 | 7 | 5 | 50 | 0 | 50 | 0.2 |
| DE15MV071BOT | 11 | 1 | 1 | 62 | 1 | 63 | 0.4 |
| DE15MV071TOP | 16 | 2 | 4 | 66 | 2 | 68 | 0 |
| DE15MV102M1 | 13 | 2 | 3 | 38 | 2 | 41 | 1 |
| DE15MV102L1 | 10 | 3 | 3 | 29 | 3 | 32 | 0.7 |
| DE15MV102M2 | 10 | 3 | 3 | 35 | 4 | 39 | 1 |

| Sample | Clays | | | | | | |
|--------------|--------------------|--------------------|-----------------|---------------------|---------------|---------------------|-----------------|
| | 2:1 Al cl. (wt. %) | 2:1 Fe cl. (wt. %) | Mg-chl. (wt. %) | Tri 2:1 cl. (wt. %) | Musc. (wt. %) | Sum 2:1 cl. (wt. %) | Sum cl. (wt. %) |
| DE15MV068G1 | 5 | 23 | 7 | 0 | 0.9 | 28 | 37 |
| DE15MV068G2 | 0.5 | 18 | 3 | 0 | 4 | 19 | 27 |
| DE15MV068C2 | 2 | 10 | 3 | 0 | 9 | 12 | 24 |
| DE15MV071BOT | 0 | 18 | 1 | 0 | 2 | 18 | 22 |
| DE15MV071TOP | 0 | 7 | 0 | 0 | 4 | 7 | 10 |
| DE15MV102M1 | 5 | 21 | 3 | 0 | 11 | 26 | 41 |
| DE15MV102L1 | 6 | 34 | 5 | 0 | 6 | 40 | 52 |
| DE15MV102M2 | 11 | 23 | 4 | 0 | 5 | 34 | 45 |

Table 4-2: Quantitative results for all 8 successive layers, of which the samples can be seen in Figure 4.23. In comparison to Table 4-2, this table represents the mineralogy of a specific lamination. (in this table clay is abbreviated as cl., chlorite as chl., muscovite as musc., dolomite as dol., calcite as cal., K-feldspar as Kspar and plagioclase as plag.).

4.3.3 Clay-specific XRD: Laminated marls

In total six different clay minerals were identified within the laminated marl lithologies. The XRD-patterns, both measured in air-dried and ethylene-glycol saturated conditions, can be found in Appendix H – XRD diffraction patterns: Oriented clay slides.

The presence of both smectite and mixed layer illite-smectite could be noticed, based on the presence of peaks at 9.9 Å & 15.5 Å (air-dried). Both of these clay minerals were already observed within the bulk measurements. The second clay mineral, characterised by a peak for both air-dried as ethylene-glycol saturated, was palygorskite. This clay mineral could not be detected with certainty in the bulk measurements, but was possibly observed in the SEM-pictures. However, in order to truly confirm this, the samples would have to be measured under heated conditions as well. The peak for this mineral should lie at 10.5 Å, however, due to a shift of the XRD-pattern a slight deviation is possible. Lastly, a peak at 7.2 Å indicated the presence of serpentine, kaolinite and chlorite. In order to truly differentiate these peaks, these clay samples would have to be measured under heated conditions. These clay minerals were already observed in the bulk measurements.

Due to the presence of multiple clay minerals, it was difficult to truly quantify the clays present within these samples. At the end it did not seem that either one of the three sequences, that contained the laminated marl lithotype, were characterised by one unique clay assemblage.

4.3.4 Clay-specific XRD: Argillaceous travertine (Bouman, 2016)

The clay minerals, present in the argillaceous travertine lithologies (described by Bouman, 2016), were not entirely the same as the ones in the laminated marl lithologies. The extracted clay content of the paleosol was insufficient and did not yield a good clay-sample. The second sample, which represented a marly horizon, was characterised by the presence of illite-montmorillonite and/or illite-vermiculite and kaolinite and/or chlorite. In contrast with the samples of the laminated marls, palygorskite was not observed. In order to differentiate illite-montmorillonite from illite-vermiculite and kaolinite from chlorite, the samples would have to be measured under heated conditions. The clay content of the marly horizon thus contained similar clay minerals as the laminated marl lithologies. The major difference, however, was the absence of palygorskite. The implications this had for the depositional environment of the laminated marls, are discussed in the discussion chapter.

4.4 Total Organic Carbon (TOC)

In total 11 samples were prepared in order to determine the amount of organic carbon and nitrogen that was present. In general, the TOC-values were rather low, ranging from 0.08 – 0.31 wt. %. However, the latter were still sufficiently high to be detected by the elemental analyser. With an exception of the laminated marls in the quarry of Cakmak, no clear variation of the carbon-content could be observed between successive layers. Furthermore, the nitrogen-content was even lower, with values ranging between 0.01 – 0.05 wt. %.

At last the C/N ratio was measured as well, which varies between 3.07 – 17.73. This ratio seemed to vary systematically for successive layers, as for example for DE15MV068, DE15MV071 and DE15MV102 (Table 4-3).

Chapter 4 – Results

| Samples | Mass | | Weight fraction | | Ratio | |
|--------------|-------------|--------|-----------------|-----------|-----------|-------|
| | sample (mg) | N (mg) | C (mg) | N (wt. %) | C (wt. %) | C/N |
| DE15MV022 | 20.192 | 0.006 | 0.023 | 0.03 | 0.12 | 4.08 |
| DE15MV067 | 18.965 | 0.005 | 0.019 | 0.02 | 0.10 | 4.24 |
| DE15MV068G1 | 21.879 | 0.004 | 0.018 | 0.02 | 0.08 | 4.97 |
| DE15MV068C2 | 19.963 | 0.004 | 0.017 | 0.02 | 0.09 | 3.85 |
| DE15MV068G2 | 21.107 | 0.005 | 0.022 | 0.02 | 0.11 | 4.55 |
| DE15MV071TOP | 19.139 | 0.003 | 0.028 | 0.01 | 0.14 | 10.26 |
| DE15MV071BOT | 20.413 | 0.004 | 0.062 | 0.02 | 0.31 | 17.73 |
| DE15MV102M1 | 20.083 | 0.008 | 0.036 | 0.04 | 0.18 | 4.76 |
| DE15MV102L1 | 19.497 | 0.006 | 0.019 | 0.03 | 0.10 | 3.07 |
| DE15MV102M2 | 18.824 | 0.006 | 0.019 | 0.03 | 0.10 | 3.46 |
| DE15MV112 | 21.620 | 0.010 | 0.044 | 0.05 | 0.20 | 4.37 |

Table 4-3: The results of the elemental analyzer for nitrogen and carbon and the measured C/N ratio.

4.5 Carbonate content

The data regarding the carbonate content of each sample can be found in table 4-4. In general, the systematic variability was rather low, with an exception for sample DE15MV068. These results could be used in order to evaluate the accuracy of the XRD-measurements.

As can be seen in Table 4-4, the XRD analyses were generally underestimating the true carbonate content. On average, the carbonate content within the samples was underestimated by 5.5 %.

| Samples | Mass | | Weight fraction | | | Difference (%) |
|--------------|------------------|------------------------|--------------------------------|----------------------------|--------------------------------|----------------|
| | Initial mass (g) | Non-carbonate mass (g) | Non-carbonate fraction (wt. %) | Carbonate fraction (wt. %) | Carbonate fraction XRD (wt. %) | |
| DE15MV022 | 10.01 | 5.25 | 52.4% | 47.6% | 39% | 8.6% |
| DE15MV067 | 10.00 | 5.61 | 56.1% | 43.9% | 34% | 9.9% |
| DE15MV068G1 | 10.00 | 5.82 | 58.2% | 41.8% | 33% | 8.8% |
| DE15MV068G2 | 10.01 | 5.33 | 53.3% | 46.7% | 45% | 1.7% |
| DE15MV068C2 | 10.01 | 4.48 | 44.8% | 55.2% | 50% | 5.2% |
| DE15MV071TOP | 10.01 | 2.73 | 27.3% | 72.7% | 63% | 9.7% |
| DE15MV071BOT | 10.00 | 2.69 | 26.9% | 73.1% | 68% | 5.1% |
| DE15MV102M1 | 10.00 | 5.15 | 51.5% | 48.5% | 41% | 7.5% |
| DE15MV102L1 | 10.01 | 6.03 | 60.3% | 39.7% | 31% | 8.7% |
| DE15MV102M2 | 10.00 | 6.80 | 68.0% | 32.0% | 39% | -7.0% |
| DE15MV112 | 9.97 | 1.88 | 18.8% | 81.2% | 79% | 2.2% |

Table 4-4: The results of the carbonate fraction and the non-carbonate fraction of the selected samples (as determined by geochemical analysis). The carbonate content, as was determined by XRD, is presented as well.

4.6 Grain size analysis

The result of the Grain Size Distribution (GSD) analysis was discussed within the size grades of gravel, as defined by Blair & McPherson (1999). This classification focuses on particles with a grain size larger than 2 mm (Blair & McPherson, 1999). The GSD-charts of the unconsolidated conglomerates are characterised by an abundance of granules and pebbles, respectively clasts with a grain size from 2 mm – 4 mm and from 4 mm – 64 mm. The latter could make up to 41 wt. % of the conglomerates (Figure 4.24).

For this procedure, different types of conglomerates were analysed, including microconglomerates. This explains the curve of sample DE15MV112, which was dominated by particles with a grain size between 0.5 – 0.125 mm (green). In general, all samples were bimodal in nature, meaning that two different grain size classes could be observed. The first class was characterised by particles with size above 2 mm. The latter represented the pebbles and granules, acting as the framework of the conglomerate. The second class was less pronounced and consisted of grains, ranging between 2 – 0.063 mm. The latter represented the matrix, present between the larger conglomerate clasts.

During the analysis itself, it was observed that the polygenetic composition on the one hand was mainly limited to the grain size class with particles between 2 and 64 mm. The matrix on the other hand consisted dominantly of quartz grains.

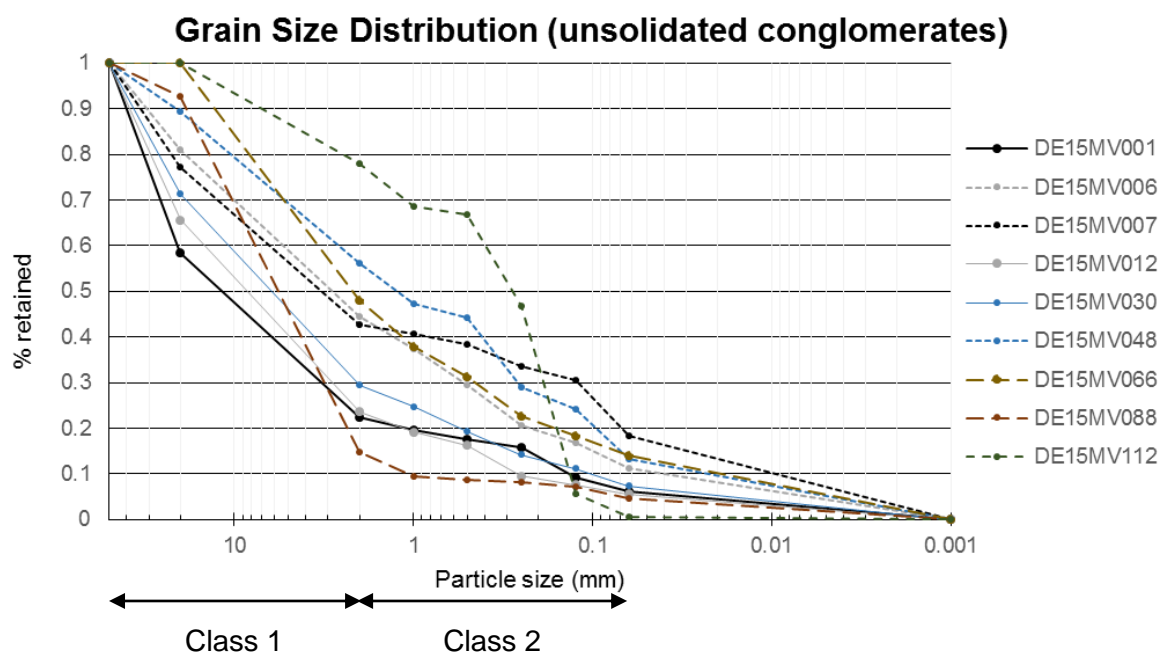


Figure 4.24: Grain-Size distribution graphs for nine unconsolidated conglomerates.

4.7 Geochemical trace and major element analysis

The results of the ICP-OES elemental analysis, associated with their detection limit, are discussed within this section.

4.7.1 Detection limit

The detection limit is defined by McNaught A.D. & Wilkinson A. (1997) as the sum of the mean concentration – *of a certain element* – in a blank with 3 times the standard deviation of the same element. In general, the mean concentration in the blank solution approached zero, reducing the formula in most cases to 3 times the standard deviation of a repetitive measurement. The concentration of all samples lied above the detection limit, which is rather low in most cases. An exception, however, was the detection limit of Ca, which was 25000 µg/g. The elevated detection limit for Ca was a consequence off a continuous decreasing Ca-content within the reference sample, leading to a high standard deviation for the repetitive measurement. This was most likely due to a faulty measurement by the machine itself, since the reference sample was homogenized. Based upon the detection limit of other elements, it was concluded that in general the analysis was executed correctly, meaning that the results could be trusted (Vassilieva, pers. communication). The detection limit for each element was plotted in Figure 4.25 as a transparent grey area.

4.7.2 Results

The results of the ICP-OES analyses can be found in Appendix I – ICP-OES results. For each element a correlative scatterplot was made with all the other measured elements, in order to deduce possible relationships between elements.

4.7.2.1 Abundance of each element

For all samples Ca was the most abundant element, with concentrations of up to 28.70 wt.%. Other major elements were Fe, Al, Mg, K, Na and Ti. Furthermore, the Ni-content of these lacustrine facies was elevated, with concentrations up to 889 ppm. A systematic variation in successive laminae could not be observed. An exception to this rule were the laminated marls that were observed in the quarry of Cakmak. For these deposits, two successive layers were characterised by a significant difference in Fe-, Mg-, Na-, Ni-, Mn-, P-, Cr-, Ba-content. It were thus especially the trace elements that expressed the geochemical variance of different successive layers.

4.7.2.2 Correlations between elements

With regard to the regression analyses, two different groups could be observed. The first one consisted of Sr, Ca and to a certain level S. The second group consisted of Fe, Al, Mg, K, Na, Ti, Ni, Mn, P, Cr, Ba, V, Zn, Co, Rb, Li, Cu, Pb and As.

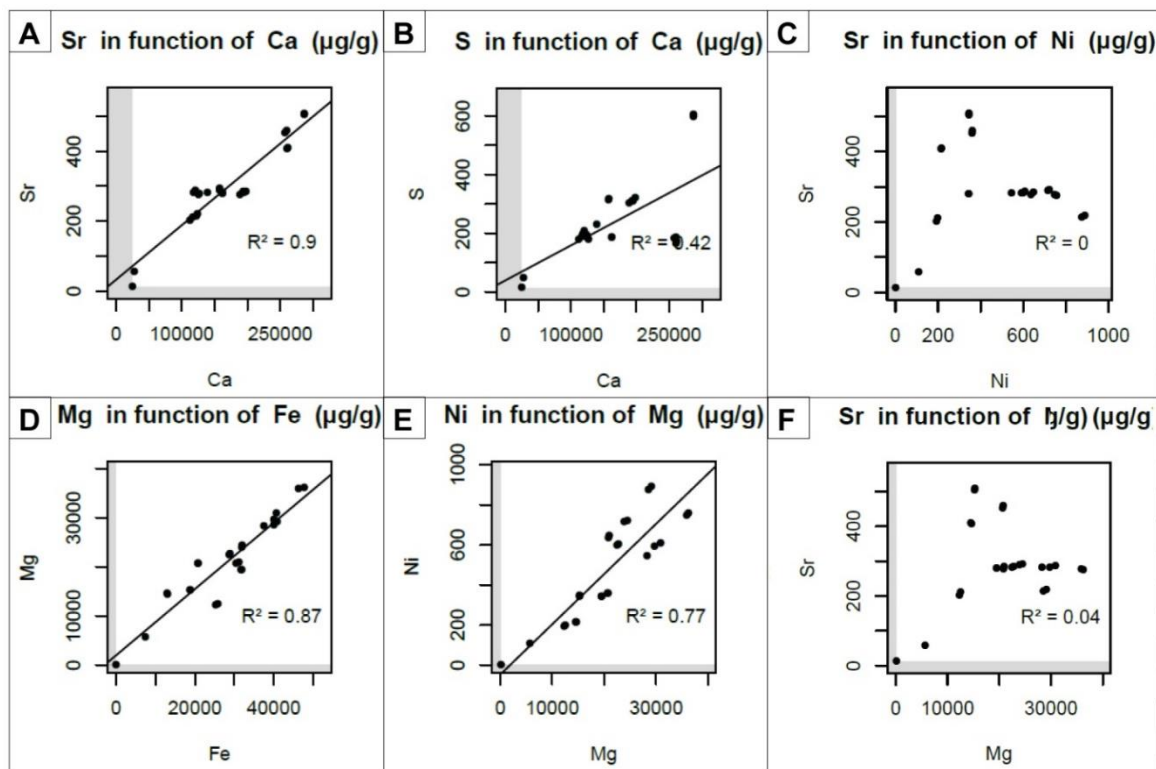


Figure 4.25: Scatterplots for the elements of Sr-Ca, S-Ca, Mg-Fe and Ni-Mg, all expressed in µg/g. A & B – The first group of elements, visualising the correlation between Ca, Sr and S. D & E – The second group of elements, as an illustrative example of the correlation between Mg – Fe & Ni – Mg. E & F - The elements of the first group do not tend to correlate at all with the elements of the second group.

Illustrative plots of these positive correlations can be found in Figure 4.25. In the latter plots A & B are visualizing the positive correlation between Sr – Ca and S – Ca, of which both concentrations were linked to one another. The correlation between the second group of elements is visualized in Figure 4.25 (plots D & E). Here, plots of Mg-Fe and Mg-Ni, which were characterised by a strong positive correlation, can be observed ($R^2 = 0.87$ & $R^2 = 0.77$ respectively). The absence of any regular correlation with Sr and any of the elements of the second group (in this specific case Ni and Mg) is visualized in Figure 4.25 (plots C & F). Similar correlations could be observed for both Ca and S. It thus seemed that the concentration of any element of group one was independent from the concentration of an element of group 2. This could clearly be seen in figure 4.25, where the concentration of Sr remained nearly constant with changing Ni and Mg concentrations.

4.8 SketchUp Pro

The resulting SketchUp Pro model lead to a correct, 3 dimensional, visualisation of the studied outcrops, respecting the metric ratios and angles as they were observed in the field, of which an overview can be found in Figure 4.26. This model can be found on CD 1 – Ballik model.

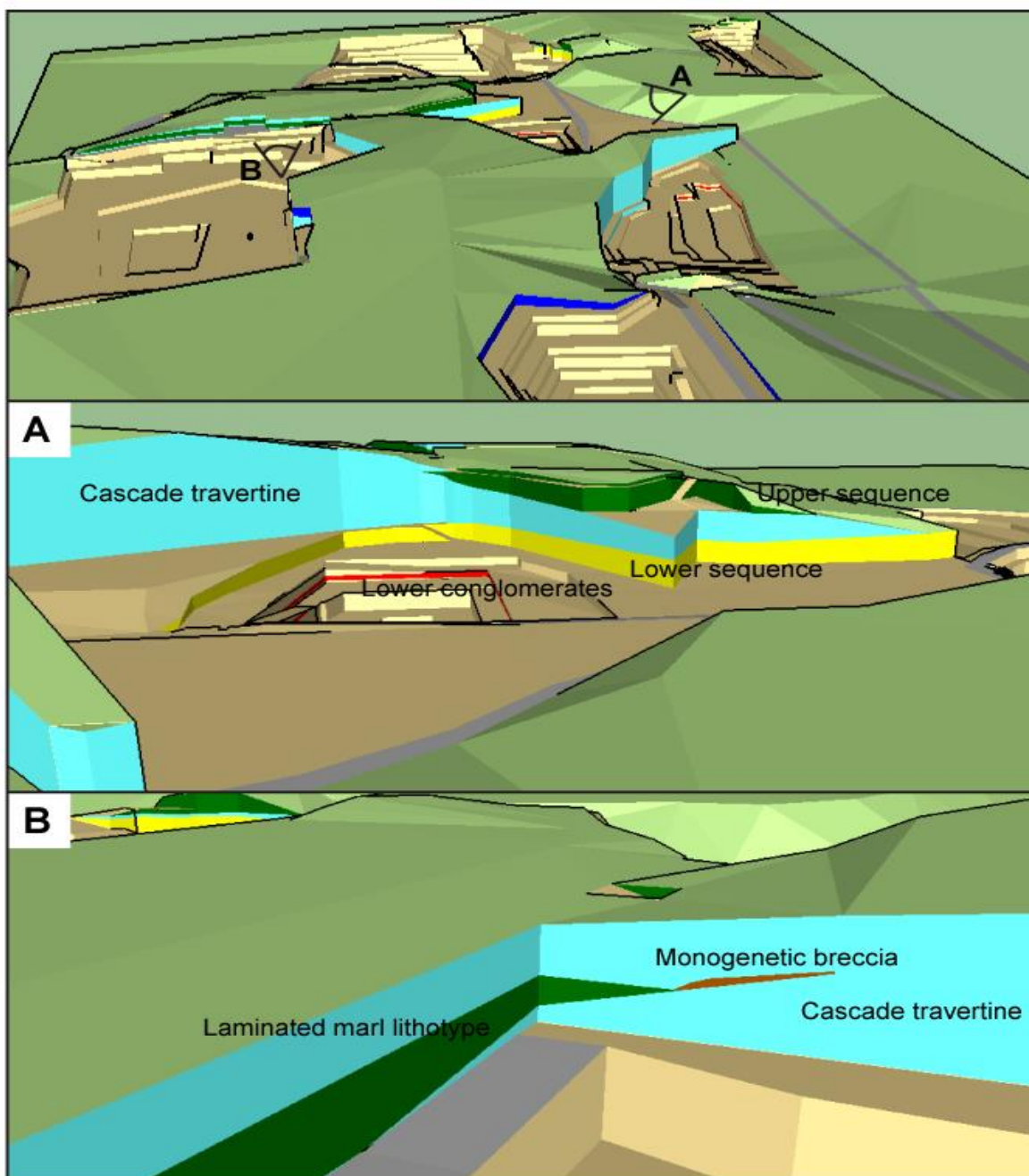


Figure 4.26: Overview of the model in SketchUp Pro, visualizing the distribution of all 4 sequences (lower conglomerates = red, lower siliciclastic unit = yellow, middle siliciclastic unit = green & cover unit = dark blue). A – Detailed section of the Faber quarry, highlighting the disappearance of the cascade travertine (cyan blue) towards the west and the on-lap of the laminated marls (green) on the travertine dome. C – Detailed section of the Cakmak Quarry, highlighting the spatial association of the monogenetic breccias with the cascade travertine and the laminated marl lithotype.

4.9 Reservoir characteristics

The results of the petrophysical measurements and of the image analysis are presented below.

4.9.1 Specific gas permeability and helium porosimetry

This section mainly focuses on the correlation of the empirical Klinkenberg corrected horizontal permeability with the ambient - *open* - helium porosity. The complete data set can be found in Appendix J – Porosity and permeability measurements.

In total, the porosity and permeability were assessed for four different lithologies, excluding the marls and tabular sandstones. Porosity ranged from 5.8 % to 39.3 % and permeability varied between 0.02 – 3035 mD. The polygenetic conglomerates are represented by its three subdivisions, while as the monogenetic breccia, gastropod-rich carbonate and coquina are kept as one group (Figure 4.27).

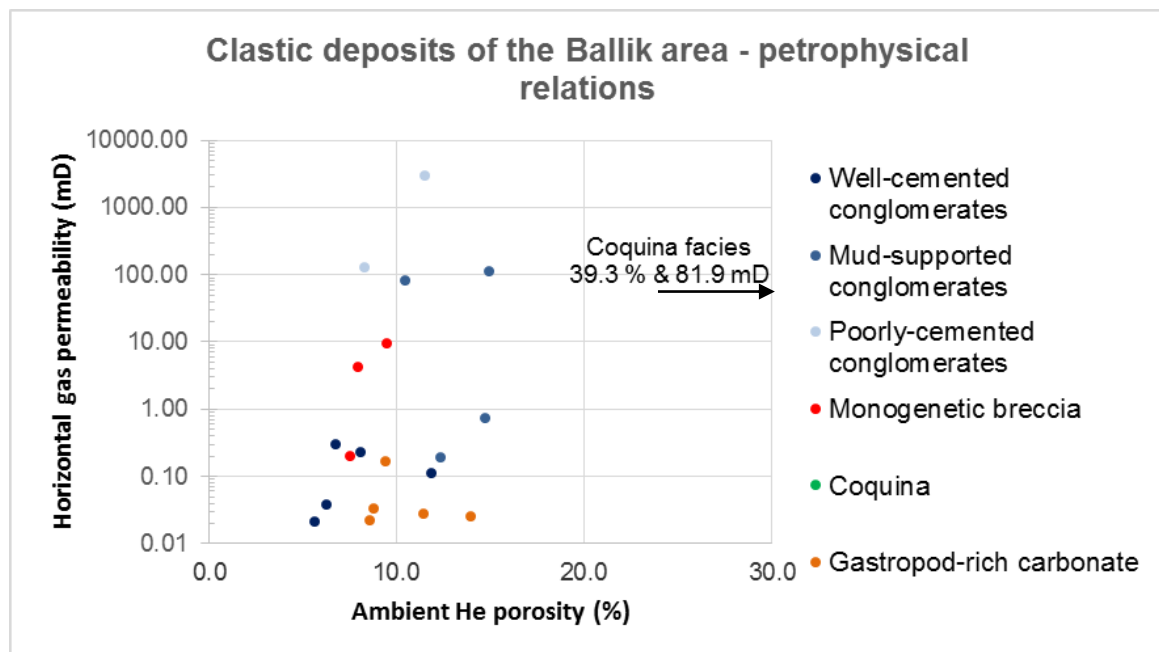


Figure 4.27: Measured ambient He-porosity (%) and empirical Klinkenberg corrected horizontal permeability (mD), plotted on a semi-logarithmic plot. Polygenetic conglomerates are presented based on its three subdivisions and are characterised by a semi-exponential relation between porosity and permeability. Monogenic breccias tend to be characterised by similar poroperm values as the mud-supported conglomerates. Permeability values of the gastropod-rich carbonate are rather low, while as its porosity is elevated. Poroperm values of the coquina lithology is the highest of all detrital deposits, however, only one data-point is available.

In general, a clear trend, regarding the permeability (and to a lesser extend porosity), could be observed for the three types of polygenetic conglomerates. The ambient helium porosity was nearly similar for both the poorly-cemented and mud-supported conglomerates, however, they were characterised by a low permeability. The well-cemented conglomerates were characterised by a slightly lower porosity in comparison to the loose conglomerate and more importantly, a very low permeability (0.02 – 0.45 mD). The mud-supported conglomerates tended to have higher permeability values, ranging between 0.19 – 113 mD. Lastly the poorly-cemented conglomerates were characterised by the highest permeabilities (131 – 3035 mD). The monogenetic breccias were characterised by similar ambient porosity as the polygenetic conglomerates (7.5 – 9.5 %) and permeability values that ranged between 0.21 – 9.45 mD. A weak exponential correlation, between the ambient helium-porosity and corrected permeability, can be observed for all of these samples (Figure 4.27).

The gastropod-rich carbonate was characterised by low permeability values, ranging between 0.04 – 0.26 mD. This in contrast to the porosity of this lithology, which was rather elevated in comparison to the well-cemented conglomerates (8.5 – 14 %). In general, the permeability remained more or less constant, while porosity values vary. The coquina lithology was only characterised by one measurement, making the data not truly representative for this lithology. Overall, additional measurements have to be carried out, in order to truly test the correlation and range of poroperm values for the detrital deposits in the Ballık-area.

4.9.2 Image analysis

In general, the 2D-porosity values (after upscaling) vary significantly from the empirically measured ambient He-porosity (Table 4-5) . The monogenetic breccias were an exception, with porosity values that averaged around the measured ambient He-porosity. Additionally the 2D-porosity in the well-cemented conglomerates underestimated the ambient He-porosity.

The porosity estimations trough image analysis for the laminated marl-facies ranged from 4.1 vol. % to 19.4 vol. %. For the mud-supported conglomerates the image analysis was strongly underestimating the total ambient porosity. Lastly, the porosity estimations for the gastropod-rich carbonate lithologies were rather elevated in comparison to the ambient He-porosity, overestimating the porosity measured porosity by a factor of 4. This overestimation indicated that in this lithology, isolated three-dimensional pores were rather common.

Chapter 4 – Results

| Lithology | Thin section | Porosity | | |
|---------------------------|--------------|----------------------|------------------------------|----------------|
| | | 2D-porosity (Area %) | Ambient He porosity (Vol. %) | Difference (%) |
| Layered marl | | | | |
| | DE15MV009 | 4.1 | n.d. | n.d. |
| | DE15MV010 | 8.4 | n.d. | n.d. |
| | DE15MV041 | 7.6 | n.d. | n.d. |
| | DE15MV067 | 19.3 | n.d. | n.d. |
| | DE15MV112 | 7.7 | n.d. | n.d. |
| Conglomerates | | | | |
| <i>Well-cemented</i> | DE15MV043 | 4.0 | 5.6 | -28.8 |
| <i>Mud-supported</i> | DE15MV044 | 2.5 | 14.7 | -83.1 |
| <i>Well-cemented</i> | DE15MV092 | 6.0 | n.d. | n.d. |
| <i>Poorly-cemented</i> | DE15MV096 | 13.1 | 8.3 | 58.0 |
| <i>Well-cemented</i> | DE15MV097 | 2.2 | n.d. | n.d. |
| Monomict Breccia | | | | |
| | DE15MV108 | 8.1 | 7.5 | 7.6 |
| | DE15MV109 | 7.0 | 9.5 | -26.7 |
| Gastropod-rich travertine | | | | |
| | DE15MV104 | 17.5 | n.d. | n.d. |
| | DE15MV105 | 27.2 | n.d. | n.d. |
| | DE15MV106 | 15.8 | 8.5 | 85.4 |
| | DE15MV107 | 11.3 | 10.1 | 12.0 |

Table 4-5: Comparison between the 2D-porosity estimates (image analysis) and the open 3D-porosity measurements (He-porosity). The difference between both techniques is expressed in percent. An underestimation through image analysis will lead to a negative difference, while as an overestimation leads to a positive percentage.

Chapter 5

Discussion

Within this chapter, the acquired results are interpreted in order to provide conclusive answers to the objectives of this research.

5.1 Facies classification

The results of several methods are integrated in order to work out a facies interpretation of the detrital deposits in the Ballık area. In total, five different facies were differentiated, being the lacustrine, fluvial, debris-flow, gastropod and coquina facies.

5.1.1 Lacustrine facies

The laminated marl lithotype was observed in all quarries. Its setting is placed within the context of a simplified depositional model, in order to explain all specific observations (e.g. zoned calcite grains, geochemical composition, laminated nature, ...) associated with these type of deposits.

5.1.1.1 Depositional setting

The laminated marls were located in a paleolow, often bordering the travertine dome itself. The areal extent of this facies, together with the presence of lateral continuous laminations, is indicating that deposition took place over a rather large area. The presence of intact ostracods and fragile algal structures implied that the depositional environment itself was rather calm. Furthermore, the rhythmic alternating laminae had similar visual characteristics as varves, however, the laminations in the Ballık area were rather thick (Boehrer & Schultze 2008; Zolitschka et al., 2015). In general, laminae in varve deposits have a thickness of several millimetres, while as the laminations in the Ballık area could have a thickness up to several centimetres. This is an indicator for a rather elevated sedimentation rate within these lakes, in comparison to (for example) polar lakes (Zolitschka et al., 2015).

5.1.1.2 *Depositional model*

In the laminated marls palygorskite was observed by XRD, however, the resolution of the SEM was not sufficiently high enough to visually confirm the presence of this mineral with great certainty. Nevertheless, this clay mineral is considered to be a tracer for arid conditions (Rodas et al., 1994; Xie et al., 2013). Botha & Hughes (1992) even suggested that palygorskite forms in sub-aerially exposed lacustrine sediments at the margin of a lake. The presence of palygorskite thus suggests that these sediments are deposited in an arid, and possibly evaporitic, environment.

Furthermore, the depositional model has to explain the presence of the alternating laminae. Organic matter did not act as a controlling parameter with regard to the lamination itself, as was confirmed by TOC-measurements. This in contrast to the carbonate- and clay-content, which varied systematically between successive laminations. Depending on whether a lamination was dominated by either the carbonate- or clay content, it will be characterised by a whitish or rather greenish colour. Furthermore, it was observed that most of these clay minerals were detrital in origin (as for example kaolinite, chlorite, muscovite, ...), indicating that the detrital influx varied systematically during the deposition of these sediments (4.2.1 Laminated marls). Additionally, the laminations were very well preserved. This requires the absence of any wave activity (cf. intact ostracods) and any benthic organisms (low TOC-values and absence of bioturbations). Nevertheless, oxidized root traces could be observed within certain parts of these deposits. All of these observations can be incorporated in two different depositional models, both giving a possible explanation for the laminated nature of these deposits. Both models consider that the non-luminescent calcite nuclei (described in 4.1.1 on page 28), observed in the lacustrine facies, were eroded from the travertine dome itself (Figure 5.1). The alternation of laminae, with either packstone or wackestone fabrics, implies that the supply of these calcite nuclei varies periodically

i) Stratification during summer

This model suggests that the packstone laminae formed during spring, when an increased run-off (associated with a period of increased precipitation) lead to an increased supply of non-luminescent calcite grains (corresponding to the calcite nuclei). The wackestone laminae are more likely to form when the lake waters are generally undisturbed. This might happen during summer, when thermal stratification might occur due to the heating of the surface waters (Figure 5.1 A). During this stratification, the clay fraction within the lake waters can settle down and give rise to the formation of wackestone laminae (Boehrer & Schultze, 2008).

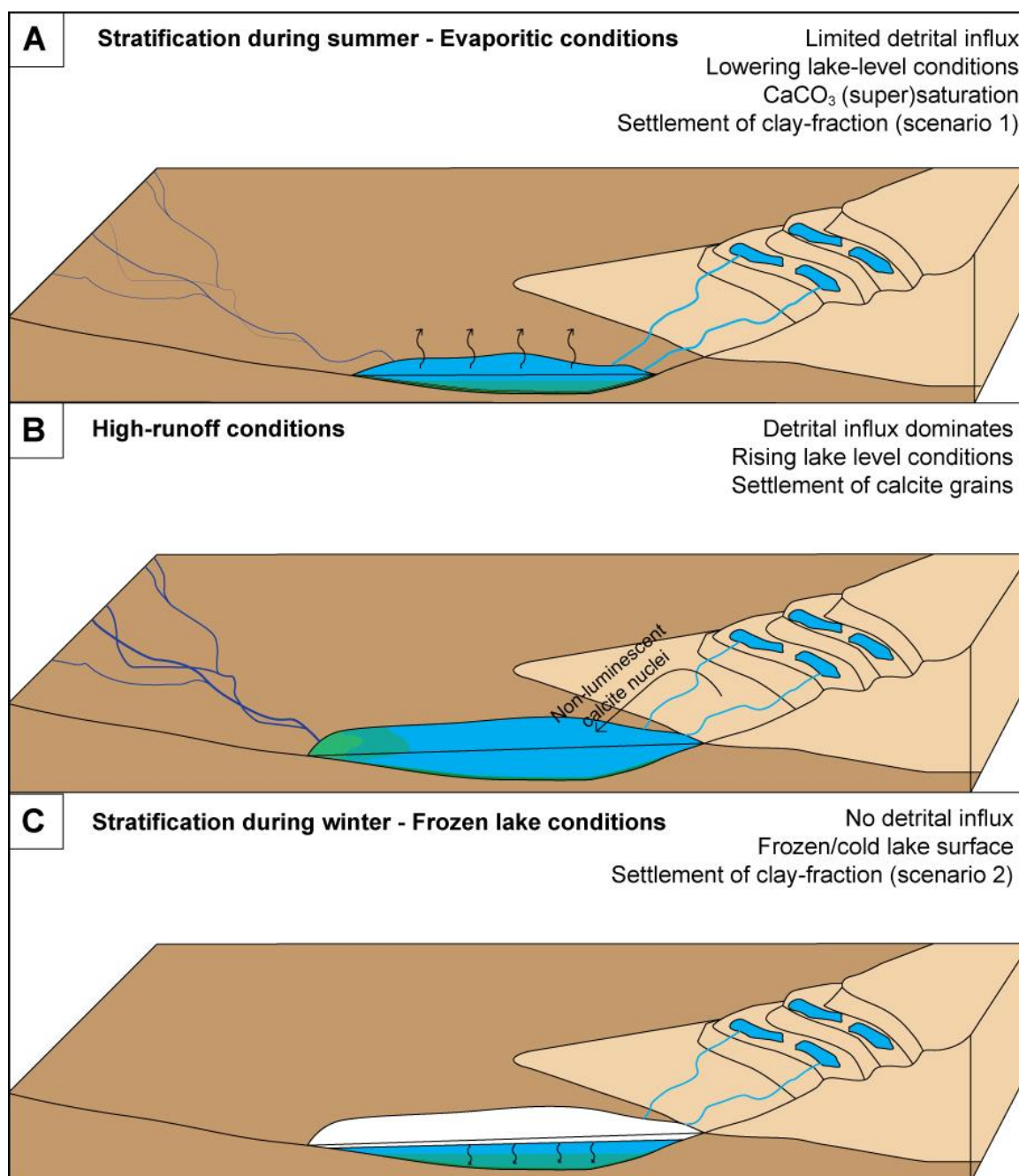


Figure 5.1: Conceptual depositional model for lake stratification during winter or summer, which is proposed for the lacustrine facies (travertine system = skin-toned, detrital deposits = brown, lacustrine = turquoise). A – During a period of a evaporitic conditions (following A and B), the waters become (super)saturated in CaCO_3 . These conditions give rise to stratification of the lake waters during summer. B – Period of high-run off, characterised by high-lake level conditions and the deposition of calcite grains. C – Ice forming on the surface of the lake gives rise to stratification during winter, allowing the clay fraction to settle down.

ii) Stratification during winter

This second model argues that the wackestone laminae are deposited during winter. The cold conditions might give rise to a frozen lake surface or to surficial waters with a temperature below 4°C . Both conditions give rise to stratification of the lake body (Figure 5.1 C). This stratification will allow grains of the clay-fraction to settle on the lake bottom.

Snowmelt will increase the run-off of the catchment area, supplying the lake waters with both detrital grains of the ophiolitic complex and the surrounding travertines (Figure 5.1 B). These calcite nuclei are likely to settle during spring and summer, during which evaporitic conditions give rise to lake water (super)saturated with respect to calcite. Nevertheless, the decreased depths of these lakes can increase the turbidity of the lake waters (e.g. wind-induced movement can reach a larger proportion of the lake body) . This causes the clay fraction to stay in suspension (Figure 5.1 C). During this period the run-off through the braided river channels is likely to decrease (decreased rain-fall, absence of snowmelt, ...). This might cause a negative water balance for the lacustrine systems, leading to exposed lake margins, giving rise to favouring conditions for the formation of palygorskite as is suggested by Botha & Hughes (1992). Unfortunately, no emergence surfaces have been observed as such in the field, with as exception root traces that were present throughout the lacustrine sediments. Nevertheless, a rhythmic variation of the lake level might also explain the fluctuating C/N ratio, indicating that the clay-rich laminae tend to be deposited during a period of a *relatively* high-lake level (Verneaux et al., 1991).

5.1.1.3 Dolomite & palygorskite – environmental tracers

A lower volumetric percentage of (luminescent) dolomite was observed within thin sections, as compared to the XRD measurements. This implies that either a large volumetric share of dolomite is non-luminescent in nature (i) or that microcrystalline dolomite crystals are present within the lacustrine sediments (ii).

The first option is rather unlikely, since nearly all grains (that do not classify as luminescent dolomite) within the lacustrine facies were either feldspars, quartz or calcite. The second theory is not confirmed by observations, however, there were several other indications (e.g. authigenic palygorskite, high Mg-content of the lacustrine sediments ...) that support the presence of microcrystalline dolomite precursor minerals. A combination of both palygorskite and fluctuating lake-levels might be an indicator of exposed lake-margins, however, no well-developed emergence surfaces have been observed. Regarding the formation of palygorskite, several mechanisms have been proposed for the formation under pedogenic conditions. The first mechanism is the transformation of precursor clay minerals (more specifically smectite), while a second possibility relates to the direct crystallization out of soil solutions (Owliaie et al., 2006; Garcia-Romero et al., 2007; Xie et al., 2013).

The presence of root-traces within the lacustrine sediments, combined with the interpretation of palygorskite and the fluctuating C/N ratio, might indicate that the

sediments were subject to pedogenic processes. The latter can lead to the formation of dolomite out of soil solutions and weathering products of palygorskite (Botha & Hughes, 1992). The evaporitic conditions at the lake margins can increase the Mg/Ca ratio within the pore fluids, facilitating the formation of dolomite within the exposed lacustrine sediments. Additionally, microbial activity can catalyse the formation of dolomite, especially within favouring conditions (high Mg/Ca ratio), due to the fact that the organic matrix of a bacterial cell preferentially binds Mg over Ca and overcomes the kinetic barriers associated with dolomite formation (Lindtke et al., 2011; Disnar et al., 2011). The biochemical behaviour of this microbial layer, also referred to as the extracellular polymeric substances (EPS), is studied in detail by Dupraz et al. (2004 & 2009). In normal conditions, the EPS is characterised by acidic molecules, which are randomly distributed and could represent hotspots for carbonate precipitation (Dupraz et al., 2004 & 2009). It is the alignment of these hotspots that may locally increase the Mg/Ca ratio, triggering the formation of Mg-rich precursor minerals.

Based on the observations that were made, in combination with the described mechanisms in literature, it thus seems likely that the authigenic formation of dolomite (precursor) minerals and palygorskite takes place during the sub-aerial exposure of the lacustrine sediments. The emergence surfaces were not truly observed as such, however, the presence of root traces, the formation of palygorskite and the fluctuating C/N ratios might imply that pedogenic processes took place.

5.1.1.4 *Zoned calcite grains*

Calcite grains within the lacustrine facies were often characterised by a strong zonation. Proximal towards the dome, these grains could be observed more often (e.g. Cakmak). The nuclei of these crystals were non-luminescent (or weakly luminescent) and sub-rounded in nature, which is in contrast with the equant cements that developed around this core.

i) Non-luminescent nuclei

The origin of these sub-rounded nuclei might be explained either due to erosion of nearby travertine occurrences (ia) or by microbial mediated processes (ib), of the first proposition is the most likely process.

ia) Erosion of the nearby travertines

The sub-rounded geometry of the core of these calcite grains, might be an indicator for some transport. Furthermore, the non-luminescent nature of this core does fit with the mineralogical characteristics of the calcite in the travertine occurrences. Additionally, the proximity of the travertine dome, the (possible) run-off of spring water and the inclined

nature of several of these travertine deposits are further arguments for an erosional origin of the calcite core.

ib) Microbial mediated processes

A second explanation for the non-luminescent core relates to bacterial mediated processes. It has been observed that cyanobacteria can catalyse the formation of calcite, either biologically-induced or biologically-influenced (Dupraz et al., 2009). The biologically-induced carbonate precipitation occurs due to a degradation of the EPS matrix. This increases the alkalinity (e.g. under influence of sulphate reducing bacteria; Dupraz et al. 2004) and the calcium concentration, leading to carbonate precipitation. This specific process has been observed in hypersaline microbialites, which is a rather unlikely setting for the studied deposits due to the absence of any saline deposits (Vasconcelos et al., 2006). The biologically-influenced precipitation takes place on the EPS matrix itself, where alkaline conditions and the presence of Ca^{2+} -ions may lead to the nucleation of calcite. The Ca^{2+} -saturation can be enhanced by evaporitic conditions, of which several arguments (fluctuating lake-levels, palygorskite, alternating carbonate-content ...) are observed within the lacustrine facies (Dupraz et al., 2009). Dupraz et al. (2004) also described the preferential precipitation in very shallow parts of a water body, which is a likely setting for the lacustrine facies of the Ballık area.

ii) Equant calcite cements

Calcite cements of a different morphology, i.e. equant crystals, did overgrow the sub-rounded core. These equant cements developed a bright – non-luminescent zonation, indicating changing pore-fluid conditions. In general, the cements of the largest crystals seem to developed in a similar direction, which thus indicates a preferential precipitation direction. Three different processes might lead to the formation of these equant cement types, being either cementation within the lake setting itself (iia), cementation in the vadose zone (iib) or the formation within the lake water itself (iic).

iia) Cementation in the lake sediments

It is likely that the lake sediments contained significant amounts of organic material during deposition, even if only a limited amount is preserved in fossil deposits (see 4.4 Total Organic Carbon (TOC)). It is possible that the organic material within the lake sediments decayed after deposition, consuming all oxygen and leading to reducing conditions (Figure 5.2 A). In calcite (over)saturated pore water this would give rise to the formation of bright-luminescent and equant calcite crystals, forming on the non-luminescent, sub-rounded calcite grains (as long as lake-stratification takes place). Assuming that the oxygen level of the lake water would have increased again, non-luminescent equant

calcite cements precipitated. Repeated changes in oxygen supply could lead to the formation of alternating bright – non-luminescent calcite rims. The advantage of the proposed mechanism is that geochemical conditions can change easily over a large area, subjecting all lacustrine sediments to similar conditions at once.

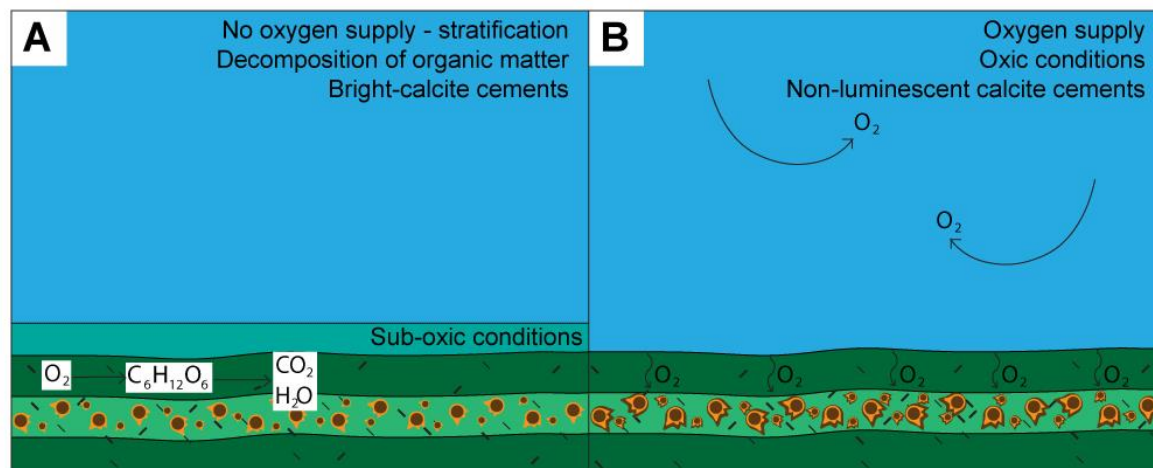


Figure 5.2: A – Decomposition of organic matter in the lacustrine sediments, giving rise to local sub-oxic conditions, favouring the formation of bright calcite cements. B – Oxidic conditions, favouring the formation of non-luminescent calcite.

iib) Cementation in the vadose zone

During sub-aerial exposure of the lacustrine sediments (as inferred from the presence of palygorskite, dolomite and possibly root traces) cementation might occur in the vadose zone. The geochemical composition of the fluids within the vadose zone can easily change, due to the influx of rain waters or a fluctuating groundwater table. However, changing the geochemical conditions contemporaneous over a broad area can be rather difficult. Furthermore, the equant cements tended to align within one direction but they did not classify as true pendant cements, based upon their morphology (Dominguez & Samaniego, 1992). Additionally, not all cements tended to align within one direction, which would be the case for the gravitational influenced pendant cements. The latter makes it more likely that the preferential growth direction is influenced by the supply of carbonate enriched waters within one direction (e.g. water flux within a specific direction, possibly influenced by evaporative pumping).

iic) Cementation within the lake water

Lastly, the cementation might occur when the calcite grains are present on the lake bottom itself. This would be similar to cementation within the sediments, with as exception that in this case the sediments are not buried yet. Here the bright cements might form during reducing lake water conditions, which can be achieved under influence of thermal stratification. In contrast, the non-luminescent cements might form within oxidizing

conditions. However, it is less likely to change the redox-conditions of a large water-body, while as it can be more easily achieved within the deposited sediments itself.

5.1.1.5 Algal structures

In the lacustrine facies algal structures could be observed. These structures were characterised by two different morphologies, being either encrusting build-up structures or elongated structures (respectively Figure 5.3 A & B).

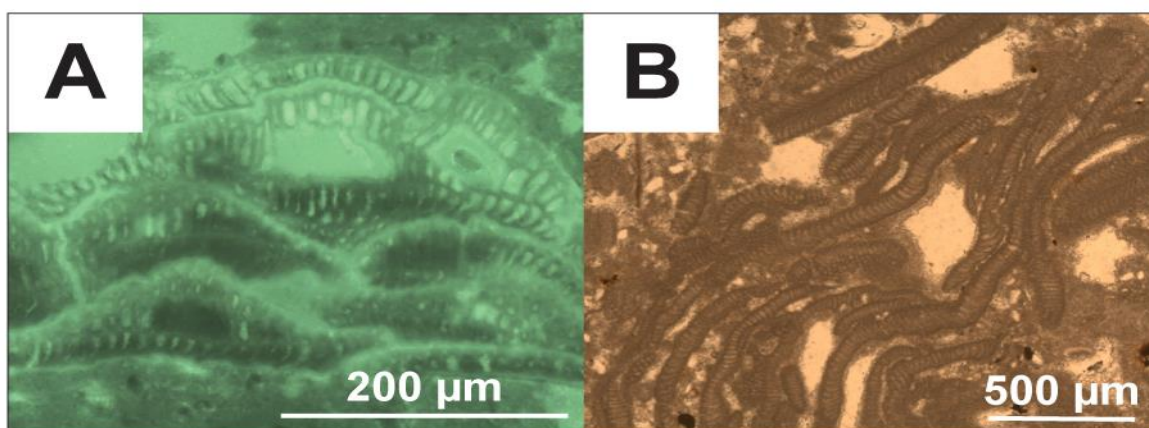


Figure 5.3: A – Encrusting algal structures, observed as small build-up structures. B – Elongated structures, present within the lacustrine facies.

It was not possible to classify the exact species that creates these structures, however, similar elongated structures were classified as cyanobacteria by Hirose & Hirona (1977). Taking into account the depositional setting (lacustrine water, evaporitic conditions, carbonate saturated, ...) and the microscopic structure, it is thus likely that these structures are lithified cyanobacteria.

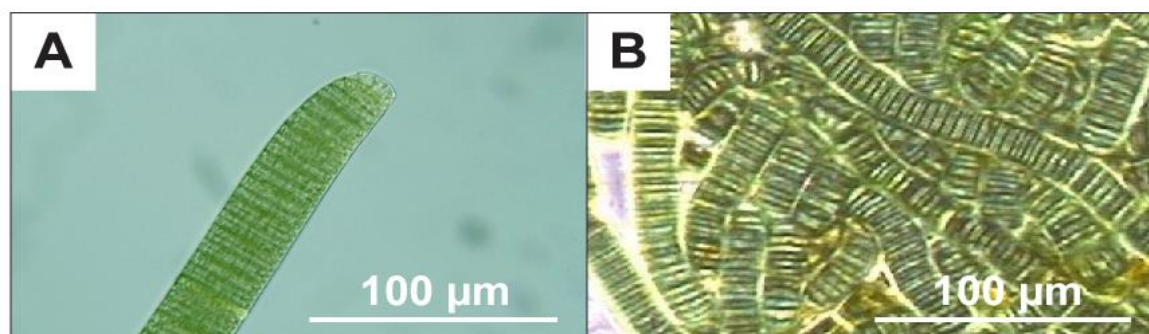


Figure 5.4: A – Example of a cyanobacterial filament. B – Lithified cyanobacteria, characterised by the presence of horizontal compartments as observed in Figure 5.3 B (modified after Hirose & Hirona, 1977)

5.1.1.6 Geochemical signal

On the scatterplots of the ICP-OES data, two groupings of elements can be observed. The first one shows a strong correlation between Sr, Ca and to a certain degree S. This can be interpreted as a signal, mainly related to the carbonate cements and calcite grains.

With regard to the Sr and S content, the adjacent travertines were enriched in Sr and S, respectively 1232 ppm and 1298 ppm (Soete, 2011). However, the concentration of all the other elements is higher within the lacustrine sediments, what might indicate that the travertines themselves mainly supplied Sr and S rich waters (apart from Ca). The second group of elements (such as Ni, Fe, Zn ...) will thus have to originate from a different, most likely detrital, source (Figure 5.5).

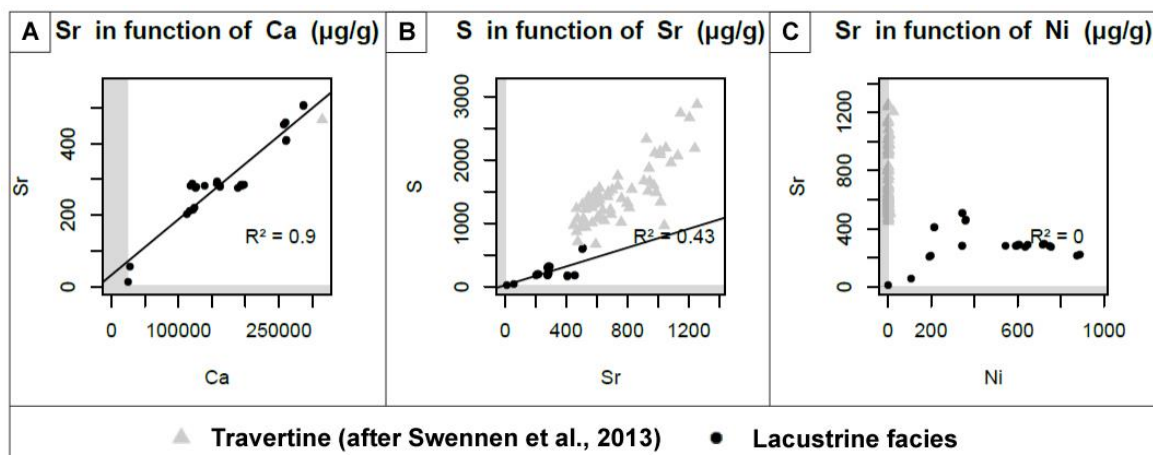


Figure 5.5: Geochemical data, expressed in ppm, of the lacustrine facies and the travertine lithologies (after Swennen et al., 2012). A - The Sr- and Ca-ratio of the travertines shows a similar trend as the lacustrine facies. B - The S and Sr data shows a similar covariation for the lacustrine and travertine samples, however, a small shift is present. C - Illustrative plot for Sr and Ni, where it can be seen that the lacustrine sediments are specifically enriched in Ni.

The overall geochemical composition of the lacustrine sediments was dominated by an elevated content of elements, characteristic for mafic rocks, with specifically high Ni-concentrations. These elements were present in much lower concentrations in the travertine deposits (Soete, 2011 & Swennen et al., 2013). The elevated concentration may be an indicator of run-off waters, originating from the region of the ophiolite complex. It is observed by Dirix (2010) that the Cr- and Ni-content of weathered ophiolite residues contained elevated concentrations (up to 5000 and 800 ppm respectively). Furthermore, the latter author also observed an elevated MgO-content. It has to be kept in mind that transport took place between the ophiolite complex and the lake location. This implies that the run-off water will be enriched specifically in the weathered products of minerals that degrade more easily (often rich in Mg, Ni ...), while other minerals will be able to resist weathering processes better. Olivine, pyroxenes and amphiboles (enriched in Mg, Ni and Fe) will weather rather easily, leading to a high quantity of weathered products of these minerals within the run-off waters. Minerals like for example chromite, which contains most of the Cr within the ophiolites, will resist weathering rather well. This mechanism might explain the fact that the lacustrine sediments are more enriched in Ni

with respect to Cr, while as the weathered – *in situ* – residues are characterised by an enrichment of Cr (Dirix, 2010).

5.1.1.7 *Lacustrine sediments as potential marker horizon*

In general, all lacustrine deposits were characterised by the same clay mineralogy. It was thus not possible to differentiate sequences from one another by the clay content of these lacustrine sediments. This indicates that the overall depositional environment and provenance area remained similar for all lacustrine sediments, independently of the studied sequence. Furthermore, the XRD-results of the lacustrine facies were compared with the argillaceous travertine lithologies (Bouman, 2016). It could be observed that palygorskite, serpentine and chlorites were not present within the travertine lithologies. The clay minerals in the latter lithology consisted of kaolinite, smectite and illite. Furthermore, the overall mineralogical content varied significantly within individual laminations, indicating that these laminations were characterised by a strong lateral variation.

The geochemical composition of these lacustrine sediments was rather uniform as well, with only a slight variation in the concentration of some elements (e.g. Fe, Mg, Na, Ni, Mn, P, Cr & Ba). In general, the relative abundance of each element was constant throughout this facies.

5.1.2 Fluvial facies

The fluvial facies consists of the polygenetic conglomerates, the tabular sandstones and the massive marls. This facies represents the second largest share in volume of all detrital sediments within the Ballik area. Furthermore, the fluvial facies often appeared on top of the lacustrine facies and next to the coquina facies.

5.1.2.1 *Depositional setting*

It was observed in the field, that several channels tended to form contemporaneously, indicating the geometry of braided-river channels. Furthermore, the presence of the massive and non-laminated marls indicated the presence of an alluvial plain in between these channels. In proximity of these channels, reeds tended to develop within adjacent marls. These reeds were encrusted by a calcite cement, in a similar manner as the reed facies of the travertine system (Soete, 2011). This thus indicates that the water, running through the braided-river system, was saturated with respect to CaCO_3 . This CaCO_3 -saturation might be due to water coming from the travertine system (Figure 2.2). The reed stems would act as a substrate for further calcite precipitation, partly due to the presence of algae and/or cyanobacteria overgrowing on the plant material (Janssen et al., 1999).

Furthermore, imbrication structures and cross-lamination, were generally indicating a flow direction from north to south (with local deviating trends from NW-SE or NE-SW). The polygenetic composition of the clasts were an indicator for a broad and diverse provenance region, which generally can be found in the north-west (Menderes Massif) or north (Ophiolite complexes). In general, most of these fluvial conglomerates tended to be well-sorted, with (sub-)rounded clasts, indicating a more distal provenance area than the Ballik area itself. An exception on this observation were the rather large and angular travertine boulders, dominantly composed of the subhorizontal facies (Soete, 2011). Their dimensions, angularity and elongated shape were an indicator for a more proximal provenance area, corresponding to the travertines of the upper or lower area.

5.1.2.2 Cementation

Most conglomerates in proximity of the travertine dome were embedded within a cemented matrix, as was observed in the Faber quarry. Conglomerates, which were initially embedded within an unconsolidated mud matrix, evolved towards their cemented counterpart in less than 400 m. The calcite cements within these conglomerates were non-luminescent in nature and thus similar to the calcite cements within the travertines (Soete, 2011). It is thus likely that similar fluids, as the ones causing the travertine precipitation, weld together these conglomerates. These fluids, that percolated through the deposited conglomerates, are either a consequence of carbonate saturated run-off waters from the travertine dome or from the progradation of the travertine dome over the surrounding detrital sediments.

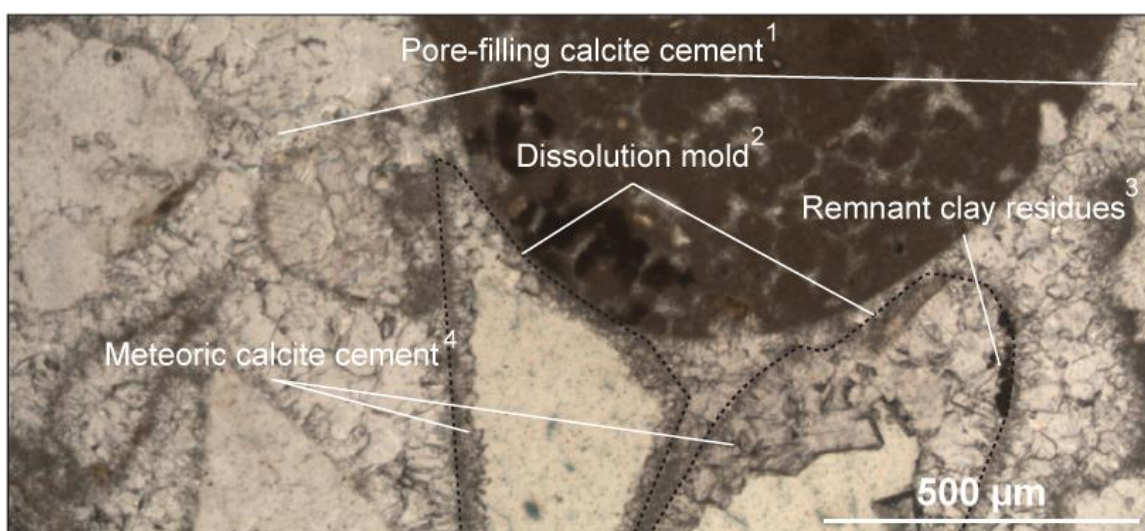


Figure 5.6: Well-cemented conglomerate with dissolution-enhanced porosity. Presence of the pore-filling calcite cement (1) in which moldic pores can be observed (2). Remnant clay residues align the dissolution mold (3), which is filled up by a second generation of calcite cement (4).

Furthermore, dissolution-enhanced porosity could be observed in certain conglomeratic beds (Figure 5.6). The molds were observed in a matrix of equant calcite cements, indicating that the dissolution of the clasts took place after the conglomerate was cemented. The molds often contained remnants of clay minerals and were in contrast to the dense matrix only partly cement reduced. The second generation of calcite cements, observed within the molds, would in this scenario originate from latter meteoric fluids, which are not able to block the pores entirely with calcite cement.

5.1.3 Debris-flow facies

The monogenetic breccias are classified as the debris-flow facies. The volumetric share of this facies is rather limited and their distribution is limited to specific settings.

5.1.3.1 *Depositional setting*

The debris-flow facies were systematically observed on top of paleoslopes, indicating a different depositional setting than the lacustrine and fluvial facies. Furthermore, this facies was characterised by the absence of any internal ordering, since clasts of all sizes were floating within a marly matrix. The rather angular shape of these clasts, which only consists of travertine, were an indicator that these sediments are only transported over a rather limited distance.

A possible transportation mechanism, creating the described features, is a debris-flow. The latter gives rise to the deposition of coarse grained deposits, due to a gravity-driven mechanism with highly-concentrated mixtures of sediment and water (McCarthy & Cadle, 1995). These deposits are characterised by their poorly-sorted internal architecture (Major, 1997; Sohn et al., 1997). This in contrast to deposits, that originate from fluvial processes, which are typically well-sorted, stratified and/or cross-stratified and dominated by grain-to-grain contacts (Sohn et al., 1997). Furthermore, the randomly oriented clasts and the, in general, non-erosive nature of these deposits are typical indicators for a debris-flow origin (Kim et al., 1995).

It is suggested by Sohn et al. (1997), who studied similar deposits in Korea, that the deposition of these rock-types was triggered by tectonic activity. Furthermore, the mud-supported character of this facies suggests that it originated from a rather small, steep and rugged catchment-area. Based upon the characteristics of these deposits, it can be concluded that they are deposited nearly in-situ. The tectonic activity might lead to an uplift of the travertine system, triggering the erosion of the paleosurface itself (in this specific case the cascade facies). Furthermore, a progradation of the travertine system after the deposition of the debris-flow facies can be observed in the quarry of Cakmak.

Additional indicators for the seismic activity were also observed within the other facies of the detrital sequences, ranging from water-escape structures to ball-and-pillow structures. It thus seems that seismicity was a likely triggering mechanism for these deposits.

5.1.3.2 *Depositional model*

The key concept of this model is the presence of a slope in combination with seismic activity (Figure 5.7 A & B). It has to be mentioned that the location of the fault is rather illustrative, however, throughout the travertine dome several faults and fractures have been observed (Van Noten et al., 2014). Debris-flows will settle when the flow velocity decreases (i.e. on rather flat surfaces, possibly adjacent to the lacustrine facies as in the Cakmak quarry). Furthermore, progradation can take place after the deposition of the debris-flow facies, causing the debris-flow to be buried underneath a new generation of travertine (Figure 5.7 C).

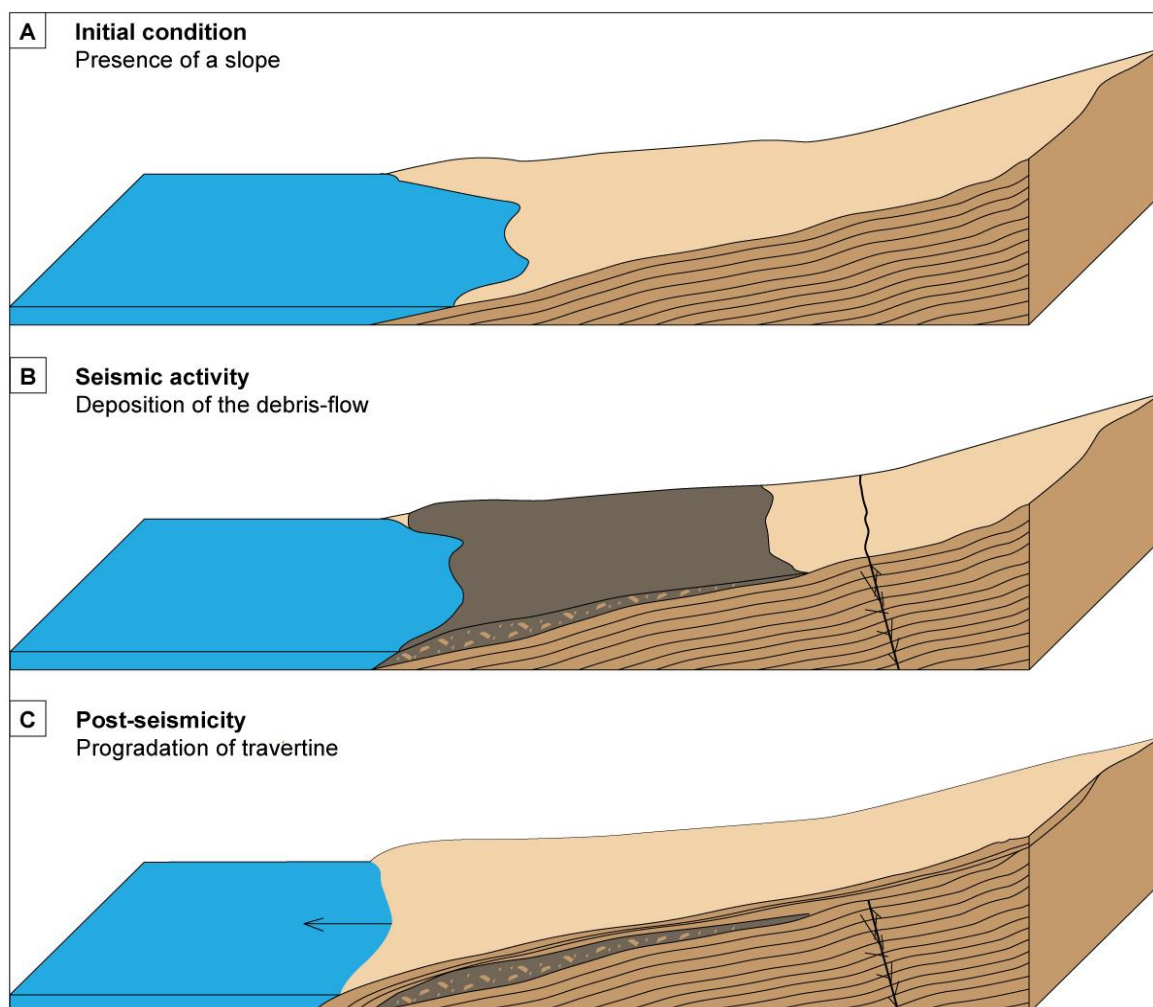


Figure 5.7: Proposed depositional model for the debris-flow facies. A - Inherent to this facies is the presence of an inclined surface. B - Seismic activity acts as a trigger for the debris flow itself, leading to brittle deformation and an increased slope. C - Post-seismic phase, during which the travertine dome will prograde over the deposited debris-flow.

5.1.4 Gastropod facies

The gastropod facies refers to the gastropod-rich carbonate lithologies, which did not make up a significant volumetric share of the total deposited sediments. This facies was closely associated with the lacustrine facies and the travertine dome itself.

5.1.4.1 *Depositional setting*

Most of the gastropods in the gastropod facies were rather intact, indicating that deposition might be largely in situ. Furthermore, the alignment of several gastropod shells in planar horizons, is an indicator for deposition in a sub-horizontal environment. Most of the characteristics (crystalline cements, depositional surface ...) of this facies tend to lean towards the travertine system, indicating that deposition took place under similar conditions. Nevertheless, an inherent difference between both facies exists. The travertine system is characterised by chemical precipitation, while the gastropod facies results from bioclastic accumulation. Furthermore, most of these gastropods were affected by dissolution processes, leading to moldic porosity. The abundance of gastropods, together with the proximity of the travertine dome and lacustrine facies, are indicators for a sub-horizontal depositional environment. This depositional environment is most likely sub-aquatic in origin, giving rise to the planar alignment of gastropods.

5.1.4.2 *Porosity inversion*

The gastropod facies was characterised with what is described as a porosity inversion. The original porosity network, present in between the gastropod shells themselves, was filled up by crystalline equant calcite cements. Afterwards, the gastropods themselves were dissolved, yielding the isolated and moldic pores. These gastropod shells were at least partly made of aragonite, making them more susceptible to dissolution in comparison to low-Mg calcite (Flügel, 2004; Marshall et al., 2008).

5.1.5 Coquina facies

Observations of the coquina are rather limited, making it difficult to interpret the facies with great certainty. Nevertheless, the depositional environment is discussed and is mainly based on field observations. The volumetric share of this facies is very limited (estimated to be lower than 1 % of the total detrital deposits).

5.1.5.1 *Depositional environment*

The shells in the coquina beds were, in contrast with those of the gastropod facies, often present as broken shell-fragments. This indicates that transport took place before these bioclasts were deposited. An additional argument for transport is the presence crossed-

bedding, reflecting a NW-SE or NE-SW flow-direction (similar to the flow-direction of the fluvial facies). A transport mechanism, that is capable of acquiring massive accumulations of gastropod shells, with beds of up to 20 cm in thickness, is thus needed to form these deposits. Two possible processes are likely to lead to the deposition of coquina beds being either fluvial transport or concentration in a shoreline environment. Fluvial lithologies are abundant in this environment and are capable of transporting gastropod shells from their biological niche to their accumulation site. The biological niche might correspond to small and isolated pools, possibly present within the alluvial plain. A second option might be that these coquina beds represent a fossil beach, concentrating gastropods that were present within the lake systems.

5.2 Reservoir characteristics

This thesis is placed within a JIP project that tries to unravel the characteristics of travertine deposits as a reservoir analogue. The observed sedimentary facies were petrophysically characterised, in order to interpolate the facies within the framework of a reservoir. The porosity and permeability values, for each facies, are discussed in this section.

5.2.1 Lacustrine facies

The lacustrine facies formed thick and lateral continuous deposits, with a length up to 500 m. The studied sediments were characterised by a 2D-porosity ranging from 4.1 % to 19.3 % (image analysis), however, it has to be kept in mind that these sediments are likely to be compacted during diagenesis. Algal structures within this facies tended to be porous, but their contribution was not relevant to the overall porosity of this facies. Furthermore, the low TOC-values did not classify this facies as a potential source rock. This might be due to the rather oxidative conditions (e.g. non-luminescent cements) to which the lacustrine sediments of the Ballık area were subjected.

It was not possible to collect information with regard to the permeability of this facies during this research. However, in general, mudstones act as impermeable horizons within a reservoir system, especially due to their very low permeability values (Broichhausen et al., 2005; Marcussen et al., 2010 & Liu et al., 2015). It is thus likely that the lacustrine facies will act as an impermeable layer within or adjacent to the reservoir, sealing the reservoir. If, for example, lacustrine sediments would be deposited on top of carbonate domes it gives rise to a sealed reservoir, which is preferentially targeted for hydrocarbon exploration. The lacustrine sediments in the Ballık area are not likely to be considered a reservoir rock itself, however, their equivalent within the Pre-Salt plays might be characterised by different reservoir properties. In general, the lacustrine settings of the

Pre-Salt are characterised by a high alkalinity and very saline conditions (Thompson et al., 2015). In the lacustrine sediments of the Pre-Salt, microbialites and stromatolites, associated with these specific conditions, have been described (Moore & Wade, 2013). Due to the presence of the latter, the Pre-Salt lacustrine sediments are likely to be more porous as the lacustrine sediments in the Ballık area.

5.2.2 Fluvial facies

The fluvial facies consisted of either conglomeratic channels, tabular sandstones or massive marls. The lithology of the tabular sandstones was laterally continuous, leading to an horizon of a well-connected reservoir rock. No porosity estimations of this lithology were available, however, they were well-sorted what might indicate that they possess a rather elevated permeability.

A strong relation between the fluvial conglomerates and the massive marls was observed in the field. Since these conglomerates were deposited within a braided-river type, they most likely form reservoir bodies of inter-connected channels. Each of these channels was laterally isolated from one another by the massive marl lithotype. Furthermore, amalgamated channels may act as vertical corridors, connecting channel networks of different generations. This may thus lead to a lateral extensive reservoir rock, with in our case porosity values ranging between 5.6 and 14.9 % and permeability values ranging from 0.04 to 142 mD (exceptionally even over 3000 mD).

The proximity of the conglomeratic channels with regard to the travertine system determines the degree of cementation of the matrix. It is thus likely that conglomerates, adjacent to the travertines, possess poor reservoir characteristics. At a larger distance these conglomerates were characterised by a significant amount of microporosity, possibly reaching up to 83 % (Table 4-5, p. 63) of the overall porosity, due to the uncemented nature of the muddy-matrix. However, it is likely that the poorly-cemented conglomeratic lithotype evolves towards the more cemented mud-supported lithotype (as was observed in the quarry of Faber). This would reduce the microporosity and thus the overall connectivity of the different pores.

Certain conglomeratic levels tended to develop solution-enhanced porosity. This might indicate that several clast types are likely to dissolve during shallow burial conditions. This solution enhanced porosity can thus lead to a significant contribution to the total reservoir porosity.

Furthermore, K-feldspars were often observed in the matrix of these conglomeratic channels. This mineral is present as detrital grains in reservoir rocks that formed within rift

basins, which fits the tectonic setting of the Lula Oil field (Soete, 2011; Wilkinson et al., 2001). The dissolution of K-feldspar takes place during diagenesis (Wilkinson et al., 2001). This might lead to an increased porosity and permeability, since these feldspars could be observed dispersed throughout the matrix. Nevertheless, the alteration of feldspar might also lead to the development of authigenic clay minerals, which can fill up (solution-enhanced) pores, thus negatively affecting the permeability (Yuan et al., 2015).

5.2.3 Debris-flow facies

The debris-flow facies can be considered as a continuous extension to the travertine reservoir system, since they were observed on top of a paleoslope without the presence of an impermeable horizon (since the debris-flow facies could be found directly on top of the travertine lithologies). The measured porosity ranged from 7.5 to 9.5 % with permeability values of about 0.03 mD. The facies did not represent a significant volume and is not likely to be of significant importance in reservoir models.

5.2.4 Gastropod facies

The gastropod facies developed on local flat surfaces inside the travertine system, often in close proximity with the lacustrine facies. In general, this facies was characterised by a rather elevated porosity (8.5 % – 27.2 %), which was dominantly moldic in nature. However, not all pores were well-connected to the overall pore network, leading to a rather low permeability (0.02 – 0.17 mD). During diagenesis, it is rather likely that all remaining gastropod fragments will dissolve, further increasing the amount of moldic porosity (Maliva, 1998).

5.2.5 Coquina facies

If the studied thin section of the coquina facies can be considered to be representative for the whole facies, the coquina facies has a great reservoir potential. The latter was characterised by both high permeability and porosity values, however, the volumetric share of this facies was rather limited. The coquina facies was characterised by the abundance of moldic porosity, due to the dissolution of gastropods and coated grains. During diagenesis it is likely that all the remaining gastropod and coated grain fragments will be dissolved as well, since they are made of aragonite.

5.2.6 Summary

It can be concluded that the detrital sediments, encasing the travertine system, are of major importance in order to understand the overall depositional environment and the reservoir architecture. The facies which were, volumetrically, the most important with

regard to the reservoir analogue were the lacustrine and fluvial facies. The latter represented a similar volume as the carbonate lithologies in the Ballık area.

With the emphasis on a reservoir analogue, the lacustrine facies could develop in between several travertine accumulations, acting as an impermeable geobody lowering the vertical connectivity. Furthermore, it might also be deposited on top of carbonate domes, acting as an impermeable seal. This could give rise to the development of important hydrocarbon traps. This in contrast with the fluvial facies, which is capable of connecting different parts of the reservoir system, both in horizontal and vertical directions. However, it has to be kept in mind that the poroperm properties of the fluvial facies might change during diagenesis.

The studied facies form a reservoir system with bodies of both poor and excellent reservoir quality. The studied deposits are therefore still considered a possible reservoir analogue. Nevertheless, the actual reservoirs (as for example in the Pre-Salt) do not necessarily consist of similar lithologies or mineralogies. However, it is likely that similar facies occur in the Pre-Salt setting, i.e. the debris-flow, lacustrine and fluvial facies.

Chapter 6

Conclusion

The goal of this thesis was to increase the knowledge on the detrital sediments, encasing a travertine reservoir analogue. In order to achieve this goal, the study focused on two main concepts, being the development of a facies classification and the quantification of its reservoir characteristics. Both of these concepts are crucial in order to increase the knowledge of the Ballik area depositional model and to extrapolate observations from the analogue to actual petroleum reservoirs.

Five different sedimentary facies, i.e. lacustrine, fluvial, debris-flow, gastropod and coquina, were studied during this research. Of all these facies, the lacustrine and fluvial facies were by far the most important, regarding the volumetric share of all detrital deposits. The fluvial facies could give rise to rather narrow and elongated channel geobodies, which regularly interconnect to one another both horizontally and vertically. With regard to the lacustrine facies, several analyses focused on unravelling the sedimentary characteristics and their potential as markers through time. Unfortunately, all studied lacustrine sediments were characterised by a similar (clay) mineralogy and geochemical composition, making it impossible to use these parameters to characterise marker beds throughout several quarries. Furthermore, the mineralogical composition within one lamination varied significantly over a short distance. This facies typically contained elements that are characteristic for mafic minerals (e.g. Ni, Mg, Fe ...). These elements give rise to specific geochemical conditions (high Mg-content, favouring the formation of both palygorskite and *possibly* microcrystalline dolomite) within these lakes, which were seasonally subjected to evaporitic conditions. This seasonal variation led to a fluctuation in detrital influx and carbonate precipitation, that gave rise to the deposition of laminated marl deposits. Within this facies zoned calcite grains were observed, possibly together with authigenic dolomite. Most likely, the nuclei of these calcite grains came from the adjacent travertine due to erosional processes. This in contrast with the equant calcite zonations, which were most likely to form within the lake sediments themselves due to changing redox conditions (related to the deterioration of organic matter and/or the stratification of the lake bottom waters). Arid and sub-aerial conditions, are confirmed by the presence of palygorskite (confirmed by XRD, speculative based on SEM observations)

and the possible presence of authigenic dolomite. However, with the exception of root traces within the sediments, no other observations with regard to pedogenic processes (e.g. emergence surfaces) were found. Cyanobacterial structures are observed as well. Finally the lacustrine facies was characterised by rather low TOC values.

Within a petroleum reservoir, each sedimentary facies might give rise to specific issues with regard to reservoir connectivity and poroperm properties. The majority of the Pre-Salt deposits are likely made of both lacustrine and fluvial sediments, next to travertine. In the Ballık area the travertine dome is encased by detrital deposits, mainly being the lacustrine and fluvial facies, making it a good reservoir analogue for the Pre-Salt lithologies. The petrophysical properties of these detrital facies are thus important with regard to the architecture of the overall reservoir analogue. In the Pre-Salt, several small carbonate domes may be present, which are all encased by similar sediments. In the Ballık area the lacustrine facies makes up a significant share, since it tends to develop in an aqueous environment present in paleolows between carbonate domes. These lacustrine sediments tend to isolate different carbonate bodies and if the latter would occur on top of such a carbonate body, they are likely to act as a seal. This could give rise to a classic domal trap for hydrocarbons. The fluvial facies might increase the lateral and vertical connectivity, due to the horizontal and vertical network of interconnected channels. However, given the occurrence and facies associations of the latter, it is unlikely that the fluvial facies will significantly interconnect individual travertine bodies.

Chapter 7

Future research

The suggestions for future work are split up in five different sections addressing specific items that that may lead to a better understanding of the detrital deposits.

7.1 Petrophysical assessment

During this research the porosity and permeability of 21 plugs was determined. However, in order to confirm the observed trends, additional measurements are needed in order to confirm that the current porperm values for each facies are representative.

7.2 Mapping of the broader region

This research mainly focused on the detrital sediments in proximity of the travertine system. It might be interesting to map the broader region, in order to characterise the extent of each sedimentary sequence. Observing these lithologies at a more distal position with respect to the travertine dome, might address the influence of the dome on adjacent lithologies (e.g. do all lithologies become less cemented at a greater distance, does the lacustrine facies forms specifically in the paleolows adjacent to the travertine dome, ...).

Additionally, a detailed knowledge of the geological formations, present within the region is essential in order to evaluate the provenance of the deposited sediments (e.g. muscovite-bearing sediments ...).

7.3 Lacustrine facies

The emphasis of this research lied on understanding the overall sedimentological properties of the detrital sediments, including the lacustrine facies. However, this facies was characterised by rather unique features (e.g. zoned calcite grains, assumed presence of authigenic dolomite, ...). A detailed study of this facies addressing these specific features might thus lead to interesting results.

This study could evaluate the clay-mineral content of several successive layers at the same location. During this research, only up to 3 successive layers have been analysed

due to the availability of samples. It might thus be interesting to evaluate more successive layers, in order to truly confirm the proposed depositional model.

In order to confirm the presence of the authigenic dolomite or the possible precursor minerals, SEM-EDX might be used. This technique might highlight high concentrations of Mg, surrounding the zoned calcite crystals.

7.4 Provenance analysis

The polygenetic conglomerates were already analysed with regard to their grain size distribution during this research. However, a detailed study of these clasts in combination with thin sections and a detailed geological map of the broader region, could lead to a better understanding of the fluvial system as a whole. More conglomerates would have to be sampled, also at a greater distance of the Ballik travertines, in order to understand the evolution of the polygenetic conglomerates themselves.

7.5 Sequence stratigraphy

It might be interesting to study the detrital sequences in the broader region with a sequence stratigraphic approach. This might, for example, highlight horizons during which a significant shift in the sedimentary system took place. This approach allows to study the evolution of specific horizons within the provenance area.

7.6 Clay-analysis

The visual analysis of the lacustrine sediments through SEM was not able to truly confirm the presence of palygorskite. Studying these lacustrine sediments with a SEM with a higher resolution might thus be useful to truly confirm the presence of this clay mineral.

Bibliography

- AKGÜN, F. & SÖZBİLİR, H., 2001. A palynostratigraphic approach to the SW Anatolian molasse basin : Kale – Tavas molasse and Denizli molasse. *Geodinamica Acta*, **14**, pp.71–93.
- ALÇIÇEK, H., VAROL, B. & ÖZKUL, M., 2007. Sedimentary facies , depositional environments and palaeogeographic evolution of the Neogene Denizli Basin , SW Anatolia , Turkey. *Sedimentary Geology*, **202**, pp.596–637.
- BARTHA, A. & BERTALAN, É., 1997. Determination of the rare earth elements of rock samples by ICP-MS using different sample decomposition methods. *Acta Mineralogica-Petrographica*, **38**, pp.131–149.
- BLAIR, T.C. & MCPHERSON, J.G., 1999. GRAIN-SIZE AND TEXTURAL CLASSIFICATION OF COARSE SEDIMENTARY PARTICLES. *Journal of Sedimentary Research*, **69**(1), pp.6–19.
- BOEHRER, B. & SCHULTZE, M., 2008. Stratification of lakes. *Review of Geophysics*, **46**, pp.1–27.
- BOTHA, G.A. & HUGHES, J.C., 1992. Pedogenic palygorskite and dolomite in a late Neogene sedimentary succession, northwestern Transvaal, South Africa. *Geoderma*, **53**, pp.139–154.
- BOUMAN, M., 2016. Reservoirkarakterisering van travertijncarbonaten. *Masterthesis in prep.*, KU Leuven
- BROICHHAUSEN, H., LITCKE, R. & HANTSCHHEL, T., 2005. Mudstone compaction and its influence on overpressure generation , elucidated by a 3D case study in the North Sea. *International Journal of Earth Sciences*, **94**, pp.956–978.
- CLAES, H., SOETE, J., NOTEN, K.V.A.N., DESOUKY, H.E.L. & SWENNEN, R., 2015. Sedimentology , three-dimensional geobody reconstruction and carbon dioxide origin of Pleistocene travertine deposits in the Ballik area (south-west Turkey). , pp.1408–1445.
- DILEK, Y. & PAVLIDES, S., 2006. *Postcollisional tectonics and magmatism in the Mediterranean region and Asia*. The Geological Society of America, Boulder. pp. 409.

- DIRIX, K., 2010. Geochemische en mineralogische studie van de Holocene sedimenten in het bekken van Gravgaz (Turkije): karakterisering en bepaling van het herkomstgebied. *Non-published master thesis*. KU Leuven, pp. 151.
- DISNAR, J., STEFANOVA, M., BRÉHÉRET, J. & MACAIRE, J., 2011. Organic Geochemistry Microbial mat development and dolomite formation under pre-evaporitic conditions during the Atlantic in a temperate area : The Sarliève Lake (French Massif Central). *Organic Geochemistry*, **42**(9), pp.1089–1098.
- DOMINGUEZ, G.C. & SAMANIEGO, V., 1992. *Carbonate Reservoir Characterization: A geologic-Engineering analysis* H. H. S. J. Mazzullo, G. V. Rieke, & Chillingarian, eds., Elsevier Ltd, New York. pp. 638.
- DUPRAZ, C., REID, R.P., BRAISSANT, O., DECHO, A.W., NORMAN, R.S. & VISSCHER, P.T., 2009. Earth-Science Reviews Processes of carbonate precipitation in modern microbial mats. *Earth-Science Reviews*, **96**, pp.141–162.
- DUPRAZ, C., VISSCHER, P.T., ARTNER, L.K.B. & REID, R.P., 2004. Microbe – mineral interactions : early carbonate precipitation in a hypersaline lake (Eleuthera Island , Bahamas). *Sedimentology*, **51**, pp.745–765.
- ERDOGAN, B. & GÜNGÖR, T., 2002. Tectonic significance of mafic volcanic rocks in a Mesozoic sequence of the Menderes Massif , West Turkey. *International Journal of Earth Sciences*, **91**, pp.386–397.
- FLANAGAN, F.J., 1986. *Reference Samples in Geology And Geochemistry*. U.S. Geological Survey bulletin (1582). Alexandria. pp. 61.
- FLÜGEL, E., 2004. *Microfacies of Carbonate Rocks: Analysis, Interpretation and Application*. Springer Science & Business Media, New York. pp. 976.
- GALPENERGIA, 2015. The Lula/Iracema Project | Brazil. <http://www.galpenergia.com/EN/Investidor/Estrategia/PrincipaisProjetos/Lula/Paginas/Projecto-Lula-Brasil.aspx>
- GARCIA-ROMERO, E., SUAREZ, M., SANTAREN, J. & ALVAREZ, A., 2007. CRYSTALLOCHEMICAL CHARACTERIZATION OF THE PLYGORSKITE AND SEPIOLITE FROM THE ALLOU KAGNE DEPOSIT , SENEGAL. *Clays and clay minerals*, **55**(6), pp.606–617.
- GARCÍA-VEIGAS, J., PRATS, E., DOMÍNGUEZ, A. & VILLUENDAS, A., 2012. Advanced applications of Scanning Electron Microscopy in Geology. In *Capitol del llibre: Handbook of Instrumental techniques for materials, chemical and biosciences*

- research. Barcelona: Centres Científics i Tecnològics. *Universitat de Barcelona*. pp. 10.
- HINSBERGEN, D.J.J. VAN, KAYMAKCI, N., SPAKMAN, W. & TORSVIK, T.H., 2010. Reconciling the geological history of western Turkey with plate circuits and mantle tomography. *Earth and Planetary Science Letters*, **297**(3-4), pp.674–686.
- HIROSE, H. & HIRONA, M., 1977. *Illustrations of the Japanese Freshwater Algae*. Uchidarokakuho Publ., Tokyo, pp. 993.
- JACOBS, P. & CNUUDE, V., 2009. “ Applications of X-ray computed tomography in engineering geology ” or “ looking inside rocks” *Engineering Geology*, **103**(3-4), pp.67–68.
- JANSSEN, A., SWENNEN, R., PODOOR, N. & KEPPENS, E., 1999. Biological and diagenetic influence in Recent and fossil tufa deposits from Belgium. *Sedimentary Geology*, **126**, pp.75–95.
- KIM, S.B., CHOUGH, S.K. & CHUN, S.S., 1995. Bouldery deposits in the lowermost part of the Cretaceous Kyokpori Formation , SW Korea : cohesionless debris flows and debris falls on a steep-gradient delta slope. *Sedimentology*, **98**, pp.97–119.
- KINGDOM, U., 1998. Hot-spring travertine facies and sequences , Late Pleistocene , Rapolano Terme , Italy. *Sedimentology*, **45**, pp. 163-180.
- LINDTKE, J., ZIEGENBALG, S.B., BRUNNER, B., ROUCHY, J.M., PIERRE, C. & PECKMAN, J., 2011. Authigenesis of native sulphur and dolomite in a lacustrine evaporitic setting (Hellín basin , Late Miocene , SE Spain). *Geological Magazine*, **148**(May 2016), pp.655–669.
- LIU, W., LI, Y., YANG, C., DAEMEN, J.J.K., YANG, Y. & ZHANG, G., 2015. Permeability characteristics of mudstone cap rock and interlayers in bedded salt formations and tightness assessment for underground gas storage caverns. *Engineering Geology*, **193**, pp.212–223.
- MAJOR, J.J., 1997. Depositional Processes in Large - Scale Debris - Flow Experiments. *The Journal of Geology*, **105**(3), pp.345–366.
- MALIVA, R.G., 1998. Skeletal aragonite neomorphism — quantitative modelling of a two-water diagenetic system. *Sedimentary Geology*, **121**, pp.179–190.
- MARCUSSEN, Ø., FALEIDE, J.I., JAHREN, J. & BJØRLYKKE, K., 2010. Mudstone compaction curves in basin modelling : a study of Mesozoic and Cenozoic Sediments in the northern North Sea. *Basin Research*, **22**, pp.324–340.

- MARSHALL, D.J., SANTOS, J.H., LEUNG, K.M.Y. & CHAK, W.H., 2008. Correlations between gastropod shell dissolution and water chemical properties in a tropical estuary. *Marine Environmental Research*, **66**, pp.422–429.
- MCCARTHY, T.S. & CADLE, A.B., 1995. Alluvial fans and their natural distinction from rivers based on morphology, hydraulic processes, sedimentary processes and facies assemblages – Discussion. *Journal of Sedimentary Research*, (3), pp.581–583.
- MCLAREN, P. & BOWLES, D., 1985. The effects of sediment transport on grain size distributions. *Journal of Sedimentary Petrology*, **55**, pp.457–470.
- McNaught, A.D. & Wilkinson, A., 1997. IUPAC. Compendium of Chemical Terminology: The Gold Book. 2nd Edition. Blackwell Scientific Publications, Oxford.
- MOORE, C.H. & WADE, W.J., 2013. *Carbonate Reservoirs: Porosity and diagenesis in a sequence stratigraphic framework* 2nd ed., Oxford: Newnes. pp. 392.
- MOORE, D.M. & REYNOLDS, R.C., 1997. *X-ray diffraction and the identification and analysis of clay minerals* 2nd ed., Oxford: Oxford university press. pp. 378.
- MUCHEZ, P., DEGRYSE, P., JOACHIMSKI, M.M., LENS, S., DEGRYSE, P., CALLEBAUT, K., DEDEREN, M., HERTOGEN, J., JOACHIMSKI, M., KEPPENS, E., OTTENBURGS, R., SCHROYEN, K. & WAELEKENS, M., 2008. Petrography , mineralogy and geochemistry of the rocks in the area of the archaeological site of Sagalassos. In *Sagalassos VI. Geo- and bio-archaeology at Sagalassos and in its territory*. Leuven: Leuven University Press, p. 28.
- NOTEN, K. V, CLAES, H., SOETE, J., FOUBERT, A., ÖZKUL, M. & SWENNEN, R., 2013. Fracture networks and strike – slip deformation along reactivated normal faults in Quaternary travertine deposits , Denizli Basin , western Turkey. *Tectonophysics*, **588**, pp.154–170.
- OJALA, A.E.K., FRANCUS, P., ZOLITSCHKA, B., BESONEN, M. & LAMOUREUX, S.F., 2012. Characteristics of sedimentary varve chronologies – A review. *Quaternary Science Reviews*, **43**, pp.45–60.
- OKAY, A., 1989. Geology of the menderes massif and the lycian nappes south of denizli, western taurides. *Mineral Resources Exploration Bulletin*, **109**, pp.37–51.
- OWLIAIE, H.R., ABTAHI, A. & HECK, R.J., 2006. Pedogenesis and clay mineralogical investigation of soils formed on gypsiferous and calcareous materials , on a transect , southwestern Iran. *Geoderma*, **134**, pp.62–81.

- PECORA, W.T., 1968. *Geological survey research 1968*. United States Government Printing Office, Washington, pp. 563.
- RODAS, M., LUQYE, F.J., MAS, R. & GARZON, M.G., 1994. Calcretes, palycretes and silcretes in the paleogene detrital sediments of the Duero and Tajo basins, Central Spain. *Clay Minerals*, **29**, pp.273–285.
- ROELANDTS, I. & DUCHESNE, J.C., 1988. AWI-1, SBO-1, PRI-1, CCH-1 and DWA-1, Belgian sedimentary rock reference materials. *Geostandards and geoanalytical research*, **12**(1), pp.13–38.
- SAARNISTO, M., 1986. Annually laminated lake sediments. Handbook of Holocene Palaeoecology and Palaeohydrology, B.E. Berglund (Ed.), John Wiley and Sons Ltd, Chichester, pp. 343-370
- SOETE, J., 2011. Travertine & Tufa: Facies-development in the travertine quarry 'Faber'. Sedimentology, diagenesis and macro-porosity characterization. *Masterthesis*, KU Leuven, pp. 146.
- SOHN, Y.K., RHEE, C.W. & KIM, B.C., 1997. Debris Flow and Hyperconcentrated Flood - Flow Deposits in an Alluvial Fan , Northwestern Part of the Cretaceous Yongdong Basin , Central Korea. *The Journal of Geology*, **107**(1), pp.111–132.
- SÖZBİLİR, H., 2002. Revised Stratigraphy and Facies Analysis of Palaeocene- Eocene Supra-allochthonous Sediments (Denizli , SW Turkey) and Their Tectonic Significance. *Turkish Journal of Earth Sciences*, **11**, pp.87–112.
- SRODON, J.A.N., DRITS, V.A., MCCARTY, D.K., HSIEH, J.C.C. & EBERL, D.D., 2001. Quantitative X-Ray Diffraction analysis of clay-bearing rocks from random preparations. *Clays and clay minerals*, **49**(6), pp.514–528.
- SWENNEN, R., ÖZKUL, M., CLAES, H., SOETE, J., CLAES, S., FOUBERT, A., VAN NOTEN, K., HUYSMANS, M., BAYKARA, O. & EL DESOUKY, H., 2013. Travertine and calcareous tufas analogue reservoir characterization. *Non published JIP report sponsored by TOTAL, ENI E&P and PETROBRAS*.
- TAYMAZ, T., YILMAZ, Y. & DILEK, Y., 2007. The geodynamics of the Aegean and Anatolia : introduction. *Geological Society, London, Special Publications*, **291**(4), pp.1–16.
- THE ECONOMIST, 2011. Brazil's oil boom: Filling up the future. <http://www.economist.com/node/21536570>
- THOMPSON, D.L., STILWELL, J.D. & HALL, M., 2015. Lacustrine carbonate reservoirs from

- Early Cretaceous rift lakes of Western Gondwana: Pre-Salt coquinas of Brazil and West Africa. *Gondwana Research*, **28**(1), pp.26–51.
- TOTLAND, M., JARVIS, I. & JARVIS, K.E., 1992. An assessment of dissolution techniques for the analysis of geological samples by plasma spectrometry. *Chemical Geology*, **95**, pp.35–62.
- U.S. GEOLOGICAL SURVEY, 2001. A laboratory manual for X-Ray Powder Diffraction. <http://pubs.usgs.gov/of/2001/of01-041/html/docs/flow/>
- VASCONCELOS, C., WARTHMAN, R., MCKENZIE, J.A., VISSCHER, P.T., BITTERMANN, A.G. & LITH, Y. VAN, 2006. Lithifying microbial mats in Lagoa Vermelha , Brazil : Modern Precambrian relics? *Sedimentary Geology*, **185**, pp.175–183.
- VERNEAUX, J., VIDONNE, A., REMY, F. & GUYARD, A., 1991. Particules organiques et rapport C / N des sédiments des lacs du Jura. *Annls Limnol.*, **27**(2), pp.175–190.
- WANG, J., NAKAZATO, T., SAKANISHI, K., YAMADA, O., TAO, H. & SAITO, I., 2004. Microwave digestion with HNO₃ / H₂O₂ mixture at high temperatures for determination of trace elements in coal by ICP-OES and ICP-MS. *Analytica Chimica Acta*, **514**, pp.115–124.
- WESTAWAY, R., GUILLOU, H., YURTMEN, S., DEMIR, T. & ROWBOTHAM, G., 2012. Constraints on the timing and regional conditions at the start of the present phase of crustal extension in western Turkey , from observations in and around the Denizli region. *Geodinamica Acta*, **18**(January 2016), pp. 209-238.
- WILKINSON, M., MILLIKEN, K.L. & HASZELDINE, R.S., 2001. Systematic destruction of K-feldspar in deeply buried rift and passive margin sandstones. *Journal of the Geological Society*, **158**, pp.675–683.
- XIE, Q., CHEN, T., ZHOU, H., XU, X., XU, H., JI, J., LU, H. & BALSAM, W., 2013. Mechanism of palygorskite formation in the Red Clay Formation on the Chinese Loess Plateau , northwest China. *Geoderma*, **192**, pp.39–49.
- YUAN, G., GLUYAS, J., CAO, Y., OXTOBY, N.H., JIA, Z., WANG, Y., XI, K. & LI, X., 2015. Diagenesis and reservoir quality evolution of the Eocene sandstones in the northern Dongying Sag , Bohai Bay Basin , East China. *Marine and Petroleum Geology*, **62**, pp.77–89.
- ZOLITSCHKA, B., FRANCUS, P., OJALA, A.E.K. & SCHIMMELMANN, A., 2015. Varves in lake sediments e a review. *Quaternary Science Reviews*, **117**, pp.1–41.

Appendices

Appendix A – Field report

Appendix B – ID-Charts for detrital facies in the Ballik area

Appendix C – Jackson Treatment

Appendix D – EA-IRMS procedure

Appendix E – Sample list

Appendix F – Bulk XRD diffraction patterns

Appendix G – Bulk XRD diffraction patterns: Laminae

Appendix H – XRD diffraction patterns oriented clay slides

Appendix I – ICP-OES results

Appendix J – Porosity and permeability measurements

CD 1

Ballik model – Sketchup Pro

Scatterplots: Geochemical correlations of elements in the lacustrine facies

Scatterplots: Geochemical correlations of elements in the lacustrine facies and travertine lithologies.

Appendices

Appendix A – Field report

In the framework of this thesis a field trip was organized which took place from the 25th of August till the 7th of September. The first objective of this field trip was to observe the sedimentary characteristics of the detrital sediments throughout all 9 quarries. Additionally, these lithologies were sampled as well, in combination with a photographic acquisition. In total four different detrital sequences were observed, which are visualized in the simplified overview in Figure 1. The field observations within each of these four sequences are discussed briefly within this appendix.



Figure 1: *Right* - Overview of the quarry of Faber, where three sequences can be observed. *Left* – Simplified overview of all four detrital sequences (Lower conglomerates = red, Middle siliciclastic sequence = yellow, Upper siliciclastic sequence = green, Cover siliciclastic sequence = blue).

1.1 Lower conglomerates

The oldest siliciclastic level that was observed are the lower conglomerates, visible in the quarries of Ece and Faber. These conglomerates occur in the subhorizontal travertine facies, as is described by (Claes et al., 2015).

1.1.1 Faber

In the quarry of Faber these conglomerates occurred as several different channels, with a thickness ranging in between several cm and a m. Imbrication structures were observed, with pebbles dipping about 30° towards the north (Figure 2).



Figure 2: Imbrication structures (highlighted in black) on the western wall of the Faber quarry, dipping towards the north.

These conglomerates tended to have a polygenetic composition, since next to travertine fragments they also contained *exotic* rock fragments (e.g. limestone, marble, quartzite ...). In the field itself, the clasts could be divided in two different families, based upon their composition and clast size. In general, the larger boulders were composed of the subhorizontal travertine facies, however, these large boulders could only be observed in the thicker units. It were these clasts that were often still quite angular in nature, as highlighted by the white arrow in Figure 3.

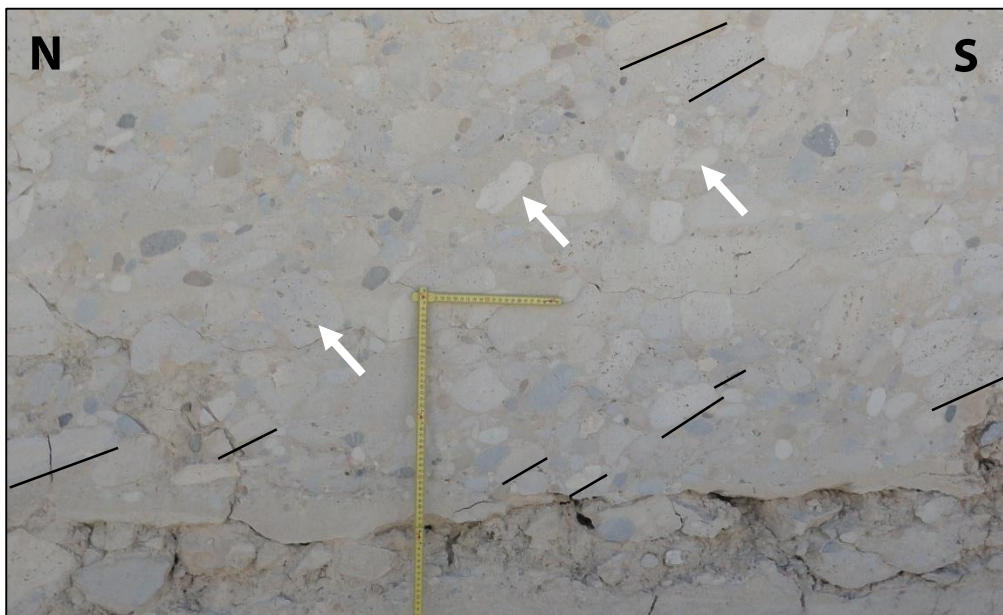


Figure 3: Sub-angular travertine boulders (white arrows) in a conglomeritic level on the eastern wall of the Faber quarry, with imbrication structures (highlighted in black) dipping towards the north.

In general, this unit was made of an alternating sequence of subhorizontal travertine and conglomerates. These conglomerates were always grain-supported in nature, observed within channels and tend to form amalgamated structures. However, they could also be observed as lenticular bodies, as can be seen in Figure 4. It was observed that the conglomeratic beds were often eroding the subhorizontal travertine facies, leading to nearly in-situ travertine blocks with a slight rotation. Throughout this unit several paleosols could be observed as well, often with the presence of some pebbles and micro-conglomerates. Some of these paleosols were observed as the lateral equivalent of a conglomeratic level, while other ones were just continuous horizons throughout the exposed section.

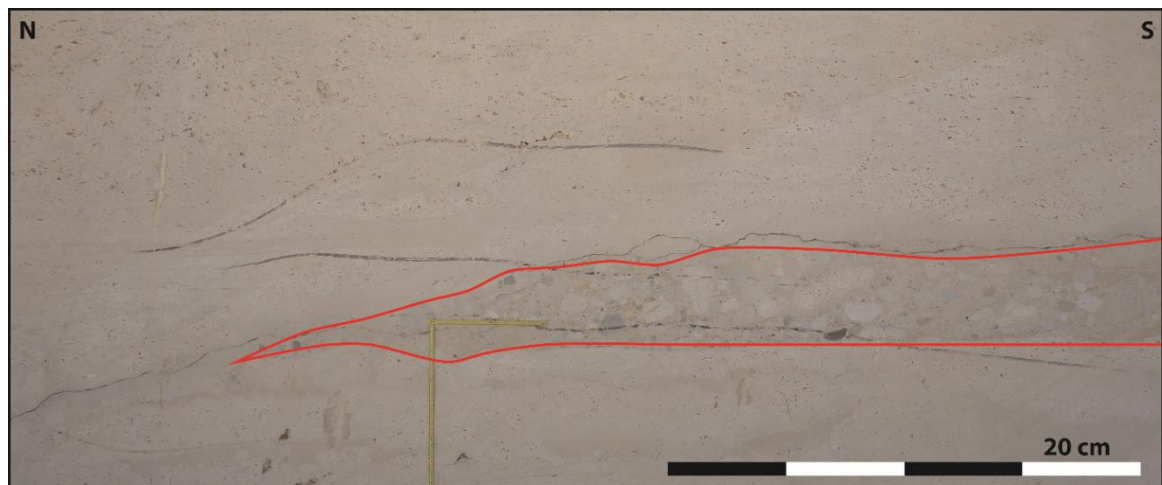


Figure 4: Lenticular conglomerate layer highlighted in red.

1.1.2 Ece

On a similar height as in Faber, some brecciated levels were observed in Ece as well. However, these beds are thinner as the ones in Faber and the overall matrix started to become more dominantly mud-supported. Furthermore, the *exotic* pebbles were absent within these breccias. Overall, the brecciated levels in Ece consisted of the subhorizontal travertine facies (Figure 5). These clasts were angular in shape are sometimes rather small. Furthermore, these clasts floated within the matrix itself and do not tended to be oriented within a specific direction.

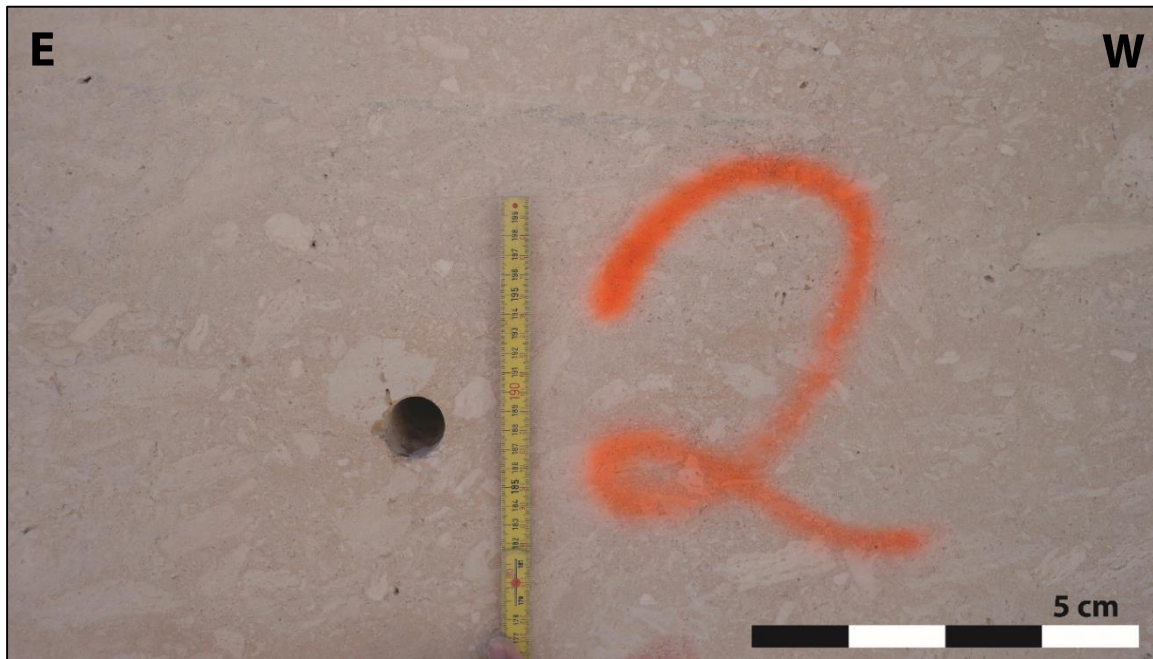


Figure 5: Composition of the conglomeratic levels in Ece (close-up of Figure 6).

Imbrication structures could be observed on the south-wall of the Ece quarry, indicating a flow direction towards the west (Figure 6). Lastly, it was observed that paleosols are rather abundant in the Ece quarry, especially towards the top of this siliciclastic sequence.



Figure 6: Imbrication structures (black lines) indicating a flow direction towards the west.

1.1.3 Summary

If we assume that the siliciclastic units in Ece and Faber were lateral equivalents from each other, an evolution in the depositional system could be observed. In general, the size of the conglomeratic beds decreases towards the east. In the western wall of the Faber quarry continuous beds, with a thickness of about a m could be observed, while as these beds seemed to break up into several smaller ones towards the east. Furthermore, these

conglomeratic beds were rather thin in the Ece quarry, where they had a monogenetic composition and more angular clasts. It could thus be observed that the amount of “exotic” pebbles decreased towards the east, just as the overall pebble-size. The breccias in the east were mainly made of clasts of the subhorizontal travertine facies, while as the conglomerates in the west were polygenetic and contained large travertine boulders. It thus seemed that these conglomerates are partly made of (locally) reworked-travertine facies, but also of eroded pebbles of different lithologies. The origin of these conglomerates seems to lie in the (north)-west, what could explain the decreased amount of *exotic* pebbles in the Ece quarry. Furthermore, the development of several paleosols, specifically in the Ece quarry, could indicate that less travertine was deposited during this period. A possible depositional setting might be an alluvial plain, on which several braided-river channels develop. The rather quick transition from the subhorizontal travertine facies towards the more energetic conglomeratic levels means that the depositional environment changed rather quickly. Making a rather catastrophic event a possible explanation for this rapid transition.

However, it is also possible that the breccias in Ece and the conglomerates in Faber do not correspond to the same depositional event. This would mean that the breccias in Ece were a rather local phenome, due to their monogenetic composition and mud-supported nature. While as the conglomeratic levels in Faber represent the development of a large fluvial system.

1.2 Middle siliciclastic sequence

This sequence was observed in the quarries of Faber, Faber West and Cakmak and was dominated by the alteration of conglomeratic channels and marls. In Faber West these conglomerates were often mud supported, while as in Cakmak they were clearly grain supported. The overall characteristics of this sequence in all quarries were given below.

1.2.1 Faber

In the quarry of Faber this siliciclastic unit had a thickness of about 9 m and was bordered by travertine deposits towards the bottom and the top. The travertines at the bottom were part of the subhorizontal facies, while as the travertines at the top were part of the cascade facies. Furthermore a pinching out geometry could be observed towards the East, since at the eastern-wall the thickness was less than 5 m.

In the western part of the quarry this sequence was dominantly composed of rather uncemented lithologies. The base of this sequence contained several erosive channels,

often with rather large clasts. The larger clasts (\varnothing 15 – 25 cm) were often made of the subhorizontal travertine facies, while as the smaller pebbles consisted of a dark-grey limestone. Within the central part of this section, the laminated marls became more dominant, leading to half a m of clearly laminated deposits. It was also within this part that coarsening upward sequences could be observed within the conglomeratic units. The top part of this sequence was dominated by erosive channels with a thickness of up to 3 m. In general, all of these channels were grain-supported, however, some mud-supported units were observed as well. Within the top part the travertine lithologies were becoming more dominant again, leading towards well-cemented conglomeratic beds. Furthermore, it was possible to observe a travertine-supported conglomerate, in which some reed-stems were present.

In comparison to the western part, which was rather uncemented as a whole, the eastern part was composed dominantly of well-cemented siliciclastic units. The base of this sequence was dominated by laminated marls, with an increasing degree of cementation towards the top. At the base an alternating package of carbonate-rich clays with silty layers rich in organic material could be found at about 1 m (located about 3 m below the top of this sequence). This alternating sequence seemed to be rhythmic in nature and contained well-developed laminations. Towards the middle part of the sequence, some erosive river channels could be observed, but in comparison to the western-wall these conglomerates were completely cemented by a microcrystalline carbonate mud. Further towards the top travertine-like lithologies could be seen, however, there were still some pebbles present within these lithologies. An overview of this western wall is given in Figure 7, highlighting the presence of an erosive conglomeratic bed.

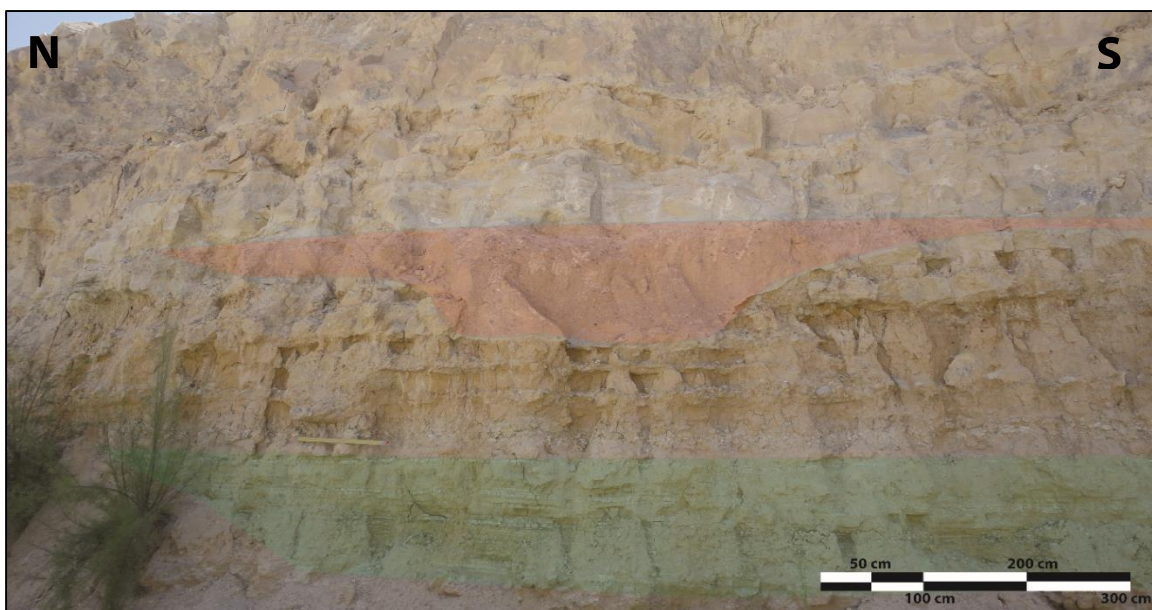


Figure 7: The western-wall of the Faber quarry with the erosive conglomerate bed (red) and the laminated marls (green).

1.2.2 Faber West

While as the middle siliciclastic unit in the Faber quarry was separated by a travertine intercalation from the upper one, this intercalation was absent in the quarry of Faber West. In this quarry the middle and upper siliciclastic sequences could be observed as one continuous sequence, often with a poor degree of exposure. The total height of this sequence was estimated to be more or less 20 m. Based upon the presence of specific carbonate enriched horizons, which were made of travertine lithologies, the total sequence could be subdivided in two smaller ones (Figure 8).

The lower 8 m seemed to match the middle siliciclastic unit as it was observed in Faber, however, the specific characteristics were slightly different as the ones observed in Faber. The first major difference was the overall abundance of grain- to mud supported conglomerates, which were less erosive as in the quarry of Faber. Additionally the pebbles within these mud-supported conglomerates were poorly sorted, leading to a poorly visible fining upwards sequence. It was only within the erosive channels that a clear fining upwards sequence could be observed, in combination of bioturbations filled with a coarse sand. The top of each mud-supported conglomerate was often rich in root traces, which were often covered by manganese-oxides. The upper part of this sequence also contained oxidation-reduction spots and was often rich in sedimentary mica-like minerals. The carbonate enriched-horizon was inaccessible and thus no information about this horizon could be collected. However, it seemed to be that the marls in between the carbonate beds were often quite red in colour.



Figure 8: An overview of the siliciclastic sequence of Faber West, with the white beds highlighted in black.

1.2.3 Cakmak

At the road towards the entrance of the Cakmak-quarry an outcrop of the same sequence could be observed as well. Standing in Faber West the connectivity of the siliciclastic unit between Faber and Cakmak could be observed, as is indicated in Figure 9.



Figure 9: Connectivity of the middle siliciclastic unit (bounded by black lines) between the Faber and Cakmak quarry.

The overall characteristics did match more closely the conditions that were observed in the Faber quarry. In general, these conglomerates were often grain-supported and were very well sorted. Additionally, these conglomerates were often deposited in erosive river channels, in which an amalgamated structure could be observed. The major difference with the conglomerates in the Faber quarry was the rather poorly-cemented nature of these beds.

1.2.4 Summary

In general, it could be observed that this sequence was dominantly composed of mud-supported conglomerates in the west, while it gradually became more grain-supported in the east. Based on the dipping of this unit, this would coincide with the flow-direction (towards the south-east) of the depositional environment.

Furthermore, it could be observed that towards the east more erosive river channels were more abundantly present, while in the west the conglomerates were often non-erosive and draping in nature. Additionally, the presence of laminated marls was restricted towards the sediments closely associated with the newly developing dome.

Regarding the developing dome a continuous travertine intercalation, which was composed of the cascade facies, could be observed in the quarry of Faber. This

intercalation was absent in the quarry of Faber West, with the exception of some carbonate-rich levels that could correlate with this travertine intercalation.

1.3 Upper siliciclastic sequence

The upper siliciclastic sequence covered most of the studied quarries, ranging from Cinkaya, Faber West, Faber, Cakmak, Ece and potentially Aglimolu Tasarim. In the quarries of Faber and Cakmak this sequence was separated from the middle one by a travertine intercalation.

1.3.1 Cinkaya

The quarry of Cinkaya was the uppermost north-western location where this sequence could be observed. An initial observation that was made was the abundance of the subhorizontal travertine facies. A rather local domal structure was present in this quarry, causing the travertine to dip both towards the north-east and south-east. Furthermore a fault, with a proximate east-west orientation could be observed in the centre of this quarry.

The north-western wall of the quarry of Cinkaya contained large-scale brecciated travertines (Figure 10). This wall is composed of a breccia with large travertine boulders, with dimensions reaching up to several metre and were quite angular in shape. The space in between the boulders was filled up by a carbonate-rich mud, which had a similar appearance as the mud of the fault itself. On top of this breccia a well-sorted conglomeratic unit could be observed, which seems to have undergone a certain tectonic rearrangement

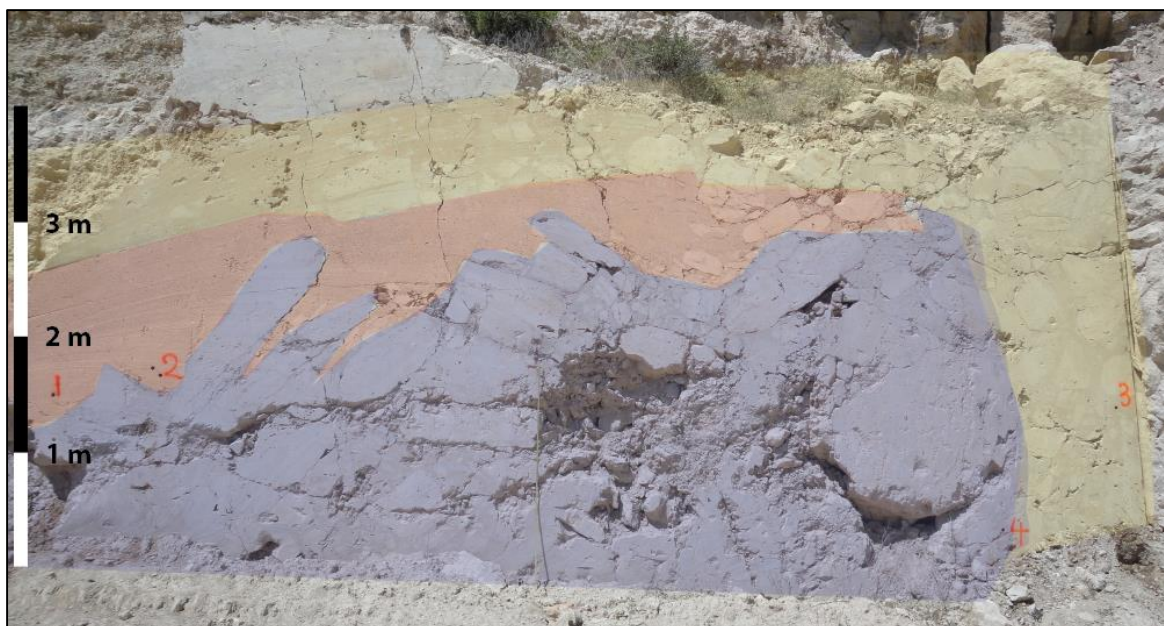


Figure 10: North-western wall of the Cinkaya quarry with travertine-welded breccia (blue), travertine-welded conglomerates (red) and mud-supported travertine breccia (yellow).

since they were draping around the large travertine boulders. Lastly, a mud-supported travertine breccia lied on top, which connected to the mud within the fault. On top of these layer reed-travertines could be observed, what could indicate that the fault itself became cemented afterwards due to the influx of carbonate-rich cements.

The travertine that aligned with the fault-like structure in the center of the quarry is enriched in gastropods. On the other hand the rather large boulders were absent here, while as the smaller conglomeratic pebbles could still be observed. These pebbles had undergone a certain tectonic activity, leading towards their chaotic structure. In general, the carbonate-mud was far more dominant in the centre of the quarry (Figure 11).

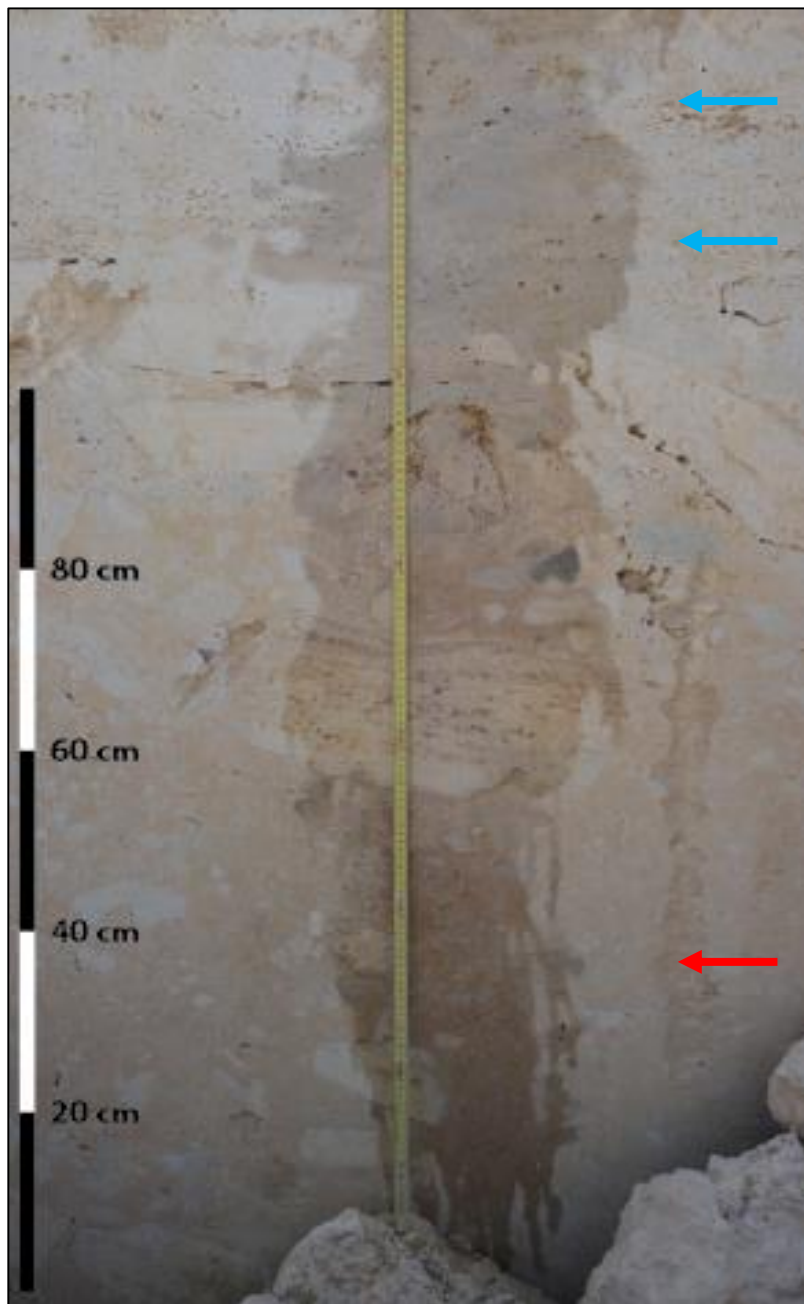


Figure 11: Breccia consisting of the sub-horizontal travertine (red arrow) facies and gastropod-rich carbonate beds (blue arrows).



Figure 12: Overview of the conglomeratic sequence in the north-western wall. Highlighted in red the porous, often powder-like, black rock.

On top of the fault structure in the north-west, a conglomeratic sequence of about 6 m in thickness could be observed. These conglomerates were very-well cemented, often with crystalline cements. It was also within this sequence that a rather porous black rock could be found (Figure 12).

To the south-west of this domal structure, laminated marls of about 2 m in thickness could be found. These marls were pinching out in between the quarry of Cinkaya and Faber West. Towards the south of the quarry of Cinkaya coarser grains became more dominant in this laminated marl. Here the marl was dominantly made of silt and contained sedimentary micas, however, petrographical observations were needed in order to confirm these observations. In between Faber West and Cinkaya, this silty lithology made place for very well sorted sandstones and conglomeratic beds. These conglomerates were most often observed in erosive channels, but also as non-erosive layers of pebbles. This could indicate the presence of a paleo-high in between Faber West and Cinkaya, potentially similar to the travertine ridge as in Cinkaya itself.

1.3.2 Faber West

As already had been indicated, the intercalation of travertine, separating the upper and middle sequence, was absent in this quarry. A major difference with all other quarries was the abundance of carbonate-cemented and travertine-like lithologies. The lower part was rich in massive marls, containing some pebbles. Erosive river channels are rather rare and if they are present they were more likely to be mud-supported than grain-supported. It was also within this sequence that silty-beds, enriched in micas could be observed. The upper-part, on the other hand contained several erosive river channels, filled with large travertine clasts (up to 20 cm). It was observed that these conglomeratic channels became more cemented with decreasing bed thickness. Furthermore, some thin travertine-like beds, made of the reed-travertine facies, could be observed as well. The abundance of carbonate-cemented conglomerates and travertine-like intercalations, could be related to the interpreted presence of a ridge. This could indicate that this ridge was still active during the deposition of this sequence, leading towards an increased cementation and the abundance of travertine-like beds towards the north-north-east.

1.3.3 Faber

In the quarry of Faber this sequenced was better exposed as in Faber West. The lower 2.5 m were composed of mud-supported conglomerates, which were non-erosive in nature. The clasts of these conglomerates were bimodal, both in size and in composition. The larger ones, being about 10 cm in diameter, were composed of the reed- and subhorizontal travertine facies. The smaller pebbles were dominantly composed of a rather dark limestone. Within this part, coarsening upwards sequences could be observed in the non-erosive conglomeratic beds.

The middle-part of this sequence was separated by the lower part by laminated marls with a thickness of about 2 m. These marls were thinly laminated (0.5 cm) in the lower part, but the thickness of the laminae increased towards the top (3.0 cm). The middle-part of this section was composed of rather sandy lithologies, in which manganese-oxidized cross-laminations could be observed. Within this part intact gastropods were present as well. These sandy units displayed channel-like geometries, with a thickness of about 2 m. On top of these sandy units a kind of nodular limestone could be observed, which was embedded in a silty matrix. Towards the top, this section consisted of grain-supported river channels, which were covered by massive marls with root-traces.

Just as the middle-part, the upper-part of this sequence started with laminated marls. These were eroded by micro-conglomerates in which cross-lamination could be seen. The

lower part of this section was dominantly made of a sandy-siltstone with a thickness of about 1 m. Within this unit some carbonate-enriched horizons could be seen, in which root-like traces could be observed. The upper part of this section was dominantly made of conglomerates, which were slightly erosive. Towards the south it could be observed that the lithologies became more enriched in carbonates. This might be related to the presence of the travertine dome, which was covered by the detritals of this sequence (Figure 13).

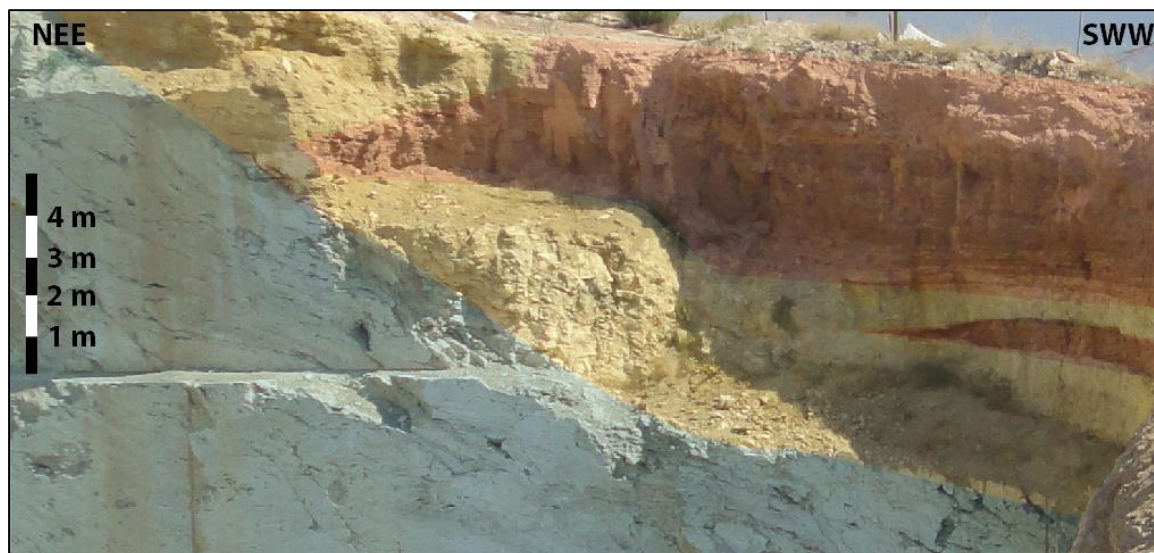


Figure 13: Most southern corner of the Faber quarry with the transition from the cascade facies (blue), to the cemented (yellow) and uncemented (red) siliciclastic sequences.

1.3.4 Cakmak

In the quarry of Cakmak, the influence of the proximity to the travertine dome on the siliciclastic deposits could be assessed. The lateral equivalent of the upper siliciclastic sequence, as observed in Faber, could be seen in Figure 14. The sequence was well-cemented in nature and had a rather limited thickness, in comparison to the sediments in the quarry of Faber. Further towards the south laminated marls could be observed. It has to be mentioned that this sequence was not observed on the same height as the other detrital deposits, however, they could belong to the same depositional system. The dislocation of this unit could be related to the paleo-topography of the travertine dome. In contrast with all the other described outcrops this one was made entirely of laminated marls, what could be related to a deeper depositional environment. This would mean that the conglomeratic sequences in Faber West and Faber were deposited on a paleohigh, while as these marls are deposited in a paleolow.



Figure 14: Well-cemented detrital deposits on top of the cascade travertine (blue) dipping towards the south. An initial observation was the degree of cementation of these marls, which was increasing towards the north (where the travertine dome is located). In the south this sequence was mainly made of uncemented marls, while as the northern section contained carbonate-cemented muds. This transition can be seen in Figure 15, where the degree of cementation increases towards the west. The equivalent of these laminated marls on the travertine dome itself, seemed to be monogenetic breccias. These breccias were welded together by a carbonate mud and tended to form paleosols in between the dome and the varve-deposits. Furthermore, these marls were covered by travertines of the cascade-facies, which tended to pinch-out towards the south-east.



Figure 15: The transition from clay-rich varves (east) to carbonate-cemented varves (west).

1.3.5 Summary

The upper siliciclastic sequence could thus be observed with great certainty in the quarries of Cinkaya, Faber West, Faber and Cakmak. It could be observed that this siliciclastic sequence tended to terminate upon the developing travertine dome. Based upon the dip direction of this sequence, the sediment seemed to originate from the north-west. Within this sequence a rather strong lateral variation could be observed, with laminated marls abundantly present near the travertine dome.

The proximity of the developing travertine dome also influenced the degree of cementation. This causes, for example, the transition from uncemented laminated marls to carbonate-enriched muds towards the travertine dome itself. The presence of a paleo-high in between the quarry of Faber and Cinkaya, caused a rather quickly changing depositional environment on both sides. Furthermore, the increased cementation near this paleo-high may indicate that it was an active during the sedimentation of this sequence (similar as the ridge in Cinkaya itself).

1.4 Siliciclastic cover unit

The youngest siliciclastic unit covered the quarries of Alimoglu-Tasarim, Cakmak and Metamar (abandoned). In general, it seemed that this sequence could be subdivided in two different sections, which were only observed both in the quarry of Alimoglu-Tasarim.

1.4.1 Alimoglu-Tasarim

The quarry of Alimoglu-Tasarim contained an overburden with an estimated thickness of about 10 m and could be subdivided into two major units. The subdivision was based upon a rapid change in the depositional environment, highlighted by an erosive contact in between both units. This erosive contact can be seen in Figure 16, where the marker horizons are highlighted by green lines. On this figure it can be observed that the lower section was eroded towards the south, leading to a decreased thickness of this section. This lower section was made of an alternation of white and greenish laminated marls, in which some horizons seemed to be enriched in organic material (and could act as marker horizons in Figure 16). These organic rich layers often contained root traces. Furthermore, towards the top some layers with gastropods and pebbles were observed as well. The uppermost top of this section contained microconglomerates, however, they did not seem to erode the underlying marls.



Figure 16: The eastern-wall of the quarry of Aglimolu-Tasarim. An erosive contact can be seen with the marker horizons (highlighted in green) and the upper unit (yellow).

This sequence could also be observed in the most western corner of the quarry of Alimoglu-Tasarim, however, in here the degree of cementation was significantly higher. This sequence as a whole, however, pinched out towards the west and thus could not be observed in the quarry of Ece. This made it impossible to truly correlate the sequences with the one on the western side of the travertine dome. On the contact between the laminated marls, erosive conglomerates and tabular sandstones, several tectonites could be observed. These tectonites ranged from ball-and-pillow structures and water escape structures. These structures could be seen on Figure 17, where the marls were draping around the sandstone blocks.



Figure 17: Ball and pillow structures (red) in the upper unit, just above the lower unit (green).

The lower section of this upper sequence did contain tabular sandstones, next to laminated marls. These sandstones often contained cross-lamination, indicating a flow direction towards the south. It was also within this lower part that carbonate beds became more dominant, often with pinch-and-swell structures. Plant material could also be observed within these carbonate beds and sometimes they tended to develop similar characteristics as the reed travertine facies. The central section of this sequence contained several coquina beds, which were often purely composed out of gastropods shells. These coquina beds were surrounded by rather fine grain-supported conglomerates, in which broken gastropod fragments were present as well. The upper part of this sequence was made of rather thick conglomerates, with a thickness up to 3 m. These conglomerates were erosive in nature and were often coated in manganese-oxide. Furthermore, the overall orientation of these channel-like geometries was north-south leading towards the quarry of Cakmak.

Further towards the east, in between the quarry of Alimoglu-Tasarim and Metamar (abandoned), a test-pit could be found. It was within this test-pit that a ridge-like travertine structure, aligned in an east-west direction, could be observed. In the northern part of this pit, conglomerates and sandstones could be observed, often with cross-lamination and manganese-oxide coating. Furthermore, certain beds were characterised by the presence of root traces. With increasing proximity towards the centre of the travertine-ridge, these lithologies became more cemented. A transition from several conglomeratic channels towards the reed-facies could be seen. Additionally, encrusting travertine horizons could be observed as well, often with a limited thickness (Figure 18).



Figure 18: Encrusting travertine on top of a fine conglomeratic bed.

In the centre of this test pit a travertine ridge could be observed. It seemed that these travertine deposits were plunging down, at the contact between the detrital deposits. This could indicate the outer-most border of the ridge (Figure 19). The travertine ridge itself was dominantly made of the reed-facies, where in the central part the reed-stems were still in-situ.

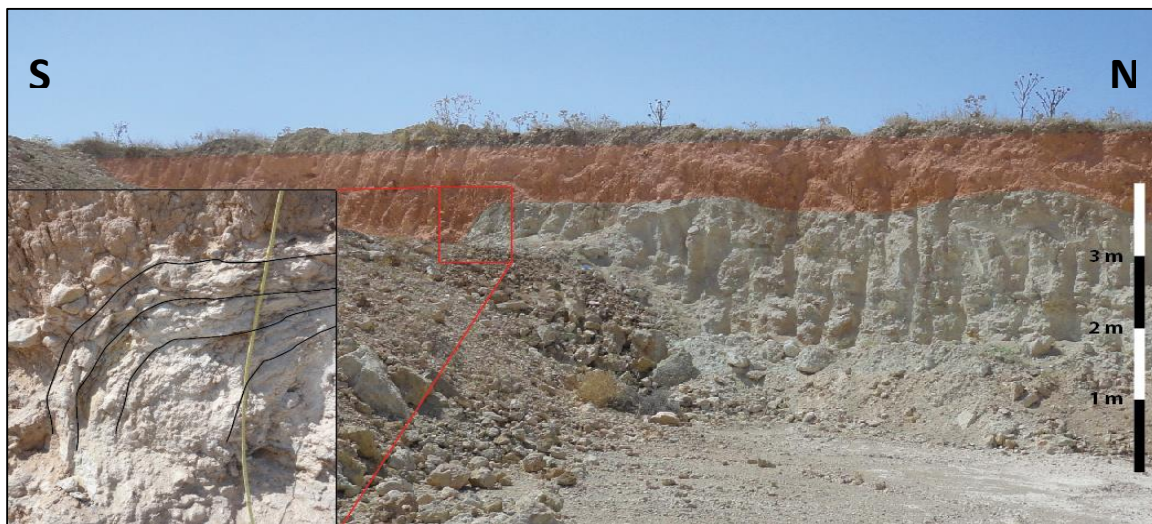


Figure 19: Central part of the travertine ridge (blue) in contact with the siliciclastic sequence (red).

1.4.2 Cakmak

The top of the travertine dome in the quarry of Cakmak was covered by the lateral equivalent of the same cover sequence as could be observed in Alimoglu-Tasarim. At first it could be seen that this unit pinched out towards the west, making it only possible to observe it in the north-eastern corner of the quarry. In comparison with the sediments in Alimoglu-Tasarim, the lower section was rather thin in the quarry of Cakmak. The thickness of these laminated marls was limited to about 1.5 m, on which erosive conglomerates could be observed. Similar as in the quarry of Alimoglu-Tasarim, some tectonites could be observed as well. These tectonites were classified as such, based upon the curving of the underlying layers (Figure 20). This made this feature rather tectonic, than purely sedimentary in origin.



Figure 20: Tectonical-triggered structure in the overburden of the Cakmak quarry.

On top of these conglomeratic channels, a metre of thinly laminated tabular sandstones could be observed. It was within these thinly laminated sandstones that several horizons, enriched in organic materials, were present. The upper part of this sequence, however, seemed to be made of fine to medium sandstones, in which hummocky cross-lamination could be observed. In between these sandstones crushed gastropod-fragments could be seen, however, in comparison to Alimoglu-Tasarim no intact gastropods were present .

1.4.3 Metamar (abandoned)

In the quarry of Metamar, the cover sequence possessed similar characteristics as the sediments in the test-pit east of the quarry of Alimoglu-Tasarim. The unique aspect of this quarry was the presence of fracture swarms, which seemed to be cemented to a certain extend. These cemented-fracture swarms tended to be orientated more or less east-west (Figure 21). Laterally of these fracture swarms, cementation occurred as well, however, the degree of cementation seemed to be related to the proximity of these swarms. This indicated that these fracture swarms were possibly pathways for carbonate-enriched fluids.



Figure 21: The fracture swarm (yellow) with vertical cemented-fractures. This cementation seems to extend laterally in the siliciclastic sequence next to it.

Appendix A – Field report

The sequence seemed to be slightly thinner as it was in Alimoglu-Tasarim, with an estimated thickness of about 5 m. The lower part of the cover sequence seemed to be made of cemented siltstones with carbonate intercalations. On top of these silty-units a rather thick coquina-bed could be observed in which intact gastropods were present. The central section of this sequence was made of erosive conglomerates with a thickness of about 1 m. It was on top of these conglomerates that the finer sandstones to siltstones could be found. It was mainly the upper section of the sequence which was influenced by the presence of the fracture swarms. This causes rather local cemented lithologies, to even pure carbonates, while as they were non-cemented at 3 m of these swarms.

1.4.4 Siray

In the quarry of Siray the detrital sequence could not be studied, since all detrital sediments were caught within a major fault zone (Figure 22). These sediments also contained intact gastropods and had a profound red colour. This could indicate that on top of this quarry some sediments were deposited with similar characteristics as the one observed in Metamar, Cakmak and Alimoglu-Tasarim. All of these studied quarries were showing traces of a certain tectonic activity (the presence of ball-and-pillow structures, fracture swarms, tectonically reactivated sediments ...), which could be related to the activation of this fault zone.



Figure 22: Large fault zone in the quarry of Siray, with an infall of red sediments.

1.4.5 Basaranral

In the quarry of Basaranlar, which is located in the upper eastern corner of the study area, no siliciclastic deposits were observed.

1.4.6 Summary

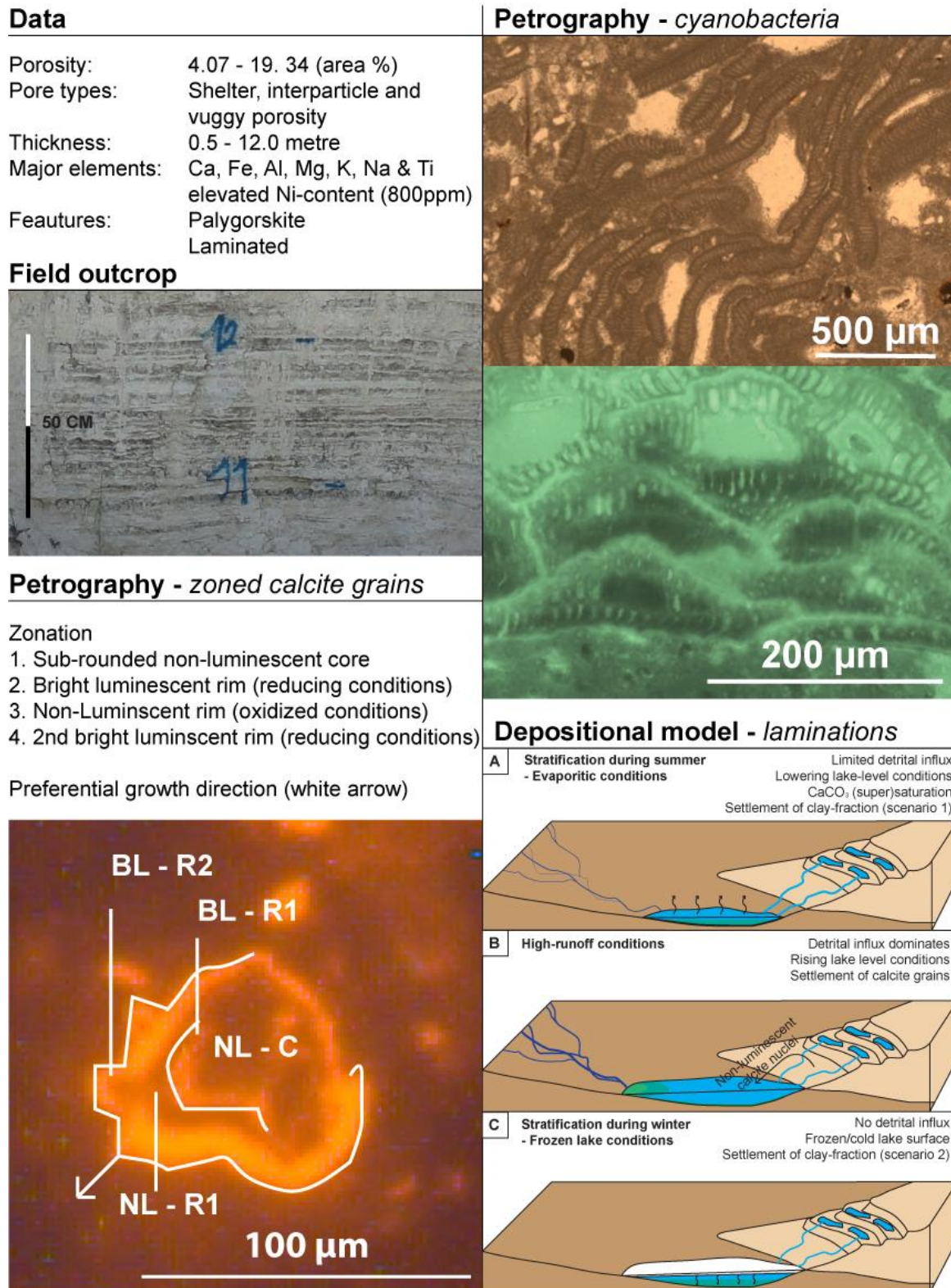
The siliciclastic cover sequence could be observed in the quarries of Cakmak, Alimoglu-Tasarim, Metamar and may have been present on top of Siray. This sequence could be distinguished from the previous ones by the abundance of coquina-beds, tectonites and carbonate-beds.

The depositional system seemed to be oriented in a north-east to south-west, meaning that the source of these sediments would lie in the north-east. This was confirmed by the dip direction of the erosional surface in between the laminated marls and the conglomeratic channels, which was dipping towards the south. Furthermore, intact gastropods were rather abundant in the north, while as they could only be observed as fragments in the south. This could indicate that they were transported from the north (Alimoglu-Tasarim) to the south part (Cakmak).

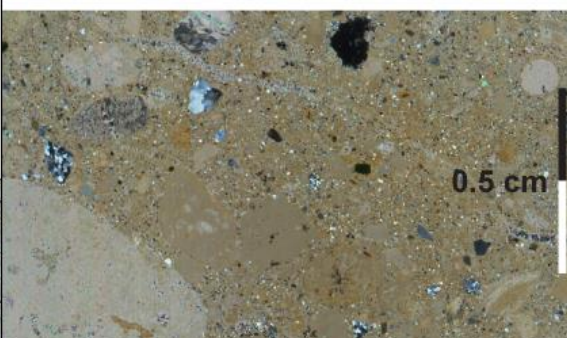
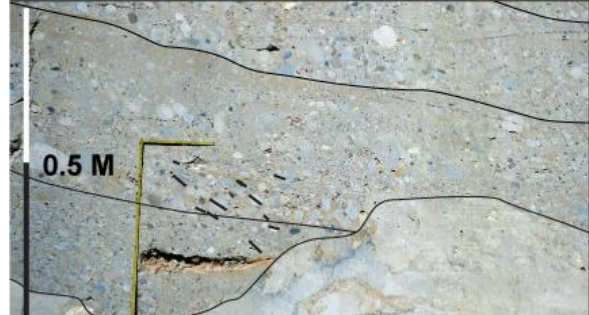
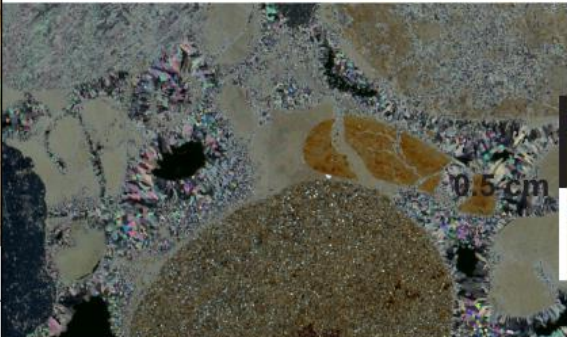
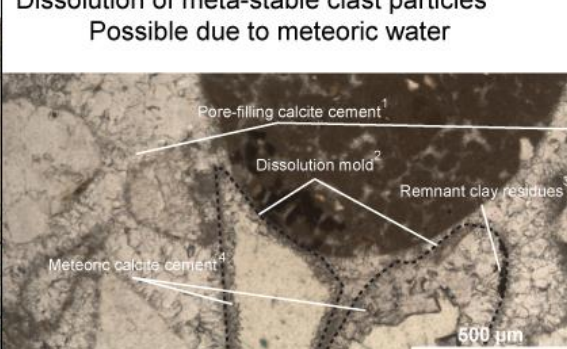
At last the presence of tectonites, fracture swarms and fault zones were considered to be an indicator for the tectonic activity in this region that took place after the deposition of the travertine dome. The presence of the red sediment in the fault in Siray could mark the most eastern extent of this cover sequence.

Appendix B – ID-charts for detrital facies in the Ballık area

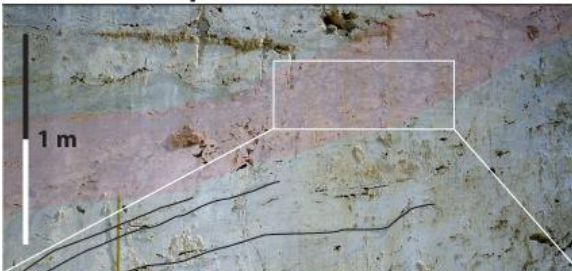
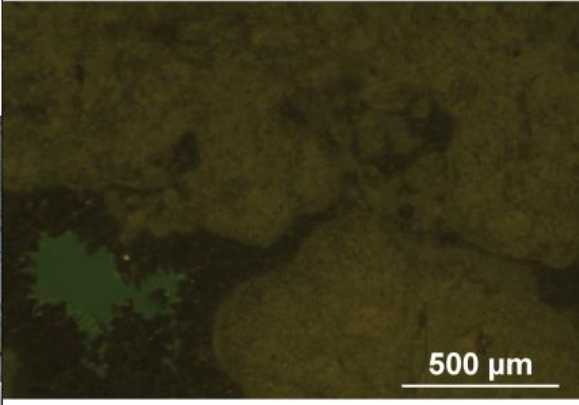
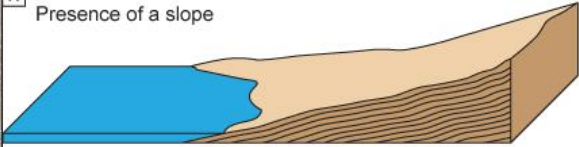
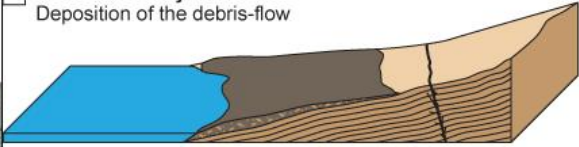
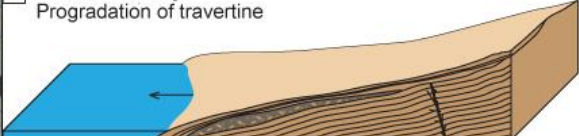
Lacustrine facies: ID-chart



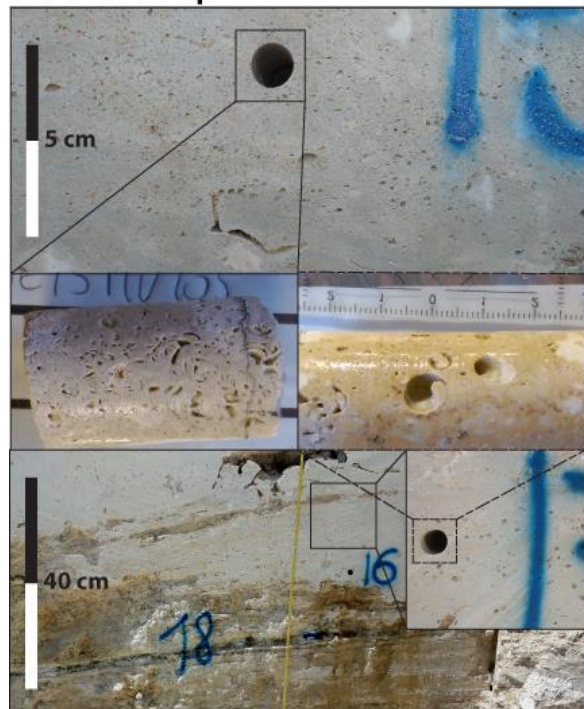
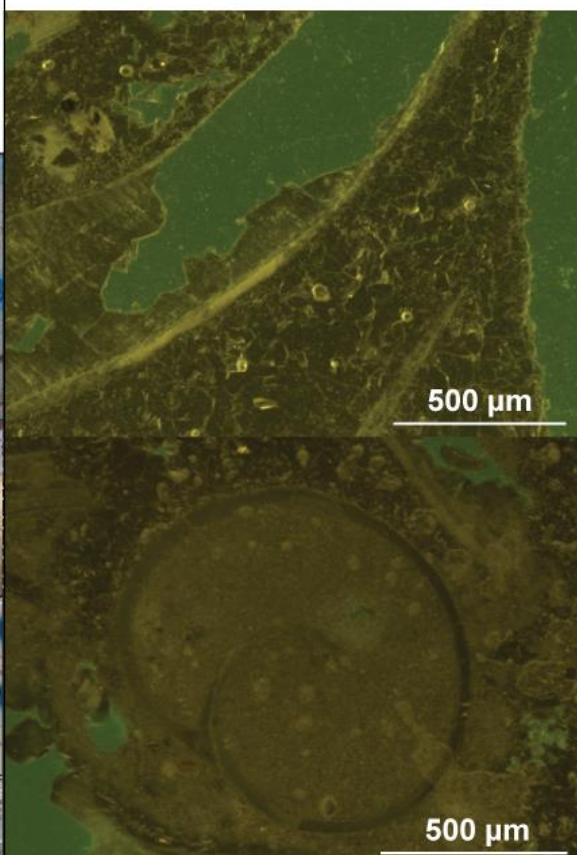
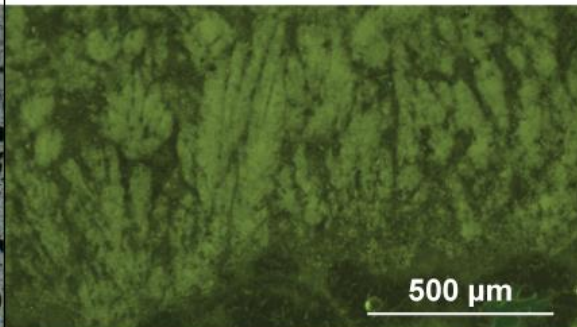
Fluvial facies: ID-chart

| Data | Petrography - <i>Mud-supported congl.</i> |
|---|---|
| <p>Porosity and permeability (conglomerates)</p> <p>Well-cemented 5.6 - 11.9 % & 0.02 - 0.30 mD</p> <p>Mud-supported 10.5 - 14.9 % & 0.29 - 123 mD</p> <p>Poorly cemented 8.3 - 11.5 % & 142 - 3143 mD</p> <p>Pore types: Interparticle, solution-enhanced & vuggy porosity</p> <p>Thickness: 0.2 - 0.6 metre</p> <p>Features: Channels</p> | <p>Clasts embedded in a microcrystalline matrix</p> <p>Calcite cements within pores</p> <p>Cemented calcite veins</p>  |
| <p>Field outcrop</p> | <p>Petrography - <i>Well-cemented congl.</i></p> |
|  <p>0.5 M</p> <p>Travertine</p> <p>Channel</p> <p>Massive marl</p> <p>Laminated marl</p> <p>Massive marl</p>  <p>2 M</p> | <p>Clasts embedded in a crystalline matrix</p> <p>Interparticle porosity</p> <p>Poorly connected pore network</p> <p>Cemented calcite veins</p>  <p>0.5 cm</p> |
| <p>Petrography - <i>Poorly cemented congl.</i></p> | <p>Petrography - <i>Dissol. enhan. porosity</i></p> |
| <p>Clasts embedded in a poorly-cemented matrix</p> <p>Microporous matrix</p> <p>Absence of calcite cements</p> | <p>Dissolution of meta-stable clast particles</p> <p>Possible due to meteoric water</p> |
|  <p>0.5 cm</p> |  <p>Pore-filling calcite cement¹</p> <p>Dissolution mold²</p> <p>Remnant clay residues</p> <p>Meteoric calcite cement⁴</p> <p>500 μm</p> |

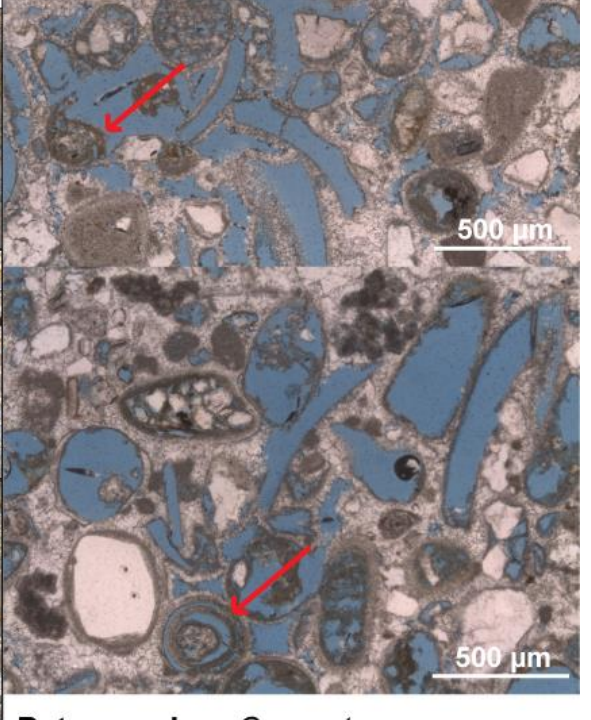
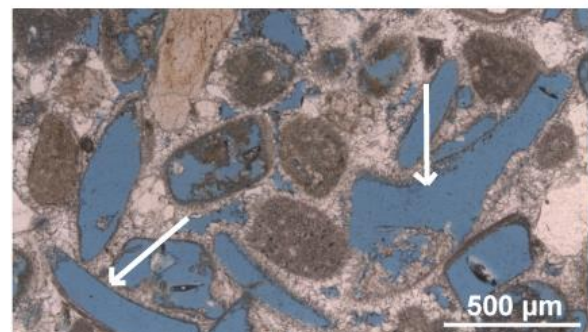
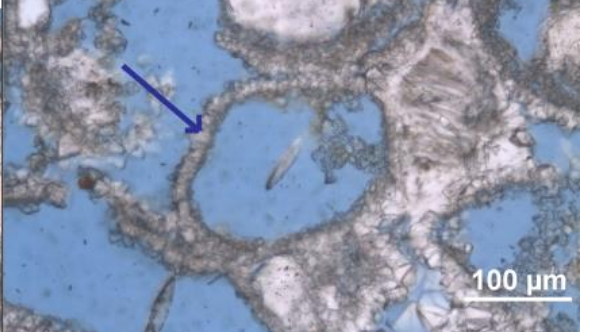
Debris-flow facies: ID-chart

| Data | Petrography - <i>Microporous clasts</i> |
|---|---|
| <p>Porosity and permeability 7.9 - 9.5 % & 0.32 - 11.8 mD</p> <p>Pore types: Interparticle and microporosity</p> <p>Thickness: 0.5 metre</p> <p>Features: Monogenetic composition Paleoslope No grain-grain contact</p> | <p>Travertine clasts contain microporosity Coated by calcite cements > Poorly connected pore network</p> |
| <p>Field outcrop</p>   |  <p>Depositional model</p> <p>Presence of paleoslope Deposition triggered by seismic activity Progradation of travertine dome</p> <p>A Initial condition Presence of a slope</p>  <p>B Seismic activity Deposition of the debris-flow</p>  <p>C Post-seismicity Progradation of travertine</p>  |
| <p>Petrography</p> <p>Small clasts trapped in a calcereous mud Interparticle porosity Presence of crystalline cements</p>  | |

Gastropod facies: ID-chart

| | |
|---|--|
| <p>Data</p> <p>Porosity and permeability: 8.7 - 14 % & 0.03 - 0.17 mD</p> <p>Pore type: Moldic porosity</p> <p>Thickness: 0.5 metre</p> <p>Features: (partly) dissolved gastropods Horizontal alligments</p> | <p>Petrography - Pore network</p> <p>Dissolution of metastable aragonitic shell Limited contact between different pores > Low permeability</p> |
| <p>Field outcrop</p>  |  |
| <p>Petrography - Pore network</p> <p>Isolated pore network Moldic pores embedded in a (micro) crystalline matrix</p> | <p>Petrography - Shrubs</p> <p>Presence of shrubs within the matrix Tend to contain microporosity</p> |
|  |  |

Coquina facies: ID-chart

| Data | Petrography - <i>Partly dissolved ooids</i> |
|--|--|
| <p>Porosity and permeability 39.3 % & 81.9 mD</p> <p>Pore type: Moldic porosity</p> <p>Thickness: 0.2 - 0.5 metre</p> <p>Features: (partly) dissolved shell fragments Coated grains Often uncemented</p> | <p>Coated grains present throughout the thin section</p> <p>Partly dissolved</p> |
| <p>Field outcrop</p>  |  |
| <p>Petrography - Pore network</p> | <p>Petrography - Cements</p> |
| <p>Connected pore network</p> <p>Moldic pores embedded in a crystalline (in the case of the cemented lithotype)</p>  | <p>Molds encrusted by microcrystalline calcite cement</p>  |

Appendix C – Jackson treatment

To maximize information about the clay minerals in a sample, one fraction is mainly studied: $< 2\mu\text{m}$ (exceptionally fr $< 0.2\mu\text{m}$). In order to ensure that the orientation in the obtained fractions is optimal, no aggregates should be present in the sample. All cementing agents are first removed. For this, the Jackson - treatment applied , it consists of three main parts :

- 1 . Solving the carbonates
- 2 . Removing the organic material
- 3 . Removing free Fe (hydr) oxides

This treatment is then closed with :

- 4 . Separating the fractions
- 5 . Convert to Ca – form
- 6 . Dialysis

After the sample is ready for :

- 7 . Apply on the glass slide

For practical reasons (centrifuge) we work on four samples per set .

1. Solving the carbonates

Carbonates do not only cement but also solve during centrifugation and cause flocculation of the clays. Its removal is done with an acid buffer , with a pH of 5 so that the minimum flocculate clays .

→ Buffer Preparation (5 liters) : 410g Na- acetate (CH_3COONa) dissolved in a gallon of water, 135 ml CH_3COOH (glacial) and dilute to 5 liters

Apply 15g (25g) of the sample into a measuring cup and add about 150ml (250ml) buffer. Cover the measuring cup and place it 30min . on a magnetic stirrer and heated to $80-90^\circ\text{C}$. Apply the material with demineralized water into the centrifuge cups (not load above). Centrifuge (2000rpm) 10min and pour supernatant into waste container cat 3. Add buffer and using an ultrasonic disintegrator for 1min. Put the sample back into the measuring cup with buffer (min.150 ml , 250ml). Cover the measuring cup and place it 30min . on a magnetic stirrer and let warm to $80-90^\circ\text{C}$.

Edit: Keep on adding buffer as long as reaction takes place (in the case of carbonate samples)

Appendix C – Jackson treatment

The carbonate cements have now been removed , the following steps (" cleaning ") are still needed to be sure to remove all of the Ca - ions (so that they can form with the organic material no complexes) and the clays to be converted in their Na- form.

- Transfer the suspensions on to the centrifuge cups with demineralized water
- Add 20ml saturated NaCl and dilute with distilled water to top
- Centrifuge (2000rpm) 10min and pour the liquid waste container in category 3
- Refill with demineralised water and add 20ml saturated NaCl
- Centrifuge (2000rpm) 10min and pour the liquid into sink

2. Removing the organic material (MnO₂ + solution)

Since this treatment with H₂O₂ is done , it should always take place after the removal step of the carbonates , for such a reaction is only effective in a carbonate-free and slightly acidic environment.

- Attach the sample, with as little as possible of the Na- acetate buffer of the centrifuge cup to a cup size
- Add steps (15ml - 25ml - ...) H₂O₂ and place the beaker on a magnetic stirrer and heated to 60 ° C , cover with a watch glass (Possibly evening which enclose and ' reacting night and then the morning until warm - or keep an eye on in the beginning!)
- Keep a close eye on the reaction and overreaction : add demineralized water !
- If the organic material is out (possibly dark color way / no response) : boil the suspension to all H₂O₂ is out

ALTERNATIVE:

Without heating (but keep an eye). Add 15ml H₂O₂ and place the beaker on a magnetic stirrer 30min. 2nd cycle : add 30ml H₂O₂ , and place 2 hours on a magnetic stirrer. Allow 1-2 days till the H₂O₂ may disappear completely. After both alternatives cleaning is again needed to exit this treatment. Transfer the suspensions on to the centrifuge cups. Add 20ml concentrated NaCl fill with demineralized water. Centrifuge (2000rpm) 10min and pour off the liquid in sink

3. Removing free Fe (hydr) oxides

Appendix C – Jackson treatment

Fe-(hydr) oxides cements can be effectively removed with Na- dithionite . However, in Fe- rich clays there is a risk that can be reduced as structural Fe therefore the quantities used are as small as possible .

The samples must be transferred to a solution in a flask

→ Solution: 8 units of 0.3 M Na - citrate per 1 unit of 1M NaHCO₃ (eg 56.47 g citrate in 640ml H₂O + 6.72 gNaHCO₃ in 80ml H₂O)

Per g sample add minimum 9ml solution , so for 15g = add minimum 135ml solution; for 25g = add 225ml. The flask with a glass rod in a warm bath shaker ' set at 75-80 ° C (the right temperature is very important !)

- Stir and add about 2g Na₂O₄S₂ (for 15g sample)
- Keep 5min. stir and repeat this another 2 times.
- After the third time leave for 15min.
- Apply the material with demineralized water to the centrifuge cups.
- Add 20ml concentrated NaCl (Cup not filled to the top with distilled water).
- Centrifuge (2000rpm) 10min and pour the liquid waste container in Category 5.
- Add distilled water and 20ml concentrated NaCl (not above).
- Centrifuge (2000rpm) 10min and pour the liquid waste container in Category 5.

4. Separating the fractions

The intention is to do analysis on two groups : < 2µm and < 0.2 microns , since for most samples the output of the fraction < 0.2 microns is not so great , this is 3/4ths of the material used . Most of the times however, we only do <2µm. Filling the centrifuge cups up to the mark , the exact centrifugation time , the rpm and temperature are very important in this process.

Fill the centrifuge cup up to the mark (!) And stir well.

For the fraction < 2 microns , centrifuge :

- Small pots : 3min (turn knob 900) at 1000rpm
- Large pots : 3min (turn knob 900) at 1000rpm

Transfer the liquid (communicating vessels) to large cups .

Repeat this procedure 2-3 (-4 - ...) times, each with a spin between the ultrasonic treatment (1 min) of the remaining material (in the centrifuge cups).

Appendix C – Jackson treatment

The remaining material on the bottom (the fraction $> 2\mu\text{m}$) is done in bowls with foil and put in the oven (90°) . After-drying , this fraction is recovered from the foil, weighed and placed in sachets.

Take 1/4th of the obtained amount of suspension to obtain the fraction $< 2\mu\text{m}$ and keep it separate and clearly mark.

The rest of the suspension is used to obtain the fraction of < 0.2 microns centrifuge :

- Small pots : 30min (turn knob to 2700) at 3000rpm
- Large pots : 37min at 3000 rpm (button set to 2700)

Transfer the liquid (communicating vessels) to large cups .

Repeat this procedure 2-3 (-4) times , fill the cups each with the remaining suspension (up to the mark !).

The remaining material on the bottom (the fraction $2\mu\text{m} > - > 0.2$ microns) is done in bowls with foil and put in the oven (90°) . After-drying , this fraction is recovered from the foil, weighed and placed in sachets.

Finally Add about 75 ml of concentrated NaCl per liter suspension to to obtain coagulation and let stand overnight (both cups with the fraction $< 2\mu\text{m}$ as those with < 0.2 microns) .

5 . Convert to Ca – form

The last flocculation of the material can be done with NaCl, but if there are smectites or smectite with mixed -layers present, it is better to do this with CaCl_2 . For in XRD analyzes, in the Na form high -charged smectites can appear as vermiculite and illite - smectites occur as illite - vermiculite . While in the Ca - form their characteristics will be preserved .

- Vacuum the clear water above the suspension road (communicating vessels) , as few tries as possible to keep water without the risk of suspension is sucked .
- Add about half a cup 1M CaCl_2 to the material in the centrifuge cups
- Centrifuge (2000rpm) 10min and pour the liquid away (as much as possible !)
- Then twice a similar procedure : but now fill the cups but each with 3-4 cm 1M CaCl_2 and centrifuge 5 min at 2000 rpm only . The material with a glass rod loosening of the soil between the centrifugations , and optionally a brief ultrasonic treatment , 20- 30s for example , perform (in the centrifuge cups) . This when the material is too much cemented .

5 . Dialysis

Appendix C – Jackson treatment

- Due to the foregoing treatments , there are a lot of excess electrolytes (for example, Cl⁻ ions) contained in the suspension , it is therefore necessary to remove this by means of a dialysis .
- Pour Ca saturation after the full (!) Fluid path
- Apply the material from the centrifuge cups with (a glass rod and) demineralized water into a semi - permeable membrane as a 'worst ' is buttoned .
- Place the sausage demineralized in a cup with 2 liters of water (clearly stating name and group!)
- Replace the water twice a day .
- After 3-5 days all electrolytes should be removed this can be tested by taking a little of the water from the beaker and add a few drops of AgNO₃. If there are still AgCl precipitation is formed, dialysis must be continued.

6. Evaporation

Put foils (with name and fraction written on it !) in bowls. Cut the ' sausages ' open and pour the material in these bowls (the membrane rinse). Place the bowls in the oven (60 °).

7. Apply on the glass slide

For the fraction < 0.2 m and < 2um the ' sedimentation technique applied . Smearmount is made only if sedimentation slides not succeed. After the material is removed from the film , it must first be returned homogenized in a mortar. After this has to be weighed and be made in the bags.

Sedimentation

For a good XRD - recording , it is necessary that there is 10 mg of clay per 1 cm² of glass plate is applied. The slides are about 14cm² , so there should be 140mg material used in total. There can be about 3.5 ml of suspension were pipetted onto a glass slide , so in this quantiteit will be the material was dissolved . As always a little loss , a little more prepared than described above:

Weigh 160mg clay material , and do it in the cut measuring cup with foot .

Leave with a plastic pipette 4ml water.

Treat this suspension with an ultrasonic desintegrator for 1min (until a homogeneous suspension is fine) - The regular tip needs to be replaced with the microtip !

Using the plastic pipette and pipette 3.5 ml of this suspension gently across the surface of the glass plate (with the name written on it)

Appendix C – Jackson treatment

Allow the plate to dry , preferably at room temperature

Smear mount

Stick the longest sides of the glass plate taped to a piece of paper , 1.7 cm release (asymmetric)

Transfer 200mg of the material in the middle of the glass plate.

Make a ' well ' in this pile and add 2 drops of distilled water until a paste is formed.

Homogenize everything and spread the paste with a Teflon stick on the glass slide.

Take another glass slide , hold it almost horizontally and smear the paste slowly evenly.

Recover in steps with new glass plates and chopsticks on the material used sticks and glass plates until everything is evenly applied.

Allow to dry.

Appendix D – EA-IRMS procedure

Sample preparation for analysis of %C, %N, $\delta^{13}\text{C}$ and/or $\delta^{15}\text{N}$

What you need:

Oven

Microbalance

Micropipette

Diluted HCl (5 to 10 %, made from HCl 37 % by dilution with MilliQ)

Ag cups (decontaminated in oven 4-8 hours at 450 °C) or Sn cups

Standards : Acetanilide (71.09 % C, 10.36 % N), or Leucine (10.67 % N, 54.89 % C)

Sample type considerations:

Keep in mind that different sample types have their specific requirements in terms of sample weights, sample preparation, and sample & standard weights.

Biomass samples: if samples are organic (e.g. plant or animal tissue, bacterial or phytoplankton culture), ~0.5 to 1 mg of sample material suffice. Keep in mind that plant tissues can have quite low N concentrations – if only N concentrations are needed (and not C concentrations) the amount of sample material can be increased to 1-2 mg.

Soil samples: the amount of sample required will depend on the N and C concentrations in your samples. As a rule of thumb: ~10 mg of material for most soil types is sufficient, for highly organic soils (e.g. peat soils) ~5 mg often suffices; for very sandy soils low in organic matter it is safer to weight out larger quantities (>20 mg, 40 mg is about the limit).

GFF filters: Important consideration is to ensure that GFF filters are precombusted (>4h at 450-500°C), and that some filters are kept and submitted as blanks. Even precombusted GFF filters have a C blank which may need to be taken into account for samples with relatively low C amounts.

For ^{13}C - or ^{15}N -enriched samples: always ask first what sample amounts are required, and give an indication of the estimated range of ^{13}C or ^{15}N -enrichment.

Ag cups versus Sn cups

All samples that need to be acidified (i.e. when organic C concentrations are required) need to be prepared in Ag cups (Sn cups will break down under the influence of HCl).

For samples where total C is determined, or only N concentrations (i.e. unacidified samples), Sn cups can be used.

Ag cups must be decontaminated before use (4 hours to overnight at 450°C – e.g. in aluminum foil, then store in glass containers). Don't do this with Sn cups (they'll be gone).

Acidification of samples:

!! Do not acidify soils or biomass samples before weighing them out. This will remove your carbonates before the sample is weighed out, and you'll not be able to correctly calculate organic C concentrations.

!! do not use other acids such as H₃PO₄, H₂SO₄, HF. 2

* For solid samples (e.g. biomass, soils ...):

Weigh the sample in Ag cups: first put the Ag cup onto the microbalance and tar the weight. Take out the Ag cup, and fill the cup outside of the microbalance (these are delicate, expensive instruments, keep them clean). Add diluted HCl with a micropipette. The amount of acid needed depends on the carbonate content of the samples, add in steps of e.g. 20 µL. The presence of carbonates can usually be observed visually (bubbling). If necessary (if the dried samples are still bubbling after the addition of diluted HCl), repeat the procedure. Soil or sediment samples with very high carbonate contents will require repeated acidification steps. Re-dry the samples at 50-60 °C at least overnight before closing the Ag cups (use clean tweezers).

!! Remark regarding closing of cups: Make sure your cups are completely closed and still intact. Make them as small as possible to avoid them getting stuck in the autosampler. After your cups are in a 96-well plate, shake the plate (with the lid properly on) and visually check that you do not see any sample material at the bottom of the wells, since (i) loss of material implies that concentration measurements will no longer be accurate, and (ii) fine material that gets into the autosampler will damage the sliding mechanism – which increases blanks and is time-consuming and expensive to repair.

* For GFF filters:

Place filters in a dessicator (without dessicant material) with a beaker of concentrated HCl on the bottom. Be careful with HCl fumes. Leave them in HCl fumes for >4h, then re-dry the filters at 50-60° overnight. To wrap up filters, use a special device (see pictures).

Standards and blanks

As **blanks**, use (depending on sample preparation):

- empty Sn or Ag cups
- when analyzing GF filters: several blank filters
- in case you use any particular sample preparation techniques, or e.g. adsorbents to trap your sample – take this into consideration and use appropriate blanks.

Standards : prepare a series of Acetanilide or Leucine standards, of different weights and bracketing the expected amounts of C or N in the sample material.

Typical standard weights: 0.2 – 1.0 mg.

Make sure the standards remain standards for subsequent users, i.e. do not cross-contaminate them, and clean spatulas before and after using it for standards. In principle, the amount of N and C in your standards should bracket the expected range you will have in your samples.

In case you also require $\delta^{15}\text{N}$ and/or $\delta^{13}\text{C}$ data, make sure additional standards are included (e.g., IAEA-N1, IAEA-N2, IAEA-C6 ...).

Organising your samples and information you need to provide.

Keep in mind that we are not a commercial service lab – read guidelines below carefully and stick to them (or ask) in order to make our work in getting them analysed less time-consuming, and to avoid confusion or errors in processing data.

!! Be clear about what data you need (C only, N only, N+C, concentrations and/or stable isotope ratios) and provide some information on the type of samples you are analysing (biomass, soils ...) and how they have been processed (acidified or not, Ag or Sn cups, ..), expected range of C and N concentrations, expected range $\delta^{13}\text{C}$ and $\delta^{15}\text{N}$ signatures ...

!! NEVER submit any samples that have been in contact with ^{14}C , or have been processed in a room where ^{14}C -tracer work is performed.

Use 96-well plates to store samples and make sure they are properly closed.

!! Order samples in the same way as they will be organised: first one or more blanks, then standards, then a series of samples, interspersed with additional standards. As a rule of thumb, include at least 2 blanks and 4 standards per set of 40 samples. For isotope work, more standards are needed – ask.

!! Provide an xls file in the following format:

-1st column: position in tray (A1, A2 ...B1, B2 ...)

-2nd column: sample name (e.g. blank, acetanilide, sample X,...)

Appendix D – EA-IRMS procedure

-3rd column: weight (mg)

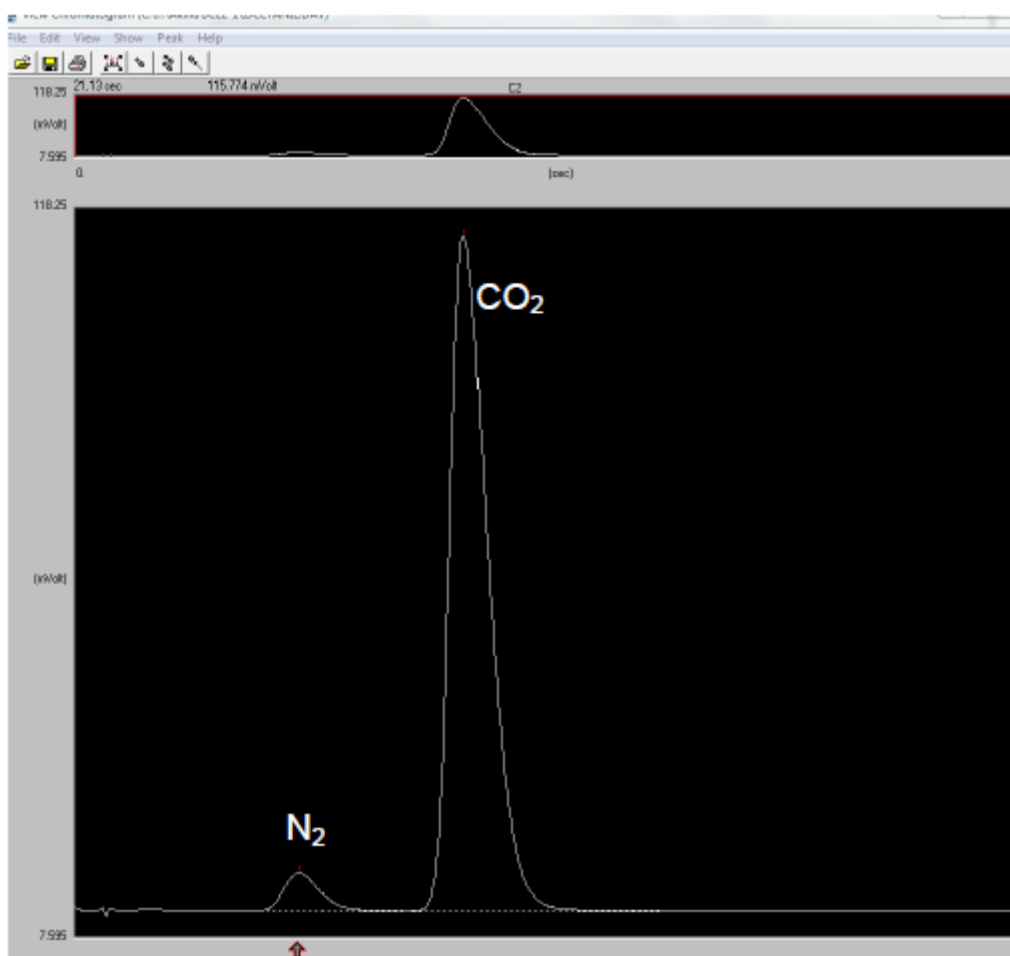
| | sample ID | weight |
|----|-------------|--------|
| A1 | Blank1 | |
| A2 | Blank 2 | |
| A3 | Acetanilide | 0.231 |
| A4 | Acetanilide | 0.465 |
| A5 | Sample1 | 0.653 |
| A6 | ... | ... |

Etc.

Also print out and leave a copy along with tray containing samples.

Processing of data:

Concentrations of N and C are based on the amount of N₂ and CO₂ detected by the EA's TCD detector (i.e. peak areas). A typical chromatogram is given below (first peak is N₂, second one is CO₂). The peak areas are proportional to the respective quantity of N and C in samples. Sample peak areas are corrected for blank contributions, and calibrations are based on the data for certified standards (acetanilide and/or leucine). A spreadsheet is available to guide you through the data processing.



Instrumentation used:

Samples are analysed using one of the following instruments: Carlo Erba 1108 elemental analyser, Carlo Erba EA1110 elemental analyser, or Thermo Flash EA/HT. When isotope data are required, these are coupled to one of the Thermo Delta V Advange IRMS's. Ask if you need more details.

If you have questions or doubts about how to prepare your samples, ask. Running samples that haven't been properly prepared is a waste of time and resources.

Appendix E – Sample list

| Samples - Thesis Michael Verbiest | | |
|--|----------------|------------------------------|
| Sample | Quarry | Brief description |
| DE15MV001 | Faber, Denizli | Fining upwards conglomerates |
| DE15MV002 | Faber, Denizli | Conglomerates |
| DE15MV003 | Faber, Denizli | Calcrete matrix with pebbles |
| DE15MV004 | Faber, Denizli | Black pebble |
| DE15MV005 | Faber, Denizli | Pure calcrete |
| DE15MV006 | Faber, Denizli | Conglomerates |
| DE15MV007 | Faber, Denizli | Conglomerate |
| DE15MV008 | Faber, Denizli | Conglomerate fragments |
| DE15MV009 | Faber, Denizli | Laminated marl |
| DE15MV010 | Faber, Denizli | Laminated marl |
| DE15MV011 | Faber, Denizli | Marl |
| DE15MV012 | Faber, Denizli | Conglomerate |
| DE15MV013 | Faber, Denizli | Travertine |
| DE15MV014 | Faber, Denizli | Conglomerate |
| DE15MV015 | Faber, Denizli | Marl |
| DE15MV016 | Faber, Denizli | Marl |
| DE15MV017 | Faber, Denizli | Conglomorate |
| DE15MV018 | Faber, Denizli | Conglomorate |
| DE15MV019 | Faber, Denizli | Conglomorate fragment |
| DE15MV020 | Faber, Denizli | Laminated marl |
| DE15MV021 | Faber, Denizli | Laminated marl |
| DE15MV022 | Faber, Denizli | Laminated marl |
| DE15MV023 | Faber, Denizli | Laminated marl |
| DE15MV024 | Faber, Denizli | Conglomorate-gastropodes |
| DE15MV025 | Faber, Denizli | Mud-supported conglomerate |
| DE15MV026 | Faber, Denizli | Nodular-limestone |
| DE15MV027 | Faber, Denizli | Siltstone-alteration |
| DE15MV028 | Faber, Denizli | Laminated marl |
| DE15MV029 | Faber, Denizli | Laminated marl |
| DE15MV030 | Faber, Denizli | Conglomorate |
| DE15MV031 | Faber, Denizli | Mudstone |
| DE15MV032 | Faber, Denizli | Carbonate mudstone |
| DE15MV033 | Faber, Denizli | Fine conglomerate |
| DE15MV034 | Faber, Denizli | Microconglomerate |
| DE15MV035 | Faber, Denizli | Conglomerate matrix |
| DE15MV036 | Faber, Denizli | Silty mudstone |
| DE15MV037 | Faber, Denizli | |
| DE15MV038 | Faber, Denizli | |

| Samples - Thesis Michael Verbiest | | |
|--|---------------------|-----------------------------|
| Sample | Quarry | Brief description |
| DE15MV039 | Faber, Denizli | Sandstone |
| DE15MV040 | Faber, Denizli | Conglomerate |
| DE15MV041 | Faber, Denizli | Siltstone |
| DE15MV042 | Faber, Denizli | Laminated marl |
| DE15MV043 | Faber, Denizli | Conglomerates |
| DE15MV044 | Faber, Denizli | Conglomerate |
| DE15MV045 | Faber, Denizli | Conglomerate |
| DE15MV046 | Faber, Denizli | Conglomerate |
| DE15MV047 | Faber West, Denizli | Massive marl |
| DE15MV048 | Faber West, Denizli | Conglomerate |
| DE15MV049 | Faber West, Denizli | Marl |
| DE15MV050 | Faber West, Denizli | Marl |
| DE15MV051 | Faber West, Denizli | Marl |
| DE15MV052 | Faber West, Denizli | Oxidation-Reduction spots |
| DE15MV053 | Faber West, Denizli | Marl |
| DE15MV054 | Faber West, Denizli | Siltstone |
| DE15MV055 | Faber West, Denizli | |
| DE15MV056 | Faber West, Denizli | |
| DE15MV057 | Faber West, Denizli | Marl |
| DE15MV058 | Faber West, Denizli | Marl |
| DE15MV059 | Faber West, Denizli | Siliclastic rich travertine |
| DE15MV060 | Faber West, Denizli | Marl |
| DE15MV061 | Faber West, Denizli | Siliclastic rich travertine |
| DE15MV062 | Faber West, Denizli | Fine conglomerate |
| DE15MV063 | Faber West, Denizli | Coarse conglomerate |
| DE15MV064 | Faber West, Denizli | Fine conglomerate |
| DE15MV065 | Cakmak, Denizli | Conglomorate |
| DE15MV066 | Cakmak, Denizli | Conglomorate |
| DE15MV067 | Cakmak, Denizli | Marl – marker horizon |
| DE15MV068 | Cakmak, Denizli | Marl – marker horizon |
| DE15MV069 | Cakmak, Denizli | Siliclastic travertine |
| DE15MV070 | Cakmak, Denizli | Coquina |
| DE15MV071 | Cakmak, Denizli | Marl – marker horizon |
| DE15MV072 | Cakmak, Denizli | Muddy travertine |
| DE15MV073 | Cakmak, Denizli | Monogenetic breccia |
| DE15MV074 | Cakmak, Denizli | Monogenetic breccia |
| DE15MV075 | Cakmak, Denizli | Gastropod-rich carbonate |
| DE15MV076 | Cakmak, Denizli | Gastropod-rich carbonate |
| DE15MV077 | Cakmak, Denizli | Gastropod-rich carbonate |
| DE15MV078 | Cakmak, Denizli | Marl – marker horizon |
| DE15MV079 | Cakmak, Denizli | Marl – marker horizon |
| DE15MV080 | Cakmak, Denizli | Gastropod-rich carbonate |

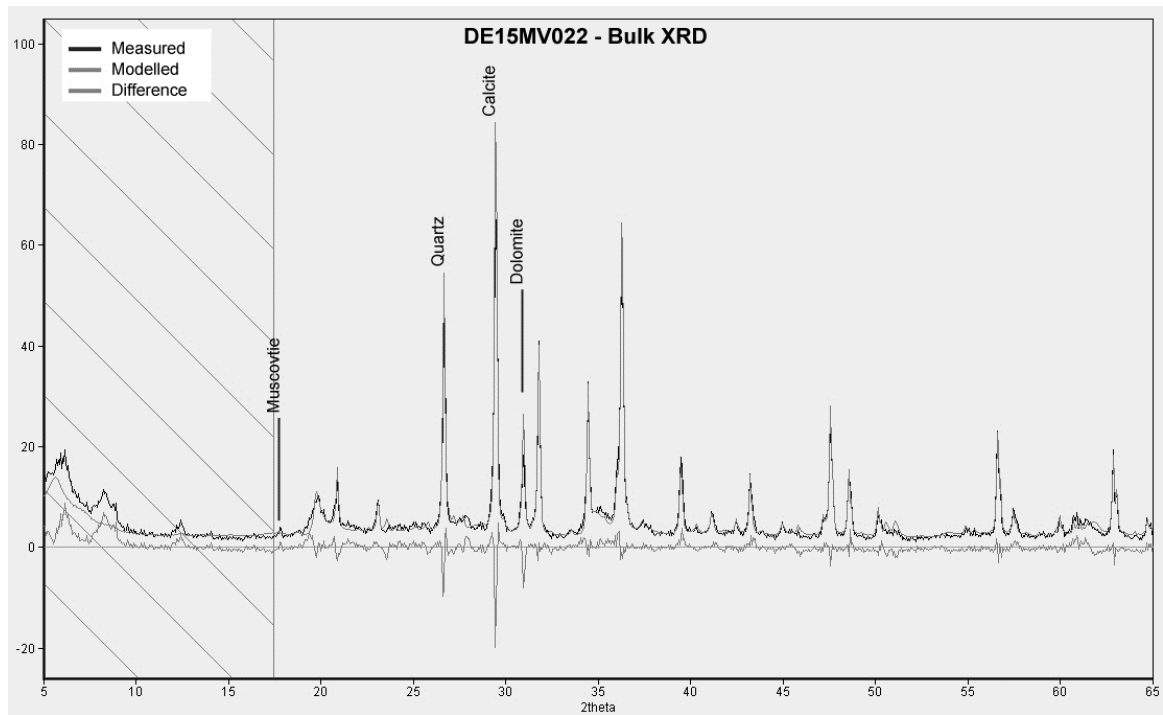
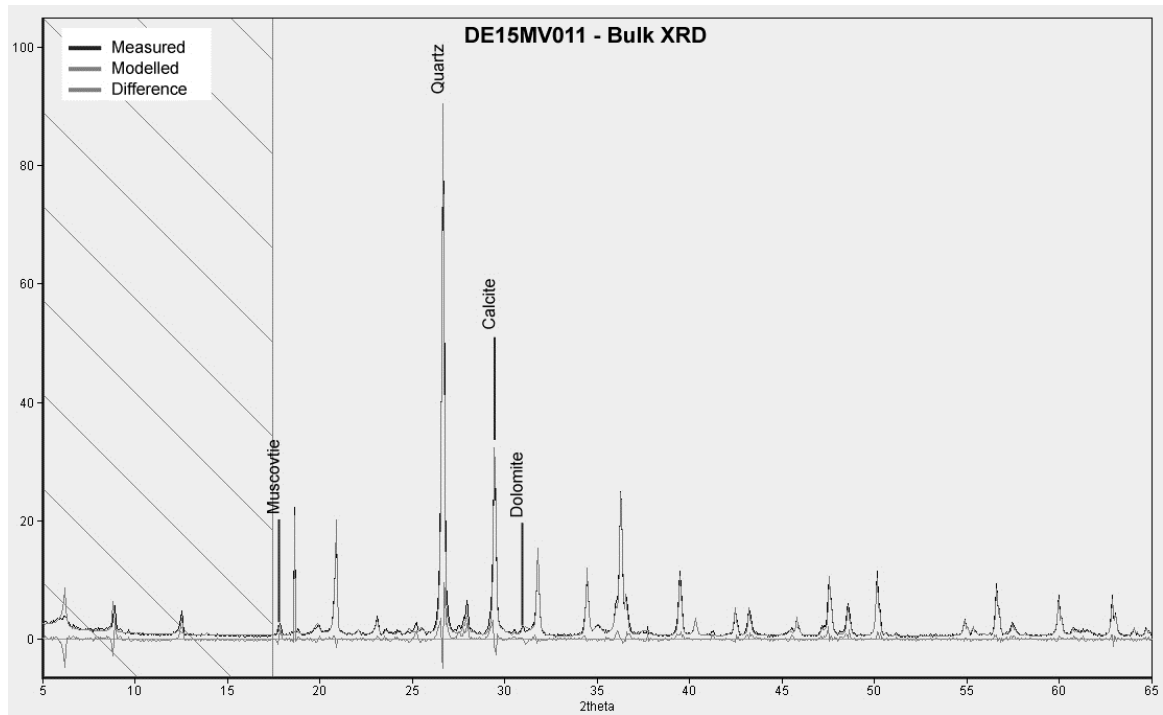
Appendix E – Sample list

| Samples - Thesis Michael Verbiest | | |
|--|---------------------------|-----------------------------------|
| Sample | Quarry | Brief description |
| DE15MV081 | Cakmak, Denizli | Marl – marker horizon |
| DE15MV082 | Cakmak, Denizli | Gastropod-rich carbonate |
| DE15MV083 | Cakmak, Denizli | Clast-rich travertine |
| DE15MV084 | Cakmak, Denizli | Marl – marker horizon |
| DE15MV085 | Cakmak, Denizli | Siliciclastic travertine |
| DE15MV086 | Cakmak, Denizli | Pebble-rich carbonate mud |
| DE15MV087 | Cakmak, Denizli | Conglomerate |
| DE15MV088 | Cakmak, Denizli | Fine-conglomerate |
| DE15MV089 | Cakmak, Denizli | Marl – marker horizon |
| DE15MV090 | Cakmak, Denizli | Sandstone |
| DE15MV091 | Cakmak, Denizli | Sandstone |
| DE15MV092 | Cinkaya, Denizli | Fine conglomerate |
| DE15MV093 | Cinkaya, Denizli | Fine conglomerate |
| DE15MV094 | Cinkaya, Denizli | Matrix – breccia |
| DE15MV095 | Cinkaya, Denizli | Matrix – breccia |
| DE15MV096 | Cinkaya, Denizli | Very fine conglomerate |
| DE15MV097 | Cinkaya, Denizli | Conglomerate |
| DE15MV098 | Cinkaya, Denizli | Pebble-plugs |
| DE15MV099 | Cinkaya, Denizli | Conglomerate |
| DE15MV100 | Cinkaya, Denizli | Conglomerate |
| DE15MV101 | Cinkaya, Denizli | Siltstone |
| DE15MV102 | Cinkaya, Denizli | Marl – marker horizon |
| DE15MV103 | Cinkaya, Denizli | Laminated marl |
| DE15MV104 | Cinkaya, Denizli | Conglomerate |
| DE15MV105 | Cinkaya, Denizli | Gastropod-rich travertine |
| DE15MV106 | Cinkaya, Denizli | Gastropod-rich travertine |
| DE15MV107 | Cinkaya, Denizli | Gastropod-rich travertine |
| DE15MV108 | Ece, Denizli | Very mud-rich conglomerate matrix |
| DE15MV109 | Ece, Denizli | Mud-supported conglomerate |
| DE15MV110 | Ece, Denizli | Very mud-rich conglomerate matrix |
| DE15MV111 | Alimoglu Tasarim, Denizli | Marl |
| DE15MV112 | Alimoglu Tasarim, Denizli | Laminated marl |
| DE15MV113 | Alimoglu Tasarim, Denizli | Laminated marl |
| DE15MV114 | Alimoglu Tasarim, Denizli | Sandy siltstone |
| DE15MV115 | Alimoglu Tasarim, Denizli | Micro conglomerate |
| DE15MV116 | Alimoglu Tasarim, Denizli | Carbonate siltstone |
| DE15MV117 | Alimoglu Tasarim, Denizli | Siltstone |
| DE15MV118 | Alimoglu Tasarim, Denizli | Carbonate siltstone |
| DE15MV119 | Alimoglu Tasarim, Denizli | Mud-supported conglomerate |
| DE15MV120 | Alimoglu Tasarim, Denizli | Coquina bed |
| DE15MV121 | Alimoglu Tasarim, Denizli | Coquina bed |
| DE15MV122 | Alimoglu Tasarim, Denizli | Fine sandstone |

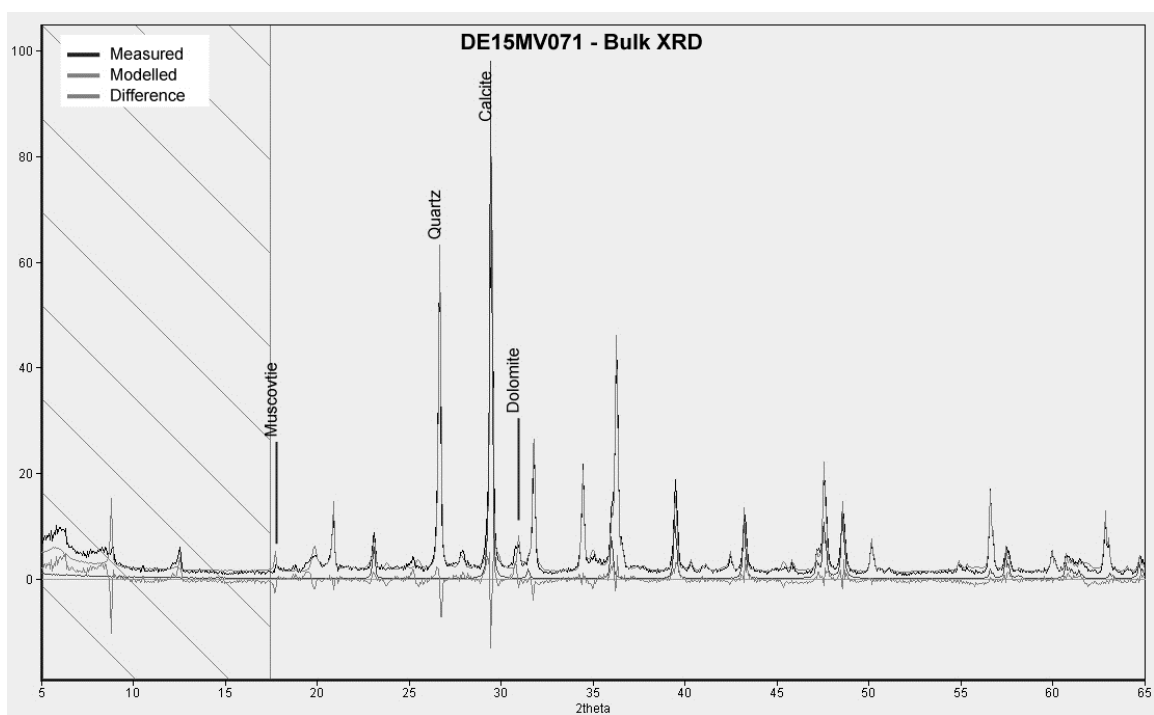
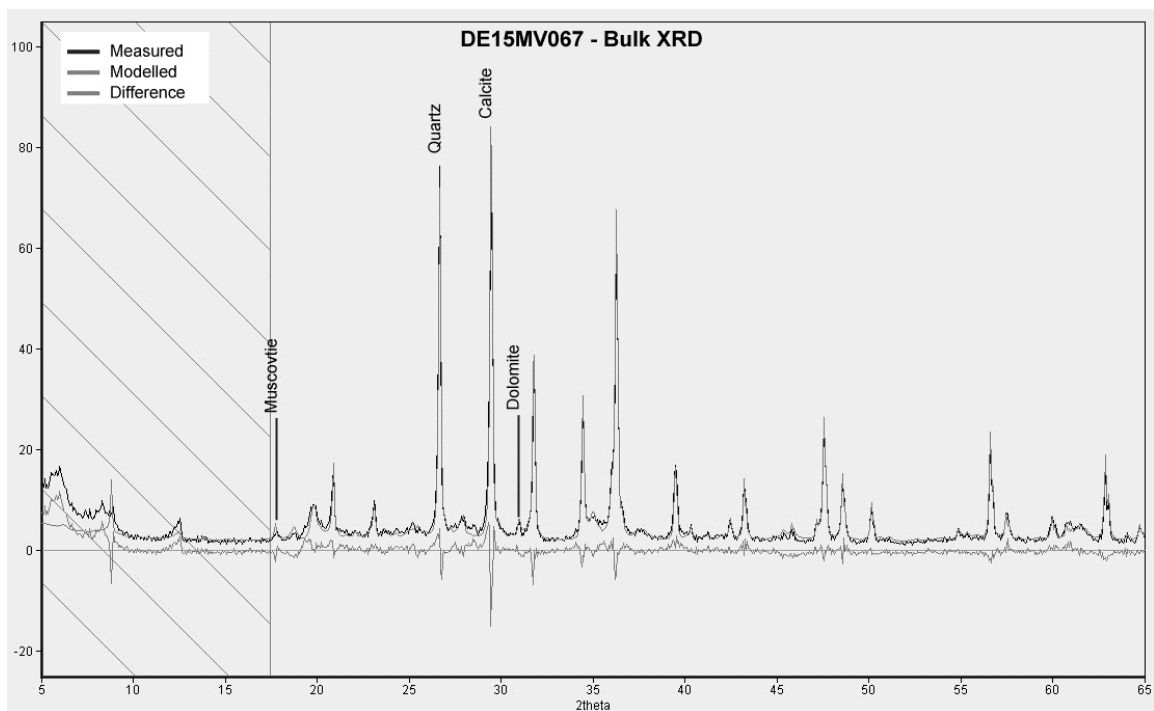
Appendix E – Sample list

| Samples - Thesis Michael Verbiest | | |
|--|----------------------------|--------------------------------|
| Sample | Quarry | Brief description |
| DE15MV123 | Alimoglu Tasarim, Denizli | Coquina bed |
| DE15MV124 | Alimoglu Tasarim, Denizli | Coarse sand |
| DE15MV125 | Alimoglu Tasarim, Denizli | Travertine with conglomerate |
| DE15MV126 | Alimoglu Tasarim, Denizli | Conglomerate |
| DE15MV127 | Alimoglu Tasarim, Denizli | Calcite crust |
| DE15MV128 | Alimoglu Tasarim, Denizli | Laminar travertine with pebble |
| DE15MV129 | Alimoglu Tasarim, Denizli | Encrusting travertine |
| DE15MV130 | Alimoglu Tasarim, Denizli | Travertine crust |
| DE15MV131 | Basaranlar, Denizli | Fault veins |
| DE15MV132 | Basaranlar, Denizli | Cement |
| DE15MV133 | Siray, Denizli | Terra rossa |
| DE15MV134 | Siray, Denizli | Veins |
| DE15MV135 | Metamar Abandoned, Denizli | Clay |
| DE15MV136 | Metamar Abandoned, Denizli | Veins |
| DE15MV137 | Metamar Abandoned, Denizli | Well-cemented travertine |
| DE15MV138 | Metamar Abandoned, Denizli | Coquina bed |
| DE15MV139 | Metamar Abandoned, Denizli | Conglomerate |
| DE15MV140 | Metamar Abandoned, Denizli | Veins |
| DE15MV141 | Metamar Abandoned, Denizli | Marl |
| DE15MV142 | Metamar Abandoned, Denizli | Vertical cemented-travertine |

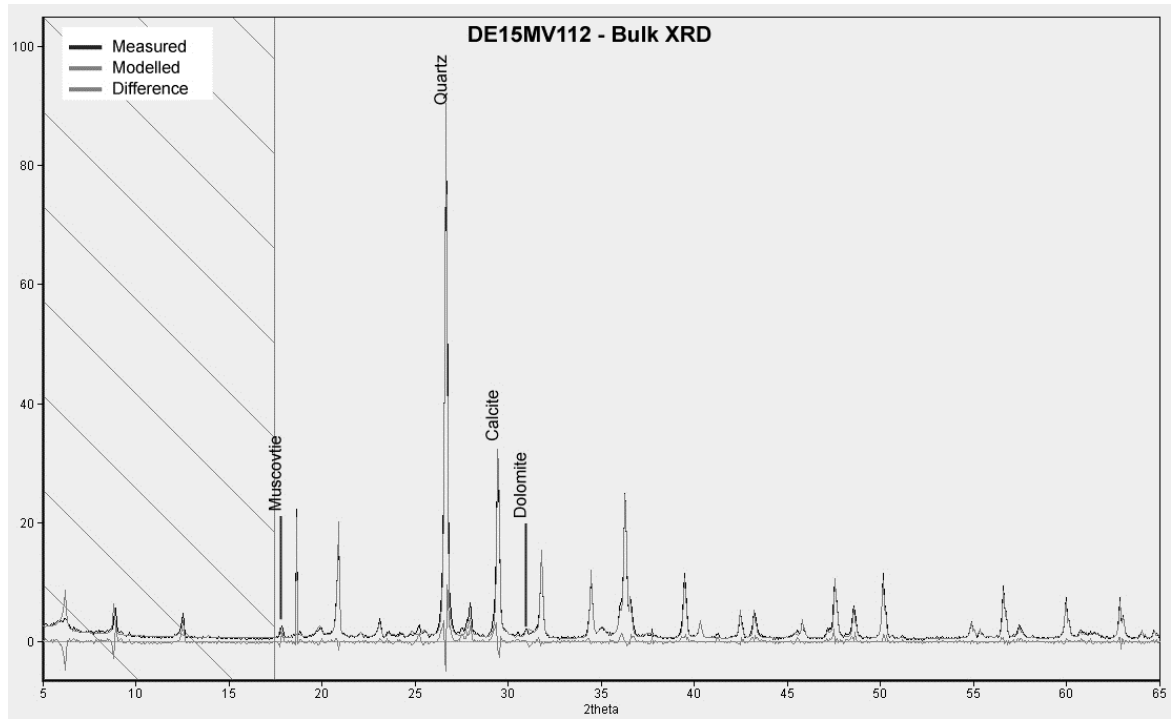
Appendix F – Bulk XRD diffraction patterns



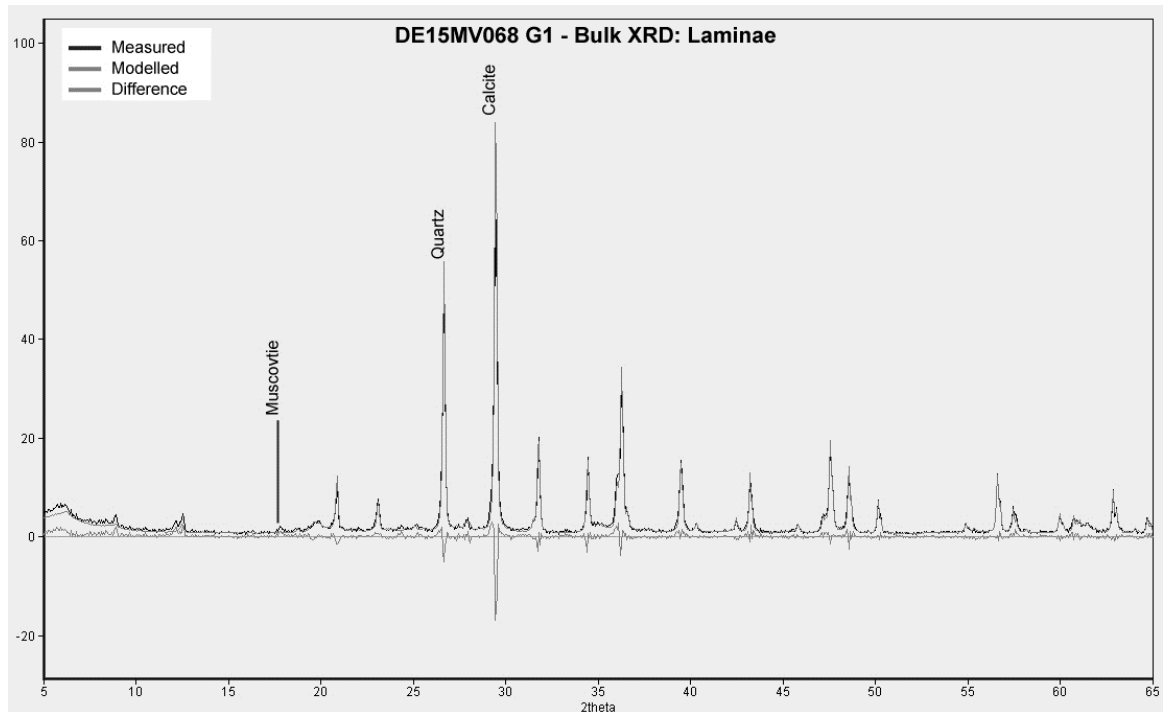
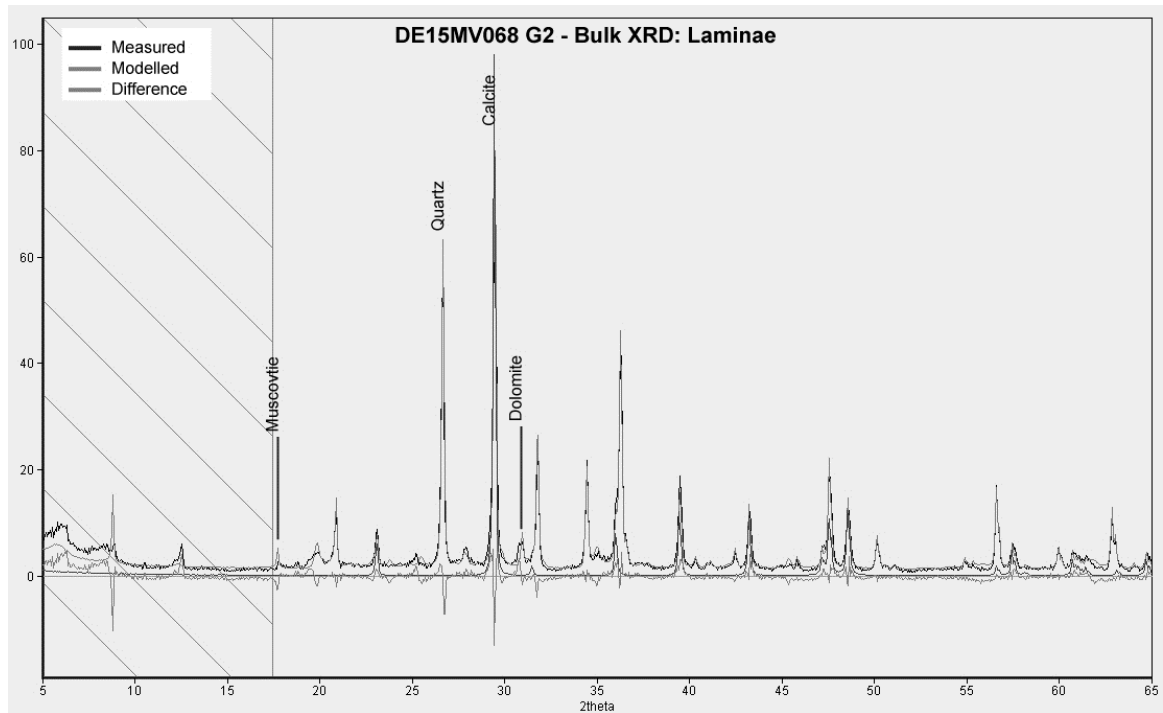
Appendix F – Bulk XRD diffraction patterns



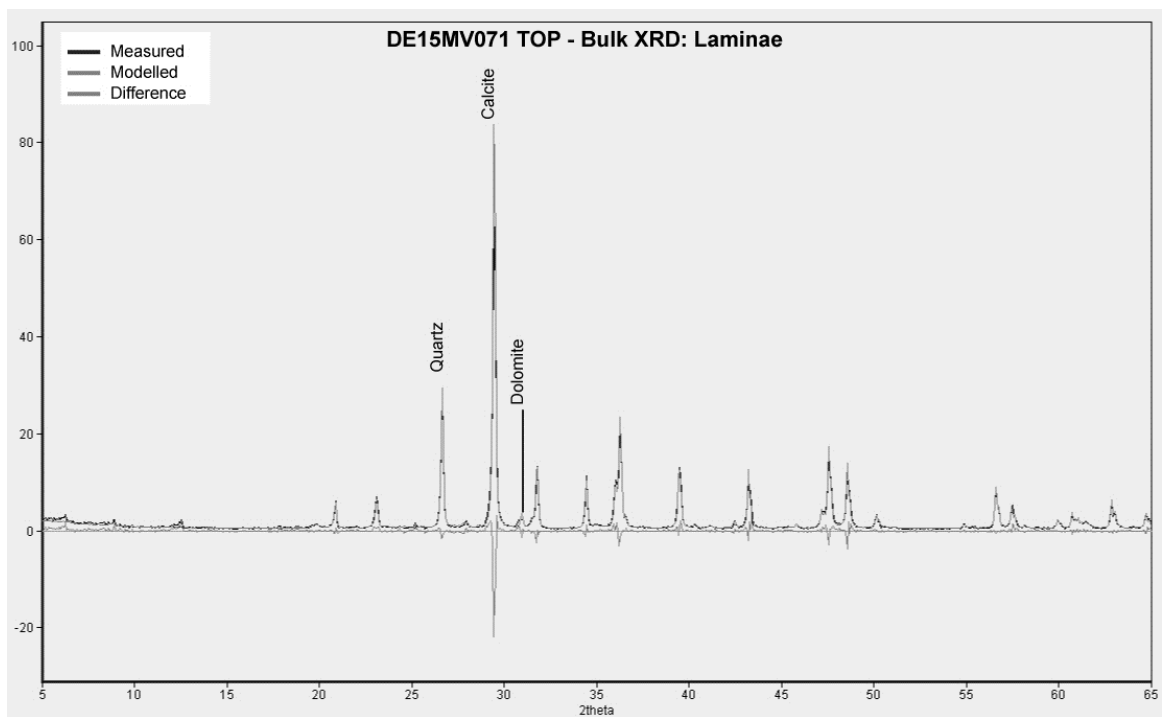
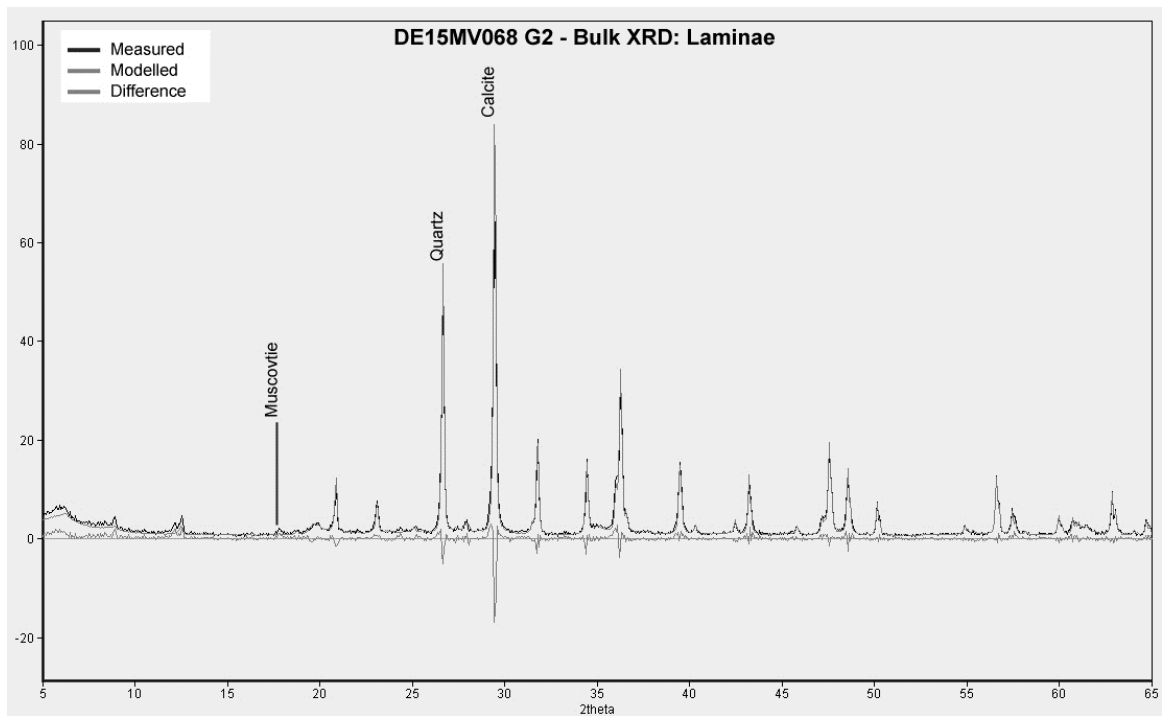
Appendix F – Bulk XRD diffraction patterns



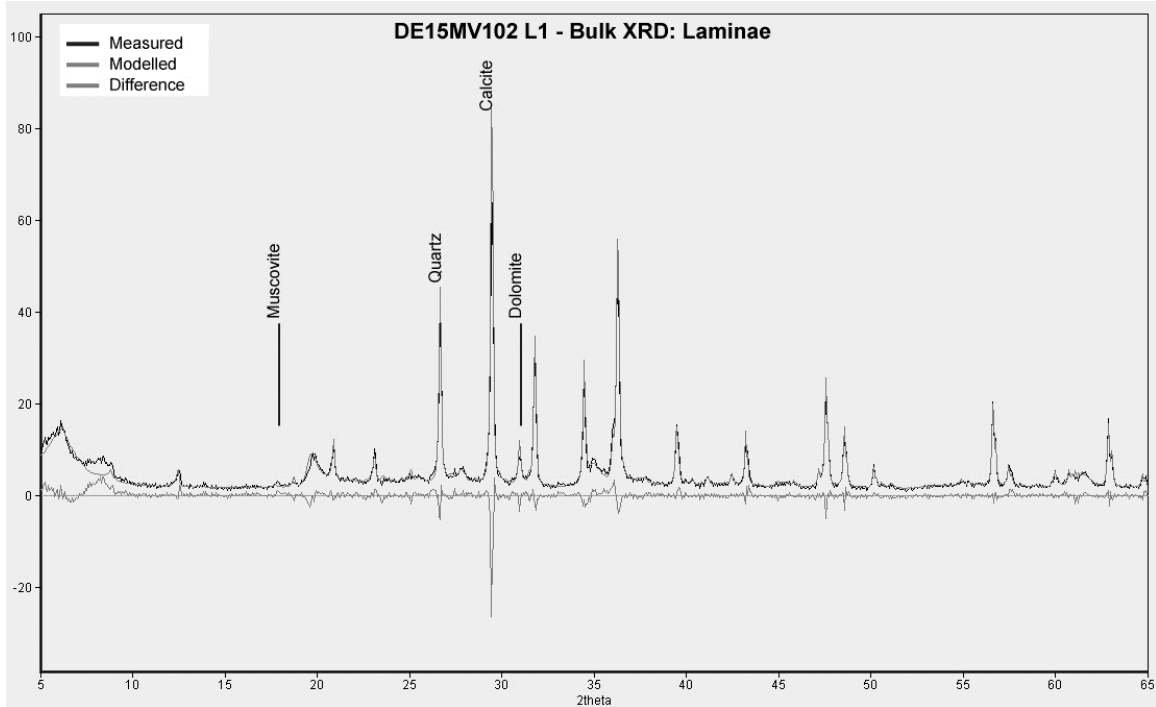
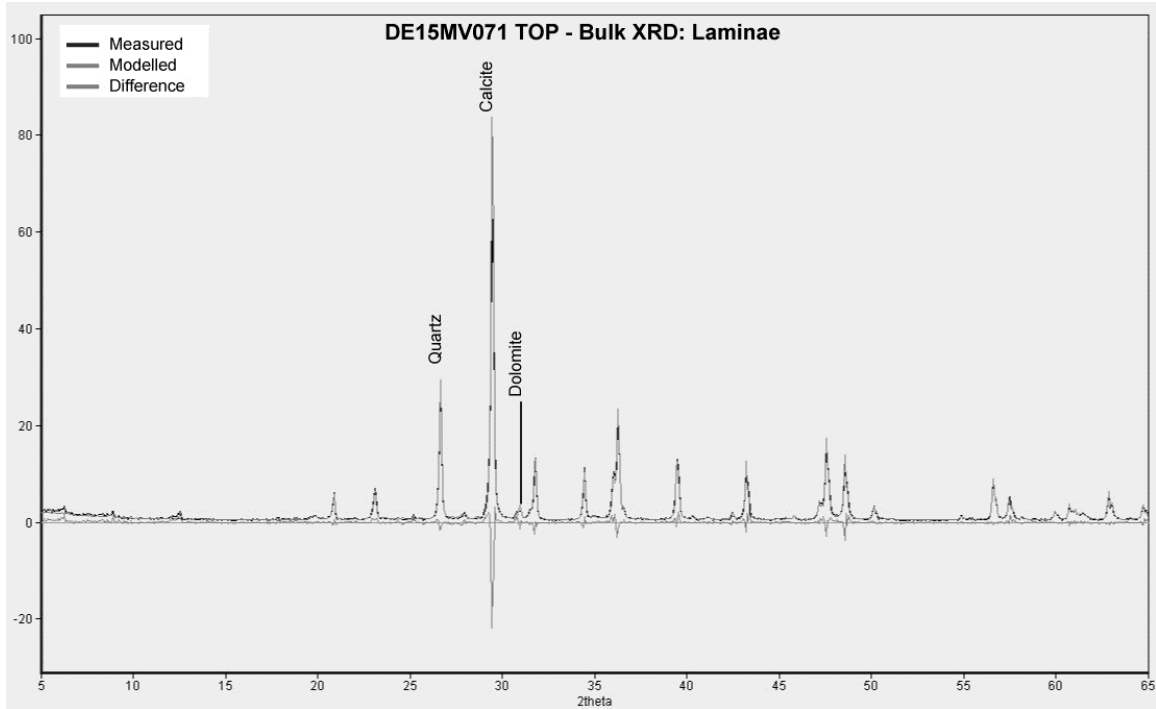
Appendix G – Bulk XRD diffraction patterns: Laminae



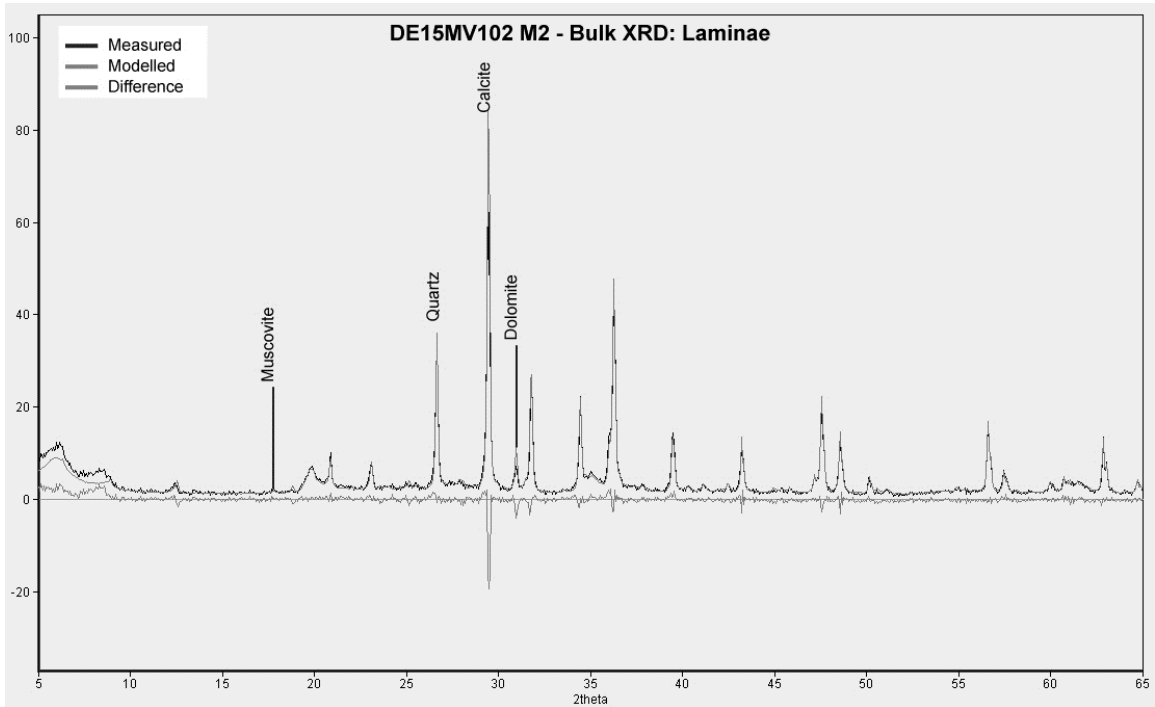
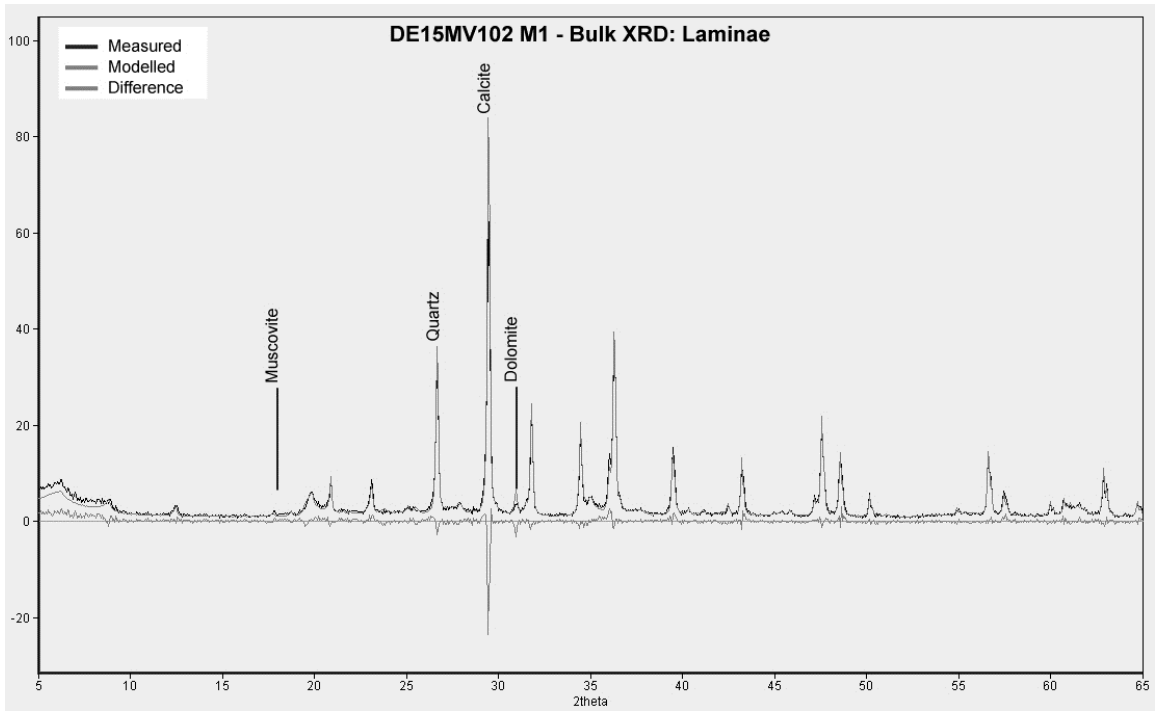
Appendix G – Bulk XRD diffraction patterns: Laminae



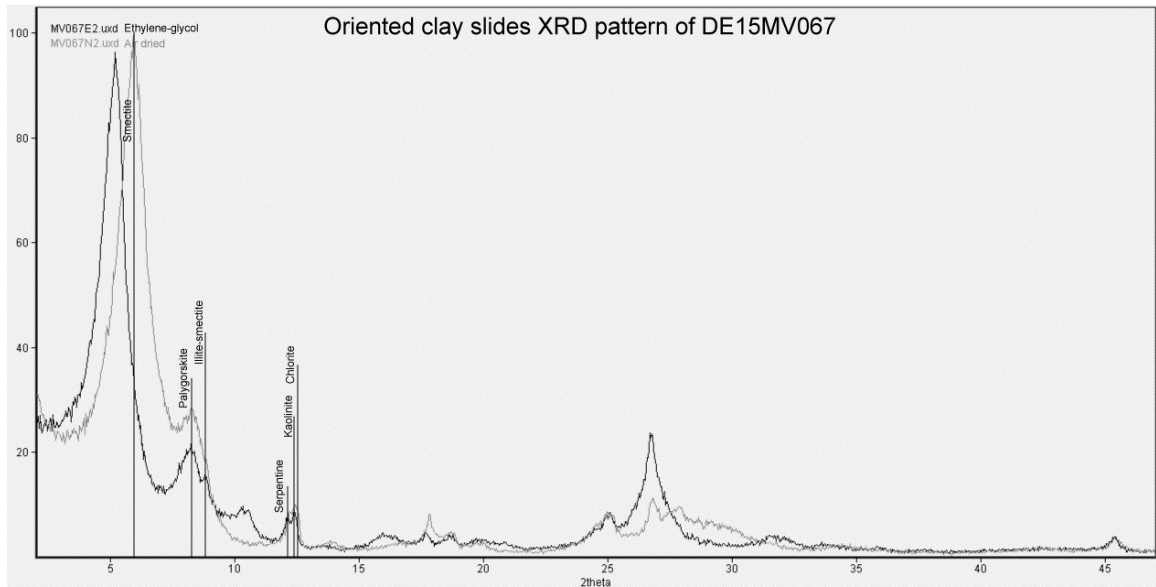
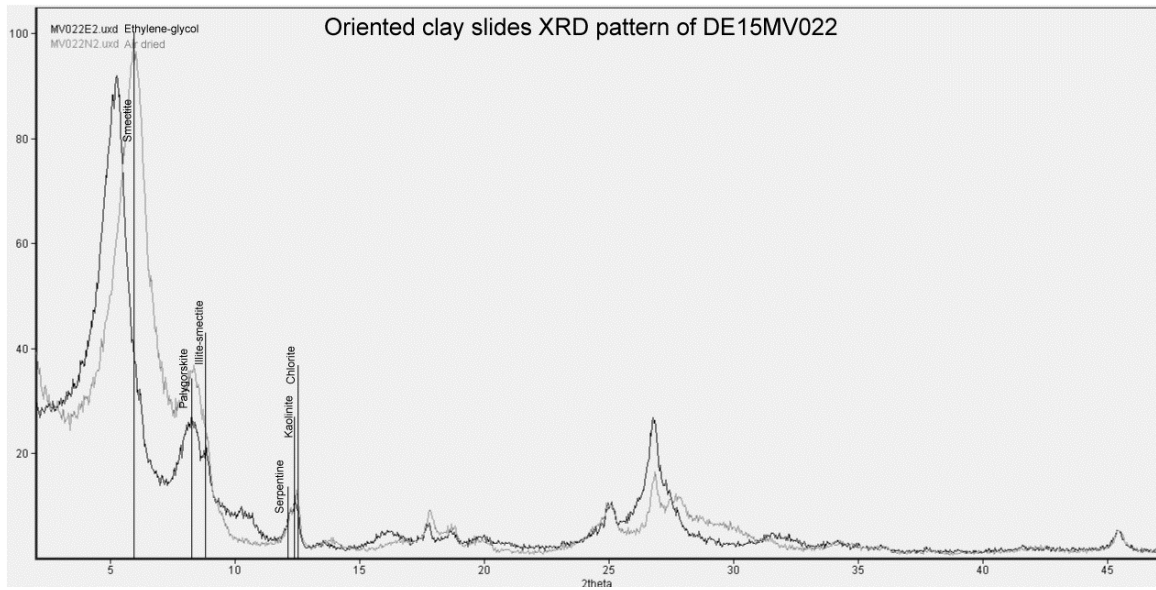
Appendix G – Bulk XRD diffraction patterns: Laminae



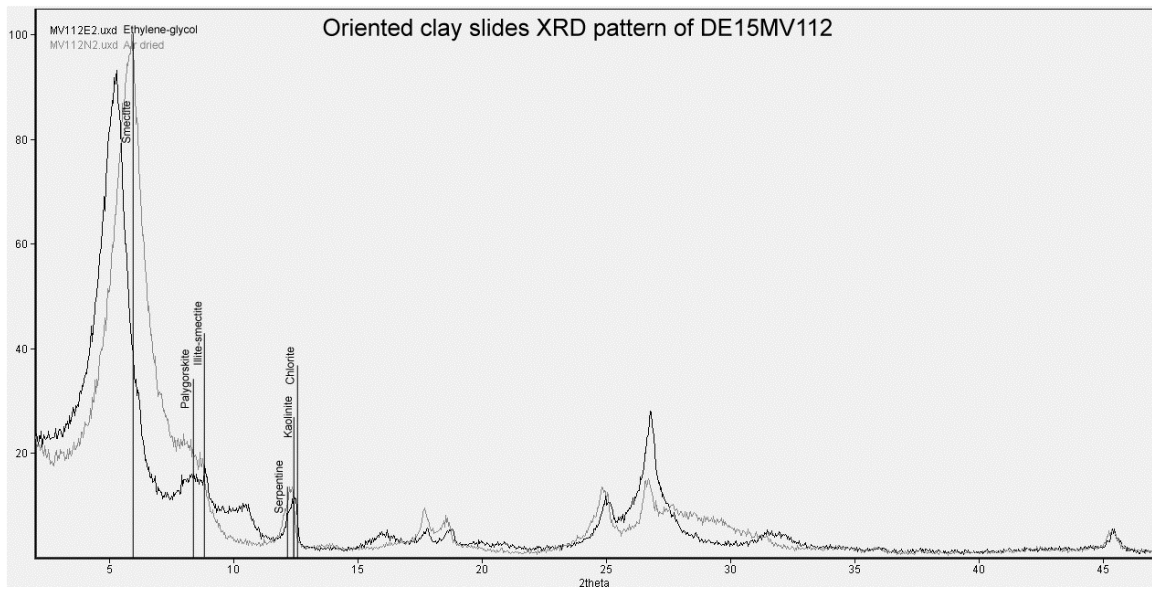
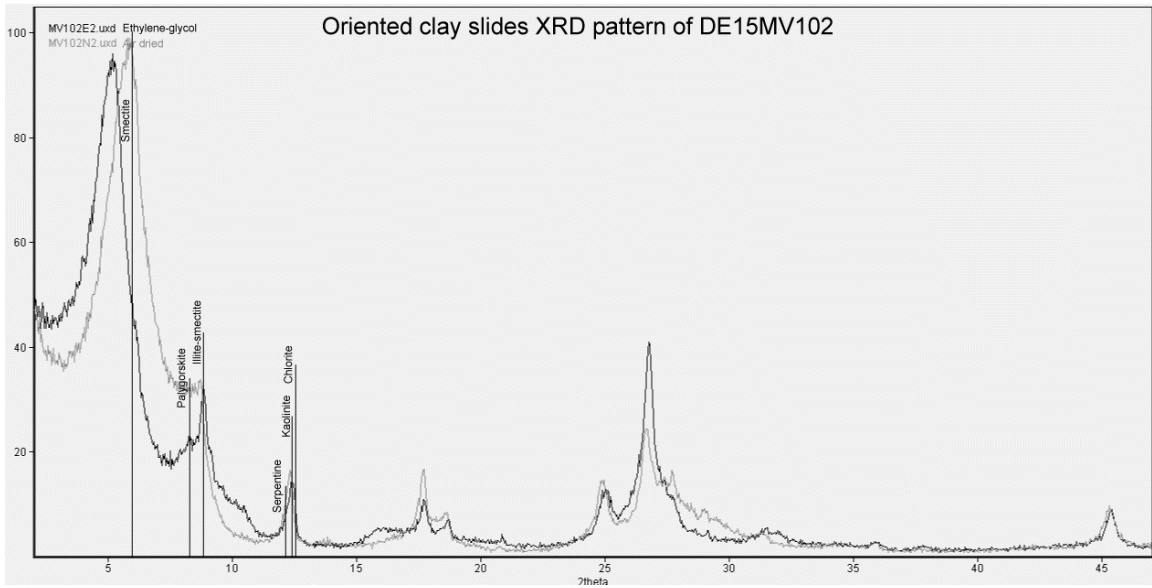
Appendix G – Bulk XRD diffraction patterns: Laminae



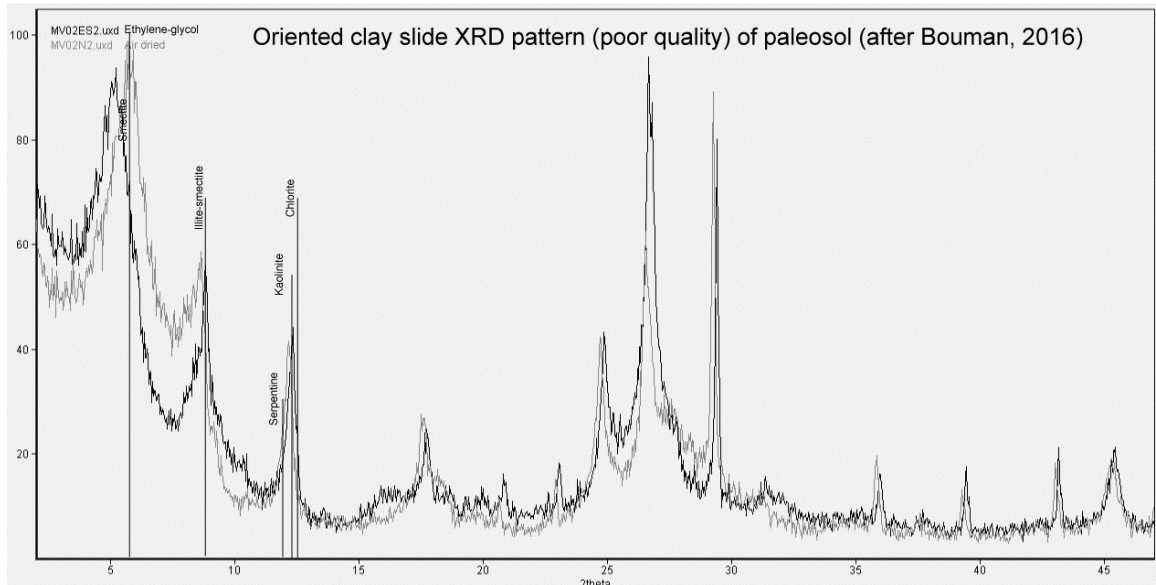
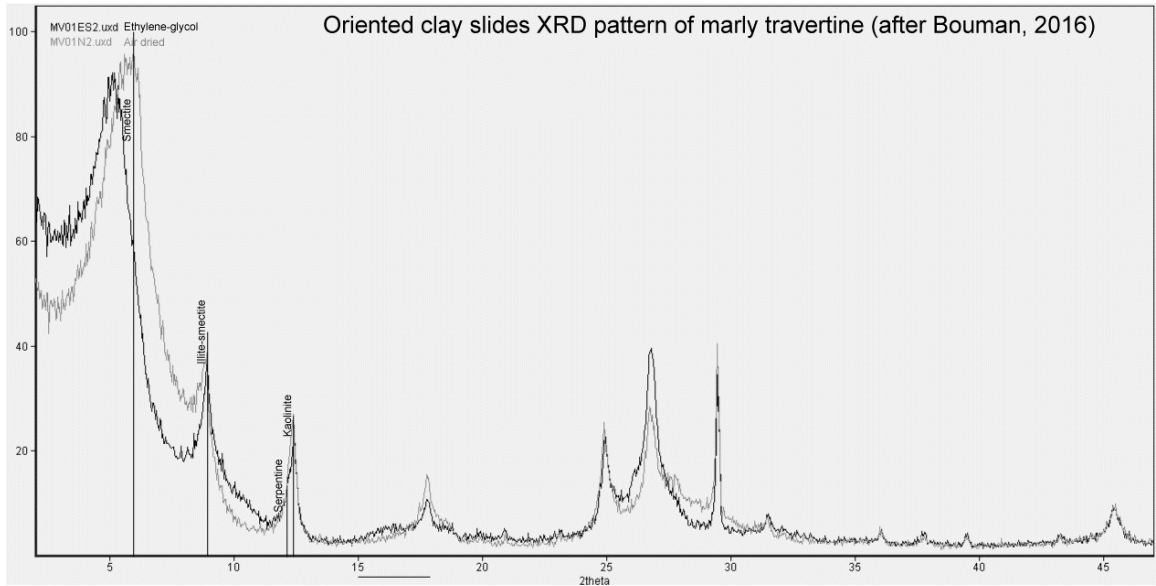
Appendix H – XRD diffraction patterns oriented clay slides



Appendix H – XRD diffraction patterns oriented clay slides



Appendix H – XRD diffraction patterns oriented clay slides



Appendix I – ICP-OES results

| Sample | <i>Major elements wt. %</i> | | | | | | |
|----------------|-----------------------------|------|------|------|------|------|------|
| | Ca | Fe | Al | Mg | K | Na | Ti |
| DE15MV011A | 11.71 | 2.58 | 3.18 | 1.25 | 0.63 | 0.56 | 0.13 |
| DE15MV011B | 11.24 | 2.53 | 3.08 | 1.23 | 0.60 | 0.56 | 0.13 |
| DE15MV022A | 12.69 | 4.62 | 3.63 | 3.59 | 0.74 | 0.22 | 0.16 |
| DE15MV022B | 12.57 | 4.77 | 3.65 | 3.62 | 0.74 | 0.22 | 0.17 |
| DE15MV067A | 12.41 | 4.08 | 3.78 | 2.91 | 0.71 | 0.26 | 0.18 |
| DE15MV067B | 12.21 | 4.00 | 3.71 | 2.85 | 0.70 | 0.26 | 0.18 |
| DE15MV068-C2A | 18.89 | 3.04 | 2.96 | 2.08 | 0.57 | 0.20 | 0.13 |
| DE15MV068-C2B | 19.36 | 3.11 | 3.03 | 2.09 | 0.58 | 0.20 | 0.15 |
| DE15MV068-G1A | 19.49 | 2.87 | 2.33 | 2.25 | 0.38 | 0.27 | 0.15 |
| DE15MV068-G1B | 19.82 | 2.89 | 2.37 | 2.27 | 0.38 | 0.27 | 0.15 |
| DE15MV068-G2A | 15.75 | 3.19 | 3.34 | 2.39 | 0.62 | 0.26 | 0.17 |
| DE15MV068-G2B | 15.78 | 3.20 | 3.35 | 2.45 | 0.62 | 0.27 | 0.17 |
| DE15MV071-BOTA | 26.01 | 2.08 | 1.42 | 2.08 | 0.22 | 0.16 | 0.07 |
| DE15MV071-BOTB | 25.73 | 2.08 | 1.42 | 2.06 | 0.22 | 0.16 | 0.07 |
| DE15MV071-TOPA | 26.15 | 1.30 | 1.43 | 1.45 | 0.24 | 0.23 | 0.06 |
| DE15MV071-TOPB | 26.04 | 1.30 | 1.42 | 1.46 | 0.24 | 0.23 | 0.06 |
| DE15MV102-L1A | 12.06 | 4.07 | 4.41 | 3.08 | 0.86 | 0.31 | 0.19 |
| DE15MV102-L1B | 11.81 | 4.00 | 4.31 | 2.97 | 0.86 | 0.31 | 0.18 |
| DE15MV102-M1A | 16.23 | 3.19 | 4.17 | 1.95 | 0.94 | 0.26 | 0.18 |
| DE15MV102-M1B | 16.22 | 3.17 | 4.21 | 1.95 | 0.94 | 0.26 | 0.18 |
| DE15MV102-M2A | 13.95 | 3.75 | 4.20 | 2.82 | 0.84 | 0.28 | 0.18 |
| DE15MV102-M2B | 2.78 | 0.75 | 0.84 | 0.57 | 0.17 | 0.06 | 0.04 |
| DE15MV112A | 28.70 | 1.87 | 1.40 | 1.53 | 0.25 | 0.13 | 0.07 |
| DE15MV112B | 28.69 | 1.89 | 1.40 | 1.52 | 0.24 | 0.13 | 0.07 |

Appendix I – ICP-OES results

| Sample | <i>Trace elements µg/g (ppm)</i> | | | | | | | |
|----------------|----------------------------------|-----|-----|-----|-----|-----|-----|----|
| | Ni | Mn | Sr | S | P | Cr | Ba | V |
| DE15MV011A | 198 | 373 | 210 | 189 | 330 | 101 | 162 | 51 |
| DE15MV011B | 192 | 356 | 202 | 179 | 331 | 102 | 154 | 50 |
| DE15MV022A | 748 | 413 | 279 | 181 | 221 | 293 | 136 | 58 |
| DE15MV022B | 756 | 422 | 276 | 183 | 224 | 283 | 134 | 58 |
| DE15MV067A | 889 | 444 | 220 | 194 | 271 | 280 | 171 | 70 |
| DE15MV067B | 876 | 437 | 215 | 192 | 261 | 287 | 168 | 69 |
| DE15MV068-C2A | 637 | 388 | 277 | 305 | 232 | 220 | 133 | 48 |
| DE15MV068-C2B | 648 | 410 | 285 | 309 | 243 | 227 | 136 | 50 |
| DE15MV068-G1A | 598 | 375 | 282 | 309 | 235 | 205 | 94 | 40 |
| DE15MV068-G1B | 604 | 381 | 285 | 323 | 232 | 188 | 94 | 41 |
| DE15MV068-G2A | 716 | 401 | 288 | 314 | 288 | 255 | 149 | 57 |
| DE15MV068-G2B | 723 | 401 | 293 | 317 | 285 | 255 | 149 | 57 |
| DE15MV071-BOTA | 361 | 667 | 459 | 185 | 168 | 103 | 147 | 44 |
| DE15MV071-BOTB | 359 | 655 | 453 | 185 | 166 | 101 | 139 | 44 |
| DE15MV071-TOPA | 216 | 745 | 409 | 172 | 213 | 65 | 66 | 29 |
| DE15MV071-TOPB | 215 | 745 | 407 | 167 | 216 | 67 | 64 | 29 |
| DE15MV102-L1A | 608 | 235 | 287 | 208 | 223 | 224 | 172 | 62 |
| DE15MV102-L1B | 592 | 232 | 281 | 198 | 215 | 224 | 169 | 59 |
| DE15MV102-M1A | 345 | 228 | 281 | 187 | 254 | 142 | 174 | 52 |
| DE15MV102-M1B | 344 | 228 | 279 | 186 | 246 | 143 | 177 | 52 |
| DE15MV102-M2A | 544 | 251 | 282 | 232 | 223 | 213 | 161 | 57 |
| DE15MV102-M2B | 109 | 51 | 57 | 47 | 43 | 42 | 32 | 11 |
| DE15MV112A | 345 | 179 | 509 | 606 | 133 | 127 | 86 | 26 |
| DE15MV112B | 345 | 171 | 504 | 598 | 139 | 126 | 91 | 26 |

Appendix I – ICP-OES results

| Sample | <i>Trace elements $\mu\text{g/g}$ (ppm)</i> | | | | | | |
|----------------|--|----|----|----|----|----|----|
| | Zn | Co | Rb | Li | Cu | Pb | As |
| DE15MV011A | 46 | 18 | 35 | 20 | 14 | 8 | 20 |
| DE15MV011B | 44 | 18 | 28 | 20 | 9 | 11 | 17 |
| DE15MV022A | 61 | 50 | 37 | 24 | 22 | 12 | 4 |
| DE15MV022B | 68 | 53 | 37 | 24 | 21 | 10 | 4 |
| DE15MV067A | 66 | 47 | 33 | 25 | 24 | 12 | 3 |
| DE15MV067B | 63 | 46 | 32 | 24 | 19 | 13 | 1 |
| DE15MV068-C2A | 46 | 29 | 29 | 20 | 15 | 12 | 3 |
| DE15MV068-C2B | 47 | 32 | 29 | 20 | 15 | 13 | 2 |
| DE15MV068-G1A | 42 | 31 | 15 | 15 | 14 | 7 | 3 |
| DE15MV068-G1B | 41 | 32 | 19 | 15 | 13 | 8 | 3 |
| DE15MV068-G2A | 52 | 36 | 33 | 22 | 16 | 10 | 1 |
| DE15MV068-G2B | 53 | 37 | 35 | 22 | 18 | 12 | 3 |
| DE15MV071-BOTA | 25 | 18 | 10 | 10 | 6 | 8 | 3 |
| DE15MV071-BOTB | 25 | 17 | 10 | 10 | 5 | 7 | 2 |
| DE15MV071-TOPA | 23 | 12 | 6 | 9 | 4 | 5 | 4 |
| DE15MV071-TOPB | 23 | 11 | 10 | 10 | 4 | 6 | 1 |
| DE15MV102-L1A | 64 | 29 | 45 | 31 | 23 | 11 | 1 |
| DE15MV102-L1B | 80 | 29 | 41 | 30 | 49 | 15 | 3 |
| DE15MV102-M1A | 56 | 23 | 50 | 32 | 19 | 14 | 4 |
| DE15MV102-M1B | 57 | 23 | 44 | 32 | 19 | 12 | 0 |
| DE15MV102-M2A | 60 | 28 | 42 | 31 | 21 | 12 | 3 |
| DE15MV102-M2B | 12 | 6 | 9 | 6 | 4 | 3 | 1 |
| DE15MV112A | 27 | 18 | 14 | 11 | 9 | 6 | 4 |
| DE15MV112B | 27 | 17 | 12 | 11 | 9 | 4 | 3 |

Appendix J – Porosity and permeability measurements

| Lithotype - Sample | <i>Petrophysical properties</i> | | | |
|-------------------------------------|----------------------------------|-------------------------------------|--------------------------------|-------------------------|
| | Ambient He porosity (% of Vb) | Gas Horizontal Permeability (mD) | Emp. Klink. Hor. Perm. (mD) | Grain Density (g/mL) |
| <i>Well-cemented conglomerate</i> | | | | |
| DE15MV033 | 6.8 | 0.45 | 0.30 | 2.71 |
| DE15MV043 | 5.6 | 0.04 | 0.02 | 2.69 |
| DE15MV045(1) | 6.2 | 0.07 | 0.04 | 2.69 |
| DE15MV045(2) | 8.1 | 0.35 | 0.23 | 2.69 |
| DE15MV110(1) | 11.9 | 0.18 | 0.11 | 2.67 |
| <i>Mud-supported conglomerate</i> | | | | |
| DE15MV044(1) | 14.9 | 123 | 113 | 2.68 |
| DE15MV044(2) | 14.7 | 1.07 | 0.74 | 2.68 |
| DE15MV099 | 12.4 | 0.29 | 0.19 | 2.71 |
| DE15MV110(2) | 10.5 | 92.6 | 83.5 | 2.67 |
| <i>Poorly-cemented conglomerate</i> | | | | |
| DE15MV040 | 11.5 | 3143 | 3035 | 2.69 |
| DE15MV096 | 8.3 | 142 | 131 | 2.68 |
| <i>Monogenetic breccia</i> | | | | |
| DE15MV073 | 7.9 | 5.57 | 4.25 | 2.67 |
| DE15MV108 | 7.5 | 0.32 | 0.21 | 2.67 |
| DE15MV109 | 9.5 | 11.8 | 9.40 | 2.67 |
| <i>Gastropod-rich carbonate</i> | | | | |
| DE15MV083 | 8.7 | 0.04 | 0.03 | 2.69 |
| DE15MV095 | 14.0 | 0.06 | 0.03 | 2.69 |
| DE15MV106 | 8.5 | 0.05 | 0.03 | 2.70 |
| DE15MV107(1) | 9.4 | 0.04 | 0.02 | 2.69 |
| DE15MV107(2) | 11.4 | 0.26 | 0.17 | 2.66 |
| DE15MV107(3) | 10.1 | 0.05 | 0.03 | 2.67 |
| <i>Coquina</i> | | | | |
| DE15MV070 | 39.3 | 90.9 | 81.9 | 2.69 |

AFDELING GEOLOGIE
Celestijnenlaan 200E, bus 2408
3001 LEUVEN, BELGIË
tel. + 32 16 32 64 60
fax + 32 16 32 29 80
www.aow.kuleuven.be

